NMI LIBRARY -- DO NOT REMOVE

BAA-102-2

[redacted]

NMI Library -- DO NOT REMOVE

Babcock & Wilcox
a McDermott company
Contract Research Division

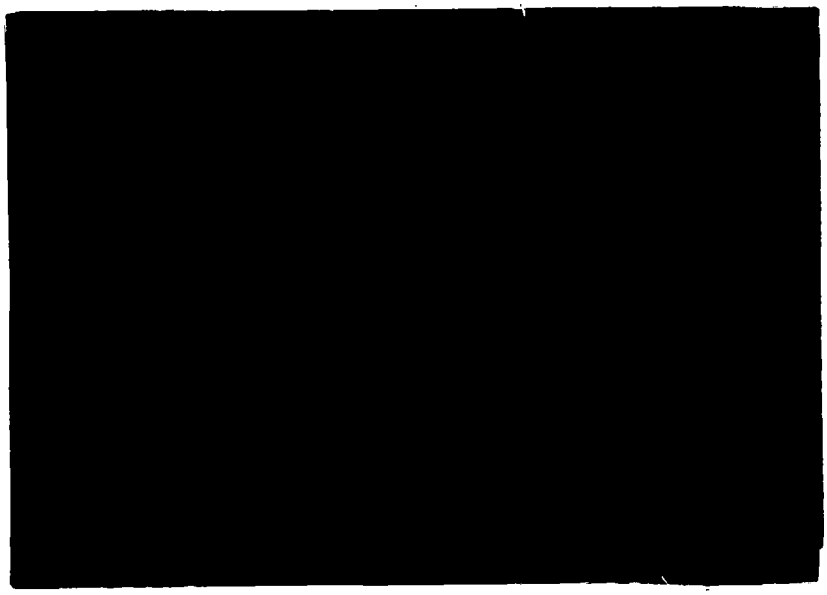

GUIDEWAY STRUCTURAL DESIGN AND POWER/PROPULSION/BRAKING IN RELATION TO GUIDEWAYS

FINAL REPORT
JANUARY 1993

GUIDEWAY STRUCTURAL DESIGN AND POWER/PROPULSION/BRAKING IN RELATION TO GUIDEWAYS

FINAL REPORT

PREPARED BY:

The Maglev 2000 Team

SUBMITTED BY:

Babcock & Wilcox
Contract Research Division
Lynchburg, VA

PREPARED FOR:

Department of Transportation
Federal Railroad Administration
Washington, DC
FRA Contract No. DTFR53-91-C-00065
B&W Contract No. CRD 1277

Technical Report Documentation Page

1. Report No.	2. Government Accession No.	3. Recipient's Catalog No.
DOT/FRA/NMI-92/25		

4. Title and Subtitle	5. Report Date
Guideway Structural Design and Power/Propulsion/ Braking in Relation to Guideways	January 1993
	6. Performing Organization Code
7. Author(s) (Principle) K.M. Falkowski, Intermagnetics Gen'l F.S. Key, Hudson Eng., S.B. Kuznetsov, Power Superconductor	8. Performing Organization Report No. CRD 1277
9. Performing Organization Name and Address Babcock & Wilcox, a McDermott company Contract Research Division P.O. Box 11435 Lynchburg, VA 24506-1435	10. Work Unit No. (TRAIS) 11. Contract or Grant No. DTFR53-91-C00065
12. Sponsoring Agency Name and Address U.S. Department of Transportation, Federal Railroad Administration 400 Seventh St. SW Room 8222 Washington, D.C. 20590	13. Type of Report and Period Covered Final Report August 1991 - January 1993 14. Sponsoring Agency Code

15. Supplementary Notes

COTR: R.M. Suever
Department of the Army, Corps of Engineers
P.O. Box 1600 Huntsville, AL 35807-4301

16. Abstract

This final report summarizes work completed in the investigation of the power, propulsion, and braking systems for five (5) different electrodynamic (EDS) Maglev configurations. System requirements and recommendations, including a cost analysis, are determined for each configuration.

The analysis considers variations in vehicle length, acceleration/deceleration criteria, airgap clearance, and maximum propulsion thrust. Five different guideway configurations have been considered, each of which is based on air-core magnets made from low-temperature superconductors (LTSC) - (NbTi, Nb3Sn) or the newer high-T_c ceramic superconductors (HTSCs).

The material requirements and cost of the guideway electrical components were studied as a function of the energy conversion efficiency, the stator block length, armature current density, stator temperature rise, and other parameters. The propulsion design focused on a dual-parallel, linear synchronous motor (LSM) with thrust modulation achieved by applying a variable frequency and voltage along the guideway. Critical design parameters were estimated using a three-dimensional computer model for the inductances, magnetic fields, and electromagnetic forces.

The study also addressed the conceptual design of the magnet, cryostat, and refrigeration subsystems. Magnetic fields, forces, AC losses, superconductor stability, heat loading, and refrigeration demands were analyzed; a specific design shows the limits of passive shielding.

17. Key Words	18. Distribution Statement
Maglev, guideway, superconductor, structural, design	Document is available to the U.S. public through the National Technical Information Service, Springfield, VA 22161

19. Security Classif. (of this report)	20. Security Classif. (of this page)	21. No. of Pages	22. Price
UNCLASSIFIED	UNCLASSIFIED	577	

REPORT LEGAL NOTICE

This report was prepared by Babcock & Wilcox and the Maglev 2000 Team as an account of work sponsored by the United States Government. With respect to any third party, neither the United States nor the U.S. Department of Transportation, nor the Federal Railroad Administration, nor Babcock & Wilcox, nor its subcontractors, nor any of their employees, makes any warranty, expressed or implied, or assumes any legal liability or responsibility for the accuracy, completeness, or usefulness of any information, apparatus, product, or process disclosed, or represented that its use would not infringe privately owned rights. Reference herein to any specific commercial product, process, or service by trade name, trademark, manufacturer, or otherwise, does not necessarily constitute or imply its endorsement, recommendation, or favoring by the United States Government or any agency thereof. The views and opinions of authors expressed herein do not necessarily state or reflect those of the United States Government or any agency thereof.

FINAL REPORT

Table of Contents

FINAL REPORT

Table of Contents
(Continued)

THE MAGLEV 2000 TEAM

This study was conducted by a consortium of firms, brought together to contribute their knowledge and experience to offer recommendations for improvements to Maglev systems and technology. Participation in the study included the following:

D. Atnafu, Madison Madison International[1]

J. P. Doran, Babcock & Wilcox Company

K. M. Falkowski, Intermagnetics General Corporation[1][2]

F. S. Key, Hudson Engineering Corporation[1][2]

R. W. Kiernan, Council on Superconductivity for American Competitiveness

S. B. Kuznetsov, Power Superconductor Applications Corporation[1][2]
(formerly of PSM Technologies, Inc.)

C. Russo, American Superconductor Corporation[1]

H. C. Yang, Prairie View A&M University[1]

(1) Contributing Authors
(2) Principle Investigators

FINAL REPORT

BACKGROUND:

One of the primary goals of the National Maglev Initiative is to develop an innovative system whereby the United States can benefit from Maglev transportation and its spinoffs. The advent of superconducting magnets in the early 1950's has progressed to the stage of commercializing large high field magnets for use in transportation systems to greatly enhance efficiency, power density and passenger comfort. This study specifically concentrates on the design of 500 km/hr - class Maglev passenger vehicles using on-board superconducting magnets. Present electrodynamic Maglev designs are analyzed and performance improvements are added to yield optimum choice of materials and ultimately deliver the highest power density per dollar. The study focuses on the economic relationship between guideway materials, structure and choice of vehicle characteristics for 5 representative guideways and 3 vehicle weight classes.

This Final Report presents the results for the three primary tasks for the Babcock & Wilcox / Federal Railroad Administration contract DTFR53-91-C-00065 - GUIDEWAY STRUCTURAL DESIGN AND POWER/PROPULSION/BRAKING IN RELATION TO GUIDEWAYS. The lead subcontractors for each task - PSM Technologies, Inc./Power Superconductor Applications Corporation for Section 1, Intermagnetics General Corporation for Section 2, and Hudson Engineering Corporation for Section 3 were supported by the remainder of the Maglev 2000 Team. Remaining Team members include American Superconductor Corporation, Babcock & Wilcox Co., Council on Superconductivity for American Competitiveness, Madison Madison International, and the Prairie View A&M Research Foundation.

CONTRACT TECHNICAL OBJECTIVE:

The objective of this contract is to investigate the power, propulsion, and braking systems for five (5) different electrodynamic (EDS) Maglev configurations. System requirements and recommendations, including a cost analysis, are determined for each configuration. Possible multiple uses for the guideway structure are identified and investigated. In addition, three superconductors are evaluated for use on Maglev systems. Through this research, it is planned that improvements can be identified which will contribute toward a technically advanced economically viable U.S. Maglev system.

EXECUTIVE SUMMARY:

This report has analyzed electrodynamic and mechanical designs for a magnetically levitated transportation system with nominal specifications:

- maximum speed: 500 km/hr (300 mph);
- passenger capacity/car: 76-200;
- vehicle weight: 26-67 metric tons (57,200-147,400 lbs);
- guideway width: 3.65 m (12 ft.)

The analysis considers variations in vehicle length, acceleration/deceleration criteria, air-gap clearance, and maximum propulsion thrust. Five different guideway configurations have been considered, each of which is based on air-core magnets made from low-temperature superconductors (LTSC)(NbTi, Nb_3Sn) or the newer high-T_c ceramic superconductors (HTSCs).

The material requirements and cost of the guideway electrical components were studied as a function of the energy conversion efficiency, the stator block length, armature current density, stator temperature rise, and other parameters. The propulsion design focused on a dual-parallel, linear synchronous motor (LSM) with thrust modulation achieved by applying a variable frequency and voltage along the guideway. Critical design parameters were estimated using a

three-dimensional computer model for the inductances, magnetic fields, and electromagnetic forces. Peak field strength in the passenger compartment at various heights has been plotted for the baseline magnet design.

A main activity addressed during this study concerns the conceptual design of the magnet, cryostat, and refrigeration subsystems. Magnetic fields, forces, AC losses, superconductor stability, heat loading, and refrigeration demands were analyzed; a specific design shows the limits of passive shielding. In particular, the choice of a dual LSM for the propulsion motor with a reduced magnet width has resulted in a passenger compartment magnetic field density at 0.5 mT, which is lower than competitive designs.

Superconductor Selection

A crucial area under consideration in a Maglev transportation system is the choice of the superconductor for the magnetic levitation and propulsion systems. Hence, two types of conventional LTSC wires were assessed:

- NbTi
- Nb_3Sn,

Both of these LTSC wires must be operated under liquid helium. In addition, four types of new high-temperature superconductors (HTSCs), using their latest performance data, were considered. The HTSCs considered are:

- YBCO ($Y_1Ba_2Cu_3O_7$)
- Bismuth-based, silver-sheathed, BSCCO-2223, $[(Bi,Pb)_2Sr_2Ca_2Cu_3O_x]$
- BSCCO-2212 ($Bi_2Sr_2Ca_1Cu_2O_{8+x}$)
- TBCCO ($TlBa_2Ca_2Cu_3O_y$)

The LTSC magnets operate in the persistent mode with negligible AC losses. Both cryostable and adiabatic coil designs were considered for each conductor type. Designs for a propulsion coil having a peak field of 5.3 T in the windings and a magnetomotive force of 600 kAT were analyzed. Preliminary optimal design of the conductor and coil show the relationship of vehicle weight and overall system efficiency to refrigeration load, vehicle vertical perturbation, AC losses, and ultimate cooling temperature.

HTSC wires appear to offer significant advantages as well as considerable promise for even further improved properties in the near future. These include:

- Stability under very high magnetic fields, (i.e., high J_c in fields);
- A range of possible operating temperatures from 20-77°K, with optimal performance probably in the 20-50°K range;
- Easier, more efficient cooling; and
- Superior stability in presence of AC losses, due to the higher temperature.

Metal micro-composite ceramic HTSC wire in long lengths up to 200 m is presently available with good windability and current-densities up to 12,000 A/cm^2, adequate for magnet coils. As a material with a longer history and experience, NbTi appears to offer higher current densities, lower cost, and higher reliability at present. Issues of HTSC wire strength need further development; HTSC magnets at 20-50°K probably will not operate in persistent mode. Trade-offs of shielding costs versus superimposed AC guideway-perturbation losses between LTSCs and HTSCs are related to the overall vehicle structure and ultimately determine the vehicle weight.

Since HTSC wire development began in 1988, the performance achieved has been increasing 100 - 1000-fold per year. Although conventional NbTi LTSC conductors will provide acceptable performance, serious consideration of HTSC-wire in Maglev applications is warranted. The optimal choice of conductor type must await the overall integrated system review. It is projected that HTSC materials will attain a 5.0 Tesla peak induction at a current density exceeding 12,500 A/cm^2 in a 30°K chamber before the year 1994. This will allow further weight reduction.

A preliminary analysis of the system's heat load and refrigeration has been completed, both for low-temperature, helium-cooled systems and for intermediate temperature BSCCO-based systems. The latter can be cooled with Gifford-McMahon or Stirling cycle refrigerators with high efficiency and reliability. The heat load was found to be surprisingly low, particularly when larger cryostats are employed, because the surface-to-volume ratio is lower and radiation losses are thus reduced.

Refrigeration is required on the vehicles, consuming approximately 16 kW of electric power, depending on whether HTSCs or LTSCs are used. Additional cooling for the compressors in the range of 3-25 kW is recommended and accomplished by heat rejection to the atmosphere.

Figure 2-1 summarizes the baseline requirements for refrigeration and vehicle superconducting magnets. A value of 5.3 T, the peak field in the magnets for the LSM, was obtained by studying the effects of neighboring magnets and materials of the guideway.

Figure 2-2 summarizes some requirements for the propulsion magnets; the LTSC persistent mode has been designed in detail, and preliminary specifications are given for the HTSC magnets.

An aluminum eddy current shield on the floor of the vehicle contains alternating flux from the guideway magnets. A further analysis for the HTSC wires operating nonpersistently at 20-50°K indicates a potential for future systems cooled with either supercritical helium, liquid neon or liquid hydrogen. Other non-liquid HTSC cooling strategies are under consideration.

Design Process

The design of the LSM preceded all other superconducting (SC) systems, followed by the levitation magnet and the null-flux guidance. The baseline thrust of 60 kN (90 kN short-time overload) resulted in 24 pairs of vehicle SC magnets spaced at a pitch of 0.57 m as optimum for a 500 km/hr system. The baseline deceleration rate of 0.25 g established the upper limit ratings on both wayside inverter and vehicle magnets.

The final design of the levitation magnets incorporated 7 SC magnets per side of the vehicle excited at 385 kAT to maintain a minimum 22 cm airgap. The unique design of the Maglev 2000 also allows the lift magnets to provide a degree of lateral stabilization when working in close proximity to the propulsion magnets. A final L/D ratio of 28 was chosen.

Guideway Evaluation

The five guideway configurations chosen for this evaluation are described in detail in Section 3 and shown in Figures 3-1 through 3-15. The five configurations are:

- Type I Flat-top guideway
- Type II Wrap around or clamp guideway
- Type III Semicircular guideway
- Type IV Inverted "T" guideway
- Type V U-shaped or channel guideway

The dimensions of each guideway were developed based on the requirements of the levitation and propulsion systems designed for each individual configuration. The average levitation Q factor is 9.5, and the overall L/D ratio is optimized as 28:1. Although each configuration offers a unique solution for a magnetically levitated transportation system, the basic structural support system is similar for all guideways.

The LSM windings are precast in epoxy in 15 - 20 m long trays. The five guideways have similar construction materials, construction technology, installation techniques, and support systems. The base structural element for all five guideways is a shop-fabricated, precast, prestressed concrete girder shipped to the site as a complete assembly ready for installation. Each girder is shop-tested to ensure continuity and prepared for field connection to the next girder. The precise field installation of the girder and the continued level orientation of the girder over the operational life of the structure is a critical concern. To accomplish this the girders are designed to rest on two mechanically adjustable supports. Each of these items may be adjusted vertically to level the girder during installation and to maintain the girders level

during operation. The stator trays are electrically connected between girders, rather than an on-site winding. A sensor system, to alert operators that the guideway supports are not within level tolerances, will be utilized to aide maintenance operations for the life of the guideway system. The sensors will also continuously monitor the girder to alert operators that the girders are responding differently to the loads imposed during operation.

The magnetic field generated by the SC magnets requires the use of new and innovative construction materials for the guideway, such as composites and fiberglass-epoxy laminates. The potential interaction between the magnetic fields from the superconducting levitation and propulsion systems and any ferrous metals requires the use of nonmagnetic materials such as fiber-reinforced plastics for reinforcing and/or anchor bolts.

The guideway configurations described above and shown in Figures 3-1 through 3-15 provide a general summary of the current research efforts for Maglev guideway support systems. However, up until this point in U.S. transportation history, no study has provided a complete design/construction estimate utilizing the same design criteria and parameters for all five configurations. The primary effort of this study is to design each of the configurations using the same design criteria and prepare a construction cost estimate for each. This will enable a rigorous comparison of each system and the advantages and limitations they present.

The development of cost criteria for estimating the construction cost of each guideway configuration includes the following items:

- Effect of banking angle on structural supports
- Engineering/geotechnical support
- Temporary construction facilities
- Site preparation and finishing
- Cast-in-place foundation
- Cast-in-place columns and T-beams
- Precast concrete girder (including aluminum levitation ladders and LSM)
- Shop installation of levitation strips, LSM, sensor system, cables and wiring

- Precast concrete girder installation and hook-up
- Contractor contingency, overhead and profit

The lowest estimated cost of the base case for a dual guideway for each configuration is provided below. The base case was developed using the following criteria/parameters:

Column spacing	30-meters (100')
Ground clearance	10.7-meters (35')
Girder vertical deflection limit	Span/1500
Column lateral deflection limit	Height/500
Superelevation limit	15°
Foundation gross allowable base pressure	192 k Pa (4000-psf)

Guideway Cost Summary

Type I	$10,044,000/mile	$6,241,000/km
Type II	$11,669,000/mile	$7,251,000/km
Type III	$10,836,000/mile	$6,733,000/km
Type IV	$11,293,000/mile	$7,017,000/km
Type V	$12,675,000/mile	$7,876,000/km

The costs provided above reflect an estimate of the engineering, fabrication and construction associated with a large civil project. The costs of the levitation, propulsion, and sensor systems have been included. The use of these numbers must be limited to comparisons of the total cost of the different guideway configurations. The design and cost data used for the comparisons of each guideway are not associated with any particular region nor is it a final design. For example, the data presented above indicate that Type I has an overall constructed cost less than Type V but does not indicate the total cost for the construction of either guideway.

The construction cost of the guideway is dependent on many variables, including site location, congestion of other facilities, terrain, accessibility of construction materials, type of soils supporting the structure, material strengths, length of span, number of supporting columns, height of structure, and the vehicle supported. The impact of the following variables on the construction cost of the guideway has been assessed: single versus double columns, span length, column lateral deflection criteria, girder vertical deflection criteria, height of the structure, seismic zone influence, and girder material strength.

CONCLUSIONS

The Type I guideway is the least costly of the guideway configurations considered. The Type III with dual LSM propulsion appears best-suited to accommodate a minimum turning radius of 1.6 km at the 500 km/hr. This type of structure can be used to parallel existing U.S. interstate highway where low radius curves are prevalent. The Type II and Type IV guideways are limited in vertical and horizontal curvature which effectively limits their upper speed to about 250 km/hr with FRA-defined guideway curvature criteria. The Type V guideway is the most expensive option, and with certain modifications to the structure side walls, can be adapted to high speed operation with 15° superelevation. The Type V guideway has the highest aerodynamic drag and consequently the highest electric power costs per passenger mile. The maximum specified roll-ramp-rate is 12 degrees per second which is only accommodated by the Type III guideway.

The study concludes that the dual LSM is a superior propulsion choice for all 5 vehicle configurations including magnetic field attenuation. The preferred lateral stabilization system is null-flux guidance loops composed of aluminum-stranded conductor. The preferred levitation system is electrodynamic, with guideway-mounted, aluminum-fabricated-ladder strips interacting with 2 sets of vehicle SC magnets. The total vehicle magnet refrigeration electrical load for all systems is 82 kW; a 475 kW on-board auxiliary generator harmonically-excited by the LSM windings provides all electrical on-board service.

The final design optimized a 200-passenger vehicle weighing 67 metric tons. The specific loading is 0.335 tons/passenger. The baseline cruising power with dual LSM propulsion is 12.9 MVA, indicating a specific power usage of 64.5 kVA/passenger at 500 km/hr. The electrodynamic design provides a lateral stiffness for guidance of 4.2×10^6 N/m and a suspension stiffness up to 3.5×10^6 N/m. It is concluded that a secondary suspension system is required to meet passenger comfort levels as the electrodynamic system proposed is especially rigid at the 22-cm airgap.

The Maglev 2000 vehicle and guideway design reflect the study's prime objective to minimize the vehicle weight and, thereby, reduce the size of the guideway and maximize the long span lengths. With the objective achieved, the cost of producing a Maglev guideway, the single largest cost for a Maglev system, is reduced when produced on a high-volume basis.

POWER, PROPULSION, AND BRAKING INVESTIGATION

1.1 Electrodynamic Design Summary

The first segment of the propulsion, levitation and guidance system concentrated on detailed design of the superconducting linear synchronous motor (LSM) for the 5 guideway types. The guideways all differ in structural layout, overall width, height, configuration of electrical components, etc., but do retain a common electrical layout for the LSM with minor differences adaptable to all 5 guideways. The LSM stator windings are cast in a nonmagnetic, prefabricated tray for rapid and modular assembly at the job site. It is important to note that, in all configurations, an "air-core" (i.e., nonferromagnetic) stator is crucial to be able to maintain an electromagnetic airgap in a range of 0.19 m to 0.23 m, yielding a nominal 0.10 m mechanical clearance between the vehicle and guideway surface. Figure 1-1 shows a cross-section of the Type II system using the dual-parallel propulsion system and dual lift.

Table 1-1 references the operational characteristics for the vehicle. Table 1-2 summarizes the vehicle configuration weights and guideway loadings. The point design is chosen at the higher speed of 500 km/hr to present performance data, magnetic field plots and design tradeoffs in block length, since the high-speed condition generally represents the greatest electrical stress on the LSM. Table 1-3 details the LSM design sequence and particularly addresses the critical mutual- and self-inductance calculations for the baseline LSM design. Terminal quantities for invertor output voltage, current, MVA, power factor, efficiency and optimum load angle are given for a 60 kN cruising thrust rating. An overload short-term rating of 96 kN is obtained for acceleration periods. The 60 kN is used as the base modular thrust value per row of 50 superconducting vehicle field magnets, realizing a mechanical output power

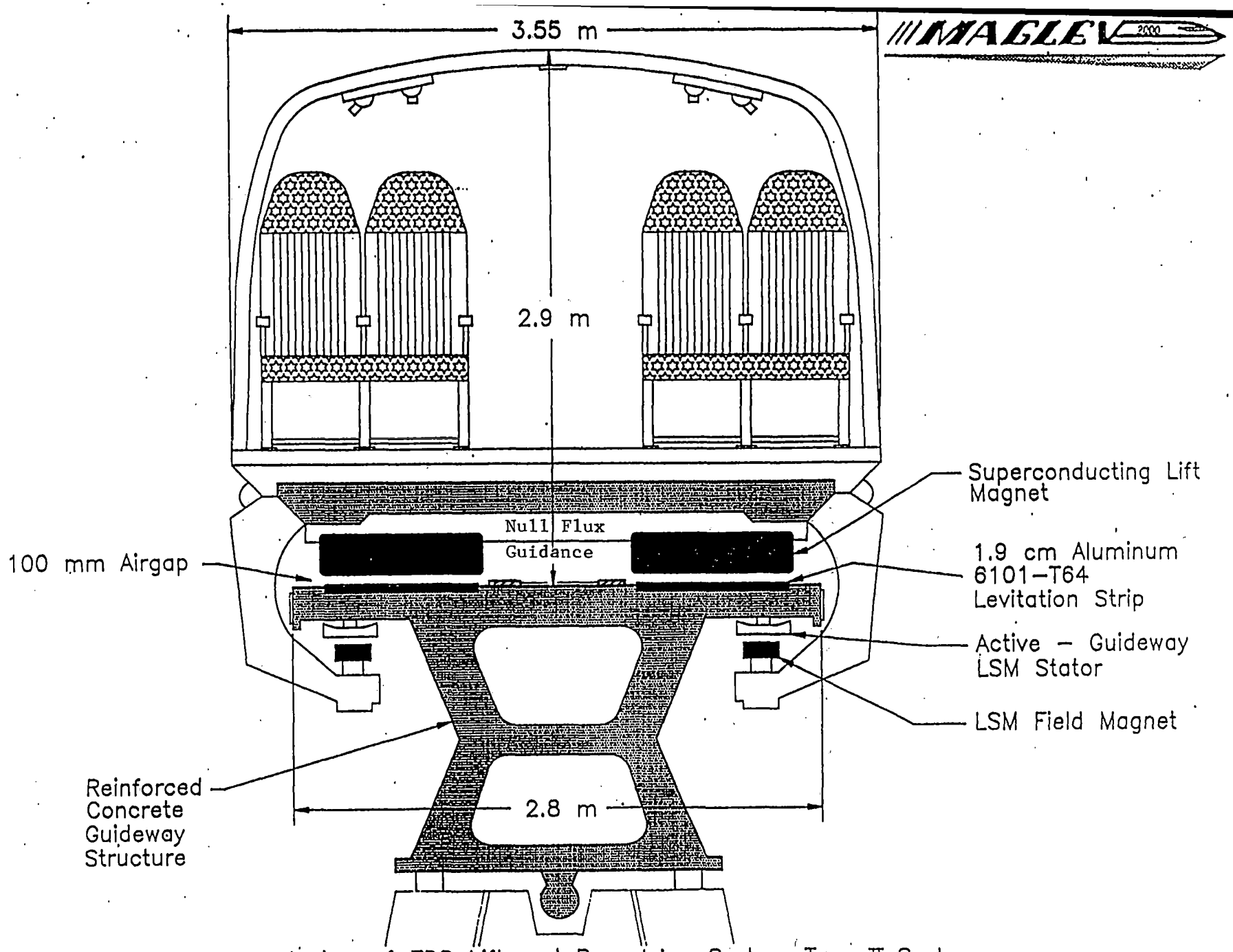

Fig. 1-1 General view of EDS Lift and Propulsion System Type II System

Table 1-1

Operational Characteristics of the Reference Maglev Vehicle

Capacity range	76, 118 or 200 passengers
Overall length	15, 23 or 39 m
Width (nominal)	3.65 m
Height (nominal)	3.2 m
Aerodynamic drag coefficient	0.26
Nominal laden weight (200 passengers)	67 tons
Acceleration	1.0 m/sec^2 (0.1g)
Deceleration - normal	2.5 m/sec^2 (0.25g)
Deceleration - emergency	10 m/sec^2 (1.0g)
Propulsion	LSM - Dual Stator
Upper speed range	400-500 km/hr.
Propulsion Magnet Refrigeration Load	41-50 kW

Characteristics At Cruising Speed of 500 km/hr.

Maximum continuous thrust	60 kN
Ground clearance	0.10-0.12 m
Magnetic drag (estimated)	12-15 kN
Aerodynamic drag (estimated)	35-37 kN
Side wind loading (100 km/hr cross wind)	70 kN
Noise, at 15 m sideline	89 d BA
Guideway aluminum for levitation strips	42 metric tons/km
Superelevation limit	15°
Maximum roll ramp-rate (Type III)	12° per second
Minimum radius at maximum speed	1.6 km
Guidance stiffness - nominal-lateral	4.2×10^6 N/m
Suspension stiffness - nominal-vertical	3×10^6 N/m
Levitation system - natural frequency	2 Hz
Guidance natural frequency	0.85-1.0 Hz
Levitation lift off speed range	48-60 km/hr.
Substation Electrical Output	12.9 MVA at 122 Hz
LSM Mechanical Output	8.33 MW
Linear Power Generator Output	475 kW

Table 1-2

Weight of Representative Vehicle Configurations and Levitation System Average Loading/Meter Guideway Length Type III, IV, V, and VI Systems

Passenger Capacity	Vehicle Length (m)	Empty Weight (kg)	Laden Weight (kg)	Guideway Loading (kg/m)
76	15	19,009	25,918	1728
118	23	29,147	35,875	1734
200	39	49,424	67,605	1733

Table 1-3

Reference Design Parameters for Superconducting Dual LSM Systems

Common Design Characteristics

Net Thrust *	60 kN
Maximum Cruising Speed, V_s	500 km/h
Mechanical Power *	8.33 MW
Field-stator Winding Separation, z_o	22 cm
On-board Power Linear Generator Drag	3.5 kN
Vehicle Aerodynamic Drag	37 kN
Electrodynamic Drag	12-15 kN
Stator Section Length, L_b (range)	0.5 - 2.0 km
Field MMF of Full-length magnets, i_f	500 kAT/600 kAT
Total Magnetic Moment of Superconducting Coils, M *	21.2 x 10^6 A-m

Conductor Material

Field Winding

Nb-Ti Superconducting Magnets		
No. of Superconducting Magnets	50	50
Mean Length, L(m)	0.53	0.53
Mean Width (round-ended), W_f(m)	0.80	0.80
Wavelength, (m)	1.14	1.14
Self Inductance, (H)	0.409	0.409

Stator Winding Cable Materials	Copper	Aluminum
No. of Parallel Conductors/phase	2	2
Active Width, W_s(m)	0.625	0.625
Conductor Diameter, d (mm)	12.7	14.6
Longitudinal Conductor Spacing	30°	30°
Conductor Length per Phase per unit guideway length *	7.99	8.01
Winding Resistance, R_s (Ω/km)	0.166	0.175
Mutual Inductance, M (mH/km)	0.95	0.95
Self Inductance, L_s (mH/km)	2.11	2.04
Leakage Inductance, L_L (mH/km)	1.16	1.09
Reactance for 1 km block section, $W_s L_L L_b$ (Ω)	0.889	0.836

Table 1-3
(Continued)

Stator Winding Cable Materials	Copper	Aluminum
Mass of Winding, (tons/km)	19.3	11.3
Lateral Offset of Field Array w.r.t. stator axis, y	-0.10	-0.10
Operating Parameters		
Field-stator Total Mutual Inductance, $N_{mag} M_{fsi}$ (uH)	6.70	6.70
Invertor Frequency, w_s (Hz)	122	122
Invertor Voltage, L-N (kV)	4.17	4.20
Phase Current, rms (A)	1031	1031
Current Density (A/mm^2)	4.09	3.55
Control Angle, B	112°	112°
Invertor Complex Power, S (MVA) *	12.9	13.0
Power Factor	0.85	0.85
Power Dissipation in 1 km block (kW)	528	557
LSM Electrical Conversion Efficiency	95.8	95.7

*per dual system

of 8.33 MW at high-speed cruise. As the overall vehicle design evolves and aerodynamic/electrodynamic drag losses are better defined, the total LSM output thrust is increased by a combination of additional field magnets and a slight boost in the stator phase current rating. It is important to note that this study has assumed design variations in the nominal working airgap of about 0.21 m are accommodated by alteration of field magnet MMF. The range of 500-600 kAT/pole (for the largest gap) is used versus alternate thrust modulation techniques such as increasing the magnet width.

The wavelength chosen for the baseline design is 1.14 m, which fundamentally establishes the 500 km/hr top speed at an excitation frequency of 122 Hz. The efficiency of the motor and field-stator mutual coupling is largely based on the ratio of wavelength to airgap. The base design has optimally chosen a wavelength to airgap ratio of 5.43:1. The field coil wavelength also establishes the main spatial attenuation of the magnetic field in the passenger compartment. One of the early conclusions of the LSM design study is that the use of a dual LSM, with individual field coils limited to one-half of a conventional LSM magnet width (and arranged in alternating N-S polarity across the vehicle width), results in a reduced passenger magnet field exposure without compromise of the magnetic field distribution at the LSM stator conductors. For this reason and because automatic roll and heave control was introduced with the dual system, all 5 guideway designs proceeded with dual stators of 800 mm active width for each winding.

The levitation system is "superdynamic" (also referred to as electrodynamic repulsive), with the vehicle containing separate superconducting lift magnets operating at 320-385 kAT/pole and a mean width of 0.48 m across the Niobium-titanium (Nb-Ti) helium-cooled superconductor, indicating an overall width of 0.58 m for the cryostat with a 1.60 m overall length. The base design for the study is a Nb-Ti superconductor, helium-cooled, operating at 4.2° K. The study also includes a design of a high-temperature superconductor (HTSC) suspension coil for operation at 20° K, extendable to 77° K using Bismuth Strontium Calcium copper oxide (BSCCO) material.

1.2 Propulsion System Design

The electrical dimensioning of the base propulsion system design has been initiated for a reference design applicable to the 5 LSM windings and interacts with a dual array of superconducting Nb-Ti field magnets located on the vehicle undercarriage to produce a nominal 60 kN (96 kN overload) thrust, continuous output, at 500 km/hr. For general layout, reference Figure 1-2 and 1-2b. The dynamics study is based on projected vehicle oscillations and anticipated eddy current intensities in the magnet wire; the final specification for wire type is made after the dynamic study. The propulsion magnets operate in a persistent-current mode with a preferred transport current of 100 A. The baseline MMF will vary between 600 kAT and 400 kAT in all parametric studies; the exact excitation is dependent on the electromagnetic airgap (19-23 cm range) and the level of braking force. In general, the most stringent system specifications are imposed by the braking duty, using the LSM in a regenerative braking mode operating up to 0.25 g deceleration. Figure 1-3 shows the Type III guideway, Figure 1-4 shows the Type II guideway, Figure 1-5 shows the Type IV guideway, and Figure 1-6 shows the Type V guideway.

Three-dimensional field calculations for a full width LSM magnet of 0.53 m overall length to fit a 0.57 m pole-pitch and a 0.80 m overall width have resulted in an internal self-inductance magnet of 0.409 H. This magnet uses a specific overall conductor cross-section of 40 mm x 40 mm square with exactly 500 turns/coil. One alternate design uses a coil cross-section of 69 x 69 mm square with overall current density of 12,265 A/cm^2. The stored energy per coil for 600 kAT excitation is 294 kJ, or, for a dual 50-magnet system the total vehicle field magnet-stored energy is 29.4 MJ for the propulsion magnets alone. One way to characterize the efficiency of a particular design is by the amount of vehicle undercarriage surface area used by the superconducting (SC) magnet array for a given thrust or power rating.

The specific result of incorporating 50 LSM magnet pairs at 500 kAT is a net propulsion force of 60 kN for a total magnet active surface area of 45.6 m^2. The specific force density loading in the base design is, consequently, 1,316 Newtons/m^2 at a base airgap of 22 cm, for

Figure 1-2

RELATIVE LOCATIONS OF PROPULSION AND LEVITATION COILS

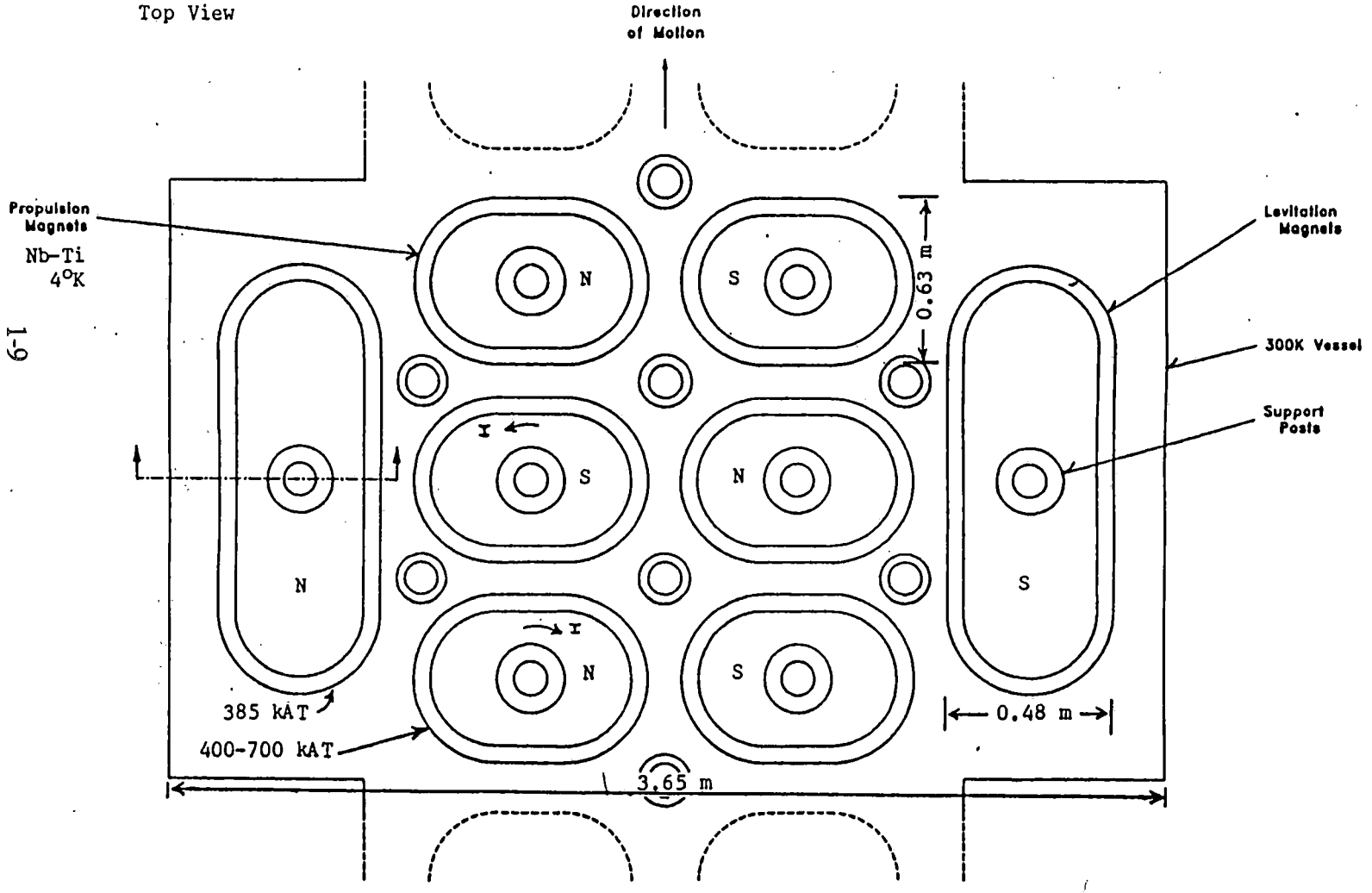

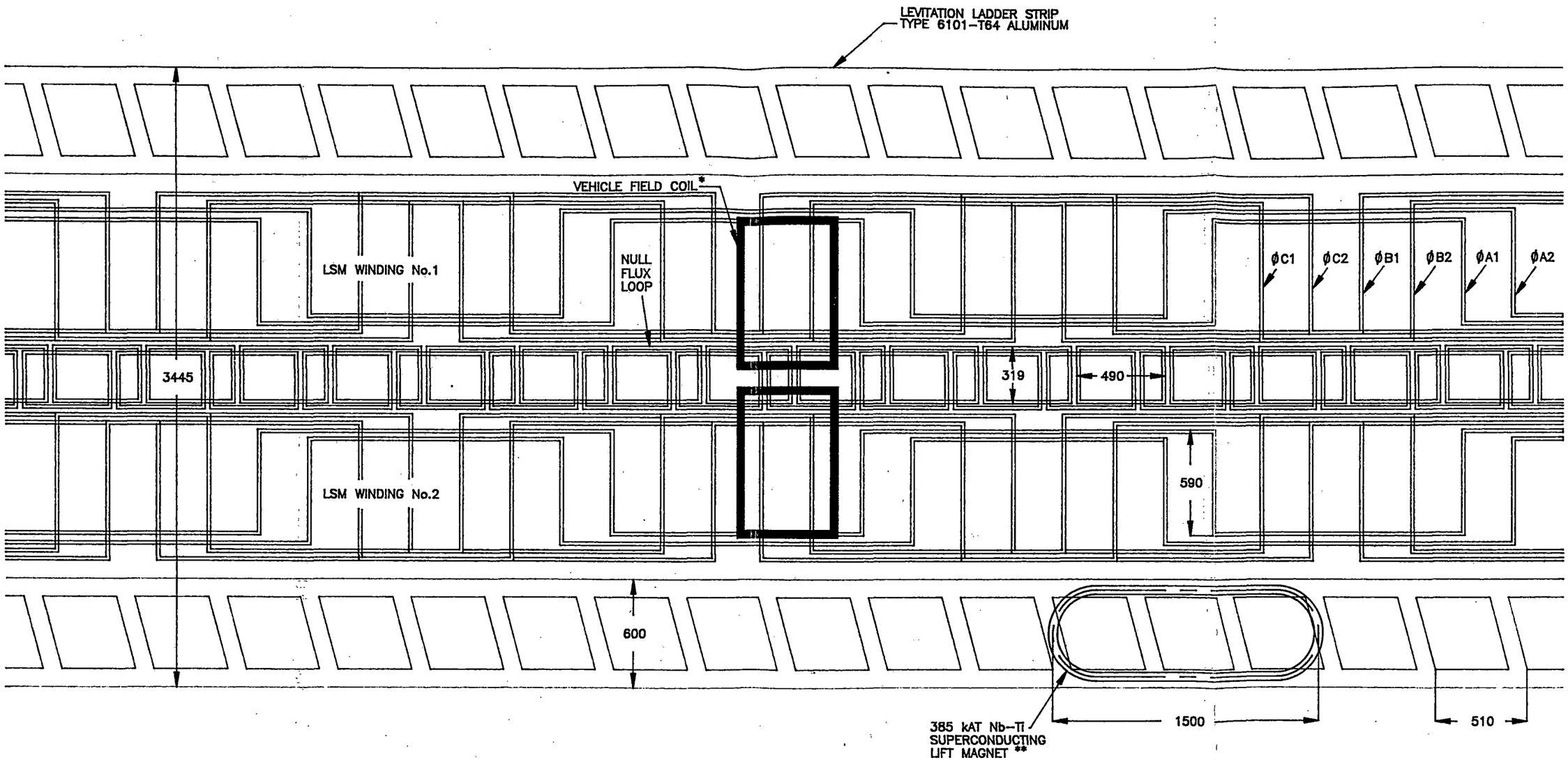

Figure 1-2b TYPE I FLAT-TOP MAGLEV GUIDEWAY WITH DUAL LINEAR SYNCHRONOUS MOTOR AND NULL-FLUX GUIDANCE LOOPS FOR 50 TONNE VEHICLE

NOTES:
*ONLY ONE VEHICLE LSM FIELD COIL SHOWN IN ARRAY OF 40 – 50 PER SIDE
**ONLY ONE LIFT MAGNET SHOWN IN ARRAY OF 5 – 7 PER SIDE OF VEHICLE

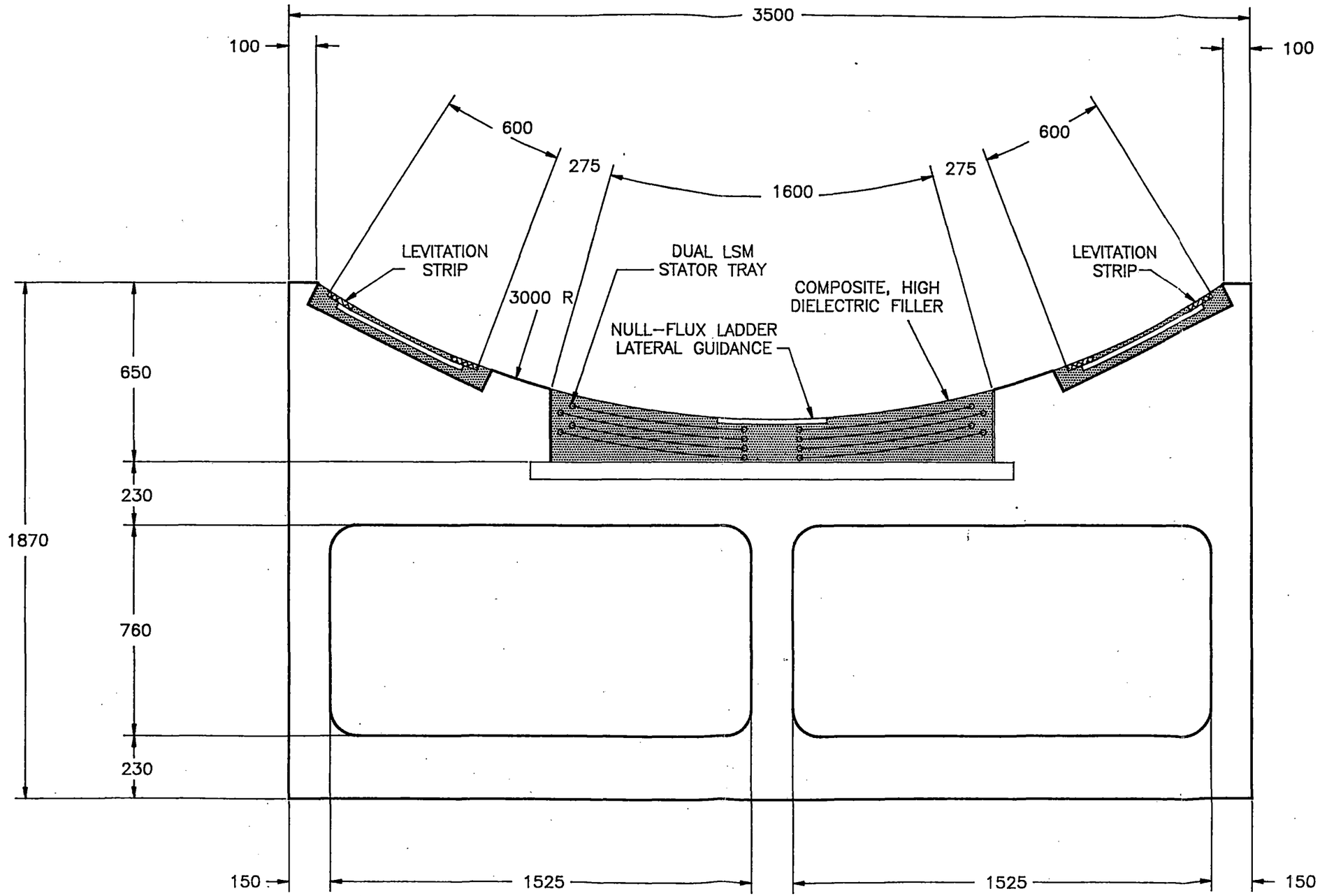

Figure 1-3 Type III Maglev Guideway

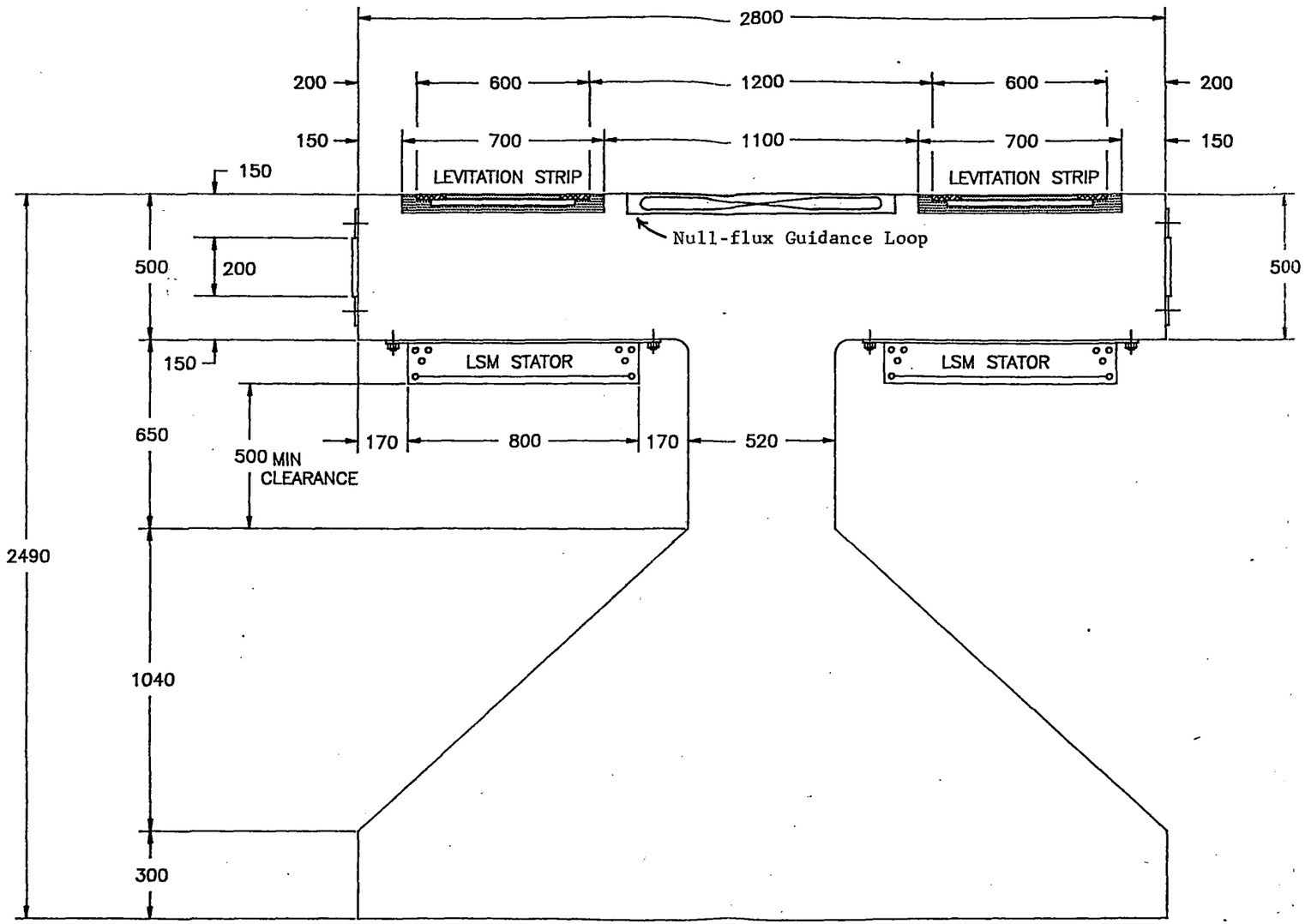

Figure 1-4 Type II Maglev Guideway

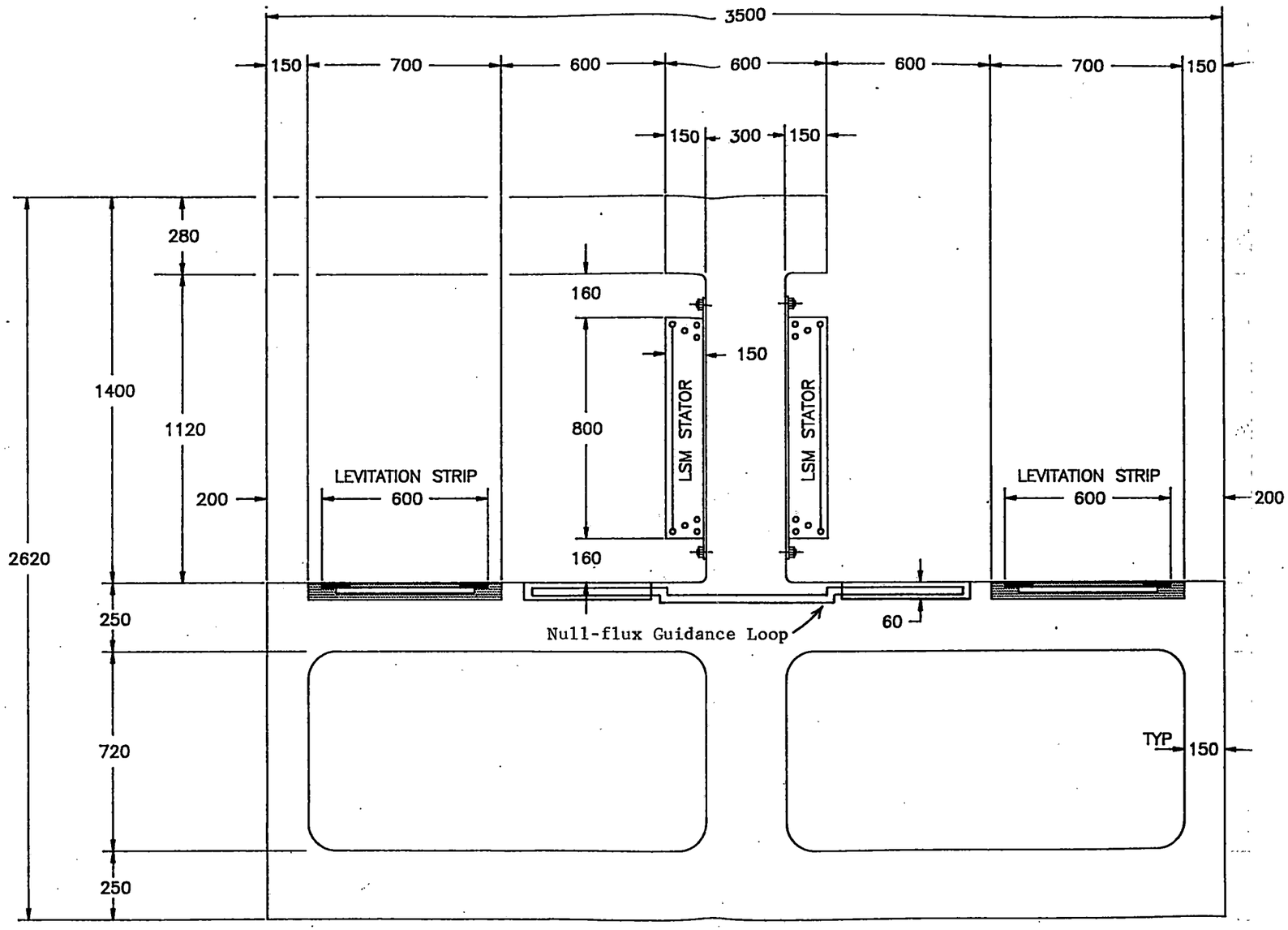

Figure 1-5 TYPE IV GUIDEWAY CROSS SECTION
INVERTED T CONFIGURATION -- DUAL LSM

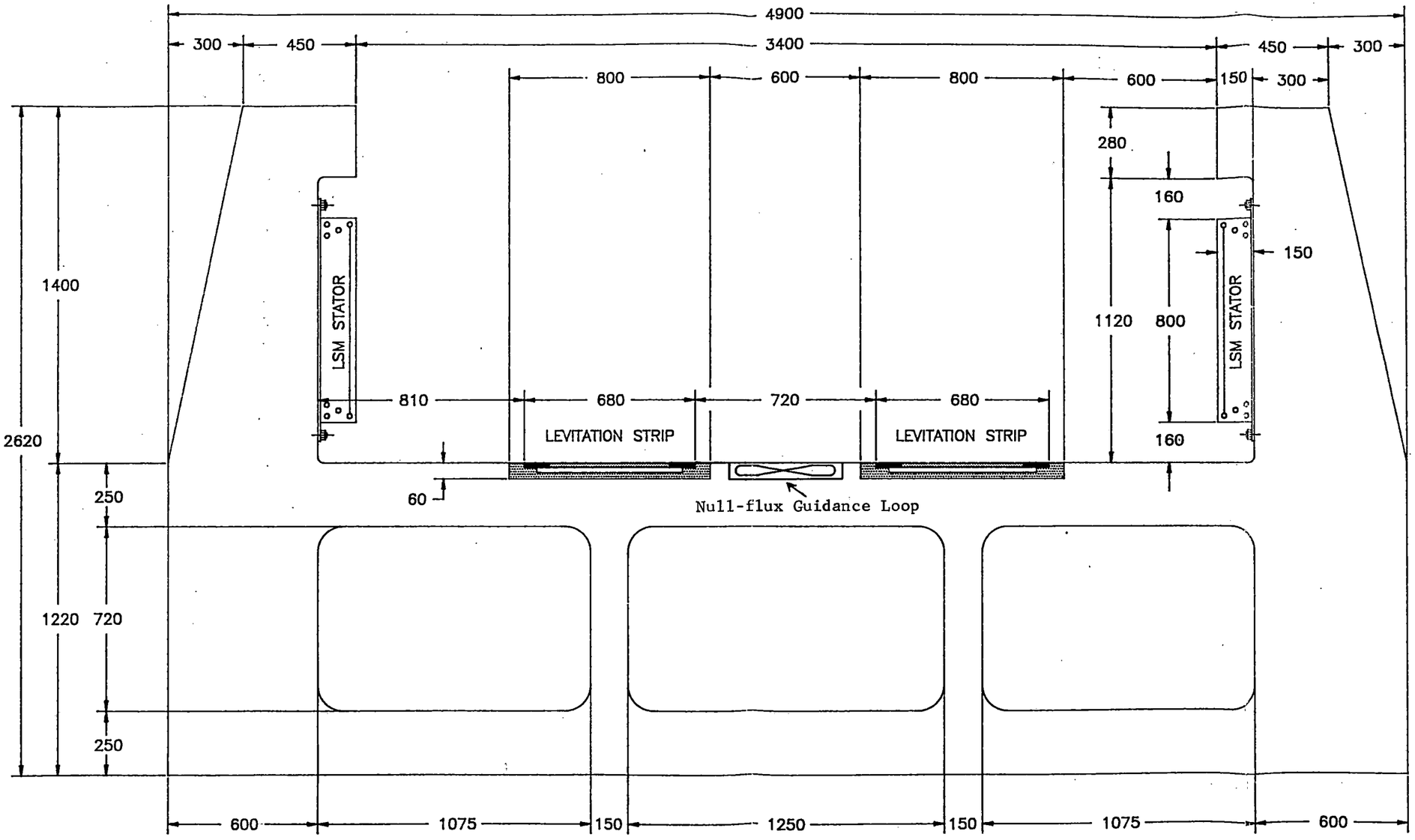

Figure 1-6 TYPE V GUIDEWAY CROSS SECTION U CONFIGURATION – DUAL LSM

the maximum overall LSM efficiency point of 95.9%. The power density of 8.33 MW output per vehicle is, consequently, 182.6 kW/m^2 baseline or 292 kW/m^2 at 60% overload factor. This is higher than comparable EMS systems such as Transrapid 07.

As vehicle passenger configurations evolve and since weights for on-board equipment are apt to increase beyond baseline designs, it may become necessary later to increase propulsive thrust capacity beyond 96 kN. The 50-magnet array results in an overall active magnet length of 28.5 m which is near the maximum for a 39-m long vehicle, which has been used by Maglev 2000 for the minimum length 200-passenger vehicle. Provisions may also be made in the preliminary design to increase the propulsion cruise thrust to 83 kN (124 kN overload) for a large 200-passenger vehicle with a 50-55 m overall length. The aerodynamic drag at 500 km/hr for system configurations Type V or Type II may attain 60-63 kN, and the residual components such as electromagnetic drag may attain up to 15 kN. To produce 83 kN forward thrust requires the full 600 kAT excitation and a magnet array of 77 magnets or 43.9 m active length covering 80% of the vehicle undercarriage. The thrust and power density remain the same as with the 50 magnet array. Figure 1-7 details the levitation ladder design.

In the reference design, Maglev 2000 has chosen a maximum magnetic field density at the guideway surface of 0.74 T, for a mean SC magnet conductor to guideway stator conductor separation of 22 cm. These numbers are specific to the Type I, II, or III guideways and for a dual (parallel layout) LSM. The advantage to increasing the field density beyond 0.74 T is a reduction in the number of SC magnets or in the surface area of the vehicle magnet array. The disadvantage to a higher field is that the shielding becomes progressively heavier, there are higher internal stresses in the magnet, and there will be higher LSM stator eddy losses in the copper or aluminum 6-phase winding. The reference design is based on a Z-directed (vertical) peak, steady-state magnetic field density of 0.62 T for a 500 kAT excitation, raising up to 0.74 T for an overload, high acceleration or high regenerative braking condition which requires 600 kAT excitation per magnet.

Reference Figure 1-8 for the magnetic field plots above the magnet plane.

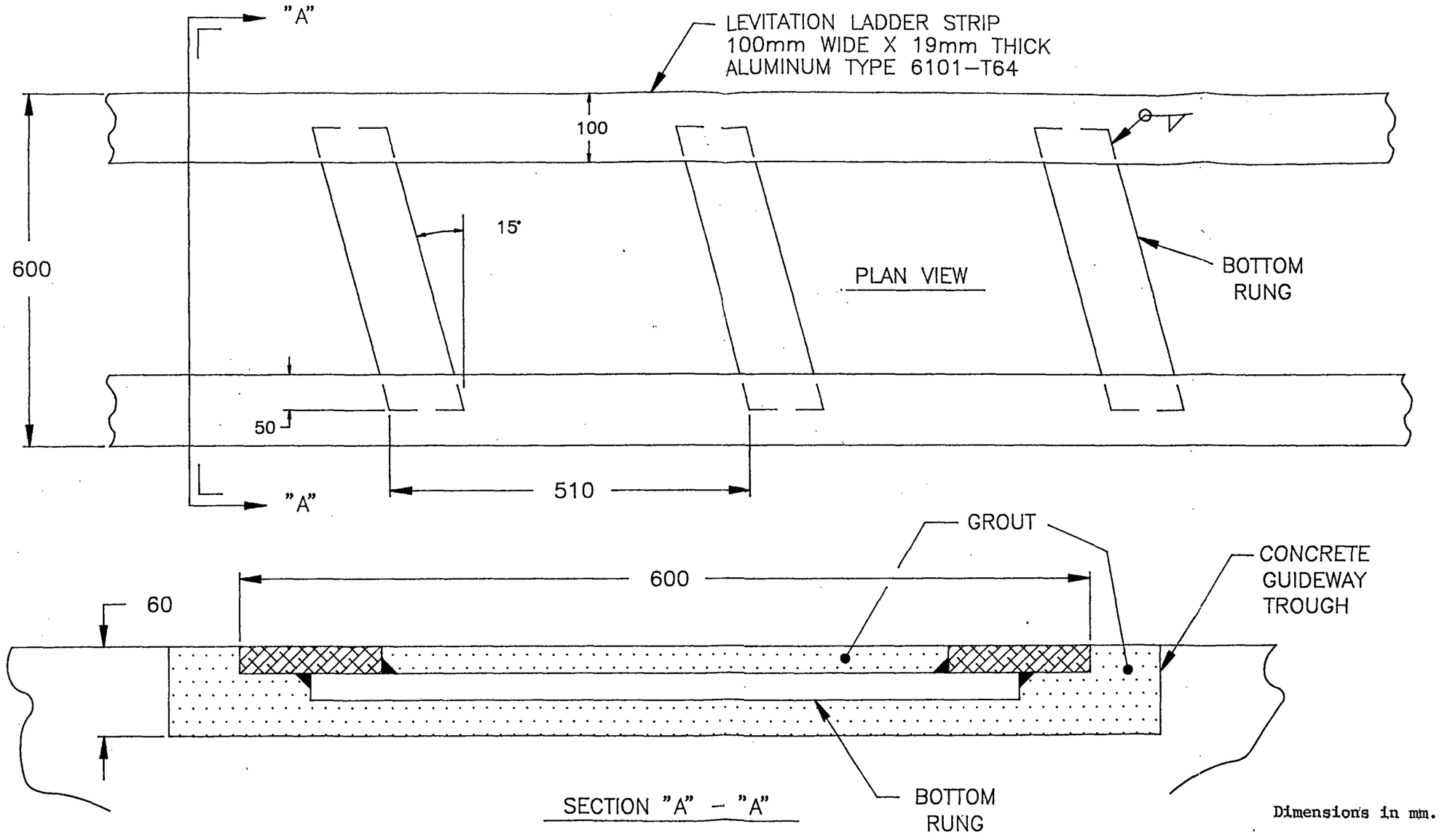

Figure 1-7 Cross section of levitation ladder strips and rungs.

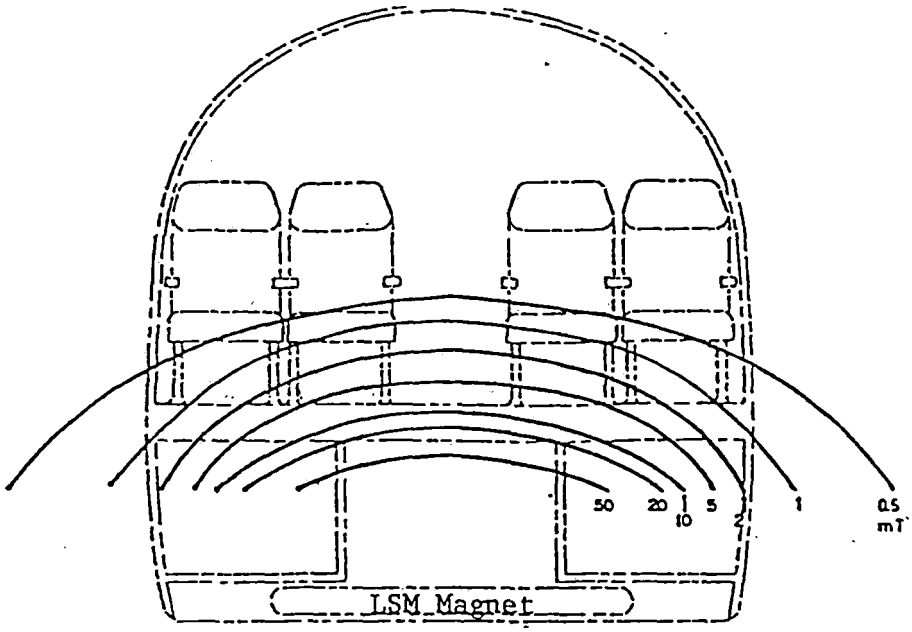

Single LSM Array Inherent Field

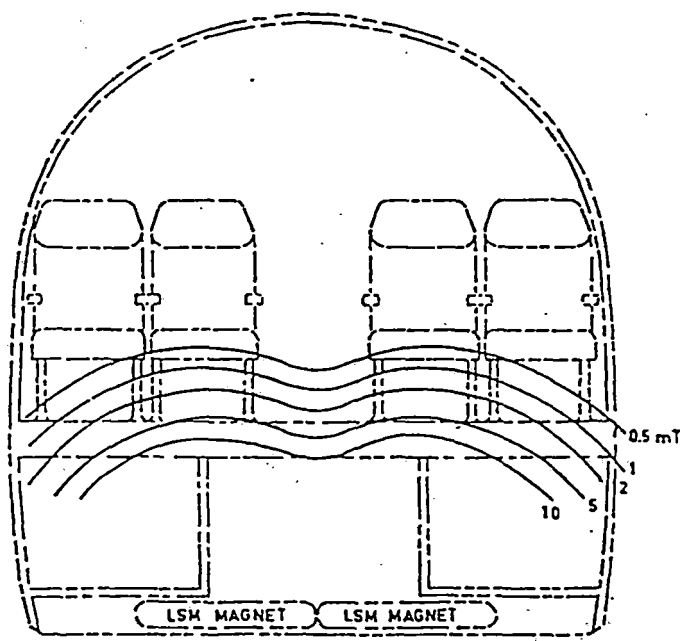

Dual LSM Array Inherent Field

Figure 1-8 Peak magnetic field densities in passenger compartment with single and dual LSM superconducting magnets at 500 kAT excitation and no ferromagnetic shielding.

The inherent (unshielded) magnetic field in the passenger compartment peaks at 24 mT for a 600 kAT excitation strength or at 20 mT for a 500 kAT MMF, located at a distance at exactly 1.00 m above the plane of the SC magnet center, representing the floor of the vehicle. With ferromagnetic undercarriage shielding (9 mm thick steel plate), the 24 mT will be reduced to 5 mT. The advantage of the dual LSM over the single width LSM is a reduction in the inherent magnetic field plot in the passenger compartment for the 500 kAT baseline excitation. The magnetic field plot in Figure 1-8 shows a dual LSM versus single LSM field, positioned over the transition from a north to south pole magnet.

With the particular LSM design presented, especially in a dual array not to exceed 0.80 m active magnet width, there appears little need for active magnetic shielding. Passive ferromagnetic shielding is sufficient and offers the additional feature of structural support for the passenger floor. A suitable shielding material is AISI Type 1020 steel, a low-cost material. Thermal calculations and the cryostat force distribution are being assessed for this type of shielding system.

The nominal acceleration is established at 0.1 G for a 42 metric ton vehicle which fundamentally calls for a 41,160 N accelerating thrust, appropriate for a 118-passenger vehicle. As the vehicle approaches the cruise speed of 500 km/hr, the aerodynamic drag (with the baseline vehicle body design) builds up to 37 kN. The electrodynamic drag remains nearly constant in the 400-500 km/hr range and peaks at 15 kN. The linear generator power pickup contributes an additional 3.5 kN of drag to provide for on-board electrical auxiliaries including HVAC and SC magnet excitation. The total calculated drag losses on the LSM are thus 55.5 kN. The invertor station and stator windings are sized to accommodate a 96 kN acceleration thrust with the thermal limit curves set by the section block length rather than by the acceleration time alone.

To accommodate a 0.1 G acceleration at high speed with 55.5 kN total drag losses requires a total LSM output rating of 96.6 kN or a 60% overload above the base modular thrust of 60 kN. The LSM stator can accommodate this in acceleration sections because of the short time duration required for the boost in stator current. For example, in a 2.0 km stator guideway

block section (worst-case condition) at 400 km/hr, the overload time is only 16 seconds, which is approximately equal to the thermal time constant of the winding. The major limitation on availability of overload thrust rating is at the invertor substation due to the commutation rating of the thyristor electronic switches for the 0-122 Hz variable-frequency supply. The Maglev 2000 group recommends tapering off the 0.1 G acceleration to 0.05 G for speeds above 400 km/hr in order to hold the maximum LSM output to 55.5 kN (drag) plus 20.5 kN (accelerating) or 76 kN total. That is, for economic capital installations or for minimizing substation kVA power demand, a limit must be placed on maximum kVA demand or utility power input. The kVA demand charge in short-haul systems (e.g., 50 km or less) becomes the largest single utility expense, exceeding the basic kW-energy charge, as discussed in detail in Section 1.4.

Consequently, the recommended invertor overload output rating (which is calculated for 1.0 minute) is 20 MVA at the substation output, with a dual 6-phase output current of 1,600 A r.m.s./phase. The nominal or continuous rating of the invertor output is 12.9 MVA, 1031 A/phase, at 4,170 V r.m.s. line to neutral. This current level can be maintained on a 24-hour basis for the invertor thyristor devices, substation step-down transformer, and protective 34.5 kV, 69 kV, or 138 kV utility switchgear. The invertor, in producing variable-voltage, variable frequency (VVVF) power, generates 5th, 7th, 11th, and 13th harmonics and, consequently, has a poor input power factor (or "displacement factor"). In an overload acceleration or medium brake mode, the substation input power is calculated at 20 MVA for the high-speed condition, a 42 metric ton vehicle, and a total LSM output of 76 kN.

The overall electrical characteristics are dictated by the brake mode deceleration specification rather than the acceleration mode. Maglev 2000 has designed the dual-LSM system with a 0.25 G deceleration rate; from 500 km/hr, the LSM inherent braking force reaches a fadeout speed, whereby an auxiliary (mechanical) brake is required to avoid very low frequency (1-4 Hz) in the stator winding. The 0.25 G brake rate at high speed requires 82 kN for which 55 kN is provided by combined aerodynamic drag and electrodynamic lift system drag and 27 kN is provided by a retarding thrust by the LSM which requires 3.75 MW peak power at the 500 km/hr point.

Braking control of the LSM is afforded by rapidly changing the invertor electrical load angle (in a 25 millisecond period) from $\beta = 112°$ to $\beta = 280° - 290°$. The 3.75 MW of available braking power is fed back into the line minus 0.70 MW for stator I^2R and invertor losses, thus injecting approximately 3.05 MW effective into the 60 Hz utility grid for a utility "power credit." Figure 1-9 shows the parametric optimization curves for LSM force, induced voltage, and stator conductor diameter as a function of the stator pole pitch.

Table 1-4 describes cost and conductor weights for two different diameters of copper conductor for the Type I LSM system indicating 16,320 kg/km and 19,307 kg/km of guideway. The addition of the null-flux guidance loops (aluminum) with the LSM conductor brings the total to 22,535 kg/km for a 12.7 mm diameter LSM stator conductor option.

Table 1-5 describes the electrical losses for Types I-V dual LSM guideway conductors operating at a nominal current of 846 A/phase for 3 parametric block lengths (0.5, 1.0, and 2.0 km), and using a specific current density of 3.36 A/mm^2. Efficiency is a strong function of current density. Table 1-6 describes the weight and cost of a 3-phase copper transmission cable from the invertor station to the LSM stator feed point. The LSM stator feed point must be installed to feed multiple (2-4) stator blocks from a common invertor. In general, this study does not advocate the use of individually-switched small stator winding sections (such as 10 m) with thyristors due to the extraordinary number of thyristor switching devices required and the inherent loss in overall system reliability by this change. The number of devices would increase from 24 per system to 2,400 for a 1.0 km block in a dual LSM configuration.

1.3 Null-flux Guidance System

The particular type of null-flux loop guidance is specially-matched to the dimensions of the LSM field magnets. In the dual LSM system, laterally adjacent field magnets are of opposite polarity, and, when a spatial unbalance in the normally symmetrically centered vehicle occurs in the LSM magnetic field, a large differential EMF is induced in the null-flux loop. The resulting induced current can typically attain 7,550 A for a 5-cm lateral sway at the cruise

Figure 1-9

Optimization Curves for Dual LSM

Force 1: Normalized from 3.174 to 4.438 N/M/AMP
Conductor Diameter: Normalized from 0.0102 to 0.026 Meters
Induced Voltage: Normalized from 164.3 to 1074.6 Volts/M

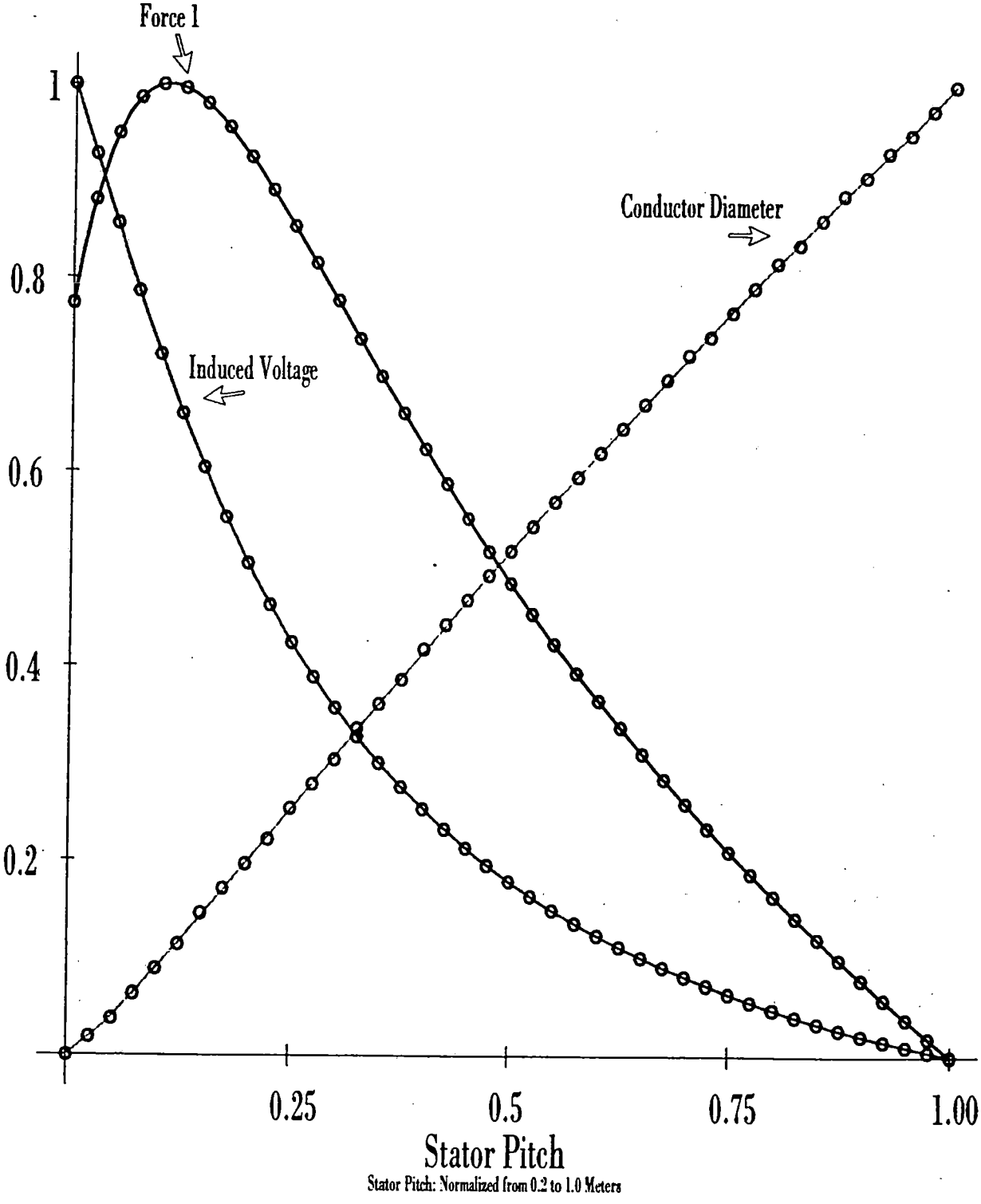

Stator Pitch: Normalized from 0.2 to 1.0 Meters

Table 1-4

Cost and Weight for Type 1 Dual LSM Stator Winding
6-Phase/Guideway Side with 212,000 or 250,000 CM Copper Conductor

Conductor dia-mm	Length/ phase/km	12 x Conductors	R/km of Guideway	Cost/km of Guideway	Weight kg
11.7	1332 m	15,992 m	2.65	$162,554	16,320
12.7	1332 m	15,992 m	2.25	$199,392	19,307

Null-flux and LSM-dual total conductor weight = 19,307 kg + 3,228 kg = 22,535 kg/km

Null Flux Loops

Mean Length of Turn = 1.542 m

Thickness = 0.011 m

Weight = 0.025 x .011 x 1.542 = .000424 cu. m. x 2,690 kg/m = 1.14 kg per loop

Total loops in 1 km = 2,832 loops @ pitch (avg.) of 0.343 m. including overlap

Total weight = 2,832 x 1.14 = 3,228 kg

Table 1-5

Electrical Losses for Representative LSM Propulsion Guideway Windings for Dual Stator Systems, at High Speed Condition of 500 km/hr and Propulsion Thrust = 60 kN

Conditions: Copper Conductors, 250 MCM, 6-phase Winding per Side,
I = 423 Amps per Conductor.

Guideway Block Length	Resistance/ Conductor (Ohm)	Stator I^2 R Loss (kW)					
		Type I	Type II	Type III	Type IV	Type V	Efficiency %
0.5 km	0.083	185	178	181	178	178	97.8
1.0 km	0.166	370	356	363	356	356	95.9
2.0 km	0.332	740*	712	726	712	712	92.1

Conductor diameter = 12.7 mm
Conductor current density = 3.36 A/mm^2
Base Mechanical Output = 8.33 MW
Base Stator Power Dissipation (423 A) = 712 kW (2.0 km block)
Net Power Input = 9.04 MW (2.0 km block)
Basic Efficiency = 92.1% (2.0 km block)

* Higher than base loss due to stray induction into parallel levitation ladder in close proximity to LSM.

Resistance calculated at 20°C condition.

Table 1-6

Weight and Cost of Guideway Transmission Cable
Strands = 19, 7 kV Insulation Type EP, Copper Conductor
Calculated per 1 km Basis

Cost/km	Cable Size (dia.)	Resistance R/km	Reactance X/km *	Impedance Z/km	Weight/km
$10,166	11.7 mm	0.166	0.358	0.422	972 kg
$12,462	12.7 mm	0.141	0.313	0.343	1150 kg

* Ohms at 20 Hz.

Cable O.D. is minimum of 7 mm over indicated inner cable size for 7 kV insulation.

speed of 150 m/s. Each aluminum-conductor null-flux (NF) loop of 30 cm width and 50 cm length has an inductance of 0.98 uH and a resistance (at 20°C) of 104 u-Ohm, and produces a restoring force of 4.2 kN or 210 kN for the entire vehicle. The guidance stiffness is thus 210 kN/5 cm or 4.2×10^6 N/m; this is considered a stiff system. The null-flux principal is applied in Type I and II systems with nearly identical component design and material cost. The Type III concept is modified from earlier patents (Ref. U.S. Patent 3,768,417) to include a dual LSM array and a center-located null-flux guidance ladder, as improvements to enhance performance and better utilize materials.

In the Type II system, using the approach of a guideway underhung LSM stator and dual outriggers attached to each vehicle, lateral guidance is accomplished by electrodynamic repulsive-inductive action against side-wall mounted aluminum strips on the concrete guideway. This is substantially different from conventional null-flux techniques and is effective in being inherently stable but has a higher steady-state dissipation loss due to the continuous repulsion (y-directed) force. A second disadvantage is that the lateral stiffness of the Type II guidance falls off (at 40 km/hr and lower speeds) at a faster rate than the NF center loop system. A major advantage is the inherent simplicity of construction and installation of the repulsive guidance strips.

Both Type IV and Type V systems do not require either null-flux or EDS inductive-repulsive ladder strips due to the continuous use of the LSM stator, which is mounted in a vertical orientation. Lateral vehicle guidance is maintained strictly by β-angle control of the LSM to modulate the horizontal force to the LSM surface. The magnitude of this force is limited to approximately 1.10 kN per unit of the peak propulsion force for a given field MMF and stator MMF. Therefore, the peak available lateral restoring force under invertor-feedback control is 2 X 76 kN = 152 kN for a 600-kAT, 50-magnet- pair excitation. This system does not have a limitation on low- or high-speed guidance fadeout but does require active, high-speed monitoring of vehicle yaw or sway motions to command a change in the invertor β-angle. The LSMs providing lateral guidance are of the same physical construction as the Type I or II, and only minor special provisions (in the master control system) are necessary to use the LSMs for repetitive lateral guidance.

As with all schemes in Type I, III, IV, and V, failure of the LSM field magnet array to produce sufficient flux (due, for example, to a cryostat failure) would result in loss of lateral guidance

performance. The Type II system uses a separate set of miniature, dedicated, guidance SC magnets mounted on the vehicle outrigger inner support leg. The active width of these field magnets are sized at a minimum of 15 cm with a limit of 20 cm width and a field strength of 90 kAT per magnet. Each vehicle would carry 8 guidance magnets per side over a span of 27 m. Table 1-7 summarizes the guidance material weights, and Table 1-8 summarizes the materials cost on guideway. The guidance material generally costs 57% of the LSM stator materials.

The recommended electrodynamic guidance system for all 5 configurations is the NF system based upon superior performance in the following areas:

1. Economics of installation and material acquisition
2. Dynamic lateral stiffness
3. Installed weight
4. Compactness of design
5. Maintenance free operation

The unique feature of NF guidance is that it utilizes the same set of SC magnets in the Maglev 2000 configuration as the main propulsion array, and its stator member is superimposed upon (or under) the LSM stator winding. A key feature is passive lateral guidance without external means for control of the NF loop resistance/inductance beyond the original installed design. In the most basic system, all NF loops are identical in dimension, material, resistivity, and electrical performance, whether for a high-speed or low-speed section. This study specifically advocates the use of a tapered electrical performance (i.e., variable X/R ratio) according to the spatial location of the NF loops with respect to designated station or low-speed sections. This method optimizes output performance and therefore minimizes overall guideway electrical weight. The implication of this design feature, for Types I-V, is an economic compromise: 3 different X/R ratio NF loops according to baseline speed in each section as in Table 1-9. The X/R ratio controls the following performance and electrical

Table 1-7

Cost and Weight for Type I Null-flux Guidance Loops
Mean Length of Turn = 1.542 m, Field MMF = 2 x 600 kAT per Pole
Length/side = 0.471 m Loop Width (mean) = 0.30 m
Conductor Thickness = 11 mm Conductor Width = 25 mm
Total Volume = .000424 cu. m. per Null Flux Loop

Single Guideway Analysis

Individual Loop Weight	Repetitive Layout Pitch	Loops per 1 km Guideway	Weight (kg) per km	Cost of Materials per 1 km
1.14 kg	0.353 m	2832	3228	$ 7,102
1.14 kg	0.157 m	6370 *	7261	$15,974

* Recommended base design for field magnets of pitch 0.51 - 0.59 m.

Table 1-8

Summary of Cost for Electric Materials
for Propulsion, Levitation and Guidance Systems (per kilometer)

Values in U.S. Dollars, 1992 Base
Materials: Aluminum Type 6101-T64 for Bar, Plate for
Levitation and Guidance Components

	Type I	Type II	Type III	Type IV	Type V
Dual LSM Stator (Cu)	162,554	162,554	165,862	162,554	162,554
Dual LSM Stator (Al)	27,120	27,120	28,100	27,120	27,120
Levitation Strip *	69,336	69,366	85,148	69,366	79,754
Null-flux Guidance	15,974	22,000	15,974	0	0
Cost in Copper/Al.	$247,894	$253,920	$266,984	$231,920	$242,308
Cost in All Al.	$112,430	$118,486	$129,222	$96,486	$106,874

Aluminum costed at specific price of $2.20/kg for bar and plate.

Aluminum costed at specific price of $2.40/kg for LSM conductor.

* Dual Ladder Type.

Table 1-9
Null-Flux Loop Selection for Optimum Utilization

	Type A Low Speed	Type B Medium Speed	Type C High Speed
Pole-pitch (m)	0.57	0.57	0.57
Speed Range (km/hr)	0-50	50-150	150-480
Reactance (u-Ohm)	0-11.76	11.76-35.3	35.3-114.7
Frequency of Induced current (Hz)	0-12	12-36	36-117
Inductance (uH)	0.98	0.98	0.98
Resistance (u-Ohm)	28	50	104
X/R Ratio	0-0.235	0.235-0.70	0.339-1.10
Loop Width (cm)	30	30	30
Loop Length (cm)	50	50	50
Vehicle Restoring Force (kN)	210	210	210
Vehicle Mass (kg)	67,605	67,605	67,605

design parameters of the NF system, independent of gross vehicle weight or overall dimensions, on the basis of the specific loading, power density and electrodynamic stiffness. In general, it is advantageous to design for a high X/R ratio on the condition that the peak induced current is high enough to yield the specified 210 kN restoring force. The high X/R ratio has the following advantages:

a. The ratio of peak asymmetrical to symmetrical rms current is maximized by having a NF loop with a high X/R ratio. In iron-cored NF systems, X/R ratios can range from 16:1 up to 22:1. In air-cored, nonferromagnetic systems, ratios of 2:1 are a limit for non-superconducting guideway loop material, independent of the number of turns per loop. The importance of high I_{asym}/I_{sym} ratio is that the transient lateral restoring force is proportional to the square of I_{asym}, whereas the effective heating of guideway conductors is based on the symmetrical and asymmetrical combined total current.

b. The higher the X/R ratio, the higher the inherent efficiency of the NF loop since less power is dissipated in the coil windings as the NF loops become "inductive limited." The NF loop X/R ratio is primarily controlled by the cross-section and specific resistivity chosen for the guideway loops. The basic loop geometry must remain near constant to coordinate with a given LSM design, and the loop inductance thus has only minor variations. The system design goal of maximizing operational efficiency is most prominent at the high-speed range, consequently establishing the design guideline of making the Type C NF loop have the highest X/R ratio. The Type A is a compromise, since its operational time is the lowest of the group.

c. A high X/R ratio produces the least sensitive variation in lateral stiffness and damping ratio to temperature changes from either ambient conditions or effects of multiple vehicle operation over a short headway period such as 45-250 seconds.

d. The high X/R ratio NF loop, when coupled electromagnetically to the vehicle field magnets, produces a lower stress on the superconducting cables for a given restoring force or stiffness coefficient. The SC vehicle magnets when receiving an AC induced counter-emf are most sensitive to the phase angle of the guideway inducted current. By maintaining a high phase angle (such as 47 degrees or higher), the interconductor forces on the SC magnet are minimized.

The specification of a Type C X/R ratio with a range of 0.339-1.10 for the highest speed sections over the intended speed range (150-480 km/hr) follows a Type B with a 0.235-0.70 X/R ratio. The fact that the X/R ratios are not spatially continuous or exactly tapered with 3 different sets does not affect the smoothness of ride since the NF loops are not in continuous use but limited to the instances of transient lateral oscillation. It is true, however, that with a limitation of 3 standard types, the NF loop performance at, for example, 140 km/hr immediately prior to a transfer to a Type C loop at the 150 km/hr zone, would be superior by the difference in ratios of 0.70:1 compared with 0.339:1. As the number of NF loop types would be potentially increased beyond 3, this effect obviously diminishes.

The mechanisms available to all 5 guideway types for NF loop control of loop resistance is by two methods:

1. Increase in guideway conductor cross-section for Type A and Type B loops to decrease resistance to 28 u-Ohm and 50 u-Ohm, respectively.
2. Change of loop material at constant cross-section according to the following schedule:

Type A	Copper	OFHC (98% conductivity)
Type B	Aluminum	6101-T (64% conductivity)
Type C	Aluminum	6061-T6 (47% conductivity)
or	Aluminum	7075

All 5 guideway types require that the NF loops be as flat as possible. The Maglev 2000 design has produced rectangular strap conductor configurations for all NF loops as an improvement over earlier circular cross-section electrical cable. The design constraint is that the internal eddy current losses in the strap conductor do not exceed those of a conventional 19- or 37-strand circular cable. The baseline design recommends that the stray eddy current losses be calculated and evaluated at a vehicle lateral displacement of 5 cm and a peak magnetic field of $\beta = 1.6$ T at the NF loop upper surface. A figure of merit for the presented design is 5.93 kW/loop for the Type C loop at 133 m/s speed which yields a specific loss of 10.4 kW per meter of guideway axial length for the basic (non-strap) resistance characteristic. Consequently, it is recommended that the stray conductor dissipation due to stranding quality be in the range of 0.30-0.59 kW/loop, as a 5-10% criterion.

1.4 Levitation System Design

The reference levitation magnet is summarized in Tables 1-10a and 1-10b for 67 ton and 36 ton vehicles, respectively. The baseline vehicle weights are 26, 36, and 67 metric tons for 76, 118, and 200 passenger vehicles, respectively, with a nominal overall width of 3.55 - 3.65 m. The heavy vehicle (freight/passenger mix) limit is 50 tons with the described design. The levitation system includes a total of five superconducting magnets (seven for redundancy) per side of the vehicle, each magnet is 1.50 m long and 0.48 m wide. The minimum value MMF of each magnet is in the range of 320,000-385,000 ampere turns depending mainly upon cornering characteristics at high speed. The field conductor is a conventional, multifilament, NbTi superconductor, in a 5.7:1 copper:superconductor matrix. The levitation ladder strips on either side of the guideway are 60 cm wide. For high speed, the levitation ladder strips have to be optimized at approximately 1.7-1.9 cm thick, whereas, at low speed, they may be thicker (approximately 2.3-2.5 cm). The levitation "lift-off" speed in the Type I system ranges from 48 km/hr to 50 km/hr. With this type of system and using type 6101-T64 aluminum, the mass of guideway aluminum dedicated to a levitation system is 31.5-38.7 tons/km of single guideway. We have assumed the worst case conditions at 500 km/hr and that the main suspension height may be as large as 22 cm from the plane of the guideway aluminum to the plane of the superconducting magnets, leaving a track clearance of 10 to 12 cm. The baseline suspension stiffness is 3 x 10^6 N/m, with a natural frequency of approximately 2 Hz; the magnetic drag in such a system at high speed has a range of 12-15 kN.

Overall dimensions for the 5 referenced guideway's levitation conductors were fixed for incorporation in overall guideway mechanical dimensioning. Table 1-11 summarizes the weight calculation for the recommended base designs. A ladder levitation strip with a skewed cross member was chosen for all 5 designs over a solid strip levitation conductor. Figure 1-2 shows cross-section and plan views. The electromagnetic calculations show a reduced electromagnetic drag at high-speed conditions (400-500 km/hr), with a skewed ladder versus simpler

Table 1-10a

Characteristics of Reference Levitation Magnet for Vehicle with Limit of 7 Magnets per Side 67 Ton Vehicle

Maximum Lift Force/magnet	12.4 Tons
Mean Width	0.48 m
Mean Length	1.50 m
Nominal Levitation Height	21 - 22 cm
Amp-turns MMF	320 kAT - 385 kAT
Maximum Design Speed	150 m/s
Magnetic Moment/Coil	230,400 - 277,200 A.T.-m^2
Number of Turns	1000
Current	320 - 385 A
Conductor Active Cross-section	38 x 48 mm
Superconductor Type	Nb-Ti
Operating Temperature	4.2°k
Coil Self - Inductance	2.5517 Henries
Coil Stored Energy @ 385 A	189 KJ
Separation Mean Coil Height to Bottom of Cryostat	70 mm
Vehicle Undercarriage Aluminum Thickness*	9 mm
Thermal Insulation Distance Between Skin and Cryostat	11 mm
Total Separation Mean Conductor to Undercarriage Surface	90 mm
Estimated Electromagnetic drag/vehicle (gap dependent)	12 - 15 kN
Lift Redundancy Factor	2.59:1

* For damper shield and mechanical structure

Table 1-10b

Baseline Suspension Magnet Specifications for 36 metric ton vehicle

Nominal lift/magnet	14 metric tons
Maximum Lift Capability/vehicle	112 metric tons
Magnet Length, l_m	1.50 m
Magnet Width	0.30 m
Suspension Height	0.21 m
Track Loop Width	0.30 m
Track Loop Pitch	1.0 m
MMF -maximum (minimum)	500 kAT (320 kAT)
Magnet Current	100 Amps
"Lift-off" Speed	14 m/s
Total Lift Magnets/Vehicle	8
Lift Redundancy Factor	3.11:1

Table 1-11

Guideway Electrical Weight Calculation for Ladder-type EDS Levitation Conductors for Aluminum Guideway Configurations

Condition: Rung Pitch = 51 cm

Guideway Type	Width Overall	Rungs in 1 km	Rung Length	Rung Weight	Side-bar Weight	Total Alum. Weight (kg/km)
I	60	1960	51.7	2.88	10,120	15,765 x 2
II	60	1960	51.7	2.88	10,120	15,765 x 2
III	80	1960	93.3	4.71	10,120	19,352 x 2
IV	60	1960	51.7	2.88	10,120	15,765 x 2
V	68	1960	80.8	4.08	10,120	18,126 x 2

All weights in kg; dimensions in cm unless otherwise stated.

arrangements and, consequently, a higher L/D ratio. The ladder yields the highest lift force per ton of conductor material for the range of design considered. A rung pitch of 51cm and a 15° skew angle were chosen. The optimum material chosen was high-conductivity "busbar" aluminum ASTM Type 6101-T64, which has 64% of the conductivity of IACS copper. Standard aluminum Type 6061-T6, the most common in general use in the U.S., has a lower conductivity of 47% of IACS and is not preferred. Further, the chosen Type 6101-T64 has an ideal layout composition with no copper content and a superior resistance to weathering and pitting in comparison with lower grade aluminum. Copper was not considered for the levitation ladder due to its high capital cost.

The base design has two parallel conductor rails, 10 cm wide by 1.9 cm thick and cut in maximum section lengths of 12.2 m. The 2 base conductors per side of guideway together have a cross section of 38 cm^2. With a specific density of 2664 kg/m_3, the two main side rails weigh 10.1 kg/m of guideway length. The transverse separation between outer rail dimensions varies from 60 cm in the Type I, II, and IV designs to 800 cm in the Type III design. The smallest inner dimension is 40 cm and is spanned by a welded, skewed, cross-member (rung), also of Type 6101-T64 aluminum and 1.9 cm long by 10 cm wide. The rungs are of the length shown in Table 1-11, according to guideway type. The semicircular Type III has the longest span for rungs due to the larger-than-average transverse (roll) motion allowable on both straight and curved guideways. The conductor weight per side for the levitation ladder is between 15.7 tons/km and 19.3 tons/km exclusive of the grouting fill material and securing bolts. If a solid aluminum flat-strip were used instead, the specific weight would be considerably higher at 30.3 tons/km for Types I, II, and IV; 34.3 tons/km for Type V; and 40.4 tons/km for Type III per side. The levitation ladder thus provides a savings of 29.2 tons/km to 42.1 tons/km for Type III, for two ladders/guideway. The conclusion of the electromagnetic field study is that it is <u>not</u> sufficient to simply reduce the thickness of the simpler flat-strip levitation strip to attain the equivalent per-unit mass as the ladder unit. The ladder configuration has a specific inductance:resistance (L/R) ratio which controls the electromagnetic drag, and this L/R ratio cannot be readily duplicated with the solid strip. The guideway rung pitch is dependent upon the choice of the vehicle levitation magnet longitudinal dimension and is chosen to be a maximum of 52% of the recommended superconducting coil axial length. In conclusion, the

Maglev 2000 team has chosen a robust fabricated aluminum ladder with the rung cross-member welded underneath the side bars in a prefabricated supply unit. The overlap of the rung under the side bar is 5 cm per side with a total weld track of 20 cm.

The calculated peak induced current per rung or side-bar is 290,000 A at a 134 m/s linear speed. The projected side-bar current density is consequently about $J=15{,}260\ A/cm^2$ cm. for a thermal period of t=3.8 ms. The expected temperature rise, ΔT, due to one vehicle passing is insignificant and calculated as:

$$\Delta T = \frac{J^2 t}{2} \text{ for J in } kA/cm^2$$

$$\Delta T = \frac{(15.26)^2\,(.0038)}{1.45} = 0.61°K$$

The maximum number of levitation magnets per side of a vehicle is to be seven and the total temperature rise per 50-ton vehicle passing at 134 m/s is 4.3°K. For the baseline 26-ton vehicle, a minimum of 4 SC magnets per vehicle side are required, and for the 36-ton vehicle, 5 magnets per side are required.

In 1992 dollars, the cost of Aluminum 6101-T64 is $2.20/kg which indicates a raw material cost of $69,366/km for dual Type I, II, or IV levitation ladder configurations. The Type III costs $85,150/km for raw materials, primarily aluminum and fiberglass-reinforced plastic (FRP).

The width of the levitation ladder is based on optimizing the following parameters:

1. Ratio of ladder overall width to mean width of vehicle SC levitation magnet.
2. Nominal levitation height. The greater the levitation height, the greater is the optimum ladder overall width. The above calculations are based on a 19-23 cm electromagnetic levitation height, and a 10 cm mechanical clearance gap.

3. The ladder reflected L/R time constant. The phase angle of the induced current with respect to the induced voltage should be in the range of 60-70° to yield a low magnetic drag and highest lift.

Figure 1-2 shows the layout of the guideway electrical conductors for a LSM, NF guidance loops and levitation ladder strips. The range of levitation magnet MMF per coil is 320-385 kAT with an isometric view of a levitation cryostat shown in Figure 1-32. It is essential to hold the levitation magnet pitch at about 3 times the rung pitch to minimize the space harmonic of the suspension forces. Thus, if the magnet length can be sized to 1.5 m long with a rung pitch of 51 cm, the pulsations of the EDS levitation force can be held to 1% of the average force. The L/D ratio of the design configuration is 26:1 to 38:1 when calculated at the upper speed of 150 m/s. The vehicle installation pole pitch of the lift magnets should be held to 2.04 m, representing a chording ratio of 0.735:1.

1.4.1 Design Constraints on Ladder Levitation Systems

The baseline guideway design specifically recommends a ladder configuration versus a solid, flat levitation strip as the preferred hardware choice, based upon the following features inherent to EDS ladder systems:

a. High lift/drag ratio at operation speeds
b. Optimization of guideway conducting material
c. Lowest guideway conductor weight
d. Concentration of guideway induced current path
e. Most adaptable to high-speed all-electric switch and high-speed banked curves

This section gives the fundamental design equations for the EDS constant-flux mode suspension systems and derives the following parametric design data for the Maglev 2000 vehicle which is used as the basis for the hardware selection.

a. Lift force versus transverse vehicle displacement
b. Lift to drag ratio versus suspension height
c. Drag force versus suspension height
d. Lift force versus suspension height

e. L/D ratio versus guideway width and magnet width

f. Drag forces versus guideway width and magnet width

g. Lift and drag force versus angular frequency

h. Levitation force versus speed.

The expression for the induced voltage in the m^{th} track loop when under constant-flux excitation is given by:

$$e_m(x) = -v_x \frac{d}{dx} \left[(I_f + \frac{1}{L_{ff}} \Sigma M_{jf} i_j) \times M_{mf} \right]$$

where I_f = initial vehicle magnet amp-turns (e.g. 385 kAT)

L_{ff} = self-inductance of one vehicle superconducting magnet

M_{jf} = mutual inductance between one vehicle magnet and track loop "j"

i_j = current in the "j^{th}" track loop

M_{mf} = mutual inductance between one vehicle magnet and track loop "m".

The induced ladder currents are expressed by the form:

$$\overset{o}{i}(x) = A(x)\, i(x) + B(x) e_m(x)$$

$$A_{(x)} = -\left[L - M(x)M^T(x)\right]^{-1}\left[R - \overset{o}{M}(x)\, M^T(x) - M(x)\, \overset{o}{M^T}(x)\right]$$

$$B(x) = \left[L - M_{(x)}\, M^T(x)\right]$$

where x is the dimension in the forward direction of vehicle motion.
Appendix A, Section 1 gives the explicit values for e_m and M matrices. A(x) is <u>not</u> periodic in the constant-flux mode.

This section presents the results of a numerical integration of guideway loop currents in a three-dimensional model which considers actual resistance and inductance of each track loop and thus calculates the exact lift and drag forces on the system. By contrast, earlier work done for the FRA by the National Laboratories neglected the exact effects of track loop resistance, thereby overestimating the net amount of lift and underestimating the electromagnetic drag. The entire system is air-core, nonferromagnetic in all respects; therefore, finite-element magnetic analysis codes are superseded by the coupled inductance formulas derived by Grover (Ref. 1-2).

One basis for evaluation is the weight of aluminum conductor per meter-length of guideway. The baseline value is 2 x 70 kg or 140 kg/m per guideway direction, which may be compared with solid levitation strips 1.0 cm thick x 82 cm wide. The electrodynamic design has to select the fundamental time constant (T) of the guideway ladder loop circuit to be able to optimize performance. The Maglev 2000 system design herein optimizes at a 150 m/s vehicle speed (540 km/hr). The Q factor of the system is defined as:

$$Q = vT = vL/R$$

where v = vehicle speed (m/s) and T = track loop time constant (L/R).

The rate of change of track current is proportional to the frequency ω of the induced current and velocity

$$\frac{di}{dt} \quad \alpha\omega = \frac{\pi v}{p}$$

where p = magnet pole-pitch (m).

The fundamental loop equation is:

$$\left[\frac{\pi L}{p} \left(\frac{v}{R} \right) + 1 \right] i = - \frac{v}{R} I_f \frac{d (L_f)}{dx}$$

indicating that performance remains constant if the ratio (v/R) remains fixed. The electromagnetic drag on a single loop (distinct from a ladder array) is given by:

$$F_D = \frac{W \Phi^2 R}{R^2 + (vL)^2}$$

where Φ is the flux linkages to the track loop.

The lift force is:

$$F_L = k I \Phi \text{ in Newtons}$$

where k is the coupling constant. If the following values are substituted:

L = 1.258 H

R = 2.01×10^{-5} ohms

T = 0.0625 sec.

and the flux linkages are taken as 5 x 10^{-4} Wbs, the lift and drag are calculated as in Figure 1-10 based on 50 vehicle magnets. The design parameters are given in Table 1-12 for the levitation vehicle magnet.

The constant-flux mode implies that the SC magnet current will fluctuate with a +/- 2% variation for the dimensions given. The ratio L/R or time constant is approximately proportional to the mass of guideway conducting material. The heavier the levitation ladder, the longer the time constant, for a given type of material.

A potentially undesirable feature of ladder guideways is the fluctuation in vertical force due to discrete loops. The ratio of magnet length to guideway rung-pitch controls this. Table 1-13 indicates the lift, L/D, and per-unit fluctuation in lift for a baseline ladder system with Q=10 at 150 m/s for variations in ratio of SC magnet length versus rung pitch. The fluctuations diminish as ladder rungs per magnet increase; there is a second minimum when the vehicle magnet length to rung pitch ratio is 1.50:1. Further, the recommendation of a multiple magnet array per side reduces the lift force pulsation well beyond single magnet arrays. In general, the per unit lift fluctuation has a minor dependence on the Q factor.

Figure 1-11 shows force versus distance along a rung pitch for values of l_m/l_t = 1,1.5, and 2.0 (the ratio of vehicle magnet length to track loop pitch). The middle case, l_m/l_t=1/5, produces the highest normalized lift force, whereas the l_m/l_t = 1.0 case produces the lowest lift force and should be avoided. The effect of varying magnet aspect ratio for l_m/l_t = 1.50 with equal W_m and W_t is shown in Table 1-14. The aspect ratio is defined as SC magnet length/SC magnet width.

Figures 1-12 to 1-14 show plots of the variation of lift force, drag force, and lift-to-drag ratio, respectively, as a function of guideway width with the magnet width as a parameter. Both lift and drag curves have well-defined maxima which occur at different values of track width. The maxima in the lift curves always occur for a magnet width to track loop width ratio close to 1.0. This is the reason for choosing the ratio as 1.0 in a number of previous examples. As

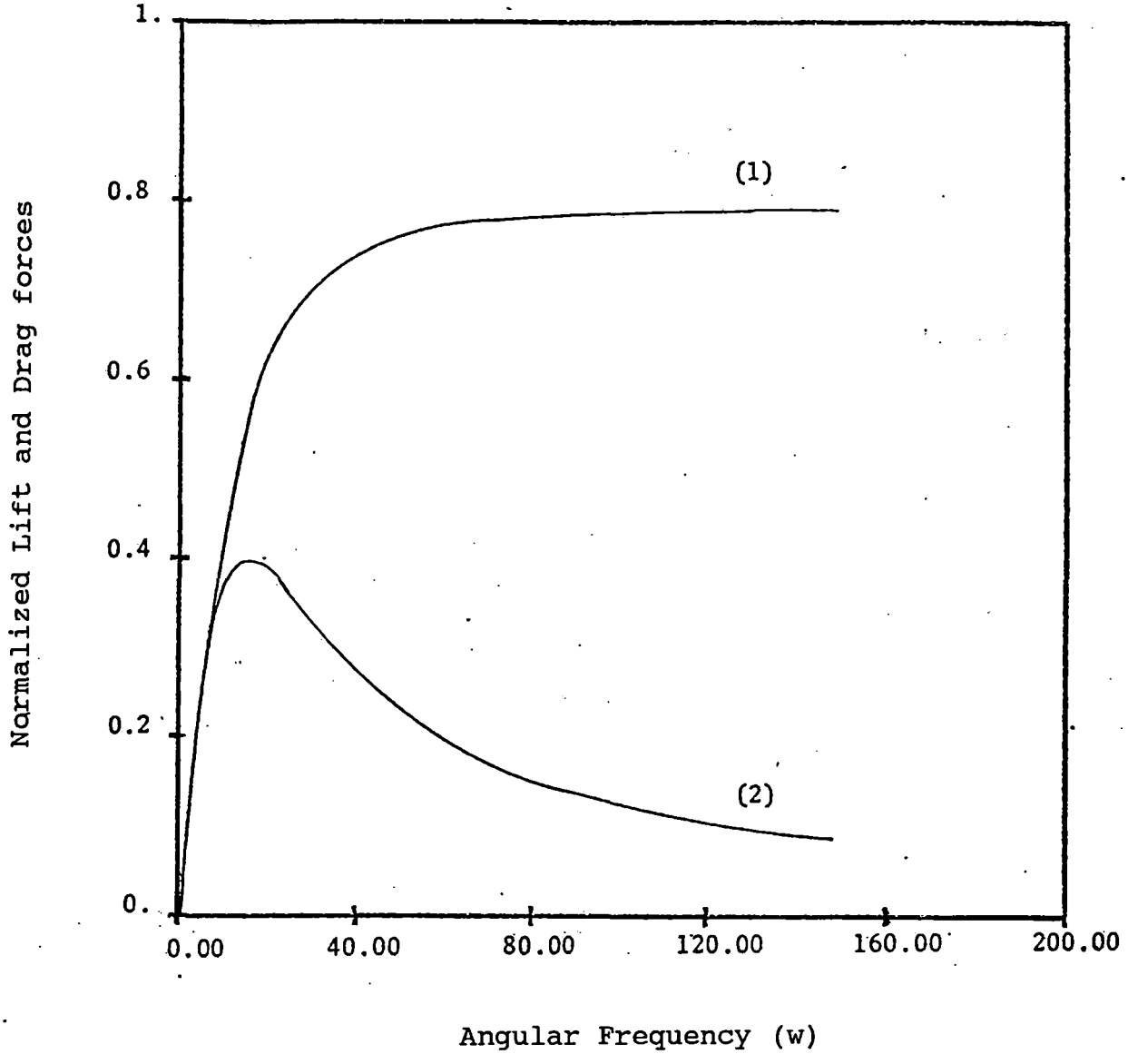

Figure 1-10 Lift and drag force versus angular frequency

ℓ_t = 1.0m, ℓ_t = 0.3m, ω_m = 0.3m

Curve (1) ℓ_m/ℓ_t = 1

(2) ℓ_m/ℓ_t = 1.5

(3) ℓ_m/ℓ_t = 2

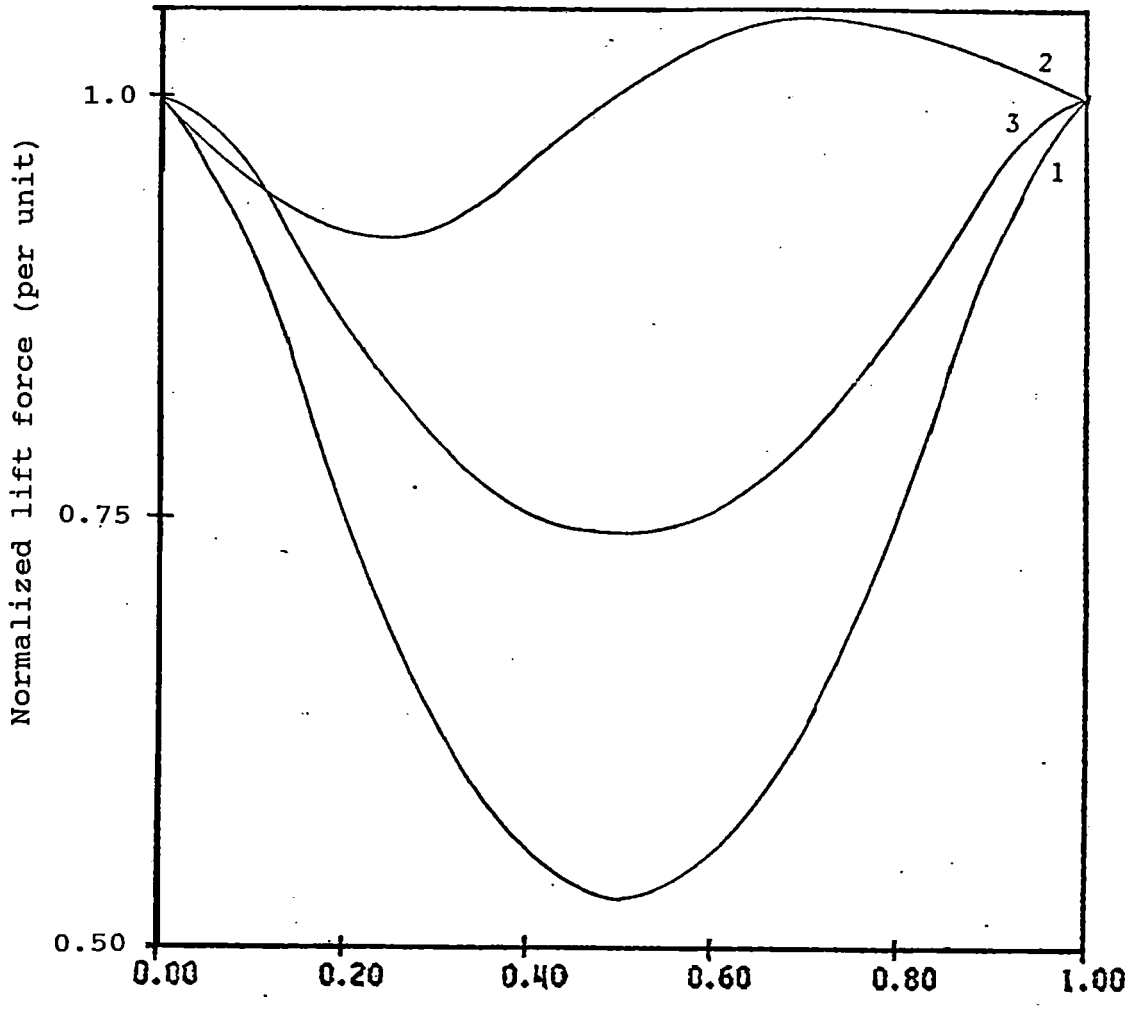

Figure 1-11 Fluctuation in lift force over a rung pitch for three different values of ℓ_m/ℓ_t

Lift Force Versus Guideway Width for Various Magnet Widths at 150 m/s Speed

ℓ_m = 1.5m, ℓ_t = 1.0 m, h = 0.22 m

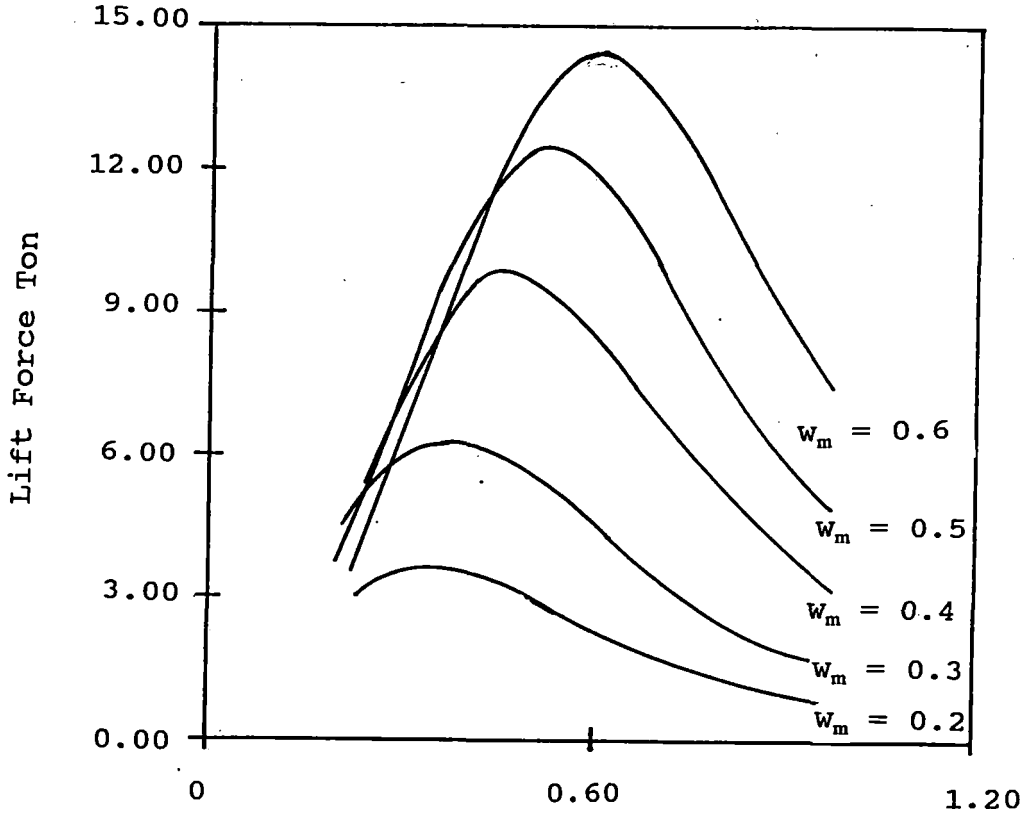

Figure 1-12

Drag Force Versus Guideway Width for Various Magnet Widths

ℓ_m = 1.5m, ℓ_t = 1.0 m, h = 0.22 m

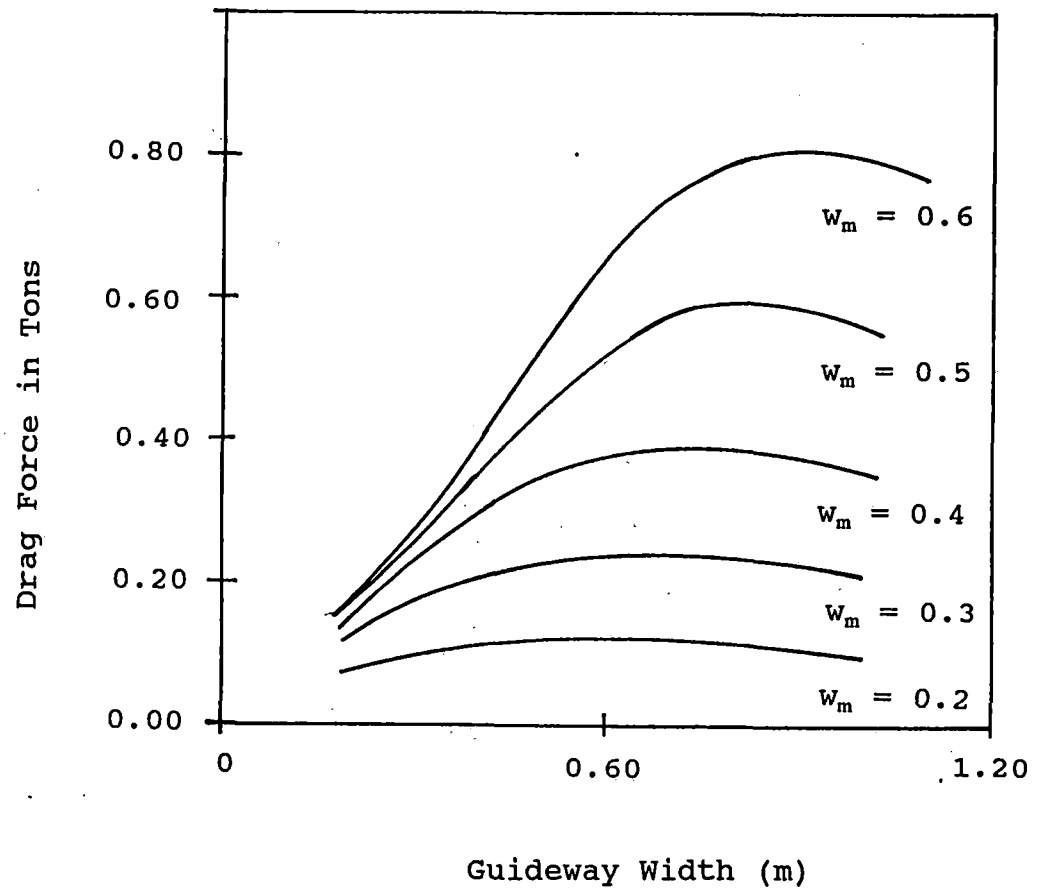

Figure 1-13

Parameters

ℓ_m = 1.5m

ℓ_t = 1.0m h = 0.22m

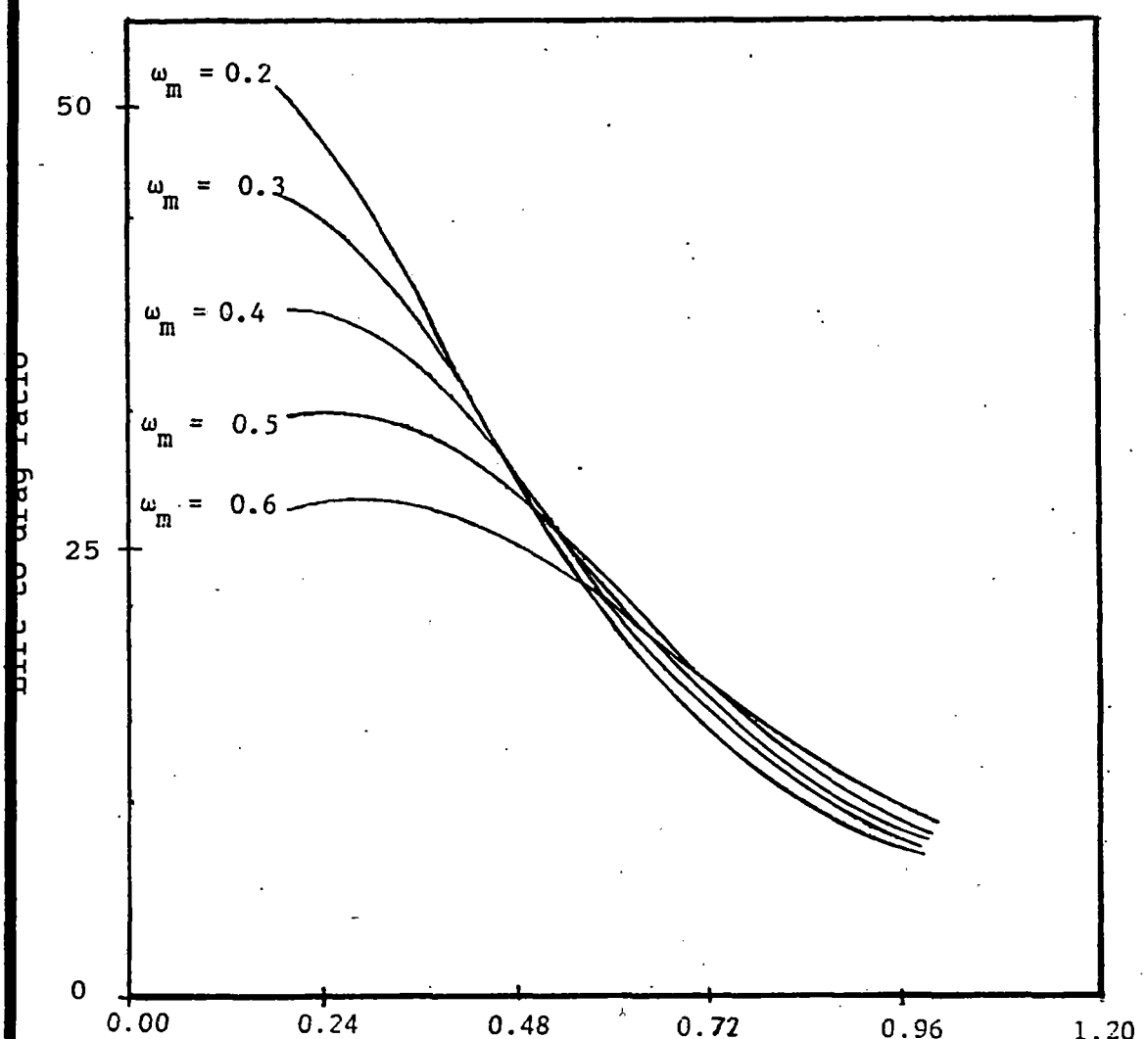

Figure 1-14 Lift to drag ration versus guideway width for different vehicle magnet transverse widths at 150 m/s velocity.

Table 1-12

Design Parameters for Levitation Vehicle Magnet for 36 metric ton vehicle

Nominal lift/magnet	14 metric tons
Maximum Lift Capability/vehicle	112 metric tons
Magnet Length, l_m	1.50 m
Magnet Width	0.30 m
Suspension Height	0.21 m
Track Loop Width	0.30 m
Track Loop Pitch	1.0 m
MMF -maximum (minimum)	500 kAT (320 kAT)
Magnet Current	100 Amps
"Lift-off" Speed	14 m/s
Total Lift Magnets/Vehicle	8
Lift Redundancy Factor	3.11:1

Table 1-13

Effect of varying lift magnet length (l_m) to track rung pitch (l_t) ratio and effect on lift force fluctuations and Q factor

l_m = 1.5 m, W_m = 0.3 m, W_t = 0.3 m, v = 150 ms^{-1}, h = 0.22 m

l_m/l_t	F_L Tons	Lift to Drag Ratio F_L/F_D	Fluctuations in F_L as percentage of average	Q
6	9.3	10.2	4	5.8
3	7.9	16.9	5.5	7.8
2	6.57	29	11.5	8.8
1.5	6.198	42	6	9.39
1.25	5.25	38	14	9.72
1	4.78	51.92	26	10.06
0.833	4.193	130	31	10.3
0.75	3.87	86	29	10.4

was observed in the results shown in Table 1-14, increasing the track and magnet widths (i.e., decreasing the aspect ratio of both) increases lift but at the expense of lift-to-drag ratio. Once again, the best system depends on both the lift required and the acceptable lift to drag ratio.

Table 1-15 shows magnitude and location of peak lift and drag forces for a 1.50-m-long lift magnets and 320 kAT excitation for different magnet widths. The L/D ratio of 26.1 is used as the baseline case with a 0.40 m lift magnet width.

1.5 Summary of Guideway Electrodynamics Design

Table 1-16 describes the total guideway electrical conductor weight for combined propulsion, levitation, and guidance systems in all 5 guideway configurations. Both copper LSM stator and aluminum LSM stator options are shown. The lightest weight systems are the Type IV and V due to the absence of the NF guidance materials. However, these systems have a much heavier concrete structure which more than offsets the reduction in conductor weight. Types I and II are both moderately light at 50,091 - 50,830 kg/km for conductors and retain efficient lightweight concrete structures. The heaviest conductor for a guideway was the Type III at 57,665 kg/km for the semicircular guideway with dual LSM propulsion. The corresponding Cost of Materials Analysis for all 5 types is given in Table 1-10. Type IV and V have the lowest electrical materials cost at $96,000 - $107,000 per km per guideway. Type I and II are in the $112,000 - $118,000/km range and Type III is $129,000/km, assuming a 100% aluminum conductor and strip. The cost of site installation of guideway electrical components is detailed in Section 4. The LSM stator winding is modular in all designs and installed in replaceable troughs along each span. Modularity of design and installation remain key feature of the described electrodynamic systems. Table 1-17 shows the combined cost of materials and fabrication labor for the principal components of the LSM at $302,000/km per single guideway direction. Table 1-18 shows the combined cost of fabrication, labor and materials for the LSM stator, NF guidance, and levitation ladder strips at $504,594/km per guideway direction, whereby the LSM represents 60% of the guideway electrical cost excluding substation frequency converter apparatus.

Table 1-14

Effect on Varying Levitation Magnet Aspect Ratio on Lift Fluctuations

l_m = 1.5 m, l_t = 1.0 m, v = 150 m/s

h = 0.22 m, $\omega_t = \omega_m$

Aspect Ratio Magnet	Ladder Loop	F_D (tons)	F_L in tons	Fluctuation as percent of average value	F_L/F_D	Q = vL/R
7.5	5	0.055	2.79	6	50	8.475
5.0	3.3	0.147	6.198	6.5	42	9.39
3.75	2.5	0.279	9.47	7	34	9.83
3	2.0	0.447	12.27	7.75	27	10.02
2.5	1.67	0.649	14.63	8	22	10.09
2.14	1.43	0.885	16.62	9	18.8	10.07
1.875	1.25	1.156	18.31	10	15.8	10.0
1.67	1.1	1.46	19.76	11	13.5	9.9
1.5	1	1.8	21.00	12	11.65	9.77

Table 1-15

Magnitude and Location of Peak Lift and Drag Forces for 1.5 m. Long Lift Magnet at 22 cm. Height

Upper Speed Case V - 150 m/s
Values per Magnet, MMF - 320 kAT

Magnet Width	Maximum Lift Force (Tons)	Guideway Width (m)	Maximum Drag Force (Tons)	At Guideway Width (m)	L/D Ratio
0.2 m	3.63	0.35	0.11	0.51	33.0
0.3	6.31	0.39	0.24	0.70	26.3
0.4	9.90	0.46	0.38	0.72	26.1
0.5	12.40	0.51	0.59	0.75	21.0
0.6	14.50	0.60	0.82	0.88	17.7

Table 1-16

Summary of Total Guideway Electrical Conductors Weight for Combined Propulsion, Levitation and Null-flux Guidance with Aluminum and Aluminum/Copper Conductor Options Conductor Weight in kg per km of Guideway

	Type I	Type II	Type III	Type IV	Type V
LSM Stator (Cu) LSM Stator (Al)	19,307 11,300	19,307 11,300	19,700 11,700	19,307 11,300	19,307 11,300
Levitation Strips	31,530	31,530	38,704	31,530	36,252
Null-flux Guidance ED Repulsion Guidance	7,261	N/A** 8,000	7,261	N/A *	N/A *
Total Weight (Al/Cu) Total Weight (Al only)	58,100 50,091	58,837 50,830	65,665 57,665	50,837 42,830	55,559 47,552

Type I = Flat-top guideway, all systems on top surface.
Type II = Flat-top guideway with LSMs mounted underneath structure.
Type III = Semicircular trough with dual LSM.
Type IV = Inverted T (Japan Railways style) with vertical dual LSM.
Type V = U-channel with separated dual LSMs, vertical.

* Incorporates LSM β-angle control for repulsive transverse guidance force.
** Uses side-wall mounted induction-repulsion transverse guidance.

N/A = Not applicable

Table 1-17

LSM Propulsion Components on Guideway
Total Cost of Materials and Fabrication/Side/Km
Applicable to all System Types

Materials	
a. Al conductor	27,120
b. Fiberglass/G-10 supports/FRP (2600)	10,400
c. Epoxy Impregnation Resin	70,000
d. Stator Fiberglass Tray	31,000
e. Inter-pod interconnects -12	60,000
Labor Cost for LSM Fabrication **	103,480
Total	$302,000

* Tray module size set at 10 m length (100 modules/km)

** Based on $12/hr cost of labor, 86.2 man-hours/module

Table 1-18

Total Cost of Electrical Materials and Labor per km of Single-Direction Guideway in 1992 dollars, Type I, II, III

LSM Stator	$302,000
Null-flux Guidance	73,374
Levitation Ladder	129,220
Total:	$504,594

1.6 Effect of Suspension Height at Cruising Speed

The height of the vehicle magnet array above the track is a dynamic parameter similar to velocity. Under normal running conditions, the lift force on the vehicle would be constrained to balance the weight of the vehicle, the vehicle height is the parameter that changes as the speed changes, assuming constant current in the magnet coils.

Figures 1-15 to 1-17 show the curves of lift force, drag force and the L/D ratio as a function of vehicle suspension height for a 1.5 m by 0.3 m magnet above a levitation ladder having a 1.0 m by 0.3 m loop size. Both the lift and drag forces decrease as the height of the magnet increases but the lift decreases faster causing the L/D ratio to deteriorate with increasing height.

In the field computations, the height of the magnets above the track was taken as the vertical distance between the plane passing through the center of the magnet and through the center of the ladder loops. In practice, the thickness of the ladder loop conductors becomes a parameter that cannot be ignored, since it will decrease the effective ground clearance of the vehicle. It may be necessary to add the radius (for conductors of circular cross-section) or half the height of the ladder loop conductor (for rectangular cross-sections) to the intended height of the magnet to allow for the conductor thickness.

Parameters

ℓ_m = 1.5m, ω_m = 0.3m

ℓ_t = 1.0m, ω_t = 0.3m

v = 150 ms^{-1}, Q = 9.39

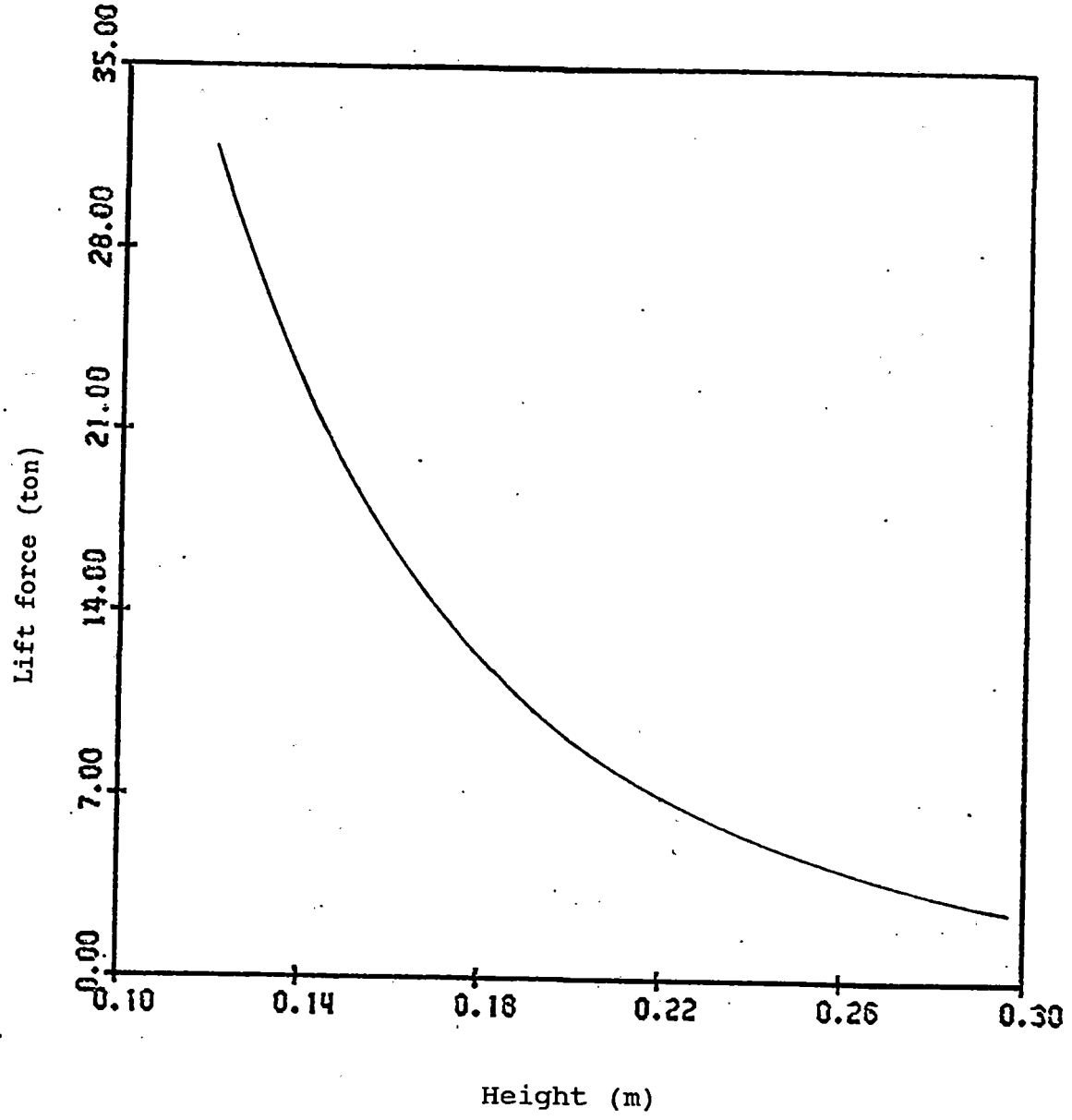

Figure 1-15 Lift force versus suspension height

Parameters

ℓ_m = 1.5m, ω_m = 0.3m

ℓ_t = 1.5m, ω_t = 0.3m

v = 150 m/s, Q = 9.39

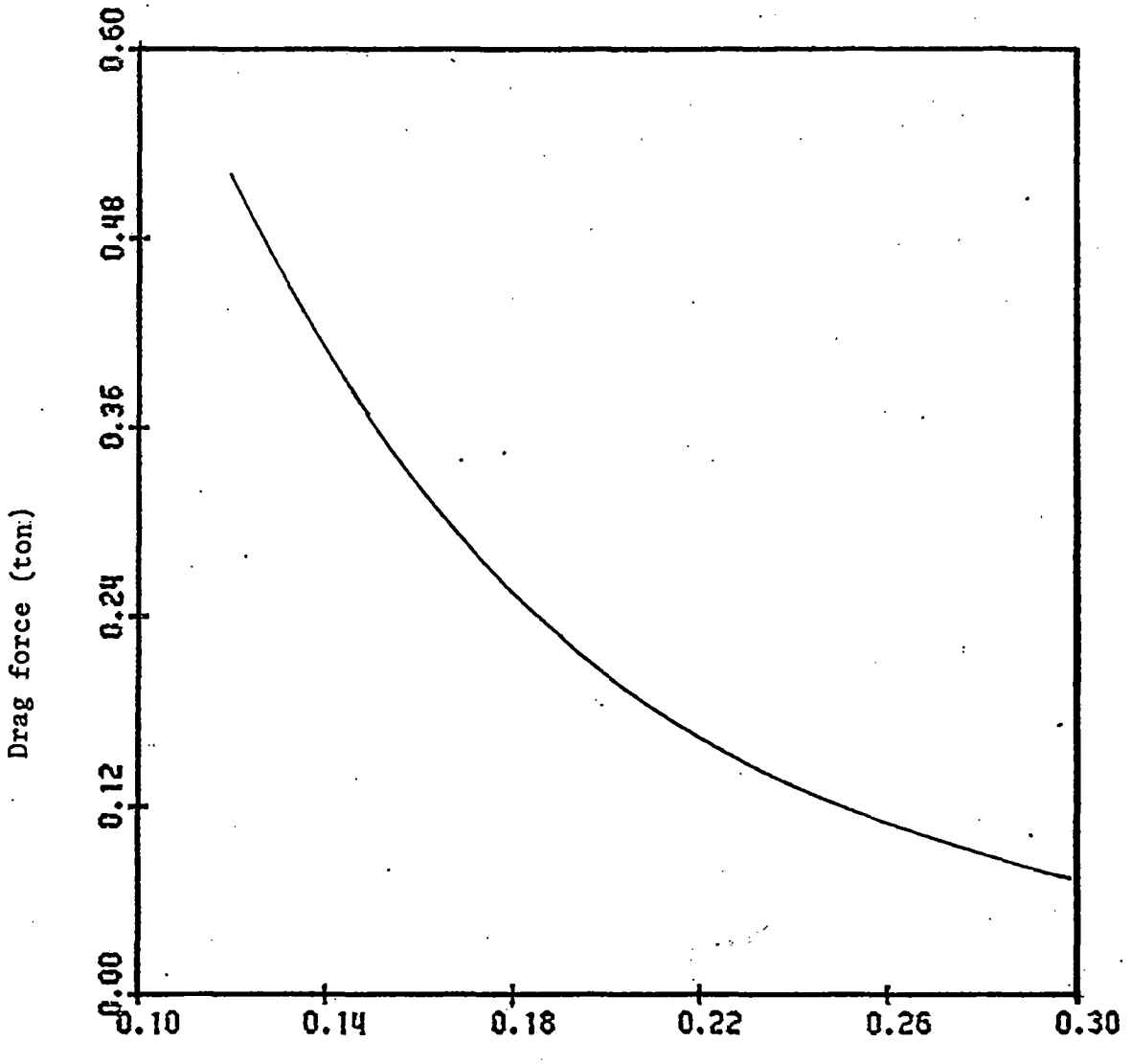

Figure 1-16 Drag force versus suspension height

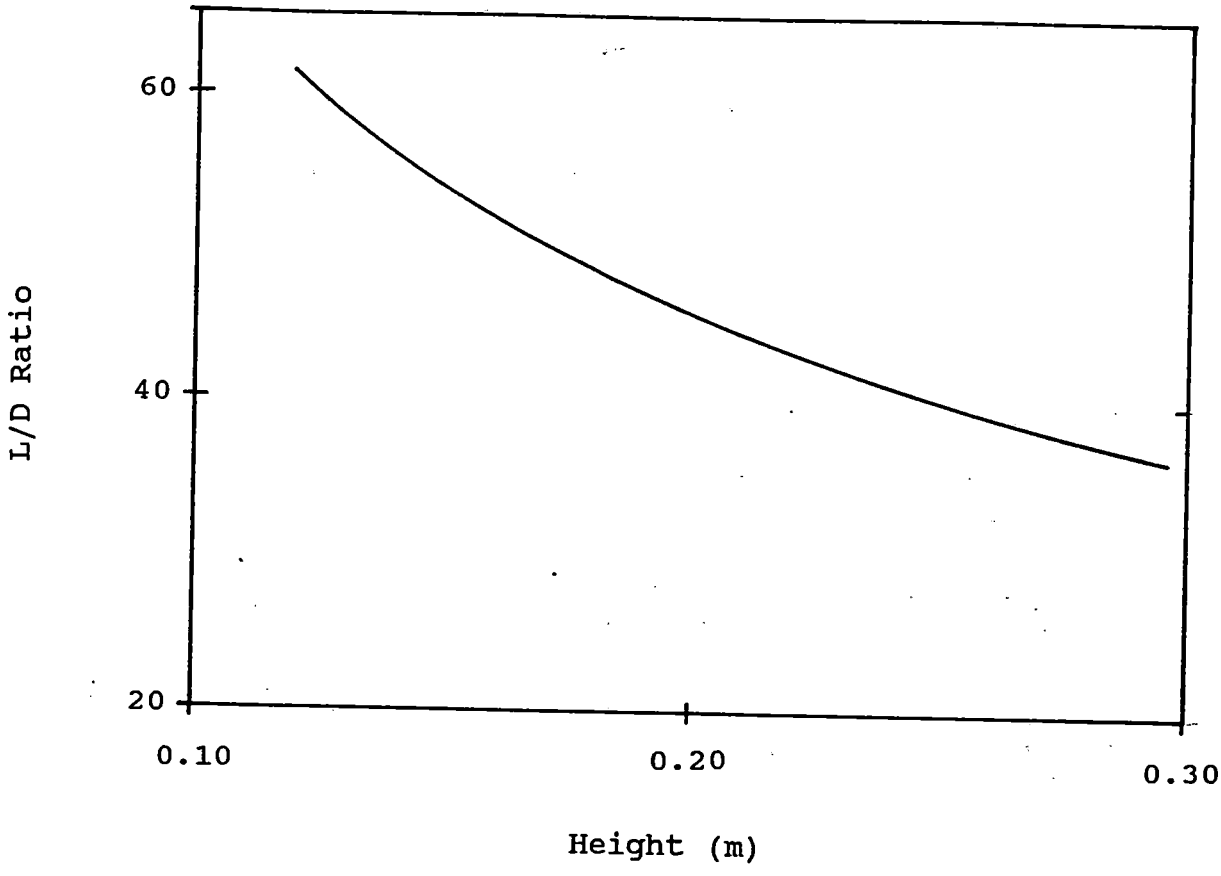

Figure 1-17 Lift to drag ratio versus suspension height

1.7 Effect on Forces of Lateral Displacement

Existing work on levitation ladders has assumed that the magnet is centrally placed above the track and hence the calculation for the transverse component of force has been neglected. This component vanishes only for the special case when the magnet is balanced symmetrically over the ladder track center-line. The lateral component of force exists whenever there is a lateral displacement of the vehicle magnet array from the guideway center-line and is always destabilizing.

Figure 1-18 shows the variation in the transverse force with lateral displacement for 4 different values of the ratio track width to magnet width (W_t/W_m). The magnet length and width were kept constant at 1.5 m and 0.3 m, respectively, and the track loop length was constant at 1.0 m. The 2 important properties of these curves are the initial slopes and the peak values; it is desirable to have both of these small. As may be seen, the performance is worst for the 2 smaller ratios (1 and 1.33) and better for the 2 larger ratios (1.67 and 2).

Figure 1-19 shows the variation of lift force with lateral displacement for the same 4 values of W_t/W_m. As would be expected, the lift force in all cases falls off steadily with displacement but much less sharply for the widest track ($W_t/W_m = 2$). In comparing Figures 1-18 and 1-19, the magnitude of the lateral force destabilizing problems becomes evident. For the worst case ($W_t/W_m = 1.33$) at a lateral displacement of 10 cm, the lateral destabilizing force is about 70% of the lift force. For the widest track, the lateral force at 10 cm displacement is 38% of the lift force, still large but a considerable improvement over the worst case.

Figures 1-20 to 1-22 show the transverse force, lift force, and drag force as functions of lateral displacement with suspension height as a parameter for the special case of a 1.5 m by 0.3 m magnet and 1.0 m by 0.3 m track loops. The drag and lift forces attenuate faster at small heights than at large heights as the lateral displacement increases. In general, for a given displacement, the ratio of destabilizing force to lift force improves slightly as height increases. For example, at a displacement of 10 cm, the ratio is about 0.98 for the 0.18 m suspension height and about 0.73 for the 0.24 m suspension height. This applies only to Type I, II, IV, and V systems.

ℓ_m = 1.5m, ℓ_t = 1.0m

h = 0.22m, v = 150 m/s

Q = 9.393

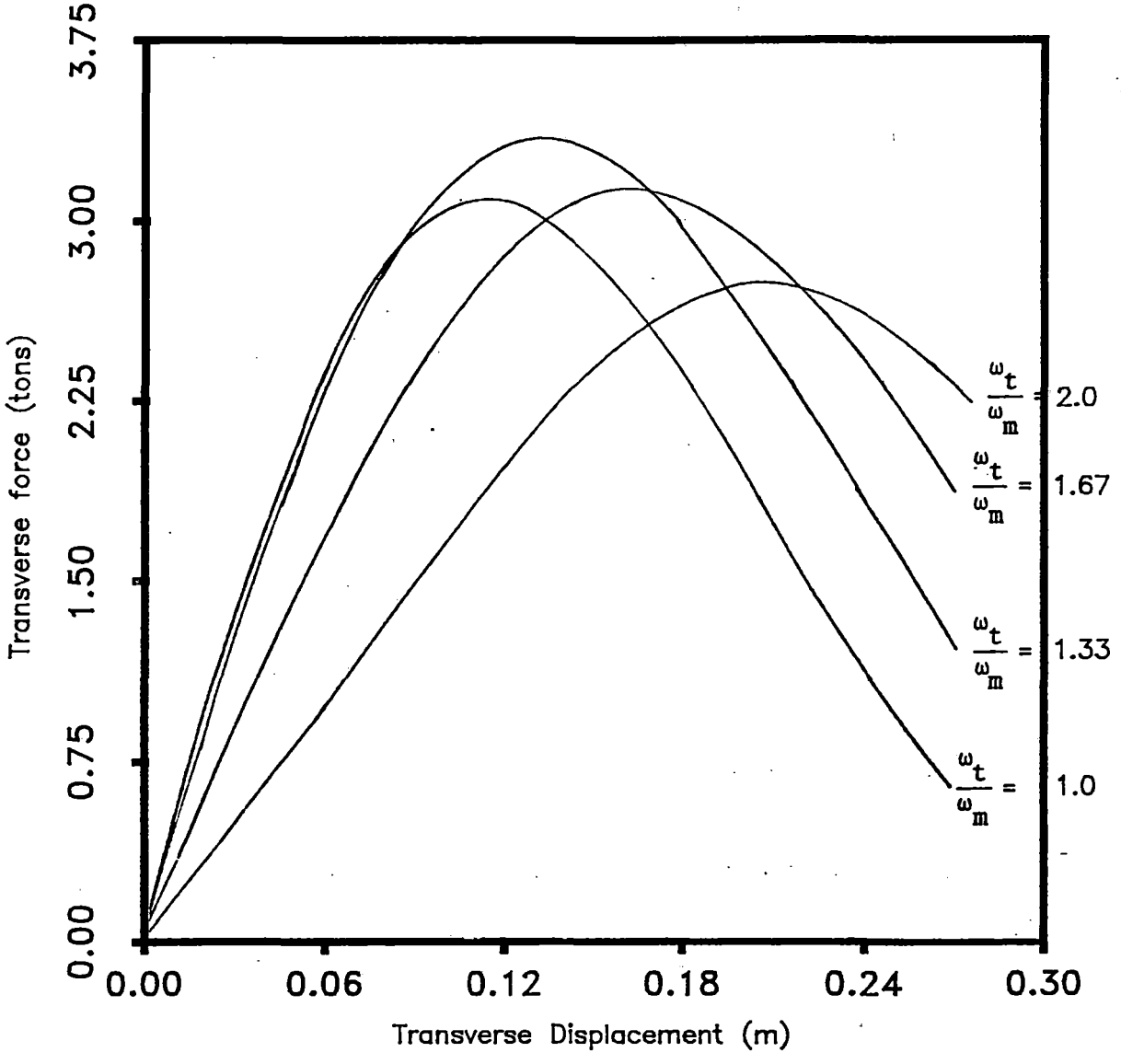

Fig. 1—18 Transverse force versus transverse displacement from guideway center—line

ℓ_m = 1.5m, ℓ_t = 1.0m

h = 0.22m, v = 150m/s

Q = 9.39

Curve (1) ω_t/ω_m = 2

(2) ω_t/ω_m = 1.67

(3) ω_t/ω_m = 1.33

(4) ω_t/ω_m = 1

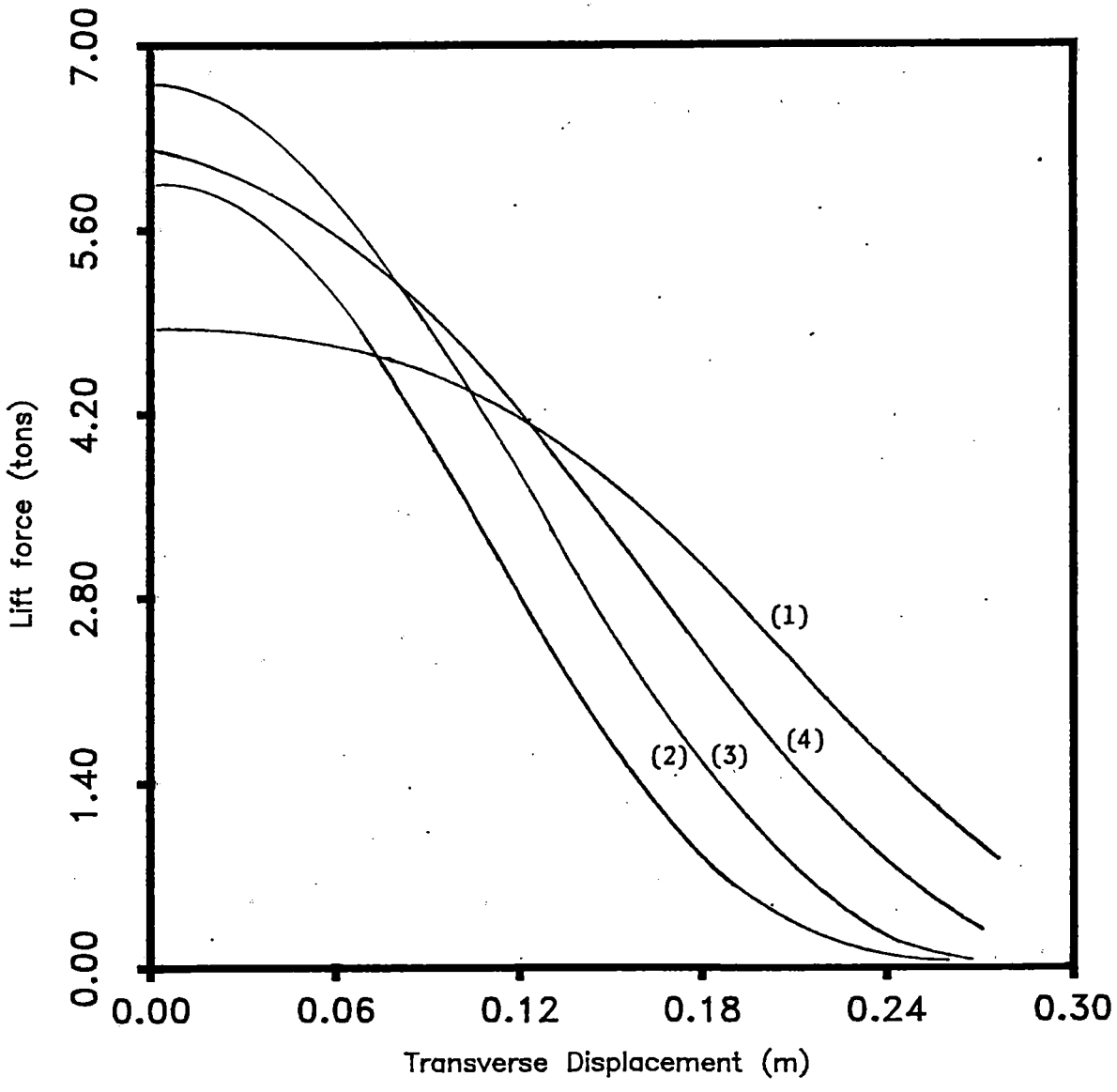

Fig. 1–19 Lift force versus transverse displacement from guideway center–line

ℓ_m = 1.5m, ℓ_t = 1.0m

ω_m = 0.3m, ω_t = 0.3m, v = 150m/s

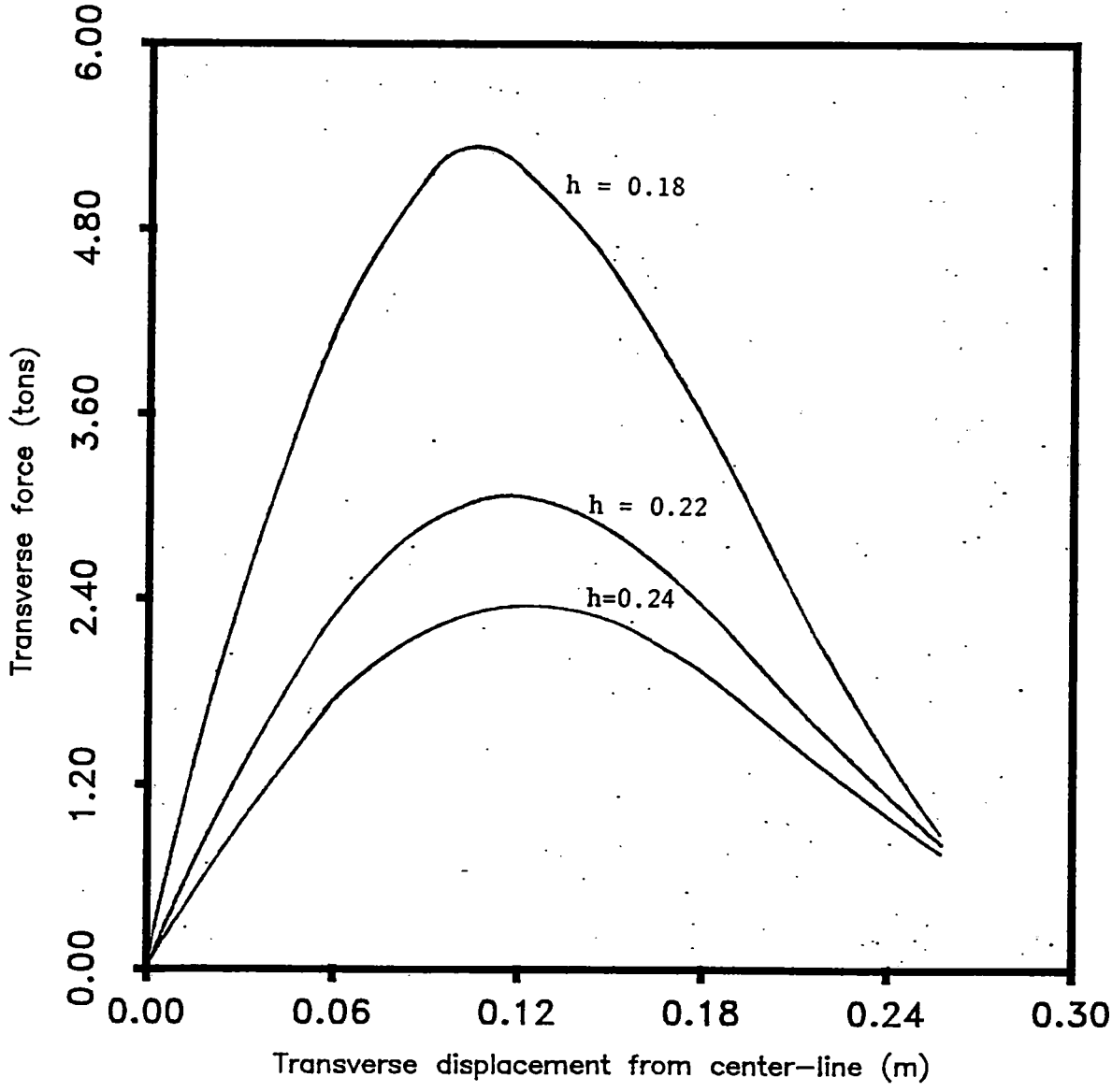

Fig. 1-20 Transverse force versus transverse displacement from guideway center-line for different suspension heights

ℓ_m = 1.5m, ℓ_t = 1.0m

ω_m = 0.3m, ω_t = 0.3m, v = 150 m/s

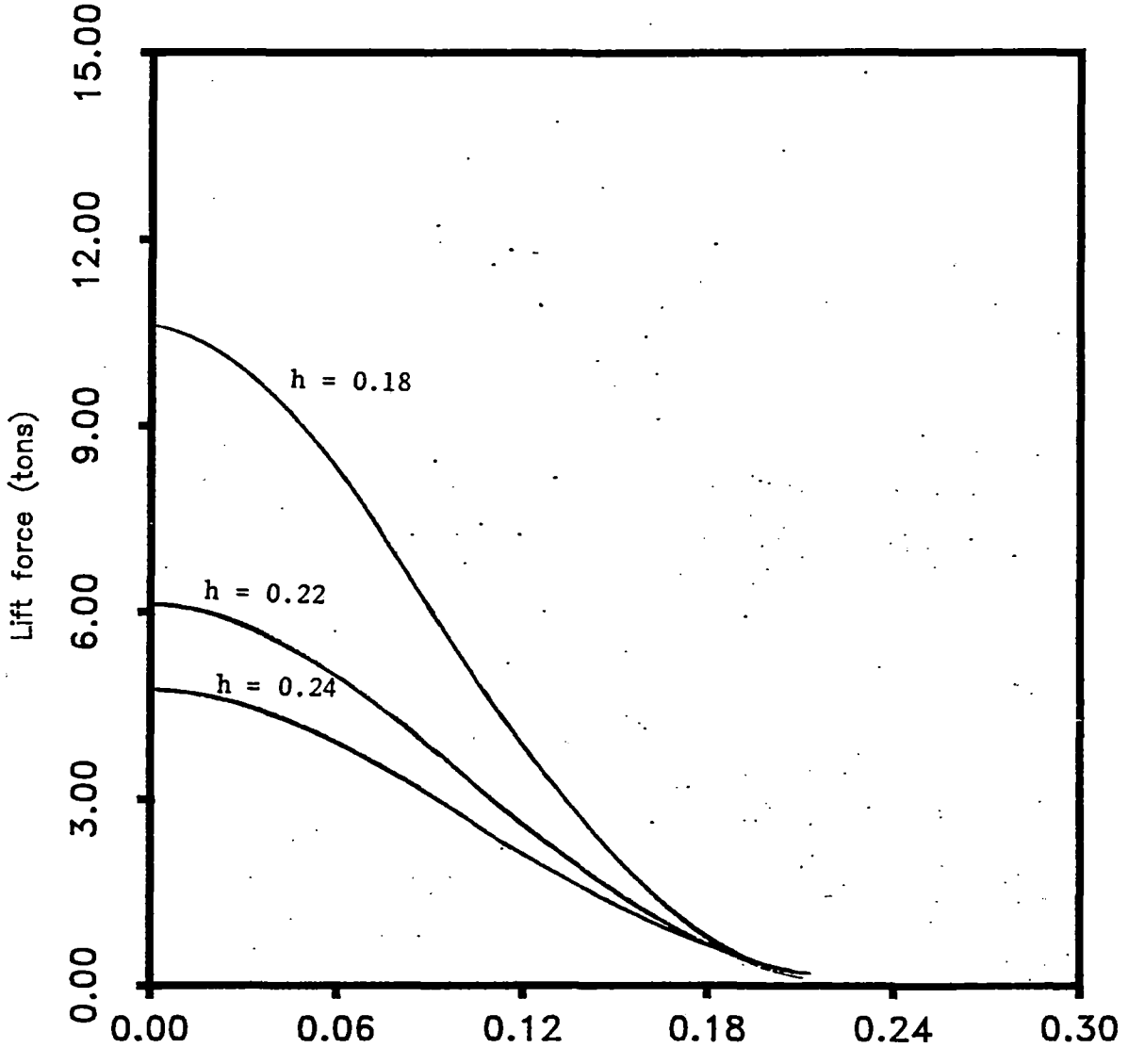

Fig. 1–21 Lift force versus transverse displacement from guideway center–line for different suspension heights

$\ell_m = 1.5, \quad \omega_m = 0.3 \qquad v = 150$ v/s

$\ell_t = 1.0 \quad \omega_t = 0.3$

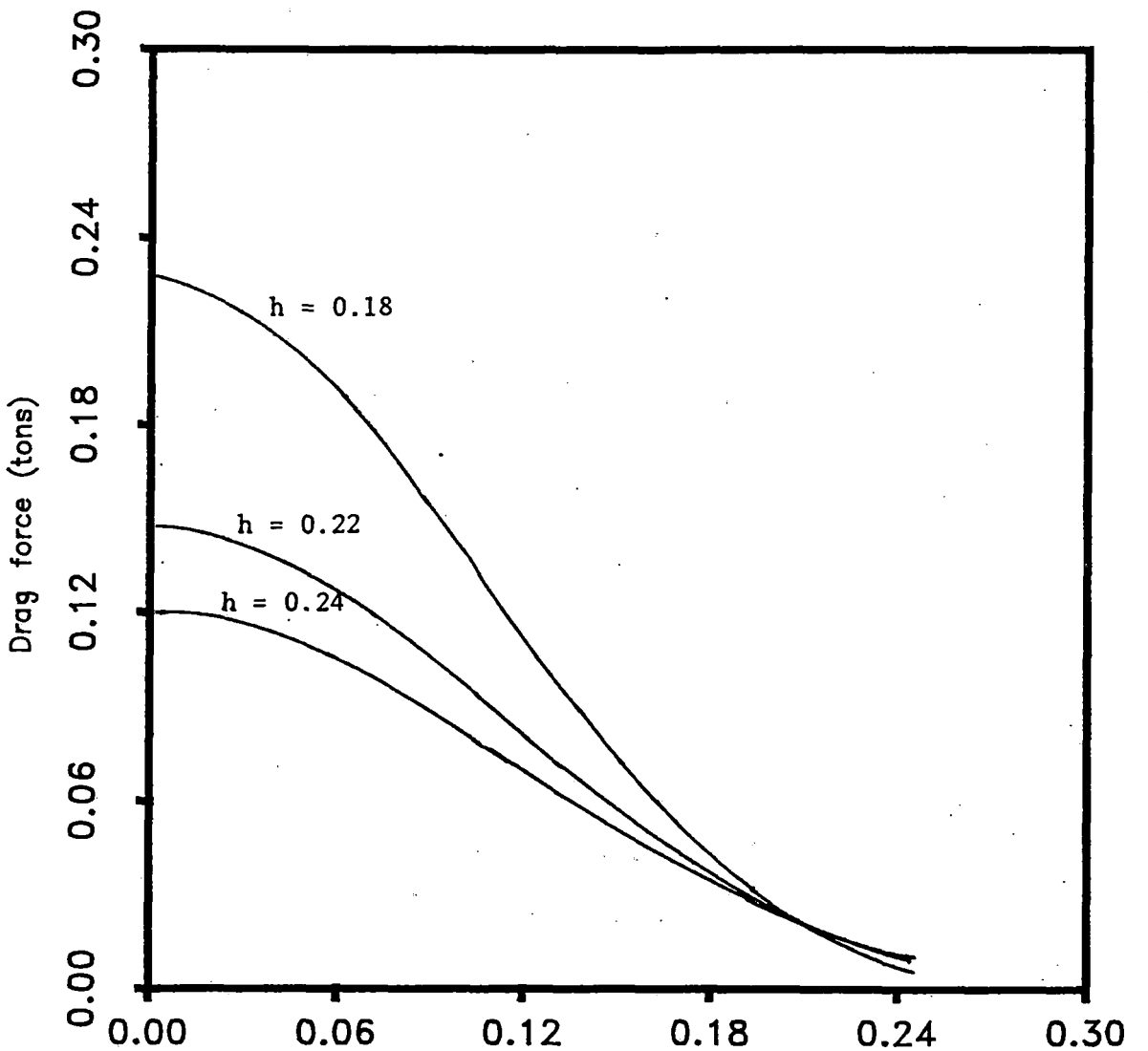

Fig. 1—22 Drag force versus transverse displacement for different suspension heights

Figure 1-23a shows the guideway roughness analysis for vertical accelerations as a function of bandwidth, at zero grade. It is concluded that 0.05 G is the acceptable limit on vehicle acceleration; at 300 mph, the minimum recommended bandwidth is 12 radians/second.

Figure 1-23b shows the guideway roughness spectrum for variations in electromagnetic airgap up to 60 mm as a function of speed and bandwidth for a 4% grade.

1.8 Substation Electrical Design

The substation apparatus per single guideway consists of a 0-120 Hz, 15.5 MW, 20 MVA rated, phase-delay rectifier-DC link - thyristor frequency invertor, which is standard industrial apparatus and commercially available at a cost of $420,000/MVA or $8.40 M for a complete VVVF Converter station including input step-down transformers. These are situated every 5 km along the guideway; however, with special switching, the spacing could be increased to every 10 km. The cost of the 20 MVA substations per double guideway is $16.8 M, situated every 5 km.

Figure 1-24 shows a system electrical layout drawing for sequential thyristor switching of an LSM active guideway in 0.625 km sections to decrease the total number of inverter substations while retaining a high overall power factor.

Table 1-19 gives the substation input apparent power with different "roll-off" rates of acceleration for a 45-ton vehicle applicable to all systems. Figure 1-25 shows substation MVA input from the utility grid and total LSM thrust for 3 different cases of high-speed operation, starting at 200 km/hr:

Case 1: Thrust ramp rate at 10 kN/100 km/hr

Case 2: Thrust ramp rate at 20 kN/100 km/hr up to 400 km/hr, then held constant at 100 kN maximum

Case 3: Thrust held at 68-73 kN for speed range 200-400 km/hr

Figure 1-23a Guideway Roughness Analysis - Vertical Direction, Zero Grade

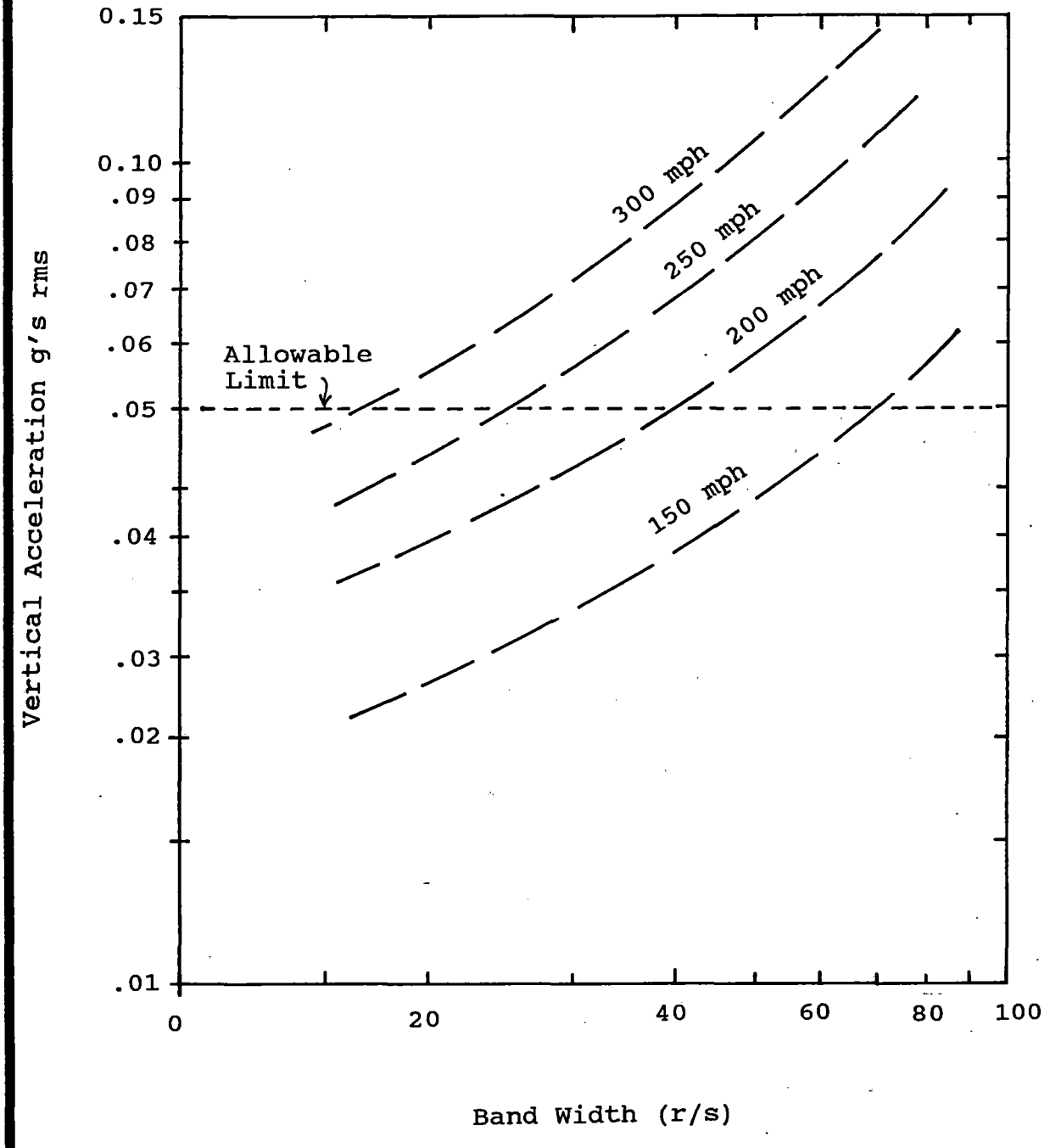

Note: Abrupt change in EM airgap is limited to 9 mm in all cases.

Figure 1-23b Ramp Analysis - Vertical for 4% Grade

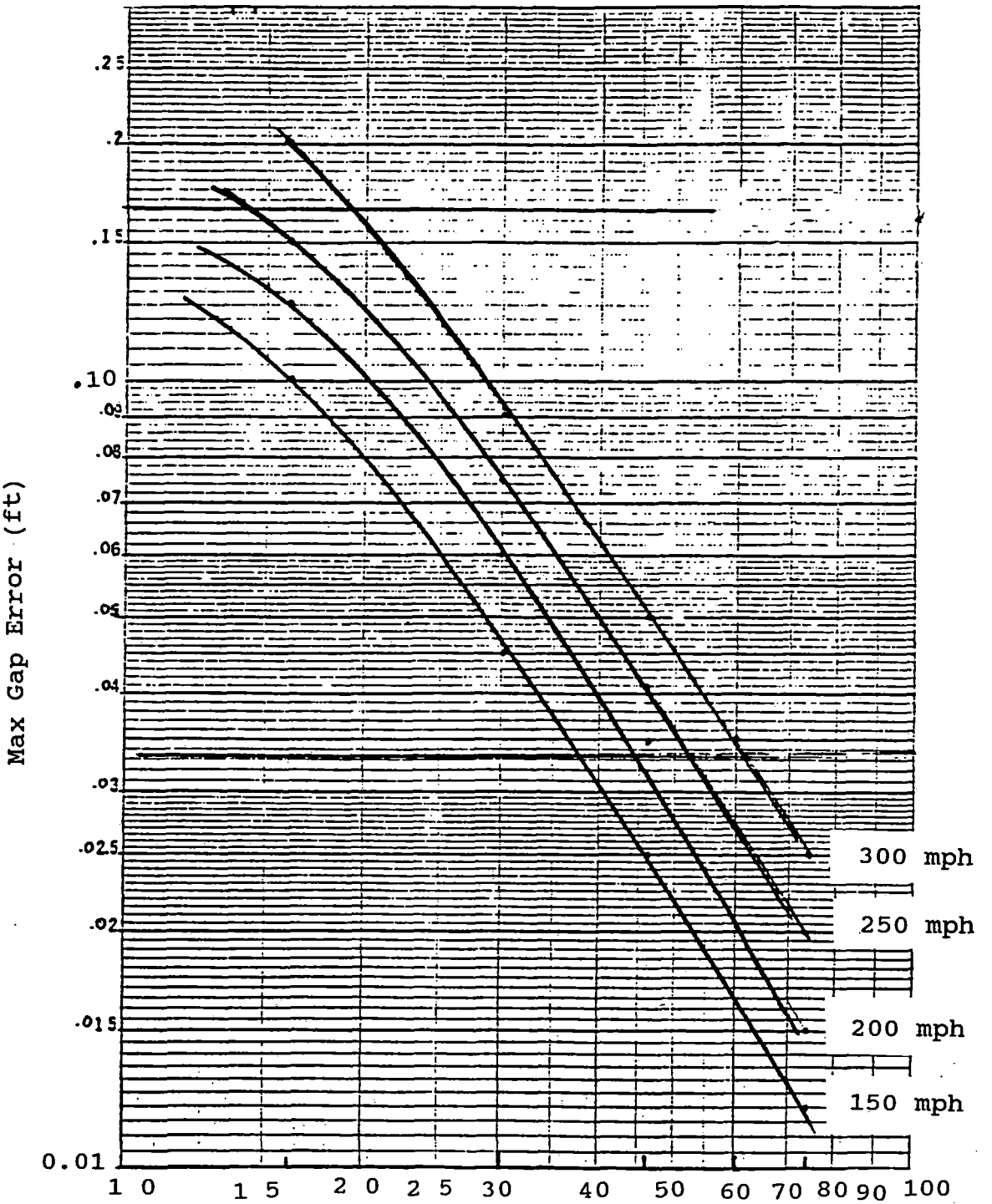

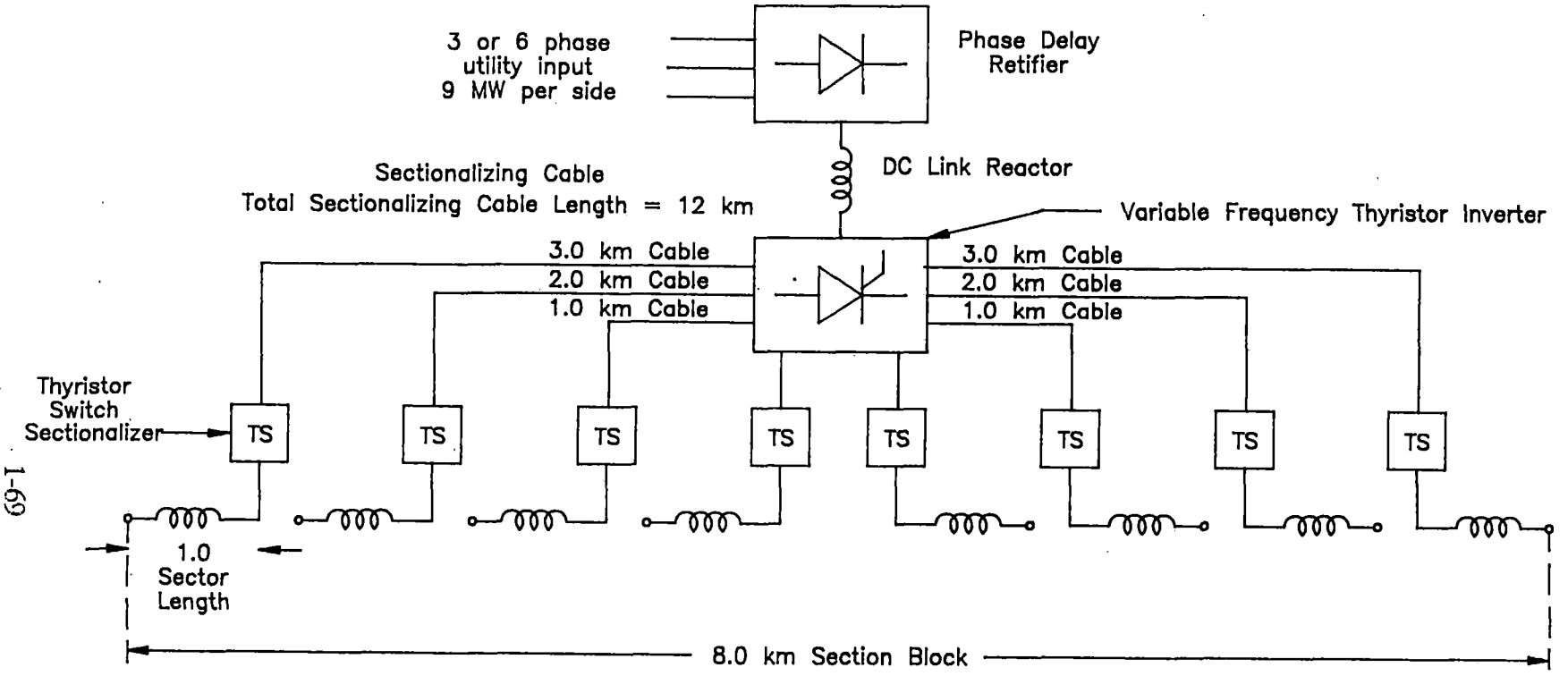

Figure 1-24 Method of reducing substation inverter kVAR and kVA demand by use of multiple sectionalizing blocks switched by thyristors for minimizing substation investment.

Figure 1-25

Substation Electrical Apparent Power Input for 45 Ton Vehicle

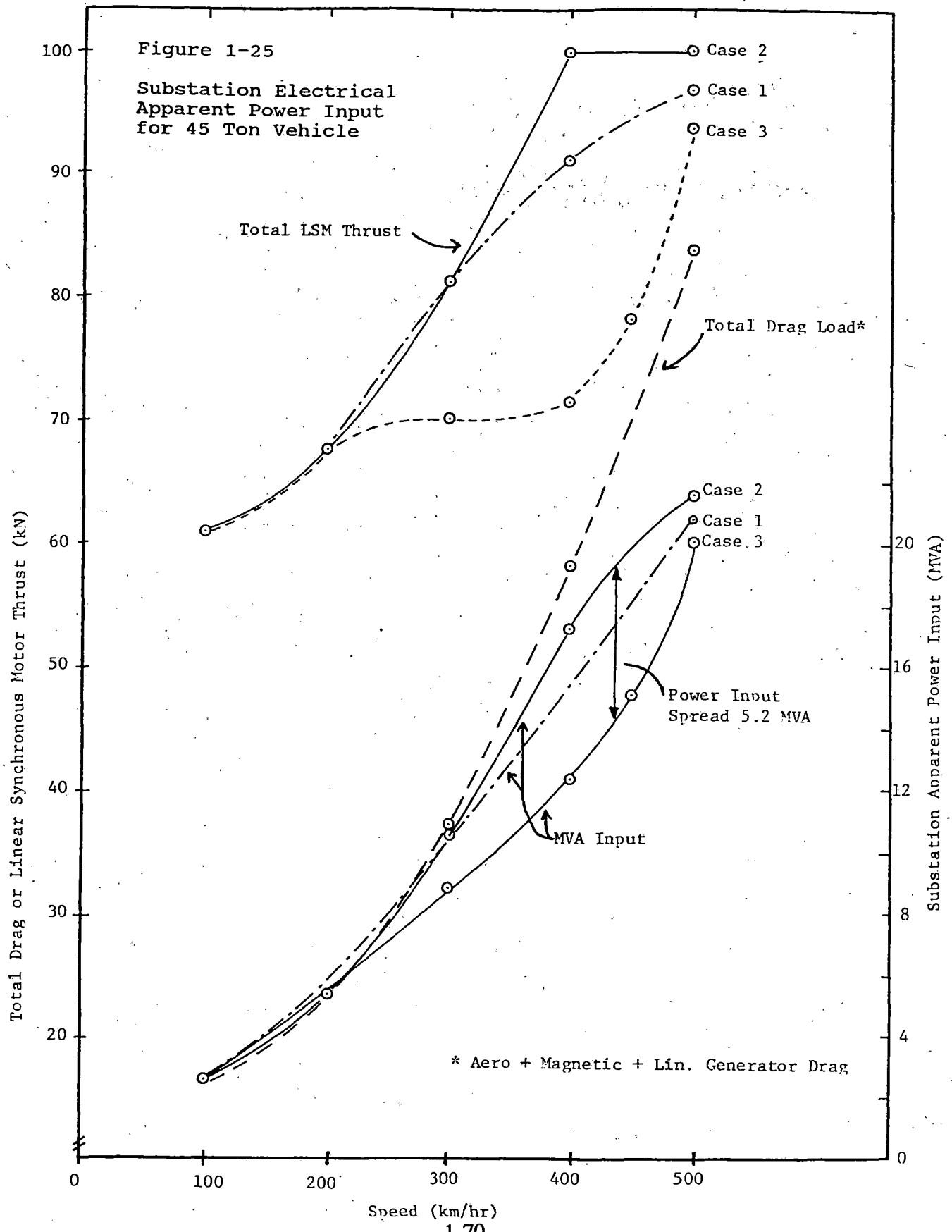

Table 1-19

Substation Input Apparent Power for High-speed Acceleration Profiles of 45,000 kg Vehicle

Case No. 1 Medium Acceleration Roll-off at 300 km/hr

Speed km/hr.	Acceleration G's	Command Acceleration Thrust (kN)	Total Input (kN)	Real Power (MW)	Substation Input (MVA)*
100	0.10	44.1	61	1.68	2.60
200	0.10	44.1	67.6	3.72	5.76
300	0.10	44.1	81.1	6.73	10.4
400	0.074	32.8	91.0	10.1	15.6
500	0.03	13.25	96.7	13.4	20.7

Case No. 2 Minor Acceleration Roll-off at 400 km/hr

Speed km/hr.	Acceleration G's	Command Acceleration Thrust (kN)	Total Input (kN)	Real Power (MW)	Substation Input (MVA)*
200	0.10	44.1	67.6	3.72	5.76
300	0.10	44.1	81.1	6.73	10.4
400	0.095	41.8**	100.0	11.1	17.2
500	0.037	16.5**	100.0	13.9	21.5

Case No. 3 Major Acceleration Roll-off at 200 km/hr.

Speed km/hr.	Acceleration G's	Command Acceleration Thrust (kN)	Total Input (kN)	Real Power (MW)	Substation Input (MVA)*
200	0.10	44.1	67.6	3.72	5.76
300	0.075	33.0	70.0	5.81	8.99
400	0.030	13.2	71.4	7.93	12.3
450	0.018	8.0	78.2	9.75	15.1
500	0.023***	10.1	93.6	13.0	20.1

* Apparent power input (MVA) assumes 76% power factor at 85% conversion efficiency for LSM and inverter/transformer station

** Limit of 100 kN propulsion system

*** Same residual acceleration as Transrapid 07

Case 3 is recommended because it yields a 3-5 MVA savings in input power over alternative schemes and therefore reduces utility demand charges by 25-30%.

The passenger throughput per guideway is designed for a 200-passenger vehicle every 37 seconds or a maximum throughput/hr of 19,460 passengers per side assuming a 20 MVA substation size at 5 km intervals.

Table 1-20 is the parametric optimization of the LSM at 500 kAT/pole and at an inverter control angle of 105°. This includes the inductance space derivative and pole-pitch optimization for a fixed propulsion force density of 4200 Newtons per meter longitudinal at 150 m/s vehicle speed.

1.9 Lift and Drag Forces Versus Speed

The detailed shapes of L/D characteristics depend upon the quantity of material, the magnet and ladder shapes, and the height and lateral offset of the magnet with respect to the ladder. This study discusses the effect that a variation in the quantity of material has on the speed characteristics.

Figures 1-26 to 1-29 show the lift and drag versus speed characteristics for a typical system in which only the quantity of track material is varied. The magnet and ladder configurations and suspension height are kept constant in all cases. The quantity of material is 50% of the referenced quantity in Figure 1-26, 100% of that in Figure 1-27, 150% of that in Figure 1-28 and 400% of that in Figure 1-29. It should be noted that changing the quantity of material in the ladder changes both the resistances and the inductances of the system (but not equally). The resistances vary almost inversely with the quantity of material. The self inductances vary roughly logarithmically, while the mutual inductances are virtually unchanged. Changing only the magnitude of the loop electrical resistance merely shifts the lift and drag curves horizontally along the speed axis but leaves their shapes otherwise unchanged. Thus we should expect that a particular value of lift or drag force should occur in Figure 1-28 at roughly one third of the speed at which the same forces occur in Figure 1-26 which has only one-third

INITIAL DISPLACEMENT

X	Y	Z
.0000	.0000	.0800

STATOR WIDTH: 1.300 METERS
CONDUCTOR RESISTIVITY: 0.294E-07 OHM-METERS
CURRENT DENSITY: 0.2500E+07 AMP/SQ. METER
PROPULSIVE FORCE: 4200.0 NEWTONS/METRE = $\dot{F}$
VEHICLE SPEED: 150.0 METRES/SECOND

FORCE(1) IS FORCE PER FIELD COIL
FORCE(2) IS FORCE PER UNIT LENGTH OF VEHICLE
FORCE(3) IS FORCE PER UNIT LENGTH OF CONDUCTOR

Table 1-20

Parametric optimization for Linear Synchronous Motor at B=105° current angle and field current = 500 kAT/pole. Dual LSM, full-width with 2 slots/pole/phase.

STATOR PITCH τ_p	MAGNET LENGTH	CONDUCTOR DIAMETER	RESISTANCE PER PHASE	INDUCTANCE PER PHASE	FORCE(1) $\tau_p \dot{F}/I$	FORCE(2) $\dot{F}/I$	FORCE(3)	STATOR CURRENT I	INDUCED VOLTAGE	SUPPLY FREQUENCY	
METRES	METRES	METRES	OHMS/M	UH/M	N/M/AMP	N/M/AMP	N/M/AMP	AMPERES	VOLTS/M	RAD/SEC	
.240	.240	.0108	.00410238	14.630	4.384	18.267	1.423	230.	945.5	1963.5	
.260	.260	.0112	.00357080	13.677	4.421	17.004	1.417	247.	880.2	1812.5	
.280	.280	.0116	.00313024	12.850	4.438	15.849	1.404	265.	820.4	1683.0	
.300	.300	.0120	.00275838	12.126	4.433	14.777	1.385	284.	764.9	1570.8	
.320	.320	.0125	.00244352	11.484	4.413	13.791	1.362	305.	713.9	1472.6	
.340	.340	.0129	.00217583	10.920	4.382	12.888	1.336	326.	667.1	1386.0	
.360	.360	.0133	.00194719	10.410	4.343	12.065	1.308	348.	624.5	1309.0	
.380	.380	.0137	.00175096	9.951	4.300	11.316	1.280	371.	585.7	1240.1	
.400	.400	.0142	.00158169	9.535	4.253	10.633	1.251	395.	550.4	1178.1	
.420	.420	.0146	.00143498	9.158	4.205	10.011	1.222	420.	518.2	1122.0	
.440	.440	.0150	.00130720	8.813	4.156	9.444	1.194	445.	488.9	1071.0	
.460	.460	.0155	.00119539	8.497	4.106	8.927	1.167	471.	462.1	1024.4	
.480	.480	.0159	.00109712	8.207	4.057	8.453	1.140	497.	437.6	981.7	
.500	.500	.0163	.00101037	7.940	4.009	8.019	1.114	524.	415.1	942.5	
.520	.520	.0168	.00093346	7.693	3.962	7.620	1.089	551.	394.4	906.2	
.540	.540	.0172	.00086502	7.463	3.917	7.253	1.064	579.	375.5	872.7	
Base → .560	.560	.0176	.00080387	7.250	3.872	6.915	1.041	607.	357.9	841.5	→ 134 Hz
.580	.580	.0180	.00074904	7.051	3.829	6.602	1.018	636.	341.8	812.5	
.600	.600	.0184	.00069970	6.868	3.788	6.313	.997	665.	326.8	785.4	
.620	.620	.0188	.00065515	6.693	3.748	6.045	.976	695.	312.9	760.1	
.640	.640	.0192	.00061481	6.529	3.709	5.795	.956	725.	300.0	736.3	
.660	.660	.0196	.00057815	6.375	3.671	5.562	.937	755.	287.9	714.0	
.680	.680	.0200	.00054475	6.231	3.635	5.345	.918	786.	276.7	693.0	
.700	.700	.0204	.00051424	6.094	3.600	5.142	.900	817.	266.2	673.2	
.720	.720	.0208	.00048628	5.965	3.566	4.952	.883	848.	256.3	654.5	
.740	.740	.0212	.00046060	5.842	3.533	4.774	.866	880.	247.1	636.8	
.760	.760	.0216	.00043696	5.726	3.501	4.606	.850	912.	238.4	620.1	
.780	.780	.0219	.00041514	5.616	3.469	4.448	.834	944.	230.2	604.2	
.800	.800	.0223	.00039496	5.512	3.439	4.299	.819	977.	222.5	589.0	
.820	.820	.0227	.00037626	5.412	3.410	4.158	.804	1010.	215.2	574.7	
.840	.840	.0231	.00035890	5.317	3.381	4.025	.790	1043.	208.3	561.0	
.860	.860	.0234	.00034274	5.226	3.353	3.899	.776	1077.	201.8	548.0	
.880	.880	.0238	.00032768	5.140	3.326	3.779	.763	1111.	195.6	535.5	
.900	.900	.0242	.00031362	5.057	3.299	3.666	.750	1146.	189.7	523.6	

Table 1-20 (Continued)

```
FIELD WINDING
-------------

FORCE CALCULATION FIELD COILS:1
COILS PER PHASE:        1
PITCH:                .570 METRES
LENGTH:               .510 METRES
WIDTH: .              .800 METRES
CONDUCTOR WIDTH:     .0400 METRES
CONDUCTOR HEIGHT:    .0400 METRES
NUMBER OF TURNS:       500
SELF INDUCTANCE: .400582 HENRIES

STATOR WINDING
--------------

NUMBER OF SECTIONS= 49
DOUBLE PARALLEL RECTANGULAR WINDING
BALANCED 3 PHASE RECTANGULAR WINDING


PITCH:                          .570 METRES
WIDTH:                          .800 METRES
PITCH DISPLACEMENT FACTOR:      .167
WIDTH DISPLACEMENT FACTOR:      .000
MIN. CONDUCTOR SEPARATION:      .025 METRES
CONDUCTOR DIAMETER:            .0127 METRES
CONDUCTOR RESISTIVITY: 0.220E-07 OHM-METRES
CONDUCTOR LENGTH:             4.807 METRES/METRE
RESISTANCE PER PHASE: 0.2087E-03 OHM/METRE
SELF INDUCTANCE PER PHASE:   1.34 MICROHENRIES/METRE
M(1,1)= 0.43037E+01M(2,1)= 0.10413E+02M(3,1)= 0.43037E+01
```

ℓ_m = 1.5m ω_m = 0.3m h = 0.22m

ℓ_t = 1.0 m, ω_t = 0.3m

Weight of aluminium per meter of track = 10.8 kg.

τ = 0.035643

$\bar{F}_{L\infty}$ = 6.2 ton

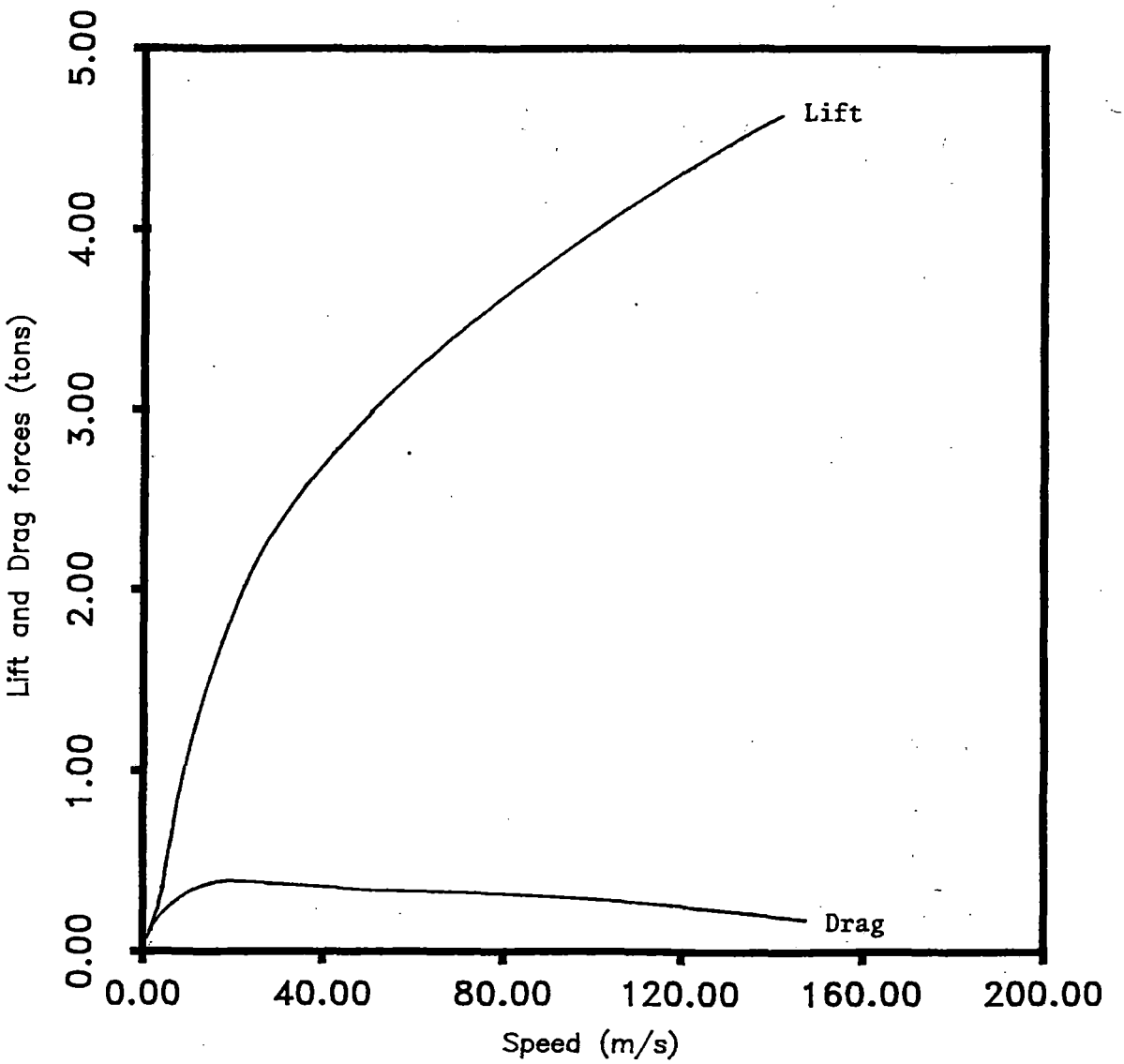

Fig. 1–26 Force vs. Speed

ℓ_m = 1.5m, ℓ_t = 1.0m, h = 0.22m

ω_m = 0.3m, ω_t = 0.3m

Weight of aluminium per meter of track = 21.6 kg

τ = 0.062612

$\bar{F}_{L\infty}$ = 6.9 ton

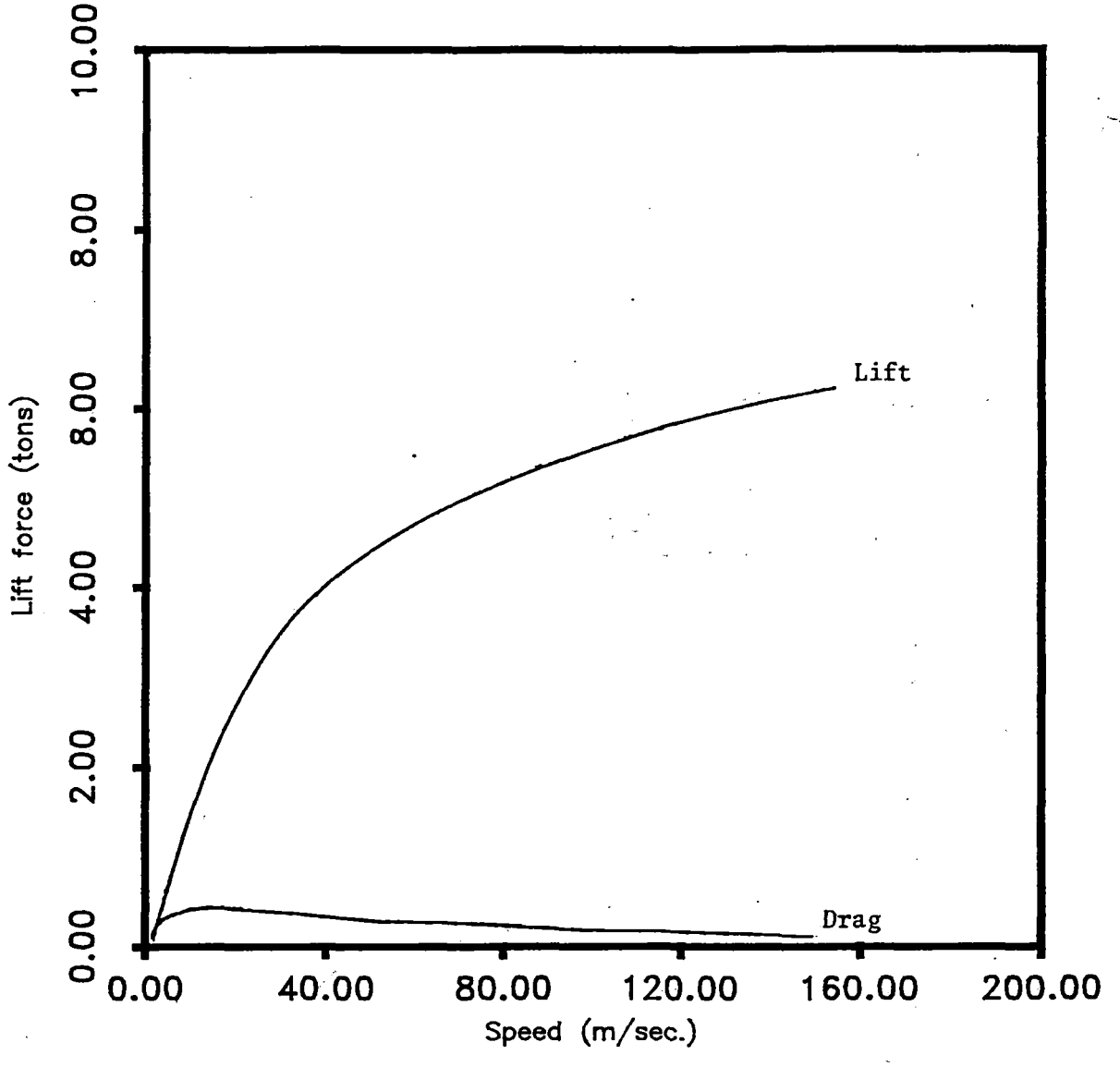

Fig. 1–27 Force versus speed

ℓ_m = 1.5m, ω_m = 0.3m h = 0.22m

ℓ_t = 1.0m, ω_t = 0.3m

τ = 0.0864, v = 150 ms^{-1}

Weight of aluminium per meter of track = 32.4 kg.

$\bar{F}_{L\infty}$ = 7.773 ton.

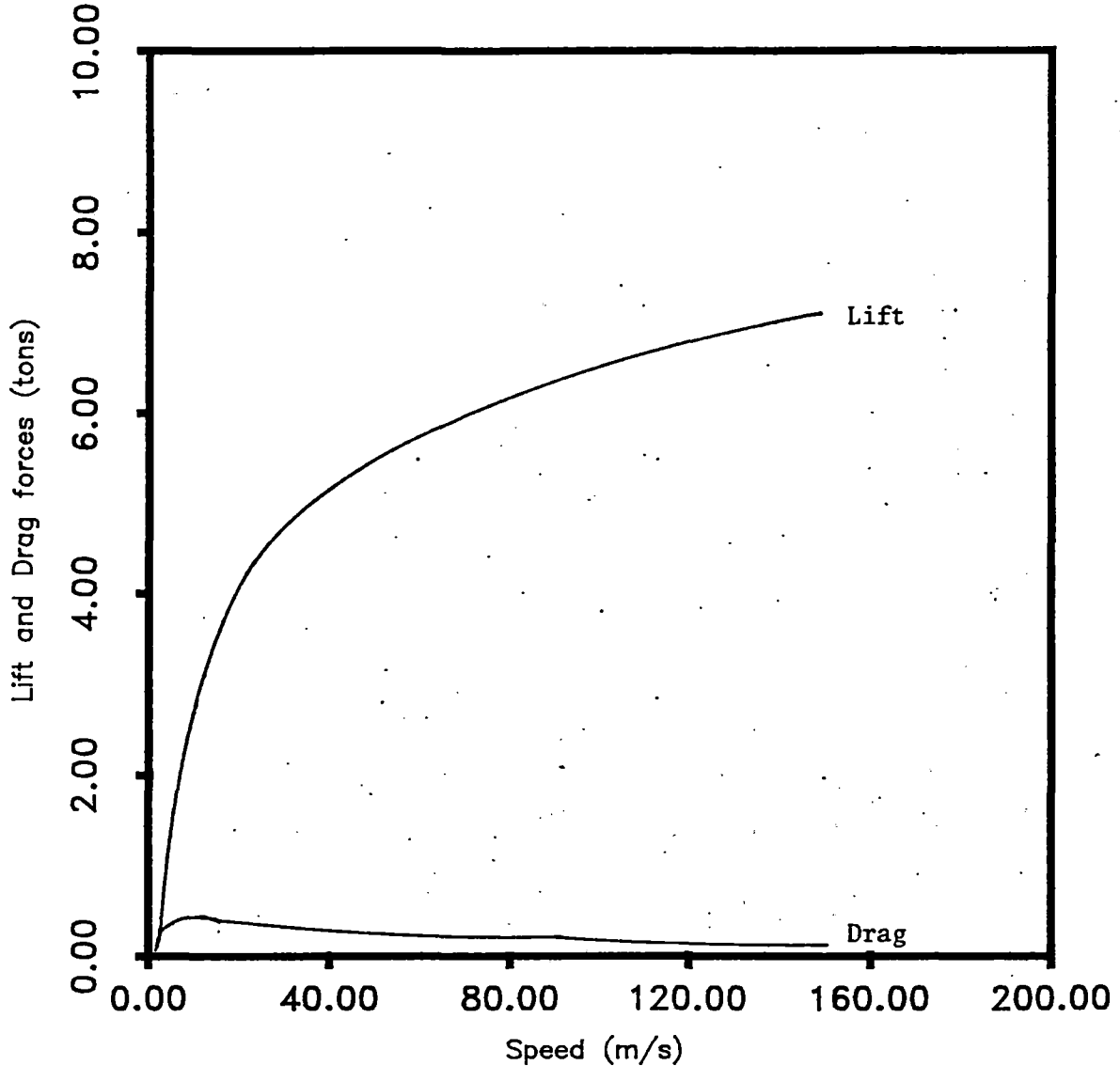

Fig. 1–28 Force versus speed

ℓ_m = 1.5m, ℓ_t = 1.0m, ω_m = 0.3, ω_t = - 0.3m

h = 0.22, τ = 0.18265

Weight of aluminium per meter of track = 86.4 kg.

$\bar{F}_{L\infty}$ = 10.13 ton

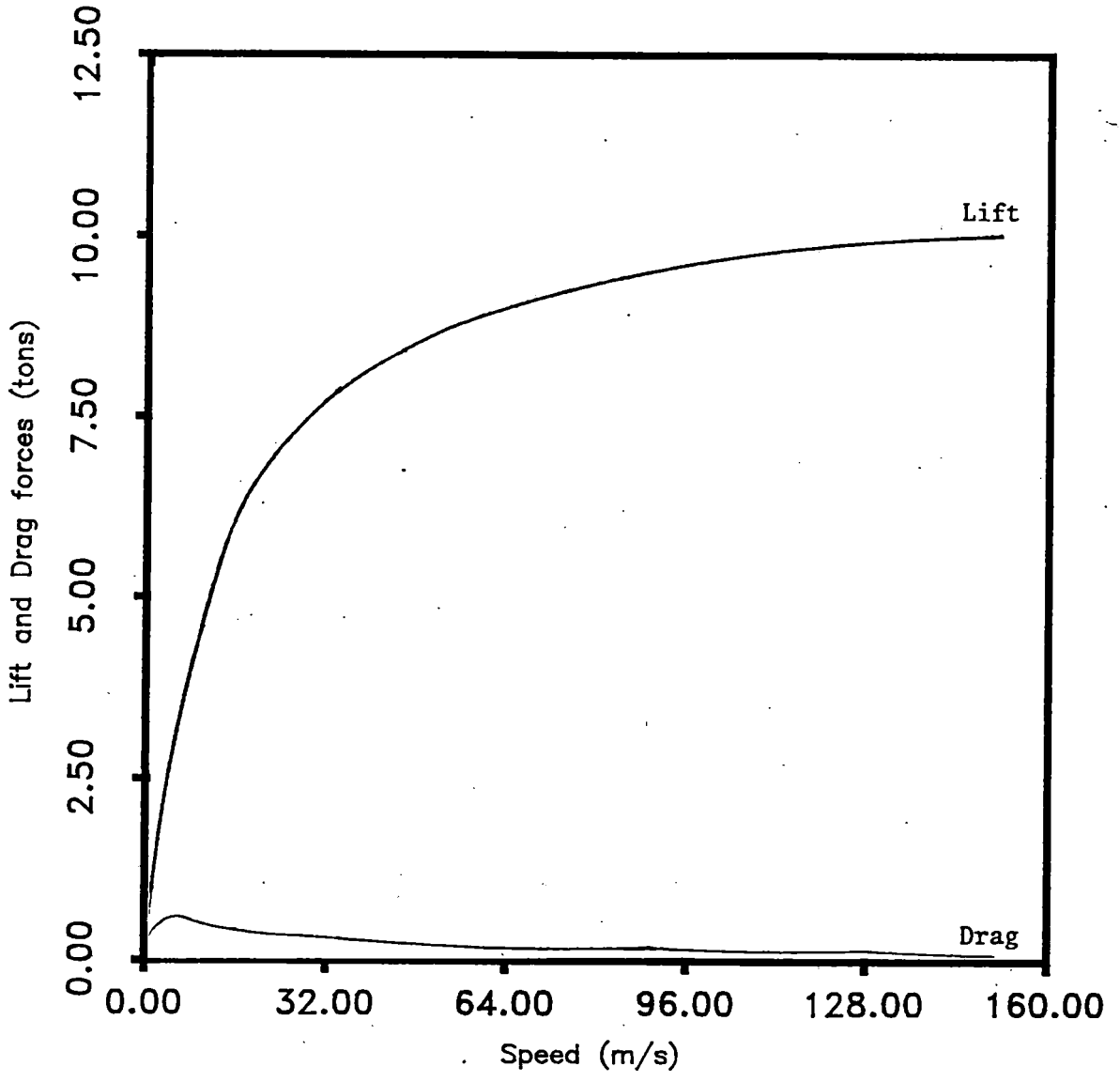

Fig. 1–29 Force versus speed

as much material. Note that the drag peak is seen to increase slightly with the quantity of material (i.e., 12% higher in Figure 1-28 than in Figure 1-26). Note, however, that the drag at cruise speed decreases with the quantity of material. A comparison of Figures 1-26 and 1-29 shows that as the quantity of aluminum per meter of track increases, the lift force obtained at cruise speed is close to its high-speed limit value. For example, in Figure 1-26, the lift force at cruise speed is only 75% of its high-speed limit value, whereas, for the system in Figure 1-29, (using 8 times the material of the systems in Figure 1-26), the lift and cruise speed is 98% of the high-speed limit value.

In summary , the shape of the lift and drag characteristics improves as the quantity of material (and therefore the quality factor Q) increases. The baseline design has a minimum value of Q = 10. The optimum performance of Type I-VI occurs when the magnet pitch is between 2.25 and 3.75 m. The fluctuations in lift can now be reduced to about 2% and the lift and lift to drag ratio is good.

In the Maglev 2000 system, the ratio of magnet length to rung pitch had been optimized to the value of 1:5. For systems in which the magnet and track loop lengths are equal, it has been found that a magnet pitch of $(n + 1/2)\ l_t$ gives optimum performance for a 2-magnet system. For example, when $l_m/l_t = 1$, using a magnet pitch of $1.5\ l_t$ gives a fluctuation of 5% compared to about 25% for a single magnet. The overall fluctuation level remains higher than for a system in which individual magnet lengths have been optimized. Figure 1-30 shows a parametric plot of the lift force fluctuations over a rung pitch for the Type I or II system.

1.10 Weight Summary of Vehicle Cryogenics

Table 1-21 summarizes the weight distribution for the LSM and lift magnet major components using a Nb-Ti conductor at 4.2°K operating temperature. The total vehicle undercarriage cryogenic weight including 20°K and 4°K thermal shielding is 23,669 kg. The Gifford-McMahon type refrigerators have been sized for a 4,545 kg weight for the vehicle. These weights exclude electromagnetic shielding and structural support beams. Section 2.0 discusses the cryogenic calculations in detail.

Table 1-21

Weight Distribution for Cryogenics
LSM & Levitation Systems for 76 Passenger Vehicle

LSM Propulsion Coil - 2 x 600 kAT	198
LN2 Shield	75
LN2 Liquid	14
20°K Shield	12
4°K Shield	45
PC Total	344 kg
Levitation Coil - 385 kAT	178
LN2 Shield	118
LN2 Liquid	24
20°K Shield	21
4°K Shield	65
LC Total	406 kg

Weight Summary

Levitation Coils (14)	5,684
Propulsion Coils (25 sets)	8,600
300°K Containment	4,840
Refrigeration Weight for 41-50 kW	4,545
Total Weight	23,669 kg

$N_m = 2$

$\ell_m = 1.5m$, $\omega_m = 0.3m$, $v = 150$ m/s

$\ell_t = 1.0m$, $\omega_t = 0.3m$, $h = 0.22m$

Curve (1) $\tau_m = 2.0$ m

(2) $\tau_m = 3.0$ m

(3) $\tau_m = 2.5$ m

(4) $\tau_m = 3.5$ m

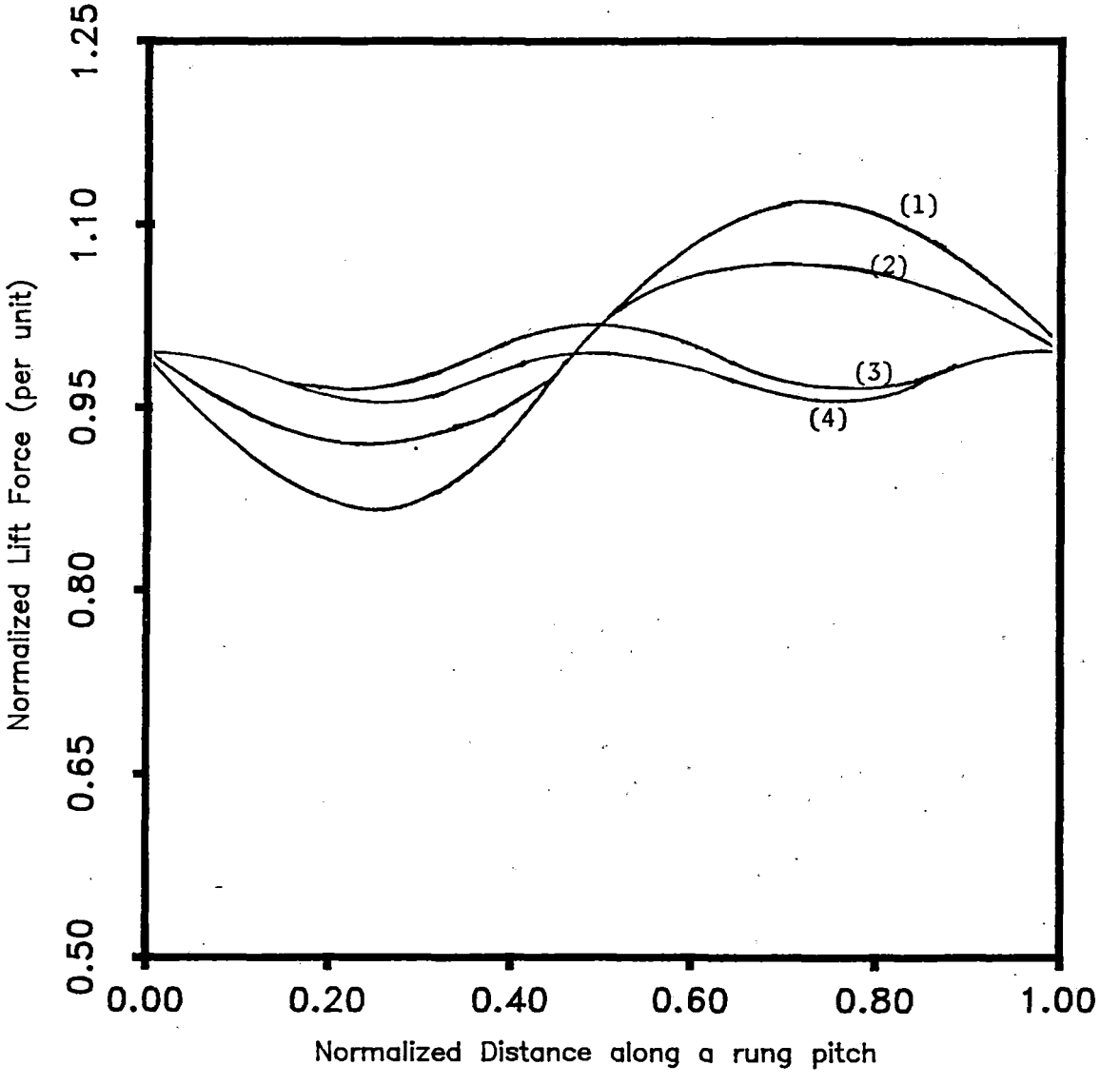

Fig. 1–30 Lift force versus normalized displacement along a rung pitch for two–magnet array

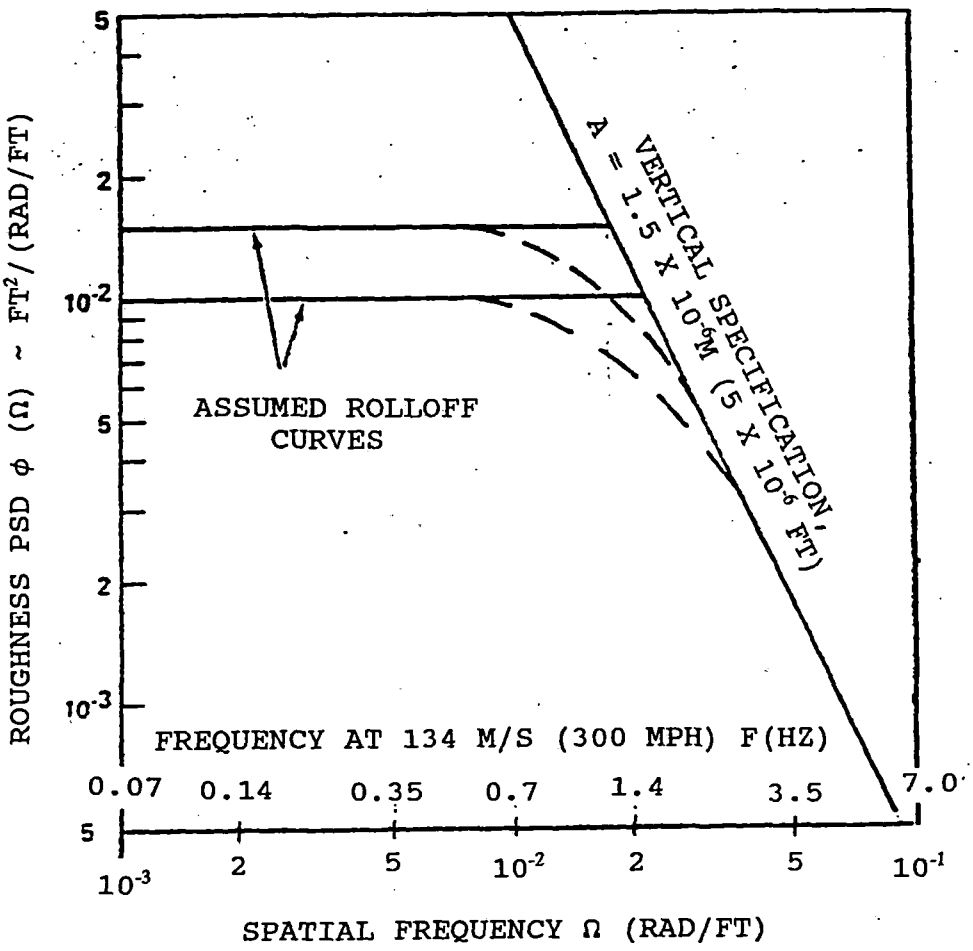

GUIDEWAY ROUGHNESS POWER SPECTRAL DENSITY RELATIONS

Figure 1-31

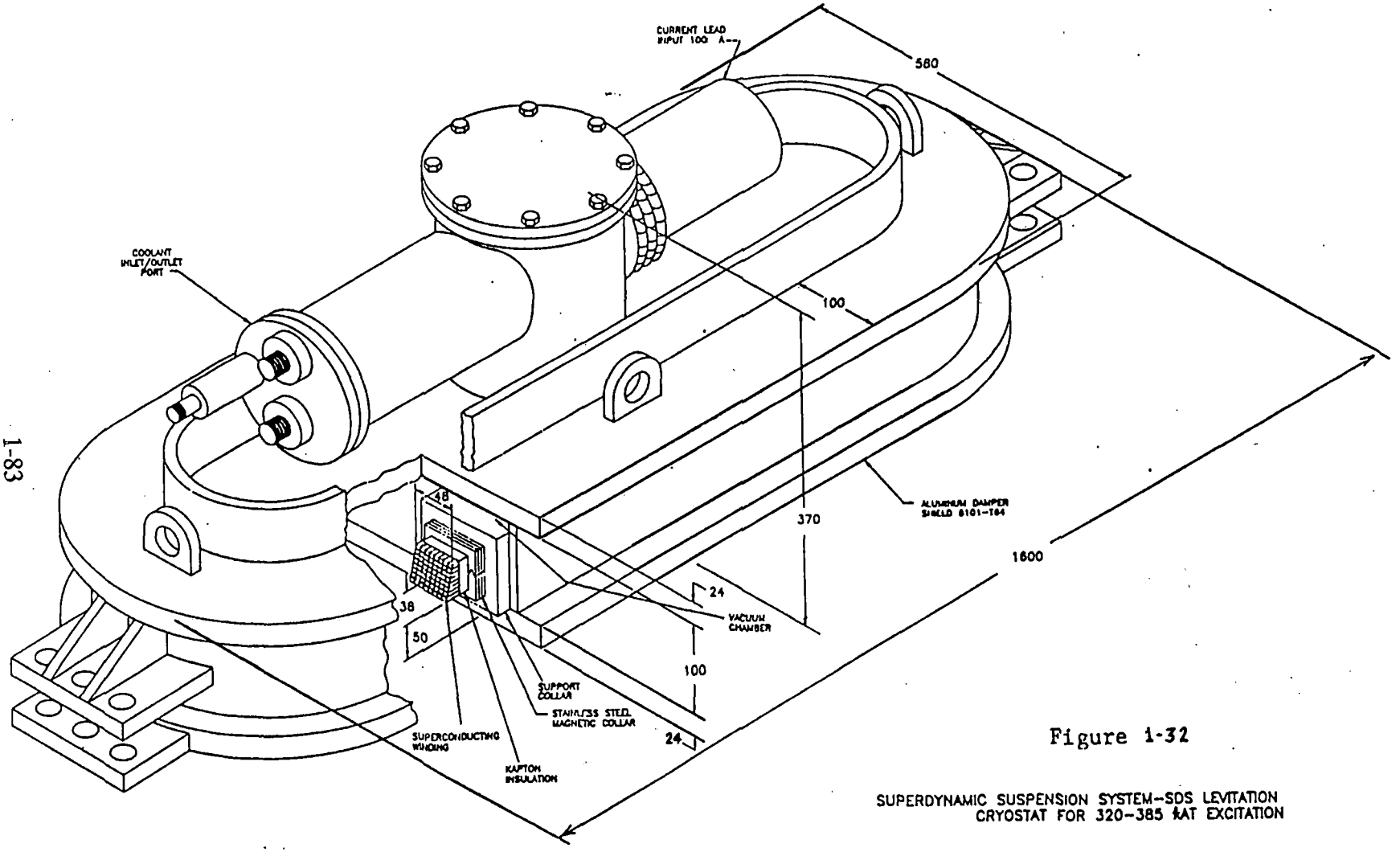

Figure 1-32

SUPERDYNAMIC SUSPENSION SYSTEM–SDS LEVITATION
CRYOSTAT FOR 320–385 kAT EXCITATION

REFERENCES

1. S. Kuntz and G. Slemon, "A Dual Linear Synchronous Motor for Maglev Vehicles," International Magnetics Conference, Los Angeles, California, June 8, 1977. See also IEEE Transactions of Magnetics, Vol. MAG-13, No. 3, pp. 1415-1417, September 1977.

2. F. W. Grover, Inductance Calculations, New York, Dover Publications, 1946.

3. S. Kuntz, P. E. Burke, G. R. Slemon, "Active Damping of Maglev Vehicles Using Superconductor Linear Synchronous Motors," Electric Machines and Electromechanics, Vol. 2, No. 4, pp. 371-384, July 1978.

4. S. Kuntz, "Active Stabilization of Roll and Yaw Moments with Dual Linear Synchronous Motor Propulsion System," Superconducting Propulsion and Magnetic Levitation for High Speed Ground Transportation, Report 77-5, The Canadian Institute for Guided Ground Transportation, Kingston, Ontario, 1977.

SUPERCONDUCTOR SELECTION

2.1 Magnetic Field Calculations

The starting point of the conceptual design is the magnetic field analysis. Computer codes were written for racetrack coil shapes from rectangular to purely circular. The magnetic field calculations are used for evaluating propulsion and lifting forces as well as magnetic shielding and are shown in Appendix A, Figures 2-2 through 2-6.

Field plots were generated for a typical propulsion racetrack coil. Figure 2-7 shows the Bz component of the magnetic field, and Figure 2-8 shows a field map in the x-y plane.

Propulsion Force Analysis

A set of analytical formulae based on the Biot-Savart law has been developed for computing the propulsion forces on the vehicle's LSM coil. The formulae describe the interaction between the three phase AC windings in the guideway and the superconducting coil on the vehicle.

The formulae consist of a finite series of terms representing the force from each segment of guideway. The series can be truncated at any number of segments. It is expected that not more than 10 terms are required.

Analytical formulae for the propulsion coil are shown in Appendix A, Figures 2-7 through 2-11. Simplified formulae for the rectangular coil that is a first approximation of the racetrack coil are shown in Appendix A, Figures 2-12 through 2-15.

Field Accuracy Study

The magnetic field for the superconducting coil was previously calculated using a thin single wire as an approximation to the finite wire bundle. We have verified the accuracy of the

System Characteristics	
Thrust	44.5 kN
Vehicle Weight	445 kN
Cruise Speed	500 km/hr (138.9 m/s)
Mechanical Power	6.945 MW
Field-Stator Winding Separation	0.21 m
Stator Block Length	2 km
LSM Configuration	Dual
Vehicle Dimensions	
length	30 m
width	3.4 m

Vehicle Field Magnets	
Number of Magnets	88–104
Mean Length (range)	0.53 – 0.85 m
Pole-pitch (range)	0.57 – 0.81 m
Mean Width	0.80 m
Field MMF (range)	400 kAT – 600 kAT
B_{peak} at Windings	5.3 T

Baseline Parameters of Linear Synchronous Motor
Figure 2-1

Propulsion Magnet Length	57–83 cm
Propulsion Magnet Width	80 cm
Field MMF	400K–600K Amp-turns
Peak Field at Winding	5.3 T
Operating Current	100 Amps
Conductor Type	Nb_3Sn or NbTi or High T_c
Conductor Stability	adiabatic or cryostable
Conductor Margin	50% cryostable
	80% adiabatic

Derived Propulsion Magnet Requirements
Figure 2-2

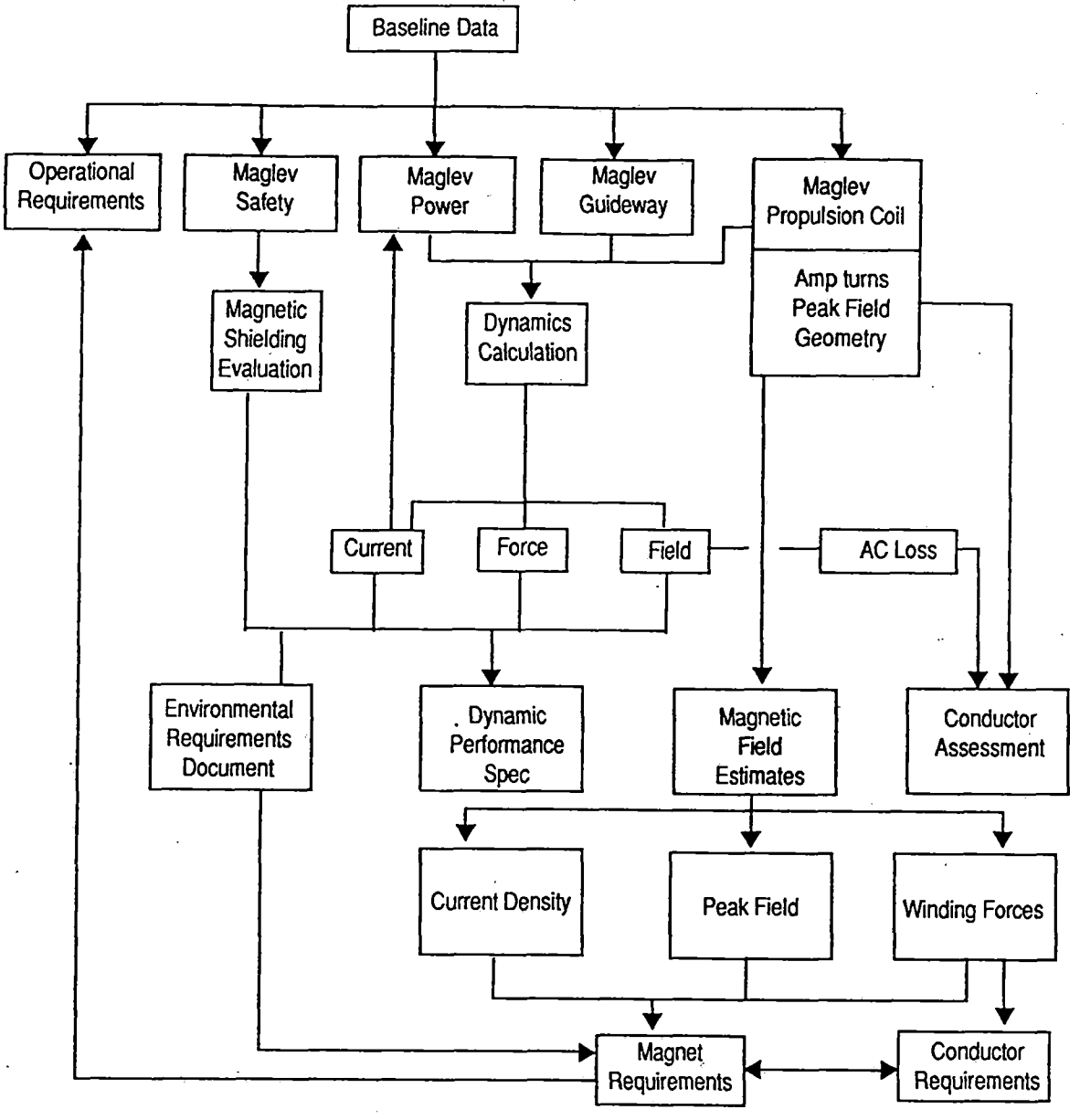

LSM Conceptual Design

Figure 2-3

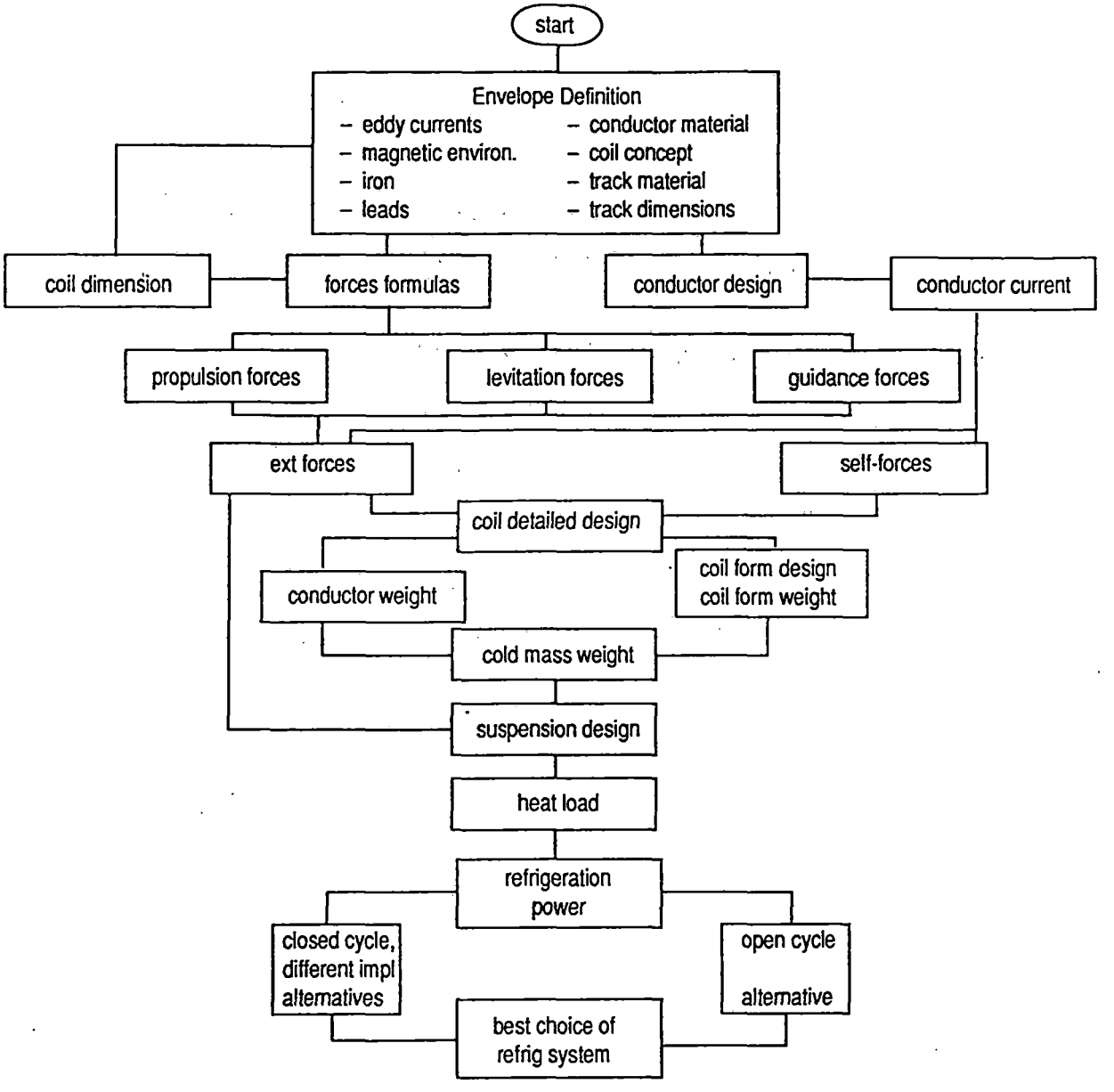

Diagram of refrigeration design process

Figure 2-4

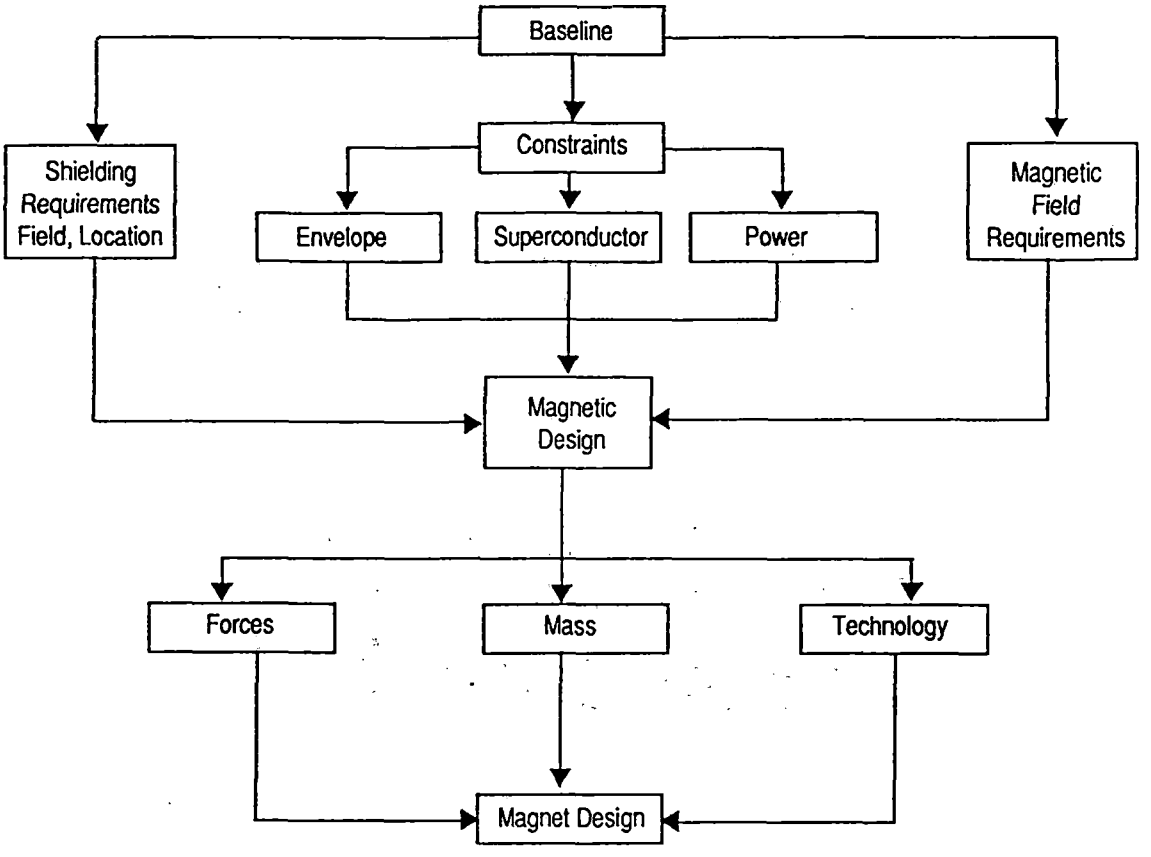

Conceptual Design Process for Active Shielding of the Magnetic Fields

Figure 2-5

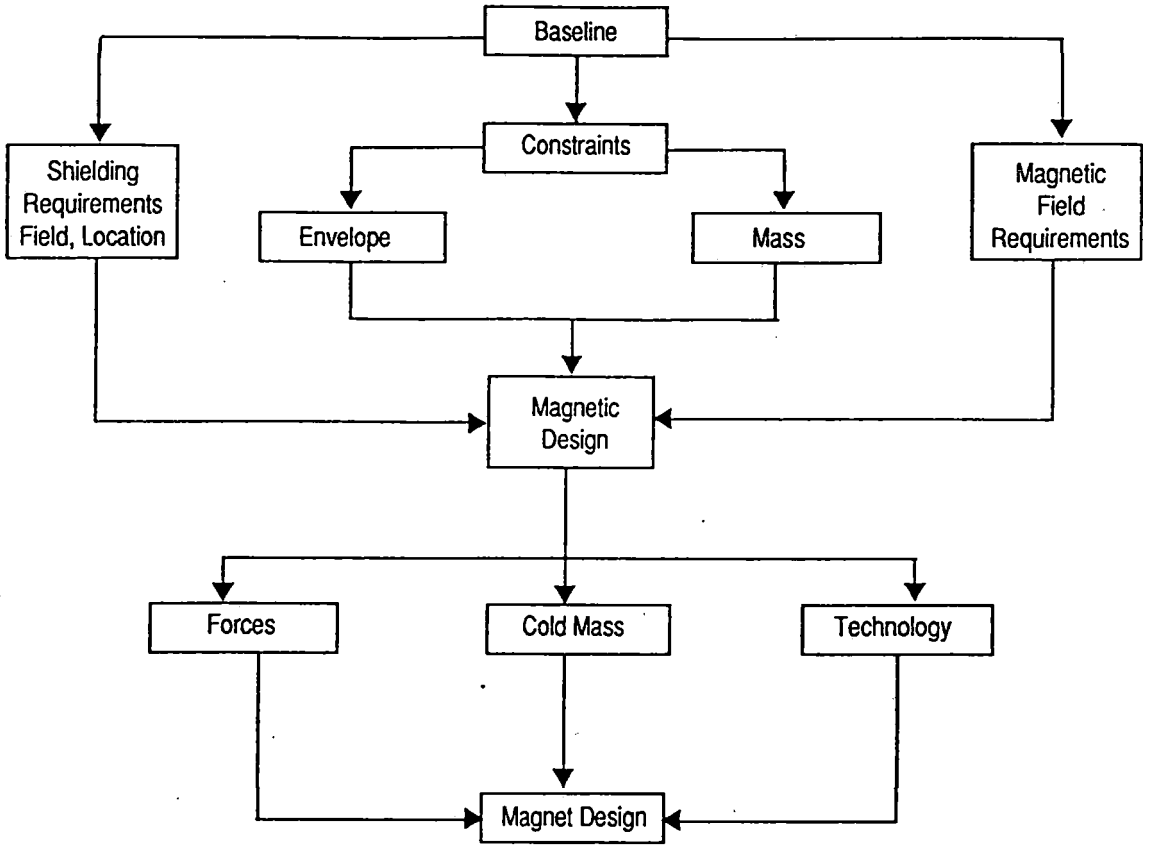

Conceptual Design Process for Passive Shielding of the Magnetic Fields

Figure 2-6

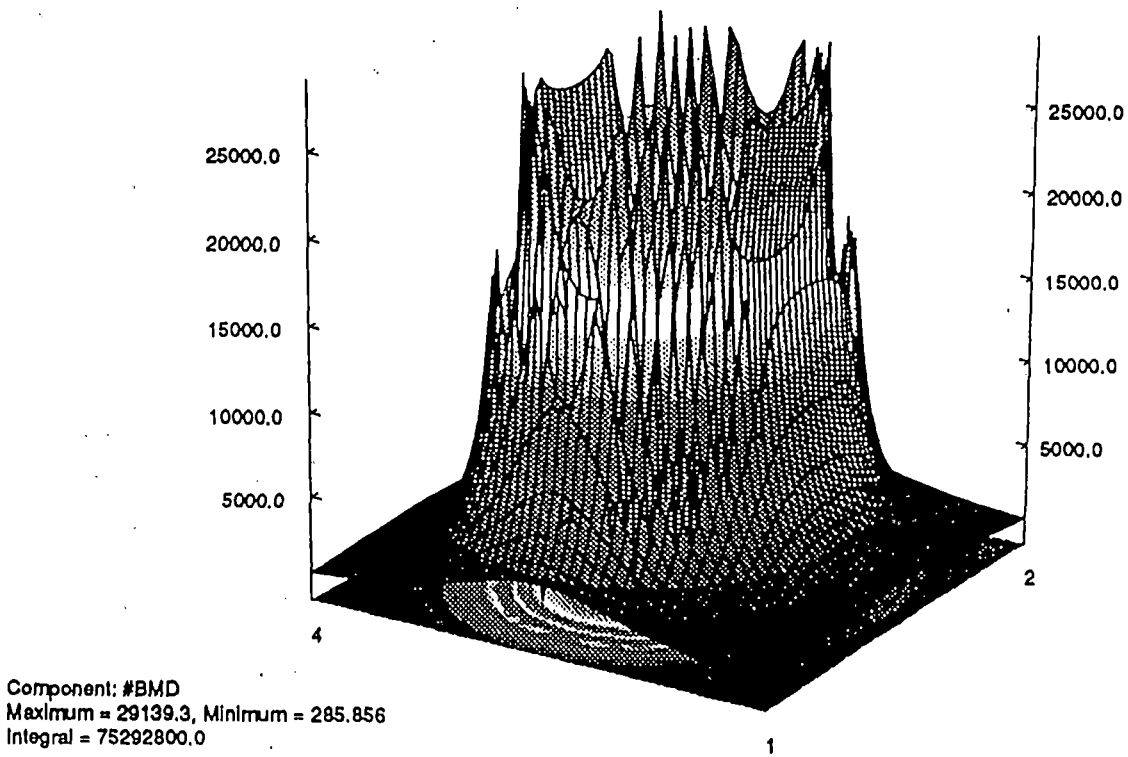

B_z component of the field of the racetrack coil

Figure 2-7

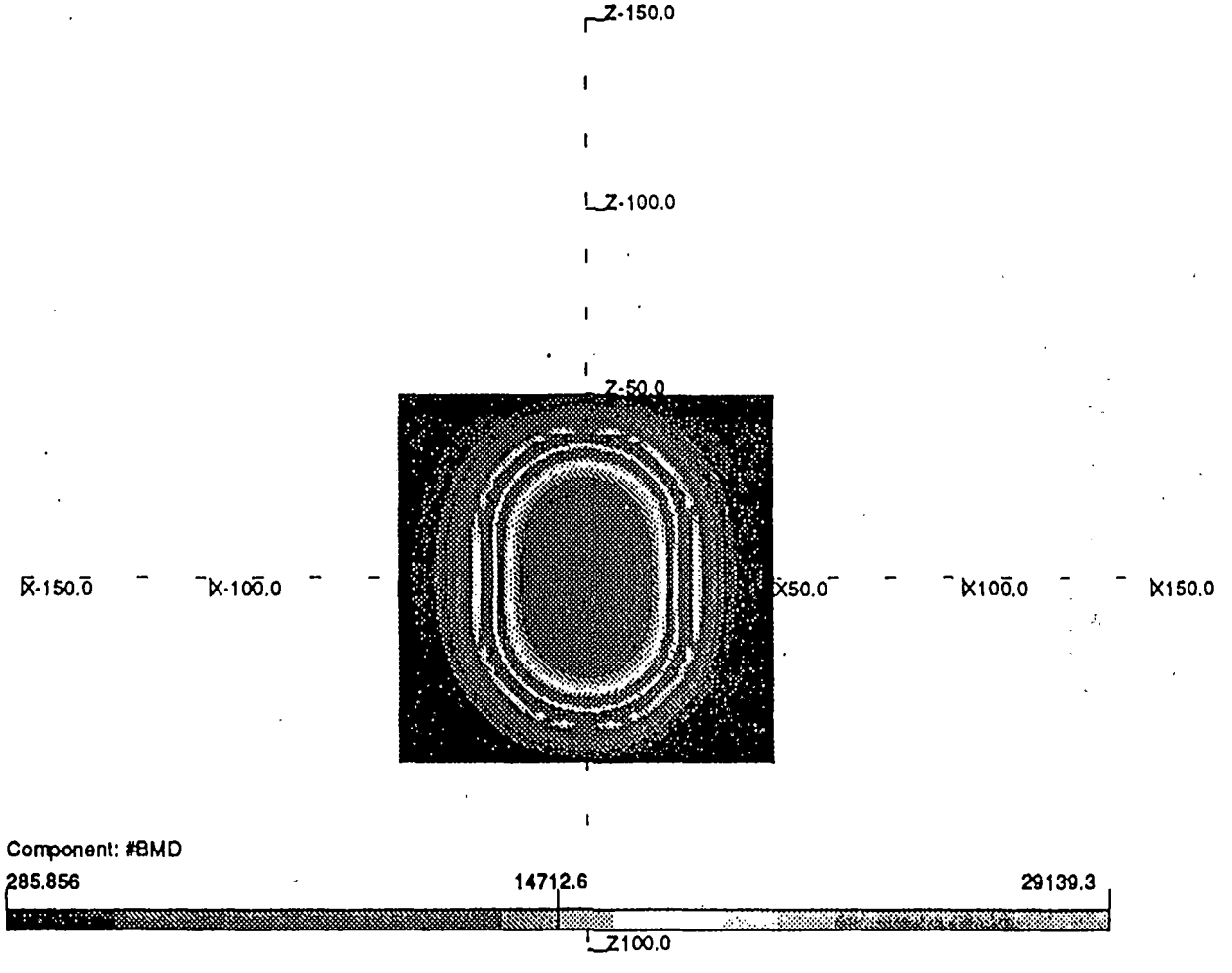

Field map in the xy plane

Figure 2-8

thin wire approximation as compared to a coil with finite cross section. The accuracy of the thin wire approximation was found to be within 1%.

Finite Element Study of the Racetrack Coil

The forces and fields on the superconductors in the propulsion coil have also been calculated using a commercial finite element software package sold by Vector Fields. The program used in this work is Tosca, which is useful for computing static or slowly varying AC fields.

The finite element calculation agrees well with previous magnetic field calculations using analytic methods. This confirmation is valuable since we can use either method with confidence in future analyses. It is particularly valuable to have an independent confirmation of the finite element method.

Fields and self forces were calculated at the circumference of the racetrack coil. Calculations were done for 400 kAT and 600 kAT. Fields and self forces are shown in Tables 2-1 and 2-2.

2.2 Emergency Forces and Fields

All the formulae used to calculate forces and fields will also be used to calculate emergency forces and fields.

2.3 Conductor and Coil Design

Conductor designs have been completed for propulsion coils with Nb_3Sn, NbTi, and high T_c compounds. Two stability criteria were used in the designs: cryostability and adiabatic stability. Cryostability criteria are usually most conservative and expensive in terms of space and material utilization, but usually produce coils with the highest operating margin.

Table 2-1

Peak Field in a 600 kAT Propulsion Coil Using TOSCA

Coil Data

Coil Shape:	Racetrack	Reinforcement Thickness (in.):	0.005
Jc (A/mm^2 @5.3T):	2900	Current Density (A/cm^2):	12265.41
Transport Current (A):	100	Total Ampereturns (Aturns):	603000
Conductor Dimension (mm^2):	0.232324	Coil Cross-Section S (cm):	6.9 x 6.9
Coil Size (cm^2):	47.61	Width (cm):	6.9
Layers:	90	Height (cm):	6.9
Turns (turns/layer):	67	Racetrack Width (cm):	57
Packing Factor:	0.587	Racetrack Length (cm):	80
Interlayer Thickness (in.):	0.003	Cu:Sc:	5.75:1
Insulation Thickness (in.):	0.0015		

Peak Field in Gauss on XZ plane (excluding coil neighbors and guideway fields)

Field along arc 0 0 33.1 21.6 0 11.5 arc radius = 21.6 cm

Coordinates		A/m^2		Gauss		
X	Z	Jx	Jz	Hy	Bm	Point
0	33.1	-12665.4	0	-39514.5	39514.5	0
3.378984	32.83407	-12509.5	1981.306	-39508.4	39508.4	1
6.674767	32.04282	-12045.5	3913.826	-39490.5	39490.5	2
9.806195	30.74574	-11285	5749.974	-39458.5	39458.5	3
12.69616	28.97477	-10246.5	7444.539	-39408.5	39408.5	4
15.27351	26.77351	-8955.79	8955.795	-39333.7	39333.7	5
17.47477	24.19616	-7444.54	10246.53	-39221.8	39221.8	6
19.24574	21.30619	-5749.97	11284.96	-39049.1	39049.1	7
20.54282	18.17477	-3913.83	12045.52	-38765.6	38765.6	8
21.22407	14.87898	-1981.31	12509.47	-38245.9	38245.93	9
21.6	11.5	4.28^{-11}	12665.41	-37121.4	37121.4	10

Table 2-1
(Continued)

Peak Field in a 600 kAT Propulsion Coil Using TOSCA

Field along line 21.6 0 11.5 21.6 0 0

Coordinates		A/m²		Gauss		
X	Z	Jx	Jz	Hy	Bm	Point
21.6	11.5	0	12665.41	-37121.4	37121.4	10
21.6	10.35	0	12665.41	-36632.9	36632.9	11
21.6	9.2	0	12665.41	-36272.1	36272.1	12
21.6	8.05	0	12665.41	-36004.5	36004.5	13
21.6	6.9	0	12665.41	-35803.4	35803.4	14
21.6	5.75	0	12665.41	-35651.9	35651.9	15
21.6	4.6	0	12665.41	-35538.7	35538.7	16
21.6	3.45	0	12665.41	-35456.7	35456.7	17
21.6	2.3	0	12665.41	-35401	35401	18
21.6	1.15	0	12665.41	-35368.7	35368.7	19
21.6	0	0	12665.41	-35358.1	35358.1	20

Table 2-2

Self Forces on 600 kAT Propulsion Coil

Coordinates		Newton/m³		Newton/cm		Lb/in	
X	Z	Fx	Fz	Fxu	Fzu	Fxu	Fzu
0	33.1	0	5.00^{8}	0	23827.24	0	13601.06
3.37894	32.83407	78278233	4.94^{8}	3726.827	23530.26	2127.346	13431.54
6.674767	32.04282	1.55^{8}	4.76^{8}	7358.551	22647.29	4200.406	12927.52
9.806195	30.74574	2.27^{8}	4.45^{8}	10802.01	21200.14	6166.001	12101.46
12.69616	28.97477	2.93^{8}	4.04^{8}	13967.73	19224.93	7973.057	10973.97
15.27351	26.77351	3.52^{8}	3.52^{8}	16771.31	16771.31	9573.397	9573.397
17.47477	24.19616	4.02^{8}	2.92^{8}	19133.85	13901.56	10921.98	7935.284
19.24574	21.30619	4.41^{8}	2.25^{8}	20980.18	10689.94	11975.9	6102.026
20.54282	18.17477	4.67^{8}	1.52^{8}	22231.57	7223.475	12690.22	4123.302
21.33407	14.87898	4.78^{8}	75776894	22778.36	3607.738	13002.34	2059.368
21.6	11.5	4.70^{8}	-1.6^{-6}	22384.2	-7.6^{-11}	12777.35	-4.3^{-11}
21.6	10.35	4.64^{8}	0	22089.64	0	12609.2	0
21.6	9.2	4.59^{8}	0	21872.08	0	12485.01	0
21.6	8.05	4.56^{8}	0	21710.71	0	12392.9	0
21.6	6.9	4.53^{8}	0	21589.45	0	12323.68	0
21.6	5.75	4.52^{8}	0	21498.1	0	12271.54	0
21.6	4.6	4.50^{8}	0	21429.84	0	12232.57	0
21.6	3.45	4.49^{8}	0	21380.39	0	12204.35	0
21.6	2.3	4.48^{8}	0	21346.8	0	12185.18	0
21.6	1.15	4.48^{8}	0	21327.33	0	12174.06	0
21.6	0	4.48^{8}	0	21320.93	0	12170.41	0

Adiabatically stabilized conductors usually produce a more efficient magnet design but are prone to training quenches. The term training quenches means that the superconducting wire has to be trained by gradually increasing the operating current. In subsequent quenches, the quench current is greater and greater until saturation.

The requirements which drive the conductor design include:

- the peak field at the winding
- the number of amp turns
- the normal operating current
- the coil size and geometry
- the insulation requirements
- the superconductor and its properties
- the matrix selection
- the coolant selection
- the reinforcement requirements from the self forces

The design outputs include:

- the conductor to current density
- the matrix to superconductor ratio
- the conductor dimensions
- the conductor mass and length

From this information one forms a coil design which has as its output:

- the coil cross section
- the number of turns
- the number of turns/layer
- the number of layers
- the inductance
- the coil energy

- for YBCO, Figure 2-9-3
- for Bismuth 2223, Figure 2-9-4

There are filament diameter limitations to satisfy cryostability conditions. They are shown for NbTi and Nb_3Sn in Figure 2-10. Data on the copper magneto resistivity effect are shown on Figure 2-11, which is typical of a matrix material.

The conductor and coil designs for 600 kAT propulsion coils are presented in Figures 2-12-1 through 2-12-10. Each figure describes coil dimensions, bundle cross section, conductor cross section, and all input and output data for different superconducting materials and different design models chosen. A summary of coil design is shown in Table 2-3.

NbTi

Conceptual magnet designs using commercially available NbTi conductor are shown in Figures 2-12-1 and 2-12-2. The conductor properties used in the study are the SSC type whose properties are listed in Figure 2-9-1. Note from Table 2-3 that the adiabatic coil is one of the smallest and most efficient in terms of weight and coil cross section. The adiabatic coils are usually potted in epoxy for added strength and reliability which is an additional advantage.

Nb_3Sn

The advantage of using Nb_3Sn for Maglev is that the critical temperature is higher so the coil should be more stable than for NbTi coils. We examined two types of coils in our studies, one adiabatic and one cryostable. Cryostable Nb_3Sn coils are usually encased, forced-flow, conductors, but for the purposes of analysis we assumed an ideal fully cryostable coil which may not be easily realized in practice, but gives us a baseline with which to make a comparison with other designs.

The coils are shown in Figure 2-12-3 and 2-12-4. Both coils are similar in size with their NbTi counterparts in Figures 2-12-1 and 2-12-2, because the current densities at low fields for Nb_3Sn are about the same as for NbTi. There is no advantage to Nb_3Sn in these configurations

since the Nb_3Sn conductor is more expensive and the coils are more expensive to fabricate using wind and react technologies.

A forced flow Nb_3Sn system has not been considered in this phase of the program. There may be some savings in refrigeration since the coil could be operated at a higher temperature using cooled He gas.

High T_c

Three high T_c superconductors were analyzed for Maglev propulsion and levitation coil applications. Some promising high T_c compounds operating at 77 K were examined in this analysis including thick film thallium compounds (TBCCO). A more practical compound is the bismuth compound (BSCCO) fabricated as a silver tape. This compound works best at 4.2 K as shown in Figure 2-9-4. The most ideal conductor would be a YBCO tape operating close to thin film values at 4.2 K, and a concept for comparison is shown in Figure 2-9-3.

The magnet designs summarized in Table 2-3 show that HTSC compounds operating at 77 K need to improve in performance to be attractive alternatives to LTSC operating at 4.2 K. BSCCO operating at 20 K may be an attractive alternative to LTSC if current density in the wire is traded for reduced refrigeration complexity. BSCCO is presently fabricated using silver. In today's market silver cost somewhat more than NbTi alloy rod. Improved current density, lower materials cost, or lower cost refrigeration approaches than can be practiced with LTSC will be required to make HTSC a competitive alternative.

AC Losses

The DC coil is under the influence of the AC current in the track windings. This creates AC losses in the coil. The losses were evaluated and are shown in Tables 2-4 and 2-5.

AC Losses Studies

Although in the conceptual design it is assumed that the AC losses in the superconductive magnet are negligible, a study was undertaken to assess the magnitude of these losses. At first we looked at low field effects. For this study the assumptions concerning the nature of the eddy current source and coil were as follows:

- The magnetic field is self field only.
- Continuous $\pm 20\%$ variation of the control current about steady state at 10 Hz.
- The actual operating spectrum is required to estimate average loss over time.
- Winding current density is 25% of critical (15,000 A/cm^2).
- Extrapolation from loss data at 50 Hz and $\pm 100\%$ variation of magnetic field.

To extrapolate the data, we made further assumptions:

- AC losses per cycle are linear at low fields.
- AC losses per cycle are independent of frequency.

Note:

- These assumptions are valid at fields less than 0.5T.
- These assumptions are linear approximations of the Bean model and agree with data taken for typical superconductors.

The calculation proceeds as follows:

From the attached figure, the AC loss per cycle at 50 Hz and 0.5T is 10 kW/m^3. The energy loss per cycle is:

$$E_0 = (10 \text{ kW/m}^3) / (50 \text{ Hz}) = 200 \text{ J/m}^3$$

The total power loss at any frequency scales with frequency and field and is given by:

$P_0 = E_0 (f/f_0) (B/B_0)$

where $E_0 = 200$ J

$f_0 = 50$ Hz

$B_0 = 0.5$T

Simplifying:

$P = 400\ B \cdot f$ W/m^3, where B is in Tesla and f is in Hz

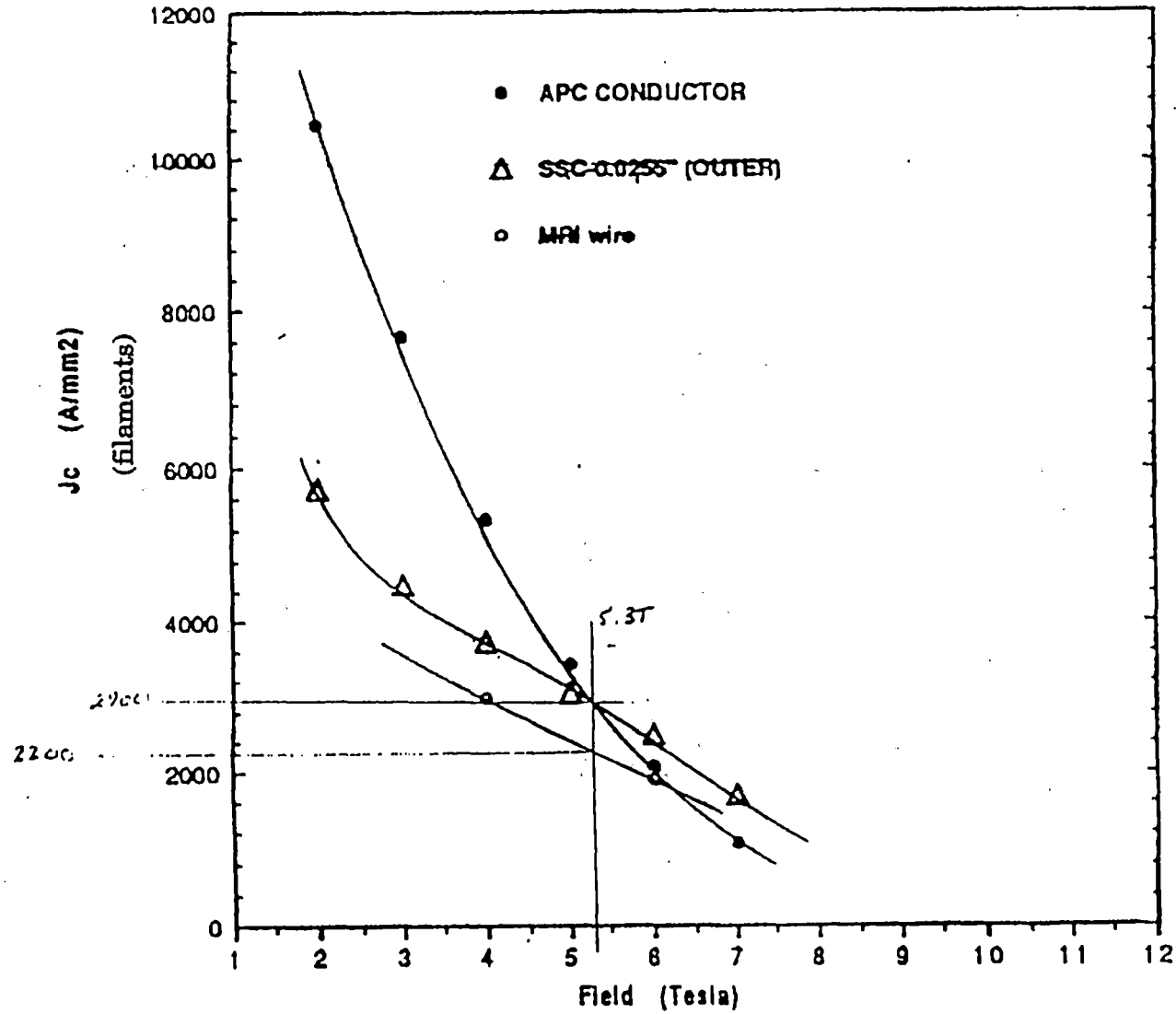

Field dependence of the critical current (NbTi)

Figure 2-9-1

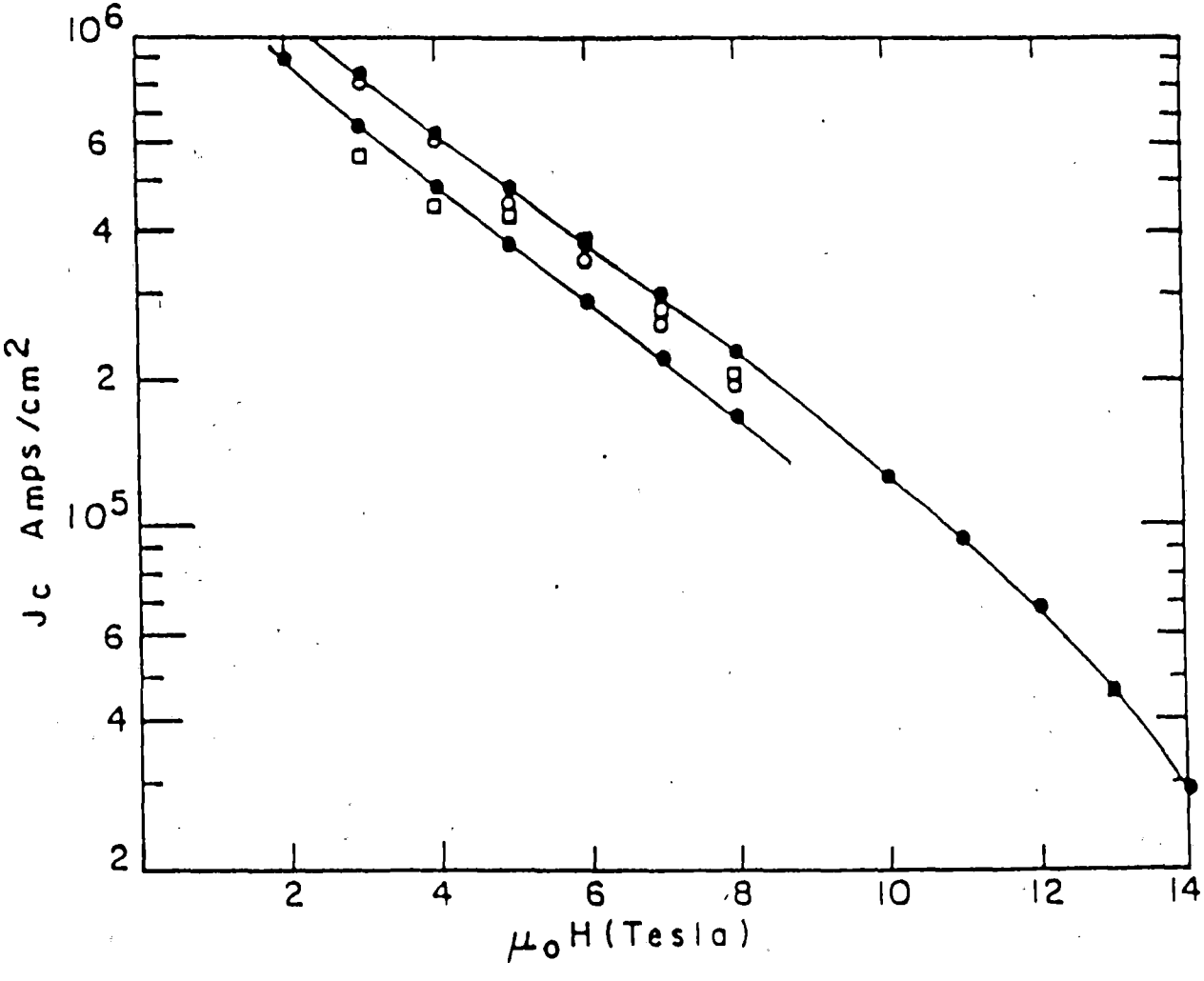

Field dependence of the critical current (Nb_3Sn)

Figure 2-9-2

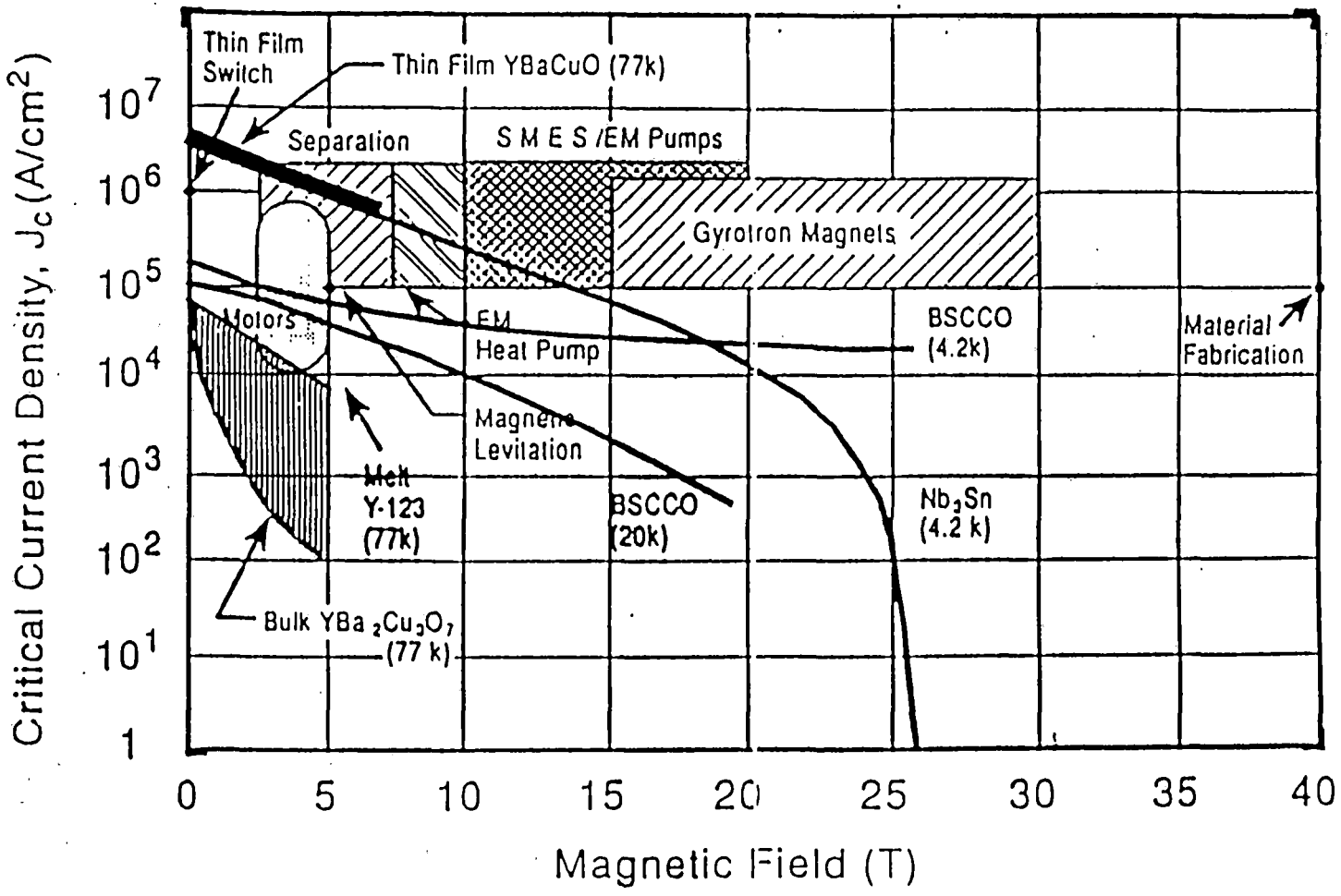

Estimated target critical current density vs. magnetic field values for various superconducting applications

Figure 2-9-3

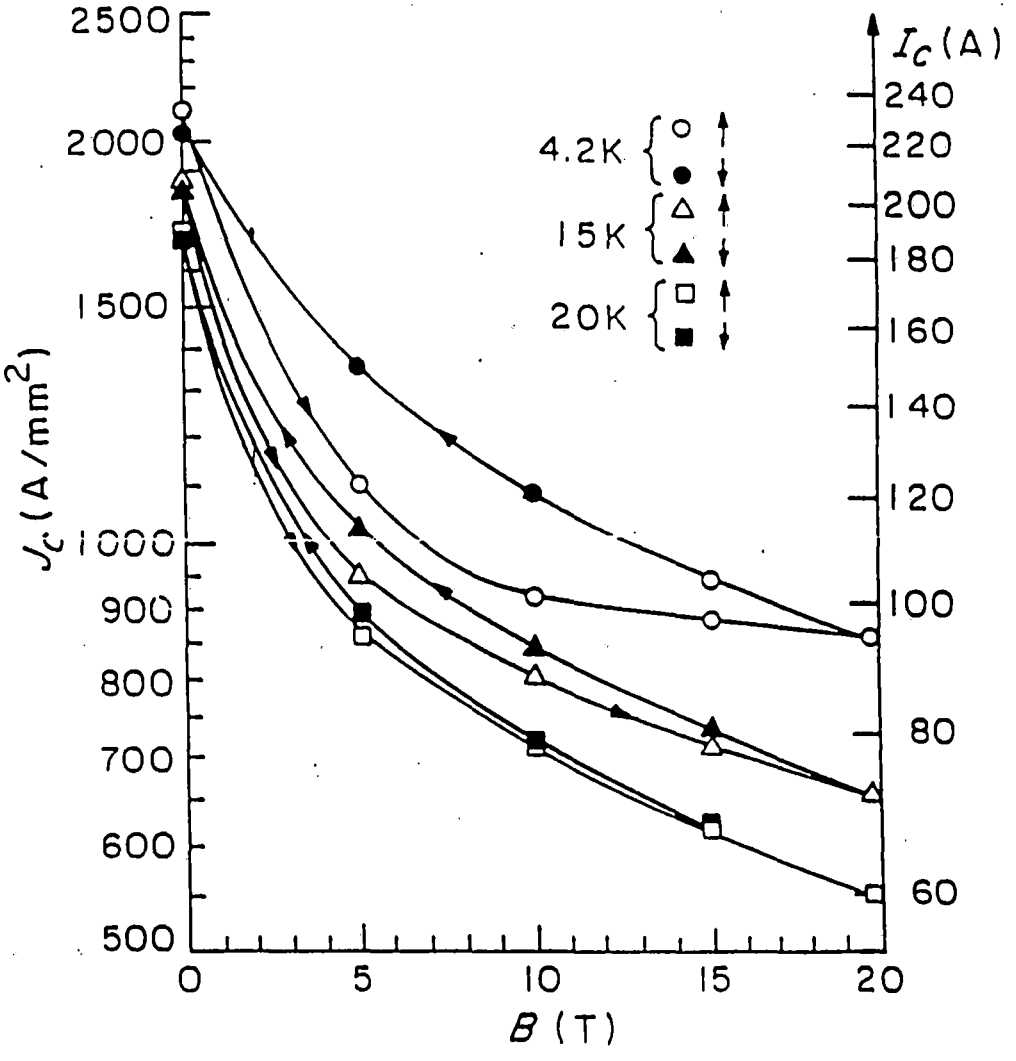

Field dependence of the critical current (Bismuth 2223)

Figure 2-9-4

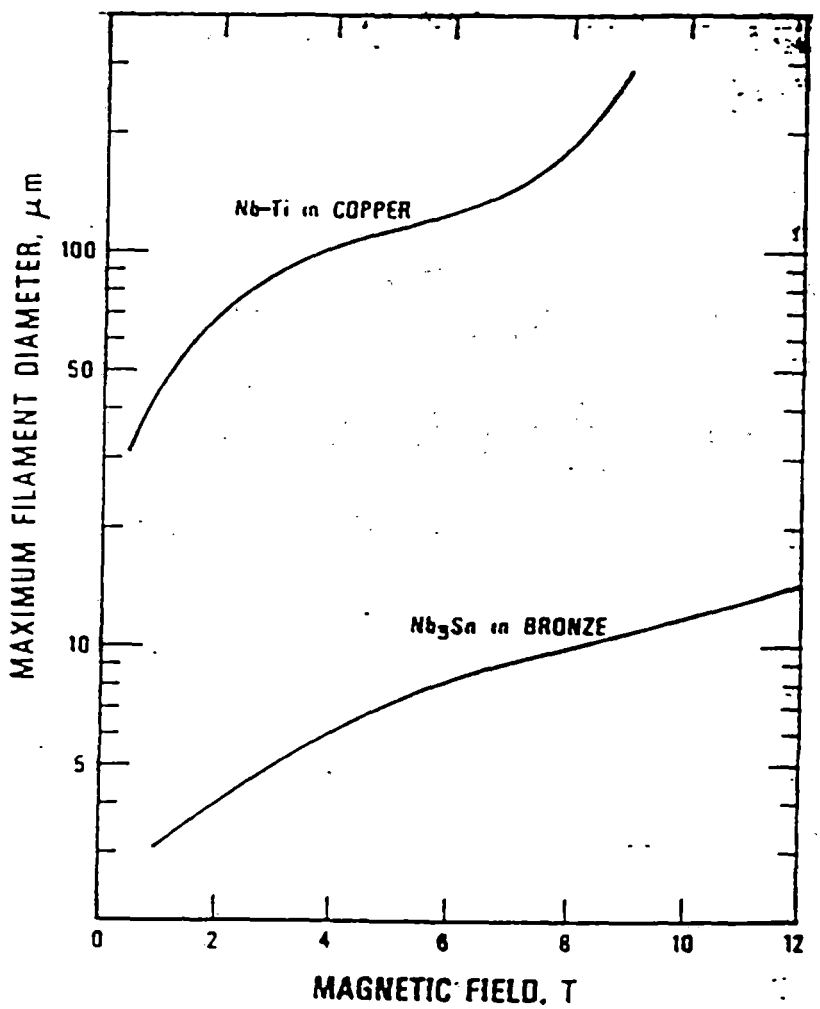

Filament diameter limits for achieving flux-jump stability in Nb-Ti and Nb_3Sn conductors, calculated using the dynamic stability criterion.

Figure 2-10

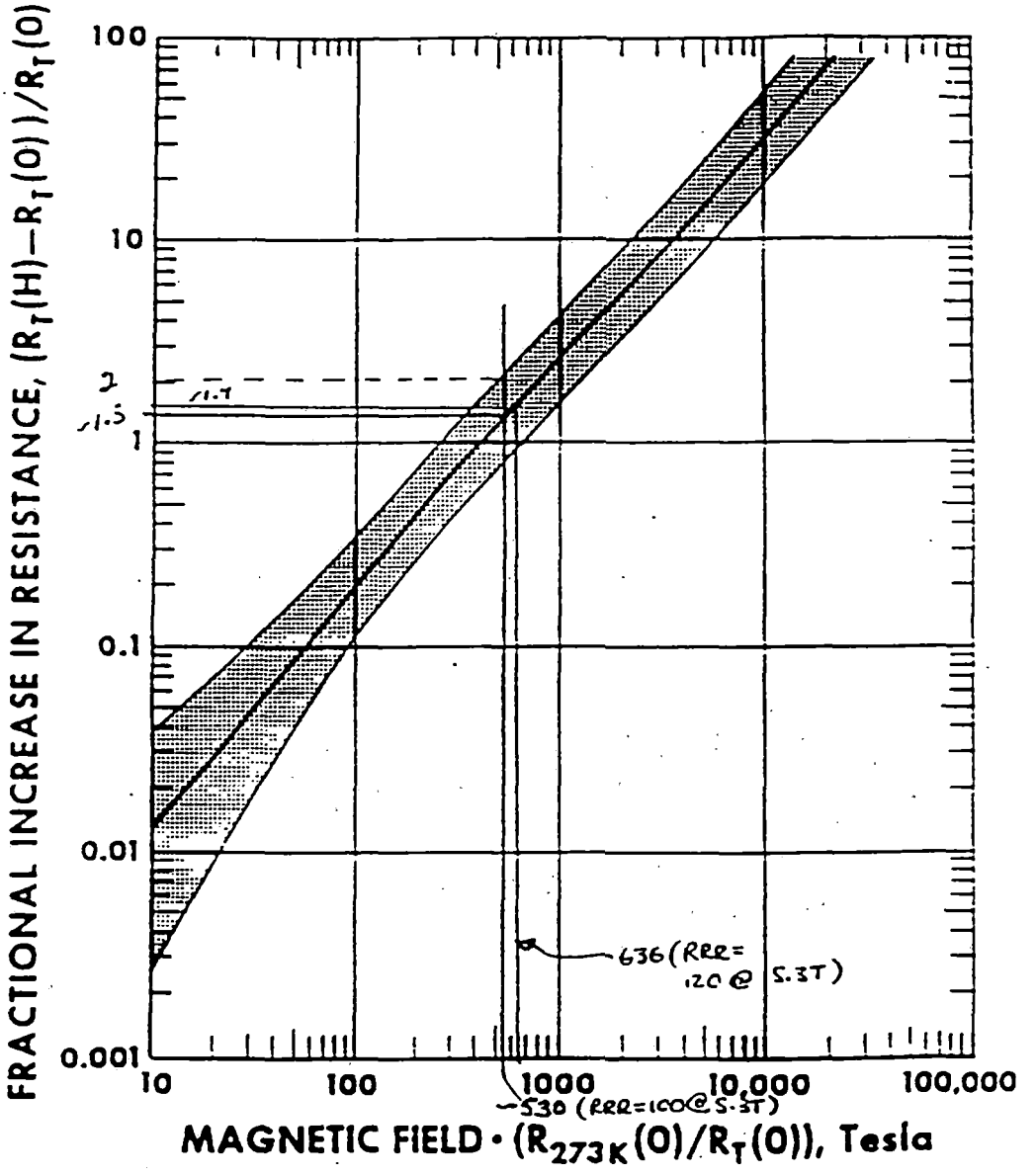

Average curve (heavy line) of the fractional change in electrical resistivity with transverse magnetic field. The uncertainty estimated from the variance of the data is shown by the shaded band.

Figure 2-11

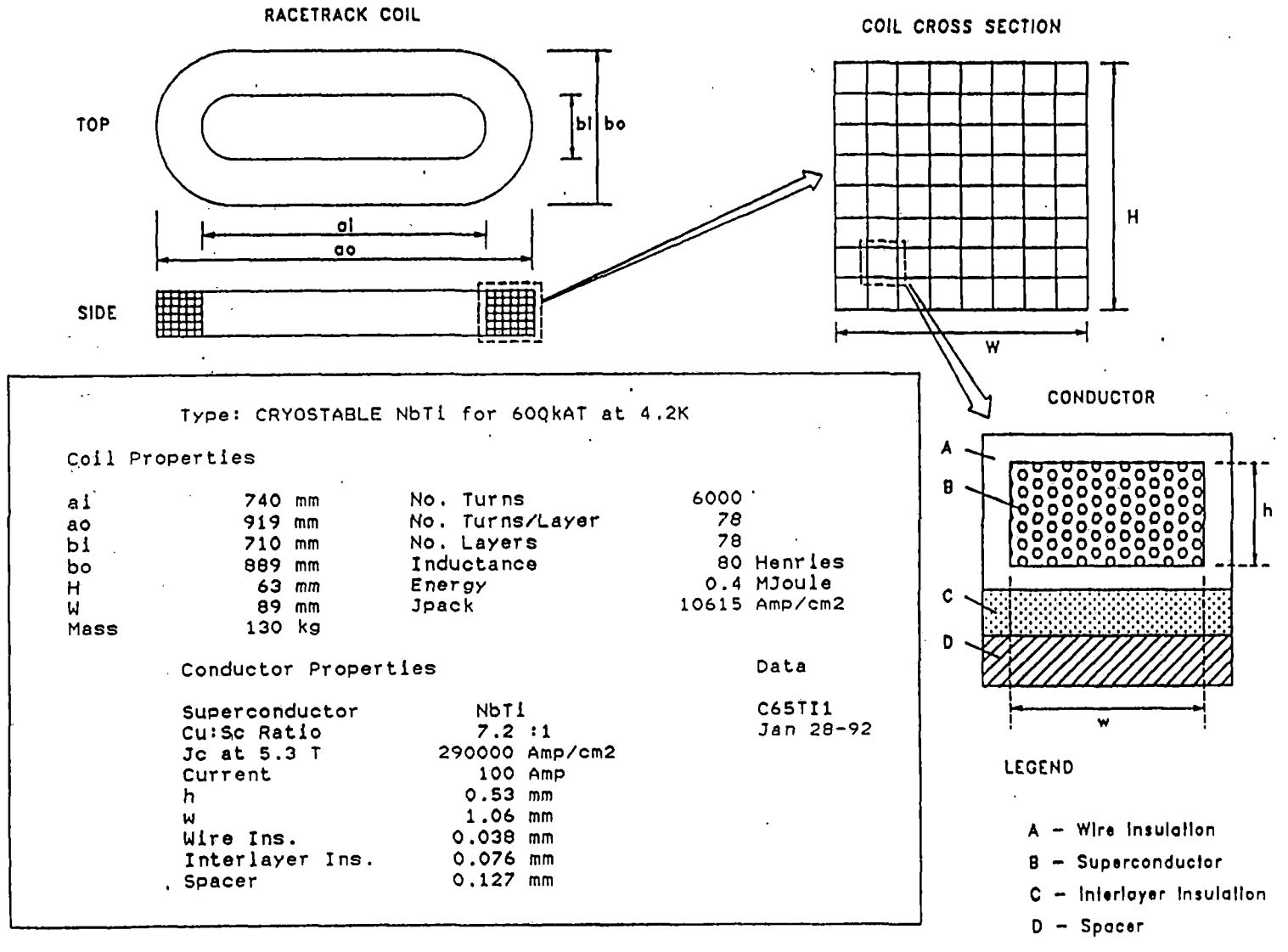

Type: CRYOSTABLE NbTi for 600kAT at 4.2K

Coil Properties

ai	740 mm	No. Turns	6000	
ao	919 mm	No. Turns/Layer	78	
bi	710 mm	No. Layers	78	
bo	889 mm	Inductance	80	Henries
H	63 mm	Energy	0.4	MJoule
W	89 mm	Jpack	10615	Amp/cm2
Mass	130 kg			

Conductor Properties		Data
Superconductor	NbTi	C65TI1
Cu:Sc Ratio	7.2 :1	Jan 28-92
Jc at 5.3 T	290000 Amp/cm2	
Current	100 Amp	
h	0.53 mm	
w	1.06 mm	
Wire Ins.	0.038 mm	
Interlayer Ins.	0.076 mm	
Spacer	0.127 mm	

Conductor and coil design parameters (NbTi – cryostable)
Figure 2-12-1

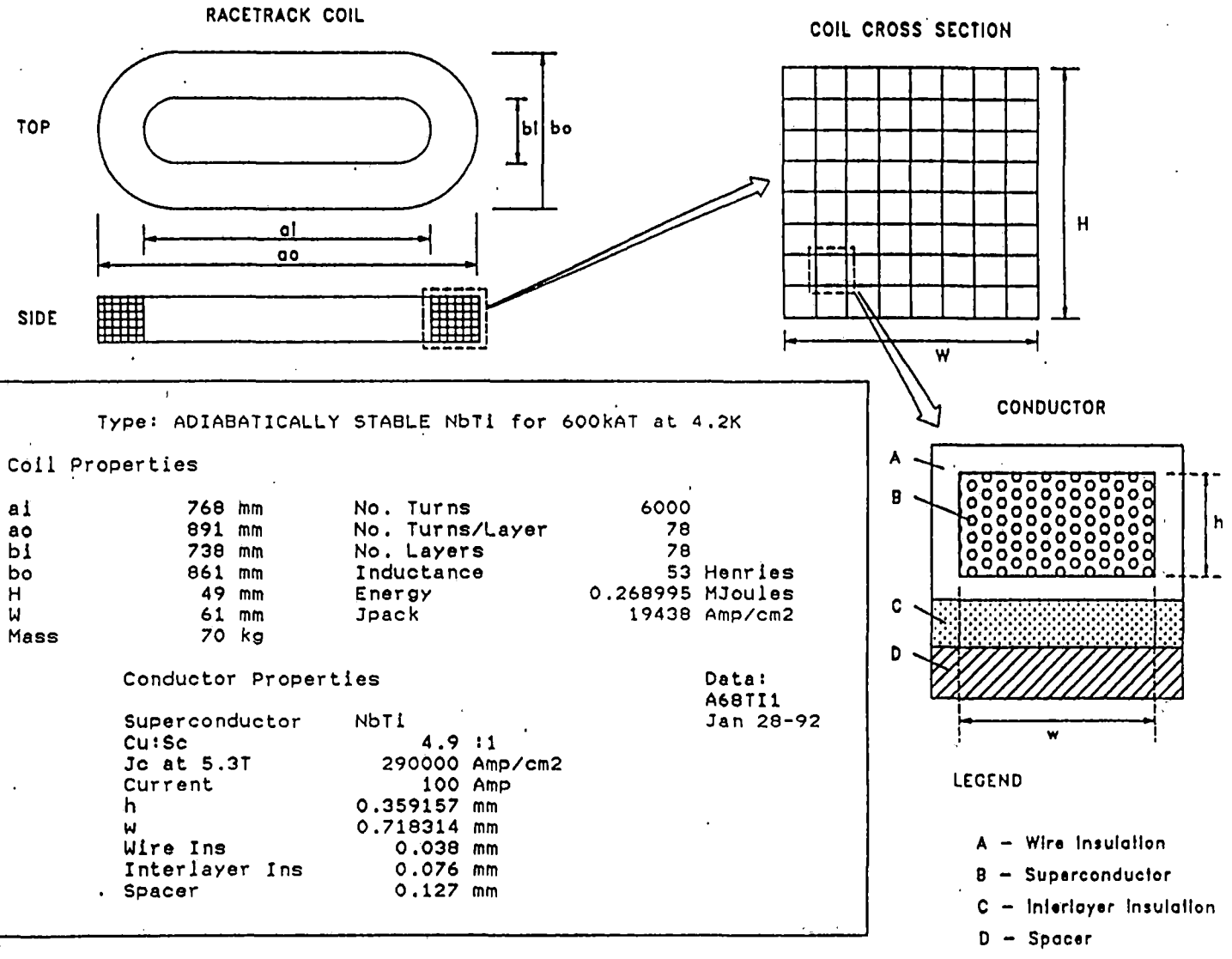

Type: ADIABATICALLY STABLE NbTi for 600kAT at 4.2K

Coil Properties

ai	768 mm	No. Turns	6000	
ao	891 mm	No. Turns/Layer	78	
bi	738 mm	No. Layers	78	
bo	861 mm	Inductance	53	Henries
H	49 mm	Energy	0.268995	MJoules
W	61 mm	Jpack	19438	Amp/cm2
Mass	70 kg			

Conductor Properties

Data: A68TI1 Jan 28-92

Superconductor	NbTi	
Cu:Sc	4.9	:1
Jc at 5.3T	290000	Amp/cm2
Current	100	Amp
h	0.359157	mm
w	0.718314	mm
Wire Ins	0.038	mm
Interlayer Ins	0.076	mm
Spacer	0.127	mm

Conductor and coil design parameters (NbTi – adiabatic)

Figure 2-12-2

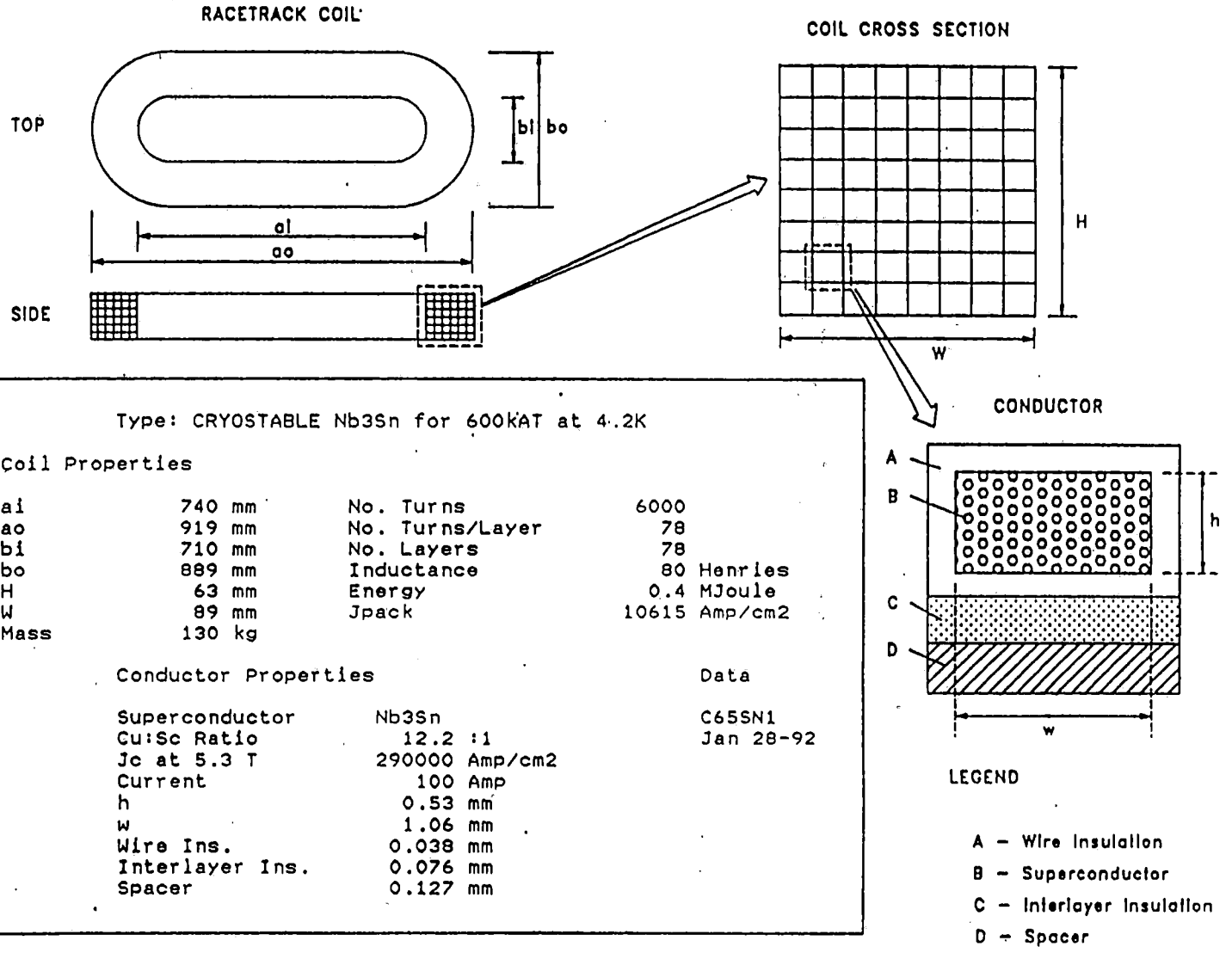

Type: CRYOSTABLE Nb3Sn for 600kAT at 4.2K

Coil Properties

ai	740 mm	No. Turns	6000	
ao	919 mm	No. Turns/Layer	78	
bi	710 mm	No. Layers	78	
bo	889 mm	Inductance	80	Henries
H	63 mm	Energy	0.4	MJoule
W	89 mm	Jpack	10615	Amp/cm2
Mass	130 kg			

Conductor Properties		Data
Superconductor	Nb3Sn	C65SN1
Cu:Sc Ratio	12.2 :1	Jan 28-92
Jc at 5.3 T	290000 Amp/cm2	
Current	100 Amp	
h	0.53 mm	
w	1.06 mm	
Wire Ins.	0.038 mm	
Interlayer Ins.	0.076 mm	
Spacer	0.127 mm	

Conductor and coil design parameters (Nb_3Sn – cryostable)
Figure 2-12-3

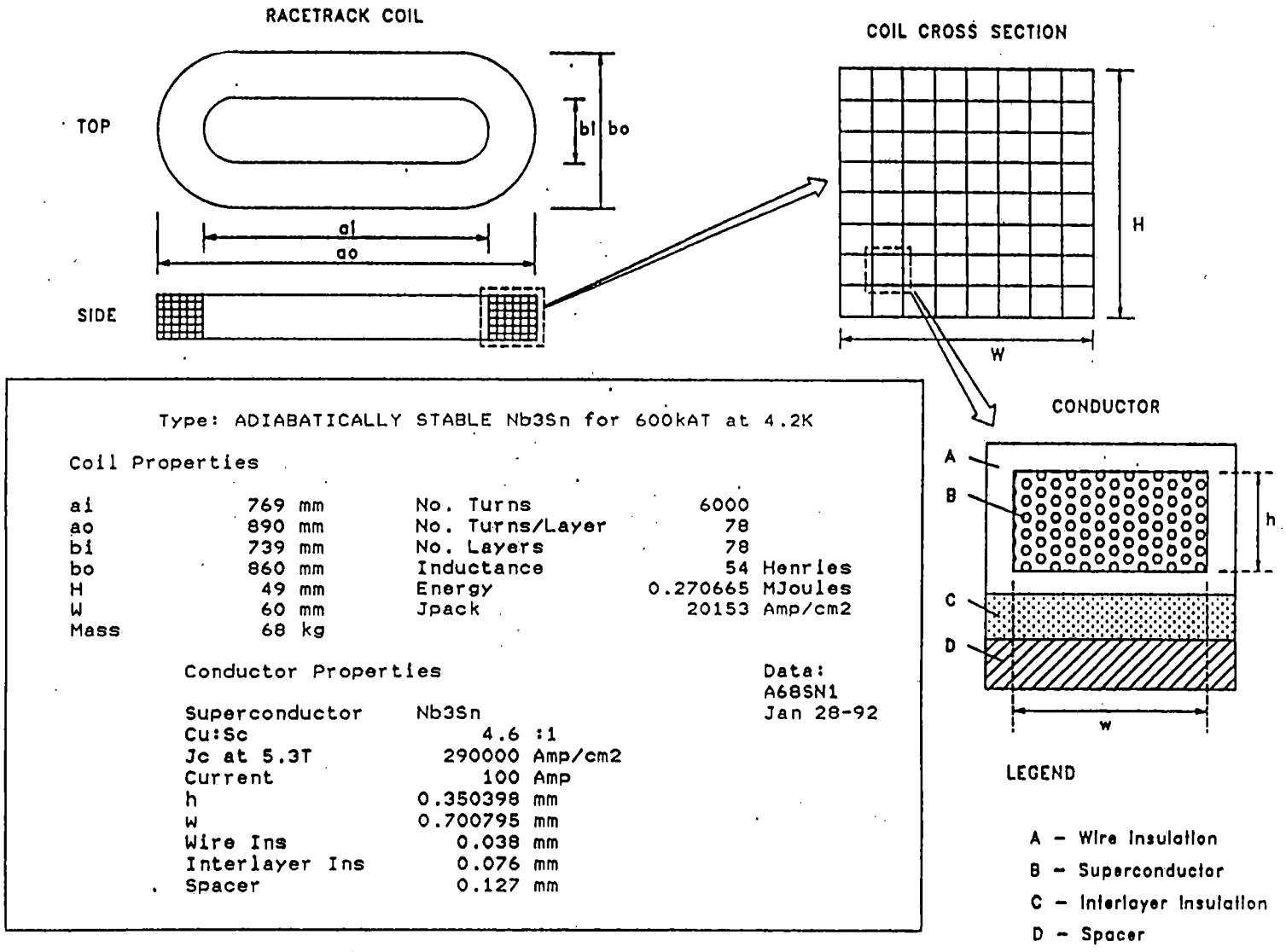

Type: ADIABATICALLY STABLE Nb3Sn for 600kAT at 4.2K

Coil Properties

ai	769 mm	No. Turns	6000	
ao	890 mm	No. Turns/Layer	78	
bi	739 mm	No. Layers	78	
bo	860 mm	Inductance	54	Henries
H	49 mm	Energy	0.270665	MJoules
W	60 mm	Jpack	20153	Amp/cm2
Mass	68 kg			

Conductor Properties

Data: A68SN1 Jan 28-92

Superconductor	Nb3Sn
Cu:Sc	4.6 :1
Jc at 5.3T	290000 Amp/cm2
Current	100 Amp
h	0.350398 mm
w	0.700795 mm
Wire Ins	0.038 mm
Interlayer Ins	0.076 mm
Spacer	0.127 mm

Conductor and coil design parameters (Nb_3Sn – adiabatic)
Figure 2-12-4

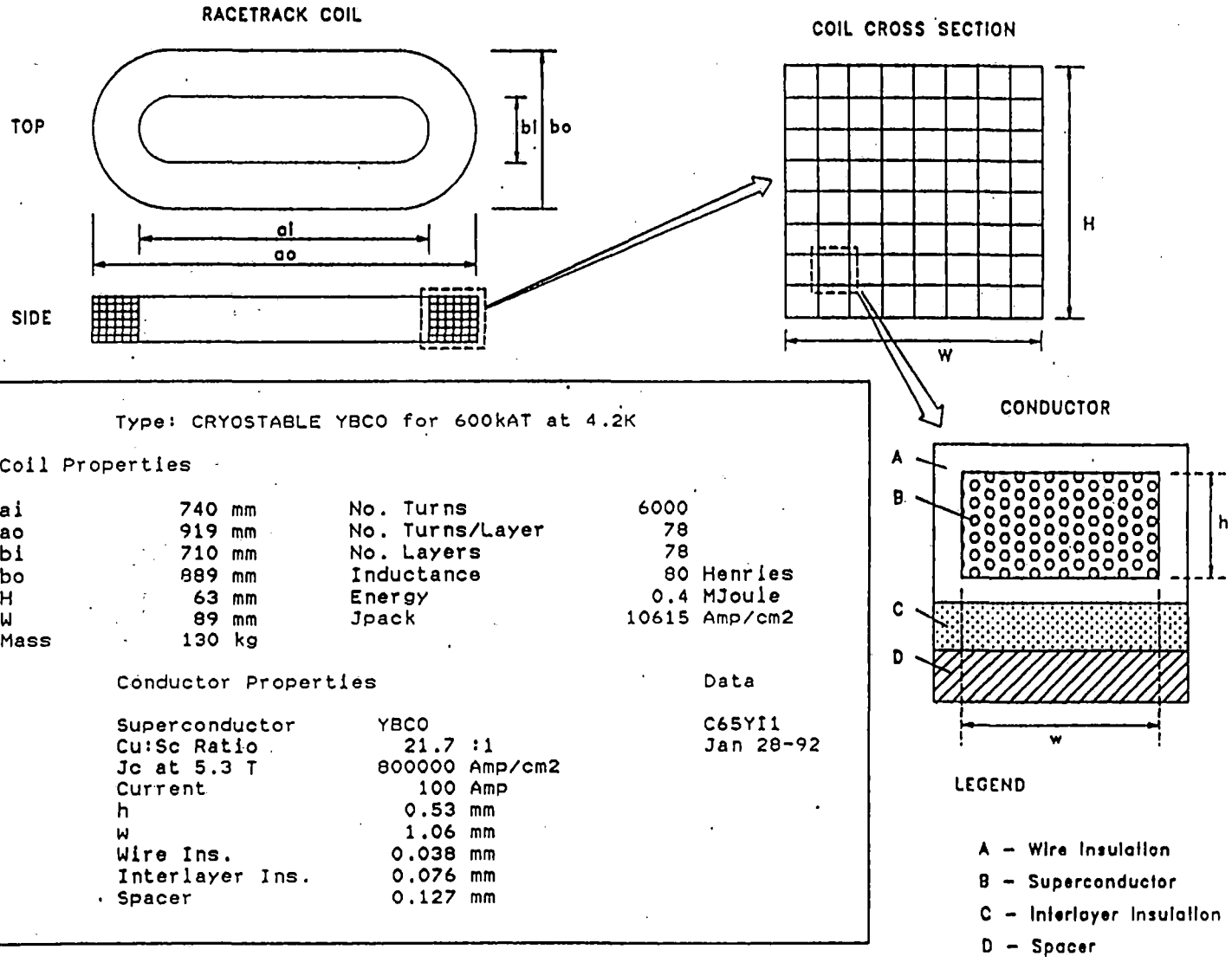

Type: CRYOSTABLE YBCO for 600kAT at 4.2K

Coil Properties

ai	740 mm	No. Turns	6000	
ao	919 mm	No. Turns/Layer	78	
bi	710 mm	No. Layers	78	
bo	889 mm	Inductance	80	Henries
H	63 mm	Energy	0.4	MJoule
W	89 mm	Jpack	10615	Amp/cm2
Mass	130 kg			

Conductor Properties		Data
Superconductor	YBCO	C65YI1
Cu:Sc Ratio	21.7 :1	Jan 28-92
Jc at 5.3 T	800000 Amp/cm2	
Current	100 Amp	
h	0.53 mm	
W	1.06 mm	
Wire Ins.	0.038 mm	
Interlayer Ins.	0.076 mm	
Spacer	0.127 mm	

Conductor and coil design parameters (YBCO – cryostable)

Figure 2-12-5

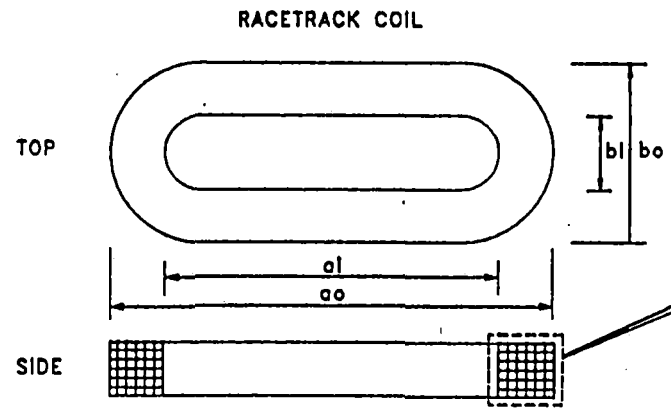

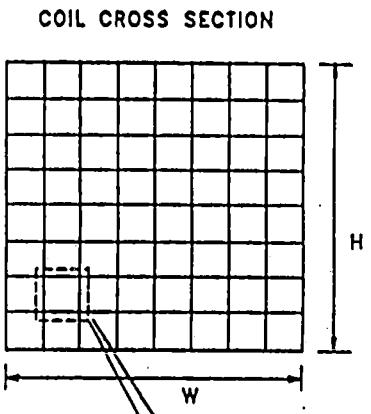

Type: ADIABATICALLY STABLE YBCO for 600KAT at 4.2K

Coil Properties

ai	772 mm	No. Turns	6000	
ao	887 mm	No. Turns/Layer	78	
bi	742 mm	No. Layers	78	
bo	857 mm	Inductance	54	Henries
H	47 mm	Energy	0.274705	MJoules
W	57 mm	Jpack	21987	Amp/cm2
Mass	73 kg			

Conductor Properties

Data: A68YI1 Jan 28-92

Superconductor	YBCO
Cu:Sc	12.9 :1
Jc at 5.3T	800000 Amp/cm2
Current	100 Amp
h	0.329943 mm
w	0.659886 mm
Wire Ins	0.038 mm
Interlayer Ins	0.076 mm
Spacer	0.127 mm

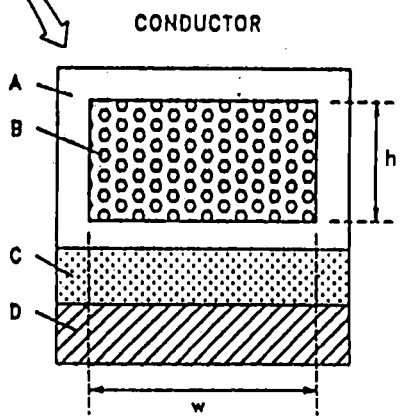

LEGEND

A – Wire Insulation
B – Superconductor
C – Interlayer Insulation
D – Spacer

Conductor and coil design parameters (YBCO – adiabatic)

Figure 2-12-6

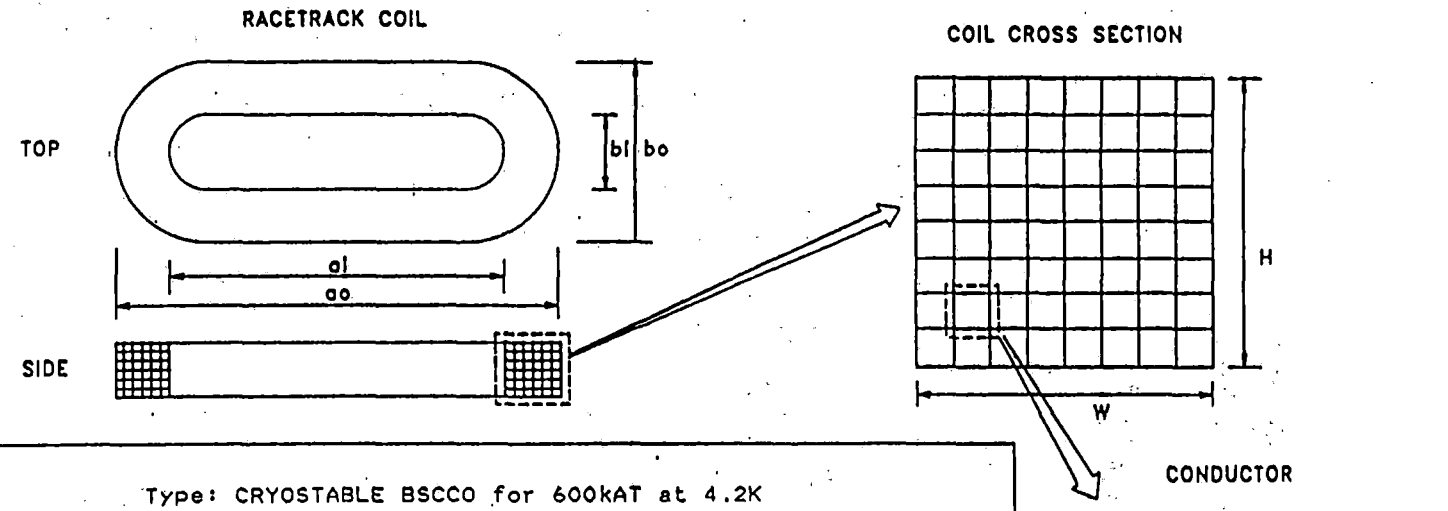

Type: CRYOSTABLE BSCCO for 600kAT at 4.2K

Coil Properties

ai	668 mm	No. Turns	6000	
ao	991 mm	No. Turns/Layer	19	
bi	638 mm	No. Layers	347	
bo	961 mm	Inductance	67	Henries
H	132 mm	Energy	0.335	MJoule
W	161 mm	Jpack	2807	Amp/cm2
Mass	578 kg			

Conductor Properties		Data
Superconductor	BSCCO	C65BI1
Ag:Sc ratio	3.7 :1	Jan 29-92
Jc at 5.3 T	110000 Amp/cm2	
Current	100 Amp	
h	0.1 mm	
w	8.43 mm	
Wire Ins.	0.038 mm	
Interlayer Ins.	0.076 mm	
Spacer	0.127 mm	

Conductor and coil design parameters (Bismuth 2223 – cryostable)

Figure 2-12-7

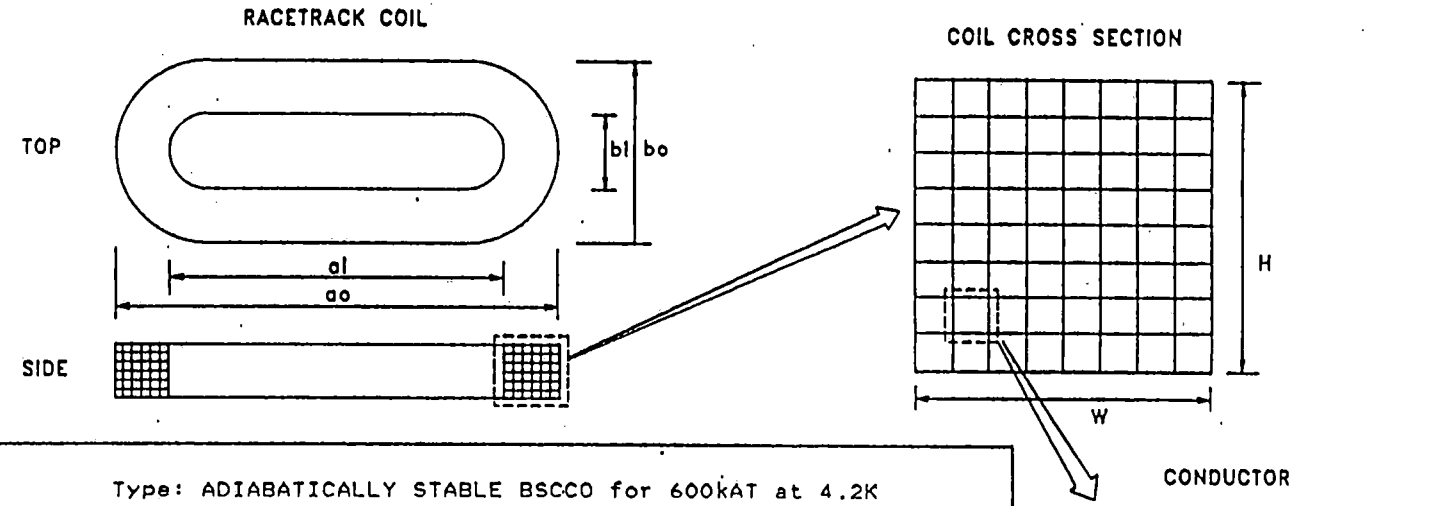

Type: ADIABATICALLY STABLE BSCCO for 600kAT at 4.2K

Coil Properties

ai	473 mm	No. Turns	6000
ao	1186 mm	No. Turns/Layer	78
bi	443 mm	No. Layers	78
bo	1156 mm	Inductance	43 Henries
H	26 mm	Energy	0.21797 MJoules
W	356 mm	Jpack	6467 Amp/cm2
Mass	250 kg		

Conductor Properties

Data: A68BI2 Jan 28-92

Superconductor	BSCCO
Ag:SC	1.1 :1
Jc at 5.3T	110000 Amp/cm2
Current	100 Amp
h	0.05397 mm
w	4.497492 mm
Wire Ins	0.038 mm
Interlayer Ins	0.076 mm
Spacer	0.127 mm

Conductor and coil design parameters (Bismuth 2223 – adiabatic)

Figure 2-12-8

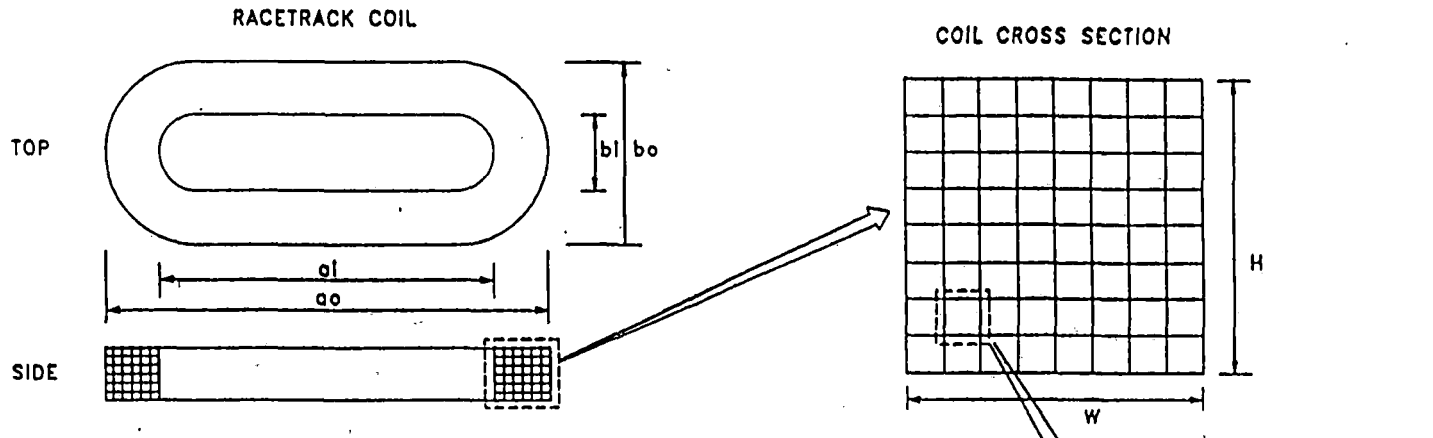

Type: CRYOSTABLE TBCCO for 600kAT at 4.2K

Coil Properties

ai	732 mm	No. Turns	6000	
ao	927 mm	No. Turns/Layer	78	
bi	702 mm	No. Layers	78	
bo	897 mm	Inductance	78	Henries
H	67 mm	Energy	0.39	MJoule
W	97 mm	Jpack	9175	Amp/cm2
Mass	176 kg			

Conductor Properties		Data
Superconductor	TBCCO	C65TL1
Cu:Sc Ratio	2.4 :1	Jan 24-92
Jc at 5.3 T	100000 Amp/cm2	
Current	100 Amp	
h	0.58 mm	
w	1.16 mm	
Wire Ins.	0.038 mm	
Interlayer Ins.	0.076 mm	
Spacer	0.127 mm	

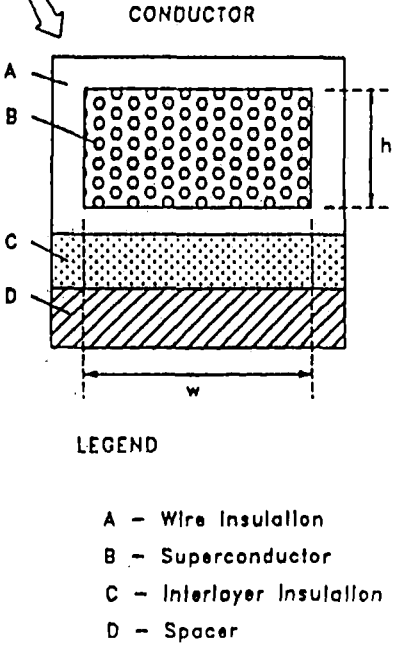

Conductor and coil design parameters (TBCCO – cryostable)

Figure 2-12-9

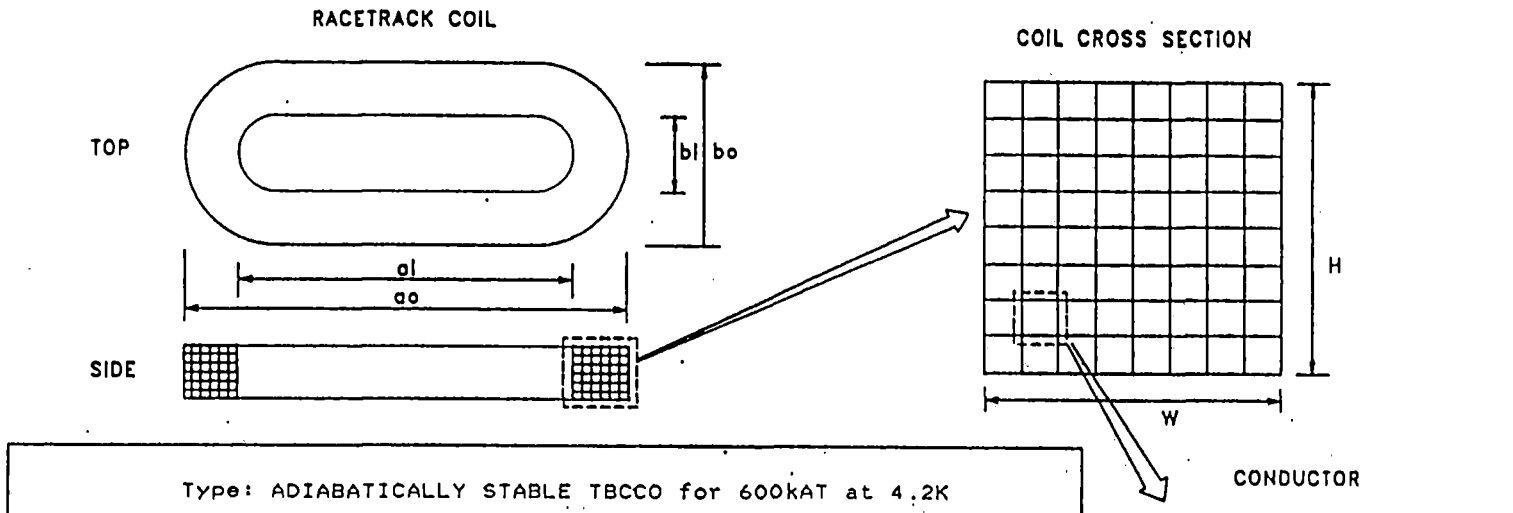

Type: ADIABATICALLY STABLE TBCCO for 600kAT at 4.2K

Coil Properties

ai	767 mm	No. Turns	6000	
ao	892 mm	No. Turns/Layer	78	
bi	737 mm	No. Layers	78	
bo	862 mm	Inductance	53	Henries
H	50 mm	Energy	0.268525	MJoules
W	62 mm	Jpack	19242	Amp/cm2
Mass	84 kg			

Conductor Properties

Data: A68TL1 Jan 28-92

Superconductor	TBCCO
Cu:Sc	1 :1
Jc at 5.3T	100000 Amp/cm2
Current	100 Amp
h	0.361649 mm
w	0.723299 mm
Wire Ins	0.038 mm
Interlayer Ins	0.076 mm
Spacer	0.127 mm

Conductor and coil design parameters (TBCCO – adiabatic)

Figure 2-12-10

Table 2-3

Summary of 600 kA Propulsion Coil Designs

Superconductor	Coil Temp. (K)	Matrix	Stability	Matrix to Superconductor	Critical Current Density (A/cm^2)	Average Current Density (A/cm^2)	Cross Section (cm^2)	Mass (kg)
NbTi	4.2	Cu	cryostable	7.2:1	290,000	10,615	56.07	130
NbTi	4.2	Cu	adiabatic	4.9:1	290,000	19,438	29.89	70
Nb_3Sn	4.2	Cu	cryostable	12.2:1	290,000	10,615	56.07	130
Nb_3Sn	4.2	Cu	adiabatic	4.6:1	290,000	20,153	29.40	68
YBCO	4.2	Cu	cryostable	21.7:1	800,000	10,615	56.07	130
YBCO	4.2	Cu	adiabatic	12.9:1	800,000	21,987	26.79	73
BSCCO	4.2	Ag	cryostable	3.7:1	110,000	2,807	212.52	578
BSCCO	4.2	Ag	adiabatic	1.1:1	110,000	6,467	92.56	250
TBCCO	4.2	Cu	cryostable	2.4:1	100,000	9,175	64.99	176
TBCCO	4.2	Cu	adiabatic	1.0:1	100,000	19,242	31.00	84
TBCCO	77	Cu	cryostable	0.0:1	10,000	3,180	186.56	510
TBCCO	77	Cu	adiabatic	0.0:1	10,000	5,561	107.07	291

Table 2-4

AC Loss Conditions

Ampere Turns	B_{max} (Tesla) Bundle Dia.		AC Field (Tesla) Bundle Dia.	Conductor Bundle Cross Section	Conductor Volume	
kA	10 cm	20 cm	10 cm	20 cm	(cm^2)	(m_3)
100	.4	.2	.08	.04	6.67	6.67×10^{-4}
200	.8	.4	.16	.08	13.3	1.33×10^{-3}
300	1.2	.6	.24	.12	20	2×10^{-3}
400	1.6	.8	.32	.16	26.7	2.67×10^{-3}
500	2	1	.40	.20	33.3	3.33×10^{-3}

- B_{max} is the peak DC field at the winding.
- AC Field is the peak AC field at the winding. AC Field is 20% of B_{max}.
- Turn length = 1 m.
- Conductor current density = 15,000 A/cm^2 (25% of J_c).

Table 2-5

AC Losses

Ampere Turns	AC Loss/Volume (kW/m^3) Bundle Diameter		AC Loss (W) Bundle Diameter	
kA	10 cm	20 cm	10 cm	20 cm
100	.320	.16	.21	.105
200	.64	.32	.85	.425
300	.96	.48	1.92	.96
400	1.28	.64	3.42	1.71
500	1.6	.8	5.33	2.66

- Data is extrapolated from known losses at 50 Hz, 0.5T.
- Losses assume DC field in the magnet is zero.

2.3.1 Near Term Capabilities of High Critical Temperature Superconductor Magnets and Transmission Lines

For power applications only two classes of the new oxide materials appear to have promise when large quantities of material are required. These families based on rare earth and bismuth perovskites have as their most common members $YBa_2Cu_3O_{7-x}$(YBCO) and $Bi_2Sr_2Ca_1Cu_2O_{8+x}$ or $Bi_2Sr_2Ca_2Cu_3O_{10+x}$(BSCCO). The thallium-based oxides are not considered here largely because of the scarcity of thallium and their near universal use in thin film applications.

The great challenge in using oxide superconductors has been to improve their critical currents in high magnetic fields, electrical contact characteristics, and mechanical characteristics. Without adequate electrical and mechanical properties, bulk-processed, oxide superconductors cannot be used in practical power applications.

Most of these challenges have been met by using microcomposite structures that mix a normal metal like silver with the superconducting oxide. Below is a description of how conventionally processed oxide-superconductor and metal-oxide-superconductor microcomposites are being developed by the oxide superconductor community.

The Present State of Conductor Development - BSCCO

The issues involved in wire, magnet, and cable development and manufacture (e.g., oxide powder production, wire shaping, wire annealing treatments and microstructure development, wire bundling techniques, etc.) are being solved.

BSCCO - Recent Results

The bismuth family of superconductors has shown the most promise to date for high-field power applications like Maglev. Most BSCCO work is oxide- or metal-precursor powder-in-silver-tube with subsequent deformation and heat treating.[1] Since this is a relatively inexpensive

manufacturing technique which may be readily scaled to production quantities, this approach shows promise for high-field, high current density applications at low temperatures (10-40 K).

Silver is one of few metals that does not seriously degrade the electrical properties of copperoxide-based superconductors. Because oxygen diffusion through silver is relatively fast compared with oxygen diffusion through the superconducting oxides, silver may also aid in achieving the proper oxygen stoichiometry in copperoxide-based superconductors.[2,3] Thus, silver is a desirable metal for use in a superconducting oxide/metal composite.

Heine et al, and a variety of Japanese workers have demonstrated exciting results for BSCCO materials at 4 K. Recent results by Carter and Sandhage[4] shown in Figure 2-13, have shown similar results at 20 K. The advent of a superconductor material which can handle currents higher than 10,000 A-cm^{-2} in fields higher than 20 Tesla leads to exciting prospects for the production of very high field magnets. From the viewpoint of Maglev, performance in the 10-40 K range at fields of 5-8 Tesla appears practical with the materials under development. Similar curves have been demonstrated for the other BSCCO compound $Bi_2Sr_2Ca_2Cu_3O_{8-x}$. It is anticipated that an additional order of magnitude in current density at high fields will be available in polycrystalline, bulk conductors within a few years. These current densities will service the Maglev industry.

Polycrystalline BSCCO materials show limited current densities in magnetic field for temperatures above 20-30 K. When adequate pinning mechanisms are found, then high critical current operation at higher temperatures in high field will be possible.

In Figure 2-24 early data[4] for 2212 material shows the effects of temperature on current density in magnetic field for material where no effort has been made to improve pinning or texture. Since T_c for 2212 is only 85 K, the critical current in the magnetic field is characteristically poor at 66 and 77 Silver-sheathed $(Bi,Pb)_2Sr_2Ca_2Cu_3O_x$(Pb BSCCO, 2223) wires have attained Jc (77K, B=0) values[5] of 17,400 A/cm^2 with recent improvements to 57,300 A-cm^{-2}.[6] Subsequent work on $Bi_2Sr_2Ca_1Cu_2O_{8+x}$(BSCCO, 2212) have shown current densities approaching 320,000 A-cm^{-2} at 4.2 K.[7] A recent review of the current state of the art is given by Otto et al. and is included in Appendix A, Section 2.

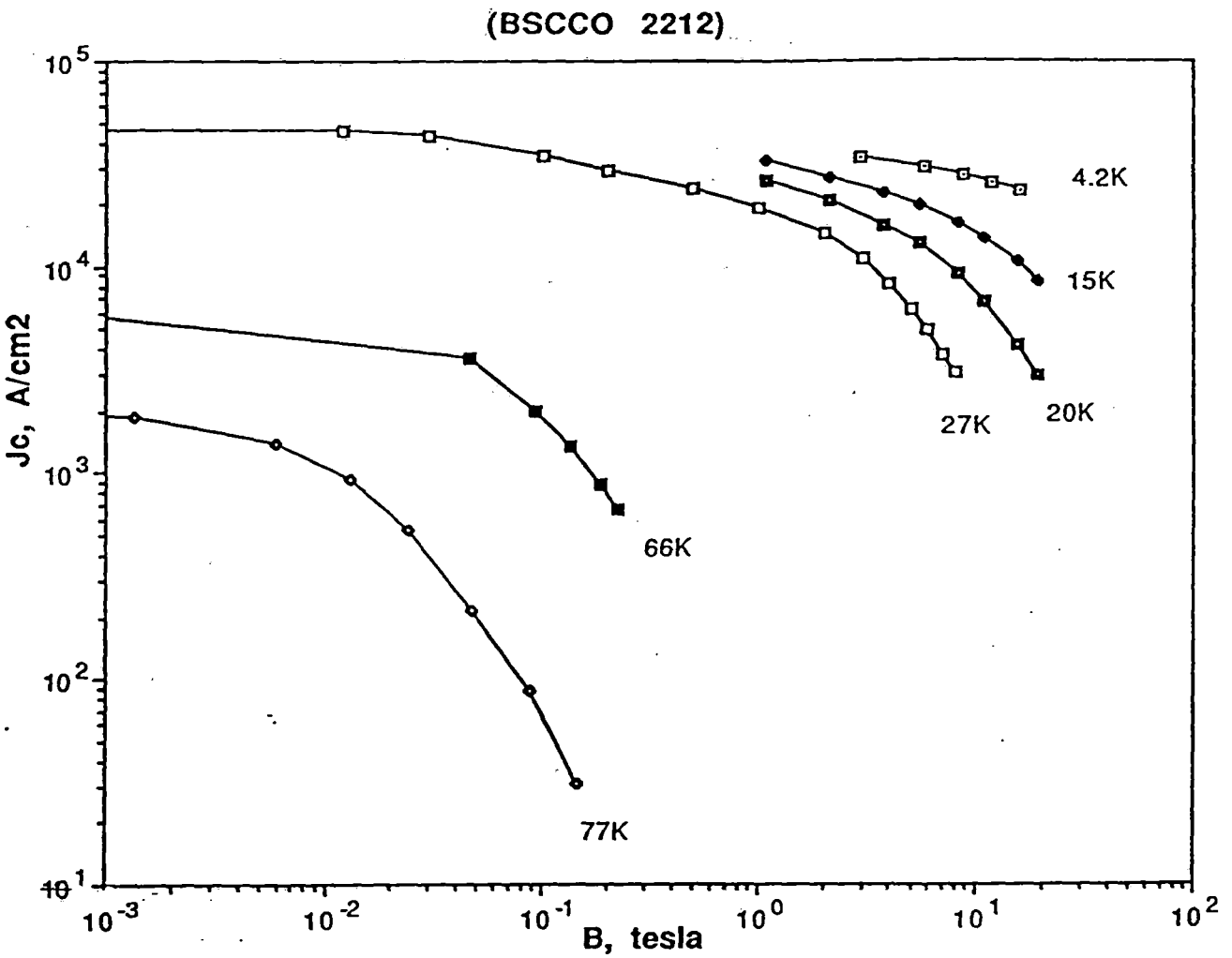

Typical Behavior of BSCCO as a Function of Field and Temperature

Figure 2-13

LOW FIELD POWER APPLICATIONS - TRANSMISSION LINES

BSCCO(2223) materials have sufficient properties for operation in low fields even at 77 K. The low fields associated with most AC applications allow the oxide ceramics to operate with good J_c's at temperatures in the 50-80 K range. The low stored energy and low magneto-mechanical stresses in low-field AC applications have removed several wire fabrication and coil design challenges apparent in high field applications. These challenges include cryostability and burnout protection.

The Case of AC Losses

Any cryocooled current-carrying application must consider the AC losses in the conductor itself and in the surrounding structure which makes up part of the cold mass of the magnet. Usually, it is the eddy current losses in the normal metal components in the cold mass which set the refrigeration requirements of the system. If eddy current losses dominate the engineering of a low-field, AC system, such as a transmission line, then the overall need for large amounts of cooling power indicate operation at the highest temperature consistent with the superconductor selected.

For example, if cryocooled copper is the stabilizer chosen for the transmission line, the AC losses in the superconductor can probably be ignored if

$$\rho 77^{HTc}(AC) < 1/10\rho 77^{Cu}(AC)$$

These low AC losses in the superconductor have been demonstrated, and the results show that high energy-density AC applications are practical at low temperatures. In fact, AC losses are so low as to be insignificant compared to other losses in the system.

The ability to operate at relatively high temperatures in low to moderate AC fields is a unique advantage for HTSC materials. Utilizing this advantage will be achieved by assuring that the HTSC remains stable under internal resistive heating and for the heat to be efficiently removed by a 50-80 K cryocooler.

Since there are losses in all superconductors operating in an alternating current environment, the higher operating temperature makes heat removal and thermal stability in the presence of AC losses easier to control. AC induced eddy current losses in the cryogenically cooled structural components will often dominate the cooling power requirements. Since cooling is less expensive at higher temperatures, AC applications which require relatively low magnetic fields will run at the highest temperature possible. At present, AC losses in unoptimized materials are approximately an order of magnitude better than high purity copper operating at the same temperature.

Materials properties are good enough now to produce 0.1 T coils with the best of the 2223 materials at 77 K. As materials properties improve, higher field coils will be produced. However, the rapid improvement in J_c performance at lower temperatures means that higher field coils will always be produced at 20-30 K compared to 77 K. Higher fields also require that a burnout protection scheme be developed for 77 K which will require considerable innovation compared to the techniques presently available at lower temperatures.

Currently, J_cxL greater than 10^9 A-cm^{-2} is achievable at 77 K in low magnetic fields with AC loss substantially better than copper operating at the same temperature. J_cxL has increased a few orders of magnitude per year since 1988. If J_cxL is a useful predictor, then low-field, commercial AC applications should have oxide superconductor wire available for first demonstrations in the 1992-93 time frame. Sumitomo and American Superconductor have already reported on components for an AC transmission line.

2.3.2 High Temperature Superconductors (HTSCs) with Potential Operating Temperatures of 20 to 77 K for Use in Magnetically Levitated Vehicles

Applications of Superconductor - Normal Metal Composites

For a majority of power applications, including Maglev, the combination of a superconductor and a normal metal composite will give optimum results, as it does for the existing metallic superconductors operating at liquid helium temperatures.[8]

Many of the reasons for using metal composites with oxide superconductors and with metal-based superconductors are the same, e.g. cryostability, normal zone propagation, ductility, etc. A

few, including thermo-mechanical properties at higher operating temperatures, are different. The extensive literature which has evolved for the use of metal-based superconductors is a useful guide for applications involving oxide superconductors.

ELECTRICAL PROPERTIES OF THE SUPERCONDUCTOR

The electrical properties of superconductors are the driving force for applications. The ability of superconductors to carry very high current densities, compared to copper, enable applications like high-field, air-core magnets. The basic parameters which describe a superconductor are the critical temperature, T_c, the critical current density, J_c, and the critical field, H_c. These are briefly described below, and a more detailed discussion is available in texts like Rose-Innes.[9]

T_c, J_c, and H_c

Superconductors operating below their critical temperature, T_c, are characterized by their lack of DC electrical resistivity, ρ. In the best low-T_c superconductors ρ less than 10^{-18} Ω-cm, which is the limit of the measurement capability by persistent current techniques. The ability of a high field magnet to operate in persistent mode with no electrical connections is important in high stability applications where very constant fields are required.

Resistivities measured in highly-oriented, polycrystalline thin films of $Tl_2CaBa_2Cu_2O_x$, and single-crystal samples of $Bi_2Sr_2Ca_1Cu_2O_{8+x}$ for 26 less than T less than 100 K have been several orders of magnitude higher than those measured in low-T_c superconductors, and the resistivity has shown strong magnetic-field orientation dependence.[10] Resistivity values will need to improve if oxide superconductors are to be used in the persistent mode.

The superconductor will stay superconducting until a critical current is passed through the wire at a given temperature and field. Most of the discussion of superconducting properties focuses on improving the critical current.

The J_c vs. B characteristics of oxide superconductors in bulk form will be a major component in determining their usefulness. Most of the practical, large-scale manufacturing techniques produce poly-crystalline materials. Therefore, critical current properties must be adequate in these wires for the applications of interest. In general, this corresponds to J_c greater than 10,000 A-cm^{-2} in magnetic fields characteristic of the application.

The critical current performance of the superconductor often drives a given application. The values of the critical current are based on the total cross-section of the active filaments including the normal conductor between the filaments but excluding outer sheaths and insulation. This has been normal practice in the low temperature superconductor industry.

The Importance of Wire Length

While critical current is an important operating parameter for coils, the ability to make long lengths of wire economically with high critical currents is a better measure of performance. Therefore the J_c xL criteria is usually more useful when considering applications where reasonable lengths of wire are required. While melt-textured and single-crystal materials have provided the best J_c performance to date, they are usually not of practical value for coil applications due to limitations on the length which can be made.

OPERATIONAL REQUIREMENTS

Wires for Maglev coils made from oxide superconductors will have several requirements which are similar to copper and metal superconductors. These will include compatibility with processing and uniformity of electrical and mechanical properties along the entire useful length of the materials.

Compatible with Processing

Compatibility with subsequent processing has been a major issue with all wire forms. In the silver and tin plated wire industry, for example, plating non-uniformities and porosity are exacerbated when the wire must be insulated with very thin high-temperature polymer insulation. This processing is done at elevated temperatures and is often sufficient to cause interdiffusion of plating and the metals, and release of trapped gases due to poor plating.

Similarly, Nb_3Sn must have all of its mechanical processing completed before conversion to a superconducting form. When a wind-and-react approach is used, the wire needs an insulation technology compatible with the winding of the material into a magnet and subsequent firing at temperatures beyond the range of polymer insulations. When a react-and-wind approach is used, the mechanical properties of the superconductor must be sufficient to survive the winding process. As a result, Nb_3Sn and related compounds are only used in situations where NbTi cannot be used. The resulting Nb_3Sn magnets are substantially more expensive than NbTi magnets mostly due to process compatibility problems.

Oxide superconductors will be no different in requiring compatibility with subsequent processing. For materials which require a wind-and-react approach, mineral insulations compatible with oxide superconductors are being developed for direct contact with YBCO materials.

To date, polymer insulations do not show promise of long term lifetime when in contact with oxides containing alkali earth material like Sr, Ba, or Ca. Materials which are sheathed in silver can be coated with conventional polymer insulation. Many successful coils have been made using technology derived from LTSC coils with polymer insulated wire with epoxy impregnation.

Mechanical Properties

Once the basic issues of sufficient critical current are addressed, most of the issues with coils will be related to their mechanical and thermal properties. In high field coils, the magnetic stresses

are close to the limits of high strength steels. In the simple case of solenoids, the stress is proportional to B^2r. Therefore, producing high field magnets with large bores will be an extremely difficult problem. Since the oxide superconductors do not appear to have high mechanical strength, some form of a strengthening member needs to be introduced.

This strengthening member needs to have a thermal expansion that matches closely to that of the oxide superconductor, and it must be compatible with the processing of the superconductor if wind-and-react processing is to be used. A rich literature of mechanical support of superconducting windings in epoxy based materials already exists for metal superconductors. It is expected that oxide superconductors will build on this existing expertise.

In order to use oxide superconductors effectively, they must have mechanical properties which allow their fabrication and their use with thermal cycling when they are superconducting. A useful empirical method for measuring the fracture toughness of a superconducting oxide/metal composite is to measure the critical current of the superconducting oxide as a function of strain and/or applied stress.

A plot of the critical current performance of the common superconductors as a function of strain is shown in Figure 2-14. More up to date information is included in Otto et al. included in Appendix A, Section 2. Note that the BSCCO materials already have mechanical properties better than Nb_3Sn. These BSCCO materials are mechanically robust and allow the production of react-and-wind coils on conventional equipment.

AC Properties

Since most of the oxide wires used in coil applications will be metal-superconducting, oxide composites of one form or another, they will have loss properties in AC fields similar to metal superconductors. There is a rich literature on the AC properties and behavior of metal superconductors in the presence of magnetic fields.

When normal metal is used in small quantities for improved mechanical properties, then interconnectivity of the normal metal is avoided and eddy current losses at higher frequencies

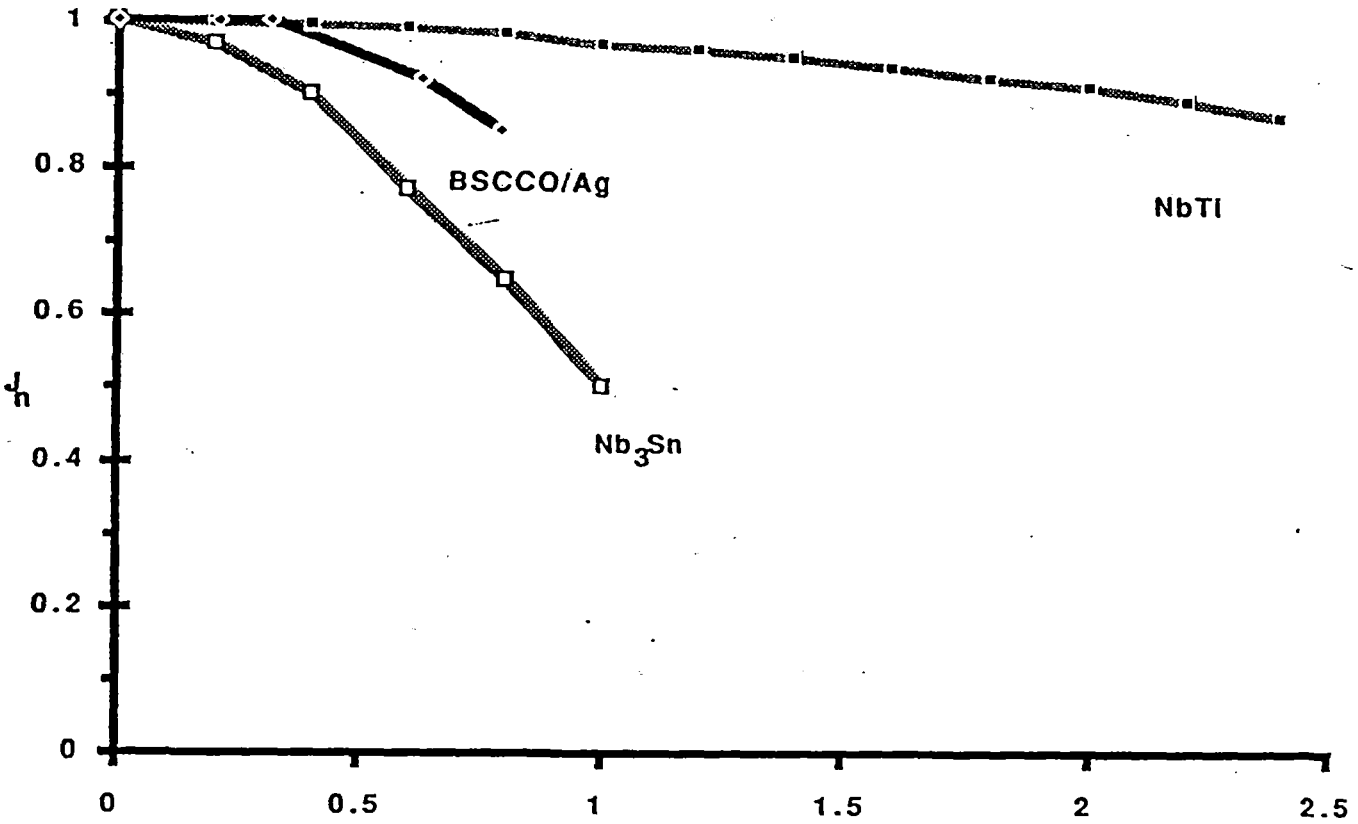

Normalized Critical Current vs. Strain for Low Temperature Superconductors and BSCCO

Figure 2-14

can be reduced. Unoptimized wires have demonstrated over an order of magnitude improvement in 50-100 Hz AC losses at 77 K compared to silver operating at 77 K. Further progress is expected as AC loss issues are further addressed.

In a Maglev magnet, there is some small component of AC loss due to the imperfections of the electrical characteristics of the guideway. For 4 K systems this will require a substantial flux shield. In a HTSC system, refrigeration requirements due to AC losses can be traded against the weight of the flux shield.

Residual Resistance

There is usually some residual resistivity in superconductors. This is especially the case under AC conditions. Simple pinning models show that in a field reversal, the flux must be depinned to change direction under the influence of the alternating field. This depinning is a nonconservative event and leads to thermal losses.

The residual resistance under low field conditions is typically very low at DC and is often connected with the losses in the normal metal under AC conditions.

Cryostability

Cryostability implies the ability of a conductor to return to the superconducting state after a small to moderate perturbation. The larger the amount of normal material in intimate thermal contact with the superconductor, the better its cryostability. The addition of silver to oxide superconductors improves cryostability, especially when the material is processed by the metal precursor route. Note, however, that the larger amounts of normal metal included usually reduces the available critical current in a given cross-section.

Normal Zone Propagation

As was discussed in the section above, the motion of flux in a superconductor causes energy dissipation. Motion of the conductor itself can cause similar dissipation. If the energy dissipated due to any cause cannot be removed from the superconductor rapidly enough, then the superconductor in the area where the dissipation occurs will convert to a normal zone.

If the current cannot be shunted around the normal zone, and there is a substantial amount of energy stored in the superconducting device, then the normal zone will heat until the material melts. Therefore, it is important to provide a current shunt around the superconductor to handle the current, and to provide a method for the removal of heat. This is especially the case when superconductors are in devices with large amounts of stored energy, like high field magnets.

The normal zone propagation velocity is related to the heat capacity, the thermal conductivity, and the configuration of the wire in a given device. Note that thermal conductivity and heat capacity are strongly temperature dependent below 80 K. In oxide superconductors the thermal conductivity is low and the heat capacity is comparable to the normal metal included for cryostability. Therefore, normal zone propagation is determined by the normal metal characteristics.

The operating temperature of superconducting devices, with large stored energy, may not be determined by the properties of the superconductor, but by the ability of the normal conductor to propagate the normal zone with sufficient velocity.

OPERATIONAL REQUIREMENTS AND CHARACTERISTICS OF HIGH TEMPERATURE SUPERCONDUCTIVITY

Current densities above 10,000 A/cm^2 have now been achieved in significant magnetic fields ($<$1T) at 77 K, the boiling point of liquid nitrogen. While the more recent results for current densities at 77 K are very encouraging, indeed, it is clear that the results currently available at lower temperatures (20 to 30 K) warrant *immediate, accelerated work on the demonstration of magnet technologies for application at the lower temperatures.* Cooling in the latter case would be achieved

by closed-cycle refrigerators. As the critical current densities at higher temperatures increase over time, the wire, cooling and magnet technologies developed now for 20-30 K operation would be directly applicable to higher temperature operations.

The operation of HTSC magnets at 20 to 30 K is also important because it:

1. optimizes superconducting properties per cooling cost,

2. does not require major innovation in normal zone propagation and magnet protection, and

3. highly reliable refrigeration technology exists and is relatively inexpensive compared to 4 K liquefiers.

4. Uses off-the-shelf components.

It is not appropriate to wait until higher current densities are achieved at higher temperatures in research samples to develop wire scale up, and to start development of cooling and magnet technologies. By that time, our foreign competition will have advanced so far in the down-stream technology development that American industry may never catch up.

In addition to the excellent current-carrying abilities of HTSC wires, American Superconductor Corporation has been able to demonstrate that HTSC wires can be made flexible. Long lengths of wire (50m) have been produced with strain tolerances of 0.5%, which is sufficient to allow for robust manufacturing processes for the wire, and to allow the wire to be formed into usable coils. While much remains to be accomplished to demonstrate all of the properties required for commercial superconducting coil applications, it is clear that the mechanical properties of HTSC wires will not be an insurmountable barrier to the development and commercialization of HTSC wire technology.

At this point, no additional scientific breakthroughs are required in order to commercialize HTSC technology. What is required is a very strong effort to overcome the significant engineering hurdles involved in tailoring HTSC properties for use in a final device. These hurdles include:

1. achieving long lengths of wire with the same properties as the research wire samples,

2. proving process capability in important specifications over long lengths,

3. proving useful magnets can be made with the HTSC wires

4. integrating cryocoolers with the HTSC magnets to take advantage of the promise of HTSC technology, and

5. demonstrating useful subsystems with all design considerations met.

Enough science exists now to allow commercialization of HTSC technology. The field is entering the development stage, and foreign competition is devoting very significant efforts to developing both HTSC wire technology and applications for this technology. Owing to the cost of capital in the United States, American industry has not been able to justify making significant investments in HTSC technology because the technology is not likely to enjoy widespread commercialization for at least five years from the present time. This barrier has not been an impediment in Japan, where industrial and government efforts in HTSC wire technology are moving forward at breakneck speed.

Energy-Storage Time Figure of Merit

Coils are normally used as energy converters, i.e., they convert electric current into stored magnetic energy residing in a volume V(m^3). Since Maglev requires a high energy density in the suspension and propulsion magnets, some form of actively cooled magnet is required. These

magnets could be actively cooled copper, LTSC, or HTSC. A useful energy-storage figure of merit[11] for coil based systems is the storage time, t:

$$t(\text{sec}) = \frac{\text{Stored Magnetic Energy (J)}}{\text{Power to Store Energy (W)}} \tag{1}$$

$$t(\text{sec}) \propto \frac{[B(\text{Tesla})]^2 V(\text{m}^3)}{\text{Cooling Power (Watts)} + \text{other losses}} \tag{2}$$

This time can be considered as the decay time for the stored energy in a short-circuited inductor with a finite resistance, or the time for a similarly configured resistanceless coil to lose its stored energy, if some of the stored energy is used to provide the cooling power.

Cryocooled Copper

For a resistive coil operating at current density J, with electrical resistivity $\rho(\Omega\text{-m})$ and winding volume $V_{coil}(m^3)$, resistive losses, which represent the cooling power required, can be expressed as

$$I^2R = J^2\rho V_{coil} \tag{3}$$

Substituting eq. 3 into eq. 2 with $V \approx V_{coil}$, and using the fact that

$$B \propto JV \tag{4}$$

gives

$$t(\text{sec}) \propto \frac{V^2}{\rho} \tag{5}$$

Note that eq. 5 is independent of J and only depends on size and resistivity. If all of the I^2R losses are totally absorbed by a closed-loop cooling system, then only the cooling system power needs to be considered.

Actively cooling and operating a copper coil in liquid nitrogen or liquid hydrogen is practical only if the resistivity is low enough to support the use of coolant. For example,

$$\rho 273^{Cu} = 1.545 \times 10^{-8} (\Omega\text{-m}) \tag{6}$$

$$\rho 77^{Cu} \approx 1/5\ \rho 273^{Cu} \tag{7}$$

$$\rho 21^{Cu} \approx 1/120\ \rho 273^{Cu} \tag{8}$$

To be efficient, the cost of cooling the copper must be less than the reduction in I^2R losses. At temperatures below 77 K the resistivity depends on the purity of the material. The number given in eq. 8 assumes that the copper is moderately pure and fully annealed.

Cryocooled Aluminum

For high energy-density applications in high magnetic fields, hyperpure aluminum operating at 20 K has been used since the late 1950's[12,13] for large magnets. Aluminum is used instead of copper because of its lower magneto-resistance in high magnetic fields, which reduces the power dissipation for a given field generated. Purcell's magnet[13] with 99.9983% aluminum has

$$\rho 21^{Al} = 2 \times 10^{-11} (\Omega\text{-m}) \tag{9}$$

Even lower values of resistivity have been obtained.

Water-Cooled Copper

To water-cool copper, the minimum water flow is governed by the equation:

$$Q(kW) = m(kg\text{-}sec^{-1}) c_p (kJ\text{-}kg^{-1}\text{-}K^{-1}) \Delta T(K) \tag{10}$$

where $c_p^{water} \approx 1(kJ\text{-}Kg^{-1}\text{-}K^{-1})$. To remove 10 kW with a 30 K temperature rise requires 0.3 kg/sec or $\approx$ 18 1/min when friction losses are included. For a small coil, head loss will probably be 40-60 psig which consumes $\approx$ 750 W of electricity.

Refrigeration Trade Offs

Good single-stage refrigerators have total efficiencies of $\approx$ 8% at 77 K and $\approx$ 5% at 50 K; two-stage refrigerators have total efficiencies of $\approx$2% at 20 K for 300 K sink temperatures; and two-stage refrigerators operating at 20 K with a series of Joule-Thompson valves to reduce operating temperature to 4.5 K for reliquefying helium will have total efficiencies of $\approx$0.4% at 4.5 K for 300 K sink temperatures. Therefore, cryocooled copper at 77 K has approximately half the energy efficiency of air- or water-cooled copper at room temperature, and LTSCs will suffer an energy penalty in efficiency and/or refrigeration sizing of $\approx$5x compared to HTSCs operating at 20 K.

Optimizing Operating Temperature for HTSC Coils Based on Application

Optimizing the performance of the superconducting magnet and refrigeration system for HTSCs can be done at several temperatures unlike the case of LTSC magnets that must operate near 4.2 K. Figure 2-15 illustrates such an optimization as analyzed by Joshi. The refrigeration load includes heat leaks from the leads and residual conduction losses for a vacuum-jacketed coil. Note that the optimum system performance occurs in the 20-30 K range.

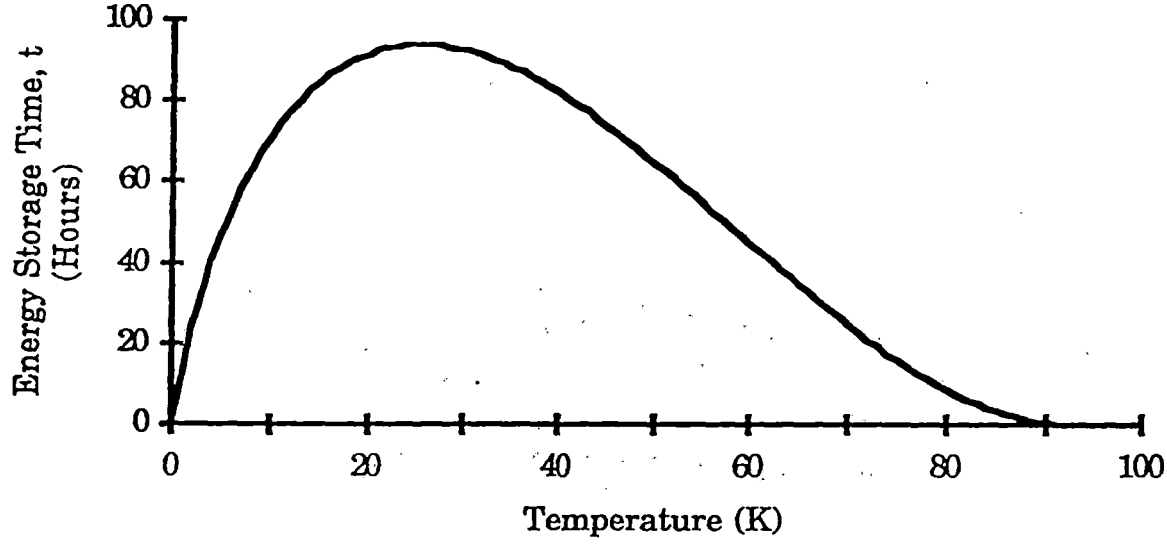

Energy-Storage Time for a 25.7 Henry Coil with a 20% of Carnot Efficient Refrigerator Attached
I = 100 A, Losses from Current Leads Included

Figure 2-15

Normal Zone Propagation and Magnet Protection as a Function of Temperature

Two of the most important magnet design issues are: 1) stability, both mechanical and electrical; and 2) protection from a quench, i.e. the uncontrolled release of magnetic stored energy due to a portion of a superconducting magnet becoming normal.

Even moderate sized (diameter $\approx$ 0.3 m, length $\approx$ 0.5 m, B $\approx$ Tesla) superconducting magnets store $\approx$1/4 MJ of energy. An uncontrolled release of this much energy is roughly equivalent to a stick of dynamite. Therefore, it is imperative to channel and distribute this energy release carefully. Brown and Iwasa[14] note that:

> . . .once a high performance magnet is driven normal over a winding volume greater than the minimum propagation zone (MPZ), it quenches. Protection is concerned with magnet longevity. Its chief objective is to ensure that a magnet suffers no permanent damage upon quenching. . . .Specifically, the peak temperature reached over the normal zone initially created must not exceed a level at which the conductor might suffer permanent damage nor must the temperature distribution be so steep as to cause large thermal strains within the winding pack, which might damage the structural integrity of the magnet. The post-quench temperature distribution, including the peak temperature is determined by the normal-zone evolution in the winding pack and the process is controlled principally by the so-called normal-zone propagation velocities. . .

Iwasa[15] has shown that for thermally isolated HTSC magnets the propagation velocity is too slow at temperatures above 20-30 K to distribute energy throughout the structure and prevent localized magnet burnout. This is largely due to the high specific heat of the superconductor and of the normal metal stabilizer at higher temperatures when compared to 4 K. Therefore, adiabatic magnets either 1) must be operated below 30 K for adequate protection, 2) must have active detection and protection schemes, or 3) require designs which allow forced cooling of the magnet.

Systems Issues for High Field Coils

If sufficient critical current in high field can be obtained in a superconductor, then issues of building high field coils are nearly totally thermal and mechanical in nature. The fields and the resulting forces in a high field high-T_c superconductor magnet are the same as in low-T_c superconductor material.

In the Maglev application, all of the suspension and propulsion forces must be transmitted through the cryogenic envelope with the attendant heat leak due to more substantial mechanical structure requirements. This imposes a larger refrigeration penalty for LTSC than HTSC.

Stability

If any microscopic motion of the conductors occurs at high fields, then a significant amount of energy is released. A motion of a single metal superconductor wire by 0.0001" can be sufficient to produce enough heat locally to drive the magnet normal at 4 K. Since the heat capacity rises quickly above 4 K, it is much easier to keep these small perturbations from driving the magnet unstable at elevated temperatures. Magnet stability at 4 K is more difficult than at higher temperatures, but magnet protection is more difficult at elevated temperature than at 4 K.

Protection

If a perturbation in the wire drives the magnet unstable and allows the formation of a normal zone, then the normal zone must either propagate quickly through the magnet (quench) or shrink fast enough so that the stored energy in the magnet cannot burnout the normal zone. Studies by Iwasa[16] indicated that the thermal properties of the coil winding tend to dominate normal zone propagation. Based on these findings, the optimum operating temperature for an adiabatic, oxide superconductor magnet appears to be 20-40 K.

Driven vs. Persistent Mode

Superconducting magnets which do not require frequent changes in field are often short-circuited with a superconducting connection after charging and running in the persistent mode. For magnetic resonance imaging magnets at liquid helium temperature this is often done with retractable current leads so that thermal loss can be reduced. Magnets which must change field frequently keep the leads firmly connected to the magnet and sustain a higher liquid helium loss. Lead loss is usually a major source of helium boil-off in DC applications of low-T_c superconductor magnets. Lead loss is a particularly serious problem in large energy storage magnets.

Two properties of the superconductor determine if the material can be run in the persistent mode. These are the index and the residual resistance. The index represents the coefficient in the equation

$$V = V_c[I/I_c]^n$$

where V is the voltage and I the current flowing through the coil. This model adequately describes the I-V characteristic of most superconductors in the transition from superconductor to normal conductor. The measurement is performed at the operating magnetic field. The subscripted variables are measured at the critical current with the given criteria. The residual resistance, R = V/I, and the inductance of the coil determines the time constant for a magnet in persistent mode. If the index of the wire is low, then only a relatively small fraction of the current density can be used to keep an acceptable value of residual resistance. Values of n = 30 are desirable for magnets operating in persistent mode since nearly all of the critical current can be used before the resistance begins to rise.

The residual resistance is directly related to the index in the transition region since

$$R = V/I = [V_c/I]\ [I/I_c]^n$$

Present oxide superconductor materials have residual resistances which are too high to allow most magnets to be run in persistent mode for acceptable times. This problem will be solved as flux pinning methods are improved for oxide superconductors.

$J_cV \approx BR^2$

The time frame for the construction of large solenoidal magnets will be related to the volume of superconductor which can be produced with a specific critical current. For a specific wire size $J_cV \approx Br^2$ is closely related to J_cxL. It also points out that the production of high magnetic fields over large areas requires very large quantities of material with good properties.

2.3.3 Refrigeration Requirements for Low and High Temperature Superconductor Devices Used in Magnetically Levitated Vehicles

Cooling Requirements

The discovery in 1986 of a whole new class of materials that superconduct at higher temperatures was truly a scientific breakthrough. The new materials, which are ceramics, exhibit their superconducting properties at temperatures which can be attained by efficient refrigerators, known as cryocoolers. The possibility of building superconducting, electromagnetic systems that could operate without the need for liquid helium changed the entire outlook regarding the widespread application of superconductivity, especially for smaller systems.

Metallic superconductor wire technology has been developed over the last 30 years, and has become a rather mature technology. Typically liquid helium is used for metallic (or low-temperature) superconductor (LTSC) applications. Cryocoolers used to provide liquid helium refrigeration between 4.2 and about 10 K in a closed cycle for LTSC wires have been limited to larger systems because of the high cost of providing a small, closed-cycle helium liquefier.

High temperature superconductors will operate in applications at temperatures from 4-77 K. The refrigeration issues for 4 K will be defined based on liquid helium and the possible addition of refluxers to reduce the boil off of liquid helium. However, cooling requirements for superconductor components in the 10-77 K range need to be addressed. The challenge of using this temperature range will be to find an adequate cooling method without the use of liquid cryogens.

Several refrigerator types cover this temperature range adequately. These range from Gifford McMahon machines (10-20 K), to pulse tubes, to Stirling cycle machines (40-80 K). Besides refrigeration capability, the ability to place the cooling at the proper points in a device and the ability to handle varying loads will be examined.

Smaller systems, like Magnetic Resonance Imaging (MRI) magnets, are successfully using liquid helium. For small, industrial systems, like Maglev, closed-cycle refrigeration, transparent to the end user, requiring conventional input power, and a minimum of special heat rejection equipment will be the most successful.

Cryocoolers

For machines with less than a few hundred watts of cooling in the 15-77 K temperature range, there are only two classes of cryocoolers with wide commercial availability. They are Stirling Cycle machines, which are the most efficient, and the Gifford McMahon (GM) Cycle machines, which are most widely used. Very large machines are often built with customized hybrid cycles for best efficiency.

Most cryopump manufacturers use oil-lubricated freon compressors which are manufactured in very large quantity for the refrigeration industry. Helium operation of these compressors forces them to run hotter. Hermetically sealed compressors have mean times between failure (MTBF) in helium service with proper deratings of > 100,000 hours. Larger semi-hermetic compressors can be rebuilt periodically. Compressor selection is part of the GM cryocooler manufacturers' art.

Stirling Cycle machines have higher thermal efficiency than GM machines. However, the only long commercial experience with small Stirling cryocoolers is with fractional-watt, common module refrigerators developed for military applications. These machines have MTBFs of only 4000 hours. With exceptional precautions, small Stirling machines should be capable of a million hour MTBFs.

Interfaces Between Cryocoolers and Devices

There is a body of literature describing the cooling of LTSC magnets in liquid helium or supercritical helium. For small adiabatic magnets where field precision and stability are important, liquid cryogens are preferred. For large systems where mechanical support members need to be included, cable-in-conduit systems with supercritical helium are often the preferred approach.

Simple conduction cooling systems with mechanical GM refrigerators have recently been attempted with Nb_3Sn superconductors operating to keep the coil at 12 K.[17] While conduction cooling was shown to be effective, the refrigerators are operating very close to their minimum temperature ($\approx$ 9 K). Temperature stability and power output[18] also need improvement in this temperature range.

The conduction cooling approach will be much more practical using HTSC coils with a refrigerator operating at $>$ 15 K. It is likely to be practical only for DC magnets, which do not generate a large amount of heat that must be removed in a short period of time; small AC or pulsed magnets may also be cooled using the conduction-cooling approach. The thermal time constant is limited by the thermal resistance between the cryocooler and the coil and by the heat capacity of the coil. Cool down times will be relatively long, and temperature stability under thermal transients will be poor compared to systems with the coil immersed in a liquid cryogen. However, the continuous operation of a Maglev vehicle, and the relatively small quantity of superimposed AC current due to guideway inhomogeneities, make this an attractive option.

Thermal transients in the 20 K range will be minimized by the relatively high thermal conductivity in this temperature range and by the 10-fold increase in specific heat of the coil at 20 K compared to 10 K.[19] Additional heat transfer mechanisms will need to be implemented for improved stability in the presence of thermal transients due to fault situations and for AC applications.

ECONOMICS OF FINISHED SYSTEMS

Economic Drivers

Several systems, like MRI magnets, small Superconducting Magnetic Energy Storage (SMES) magnets, and High Gradient Magnetic Separation (HGMS), are existing products built with superconductors. The economics of a Maglev system should be similar to these systems with either LTSC or HTSC. The move to actively-cooled, closed-cycle systems has been driven by superior performance or the value added from the use of superconductors compared to systems which use conventional conductor technology and room temperature cooling systems. Both of these reasons apply to Maglev.

Improved performance and reduced life cycle cost of superconducting versus normal conducting systems have led to the development of the MRI magnet market of several hundred units per year, an embryonic HGMS market, and an emerging small SMES market. For these markets to be industrially viable, the installed or fixed cost of the cryogenics and superconductor must be reduced, while the operating or variable cost and the system's reliability must be deemed acceptable by the user community. An example of these economic drivers will be given in the purchase cost section below for small SMES applications.

Life Cycle Cost

Life cycle cost is often defined as a combination of the fixed and variable costs of a system over its useful lifetime with some form of discounting of operating costs and depreciation of the fixed cost.

Fixed Costs

The typical cost of the cryogenics in small-to-moderate sized applications has been 5-10% of the system's price, $16,000 for 50 W at 50 K being typical, but 20-30% savings can be obtained in quantity purchases. Magnets with dewar have cost about 25% of the system price in those applications where the magnet is a key component in many operations where no substitute can be found, e.g., MRI systems.

Green and Byrns give estimate[20] of the cost of refrigeration with closed cycle liquid helium refrigerators. Since the magnets in a Maglev system are relatively small, one would expect that the cost of a closed cycle refrigerator would be high compared to an open dewar arrangement in a LTSC system.

HTSC magnets, on the other hand, can use inexpensive, two-stage, Gifford-McMahon cycle refrigerators for 20 K operation, or Stirling cycle refrigerators for 77 K operation and meet the above cost targets, even for magnets as small as those used in Maglev systems.

Operating Costs

A closed cycle refrigeration system needs to be cost competitive in operation both with a conventionally cooled room temperature system as well as with cryogen-cooled systems. For large systems, liquid nitrogen costs $\approx$ 6¢/liter, liquid helium costs $\approx$ $4/liter, and industrial electricity costs $\approx$ 6¢/kWh. The electric cost on board a Maglev vehicle may be several times

higher than this number. Therefore, some estimate of on-board electric cost needs to be generated.

System Reliability

Closed cycle systems have the potential for being more reliable than open cycle systems that depend on evaporation for cooling. Open systems are prone to icing, as well as valving and sensor problems. Closed cycle systems are subject to mechanical failures and electrical outages.

Single-stage, Gifford-McMahon refrigerators offer approximately half the efficiency of a comparable Stirling Cycle refrigerator. However, GMs have a much larger installed base, and are probably lighter than an equivalent Stirling machine. The two-stage GM machine is the most common, small refrigerator used in the 20 K range. These have demonstrated reliable performance with > 70,000 hours MTBF.

CONCLUSIONS

The integration of HTSC coils and GM cryocoolers will be a practical solution for high field operation of DC magnets in the 20-30 K range. AC applications will be handled by Stirling or GM machines in the 50-80 K range. Novel integration schemes are possible which will enhance the value of the overall system. LTSC magnets will either run with liquid helium only, avoiding the weight penalty of the cryocooler, or with a high efficiency, light-weight cooler yet to be developed.

SUMMARY

Operational requirements and characteristics of high temperature superconductors (HTSC) indicate that low field and AC applications will require refrigeration in the 50-77 K region and high field DC applications will require refrigeration in the 20-30 K range. Very high field magnets will require 4 K refrigeration.

A figure of merit, t, is developed which relates the stored energy in coils to the power required to cool them. HTSC materials give the highest figure of merit when compared to cooled normal metal and low temperature superconductors. Optimizing t shows that the best operating temperatures are in the 20-30 K range. This temperature range is also the best operating range to implement conventional magnet protection schemes for adiabatic magnets.

Low cost refrigeration will be essential for small systems using HTSC or LTSC to be economical. The typical first cost of cryogenics in small to moderate sized systems is usually 5-10% of systems price. A closed cycle refrigeration system also needs to be cost competitive in operation both with a conventionally cooled room temperature system, and liquid cryogen cooled systems.

2.4 Refrigeration and Heat Loads

Cryostat

Three cryostat systems were considered in the conceptual design. For all systems, it was assumed that there would be a liquid nitrogen reservoir near or about the magnets. Liquid nitrogen could be eliminated by additional on-board refrigeration.

The first system, System 1, uses three separate shields (80 K, 20 K, and 4 K) to maintain a liquid helium environment for the superconducting magnet. For this configuration, shown in Figure 2-16, a refrigerator is required to maintain the 20 K shield. System 1 assumes that everything reasonable is done to lower the liquid helium boil-off and 4 K refrigeration requirement. It assumes that the required space is found for the gas cooled 20 K and 80 K radiation shields and that the primary load-bearing supports are gas cooled at 20 K and 80 K heat intercepts and that adequate room is found for these critical support members.

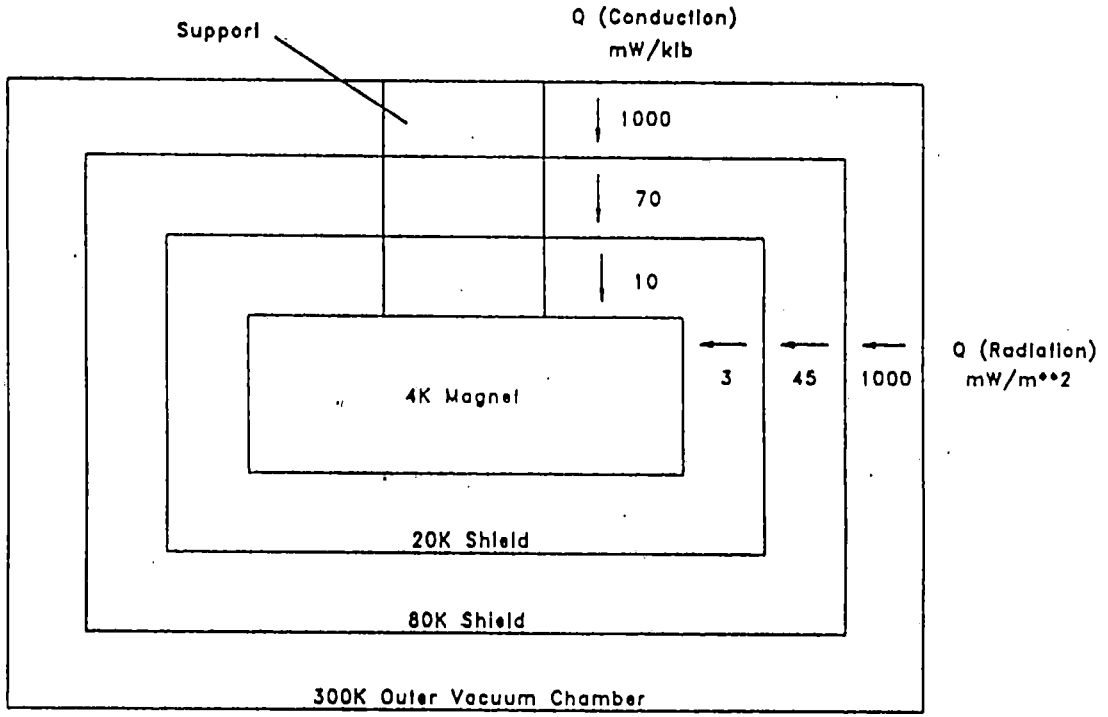

CRYOGENICS:

- 4K magnet cooled by pool boiling or 4K refrigerator.
- 20K shield and support intercept cooled by 20K refrigerator.
- 80K shield and support intercept and eddy current shield cooled by LN2 or 80K refrigerator.

Magnet/cryostat: cryogenic description (System 1 – refrigerated 20K heat shield)

Figure 2-16

A second configuration, System 2, shown in Figure 2-17, also contains three shields, but no refrigerator is required. It is assumed that liquid nitrogen and liquid helium would be provided externally from a ground-based reservoir or that a liquifier would be carried on board. System 2 also assumes that all of the above care goes into the design of the cryostats. System 2 differs from System 1 in that the 40 K low temperature radiation shield and the 40 K thermal intercept on the supports are cooled strictly from the liquid helium boil-off gas (pool boiling).

The third system, System 3, shown in Figure 2-18, contains only one thermal shield, an 80 K shield. System 3 makes an obvious simplification and saves space by eliminating the 20 K and 40 K radiation shields and thermal intercepts on the supports below 80 K. This simplification increases the size of the 4 K refrigerator significantly.

Figures 2-19 to 2-23 show the conceptual design of the cryostat for the propulsion and levitation magnets in configurations I and V.

Heat Loads

Typical heat load calculations have been tabulated for the three cryostat systems using the analysis in Figures 2-7 and 2-8. The major assumptions for the heat load calculations are listed below.

1. The on-board magnets are operated in persistent mode with the high current leads retracted.

2. The magnets at 4 K are shielded from heat-producing eddy currents using conductive shields at 300 K or 80 K or both.

3. The weight of a car that needs to be supported by the magnets at 4 K is assumed to be 445,000 kN.

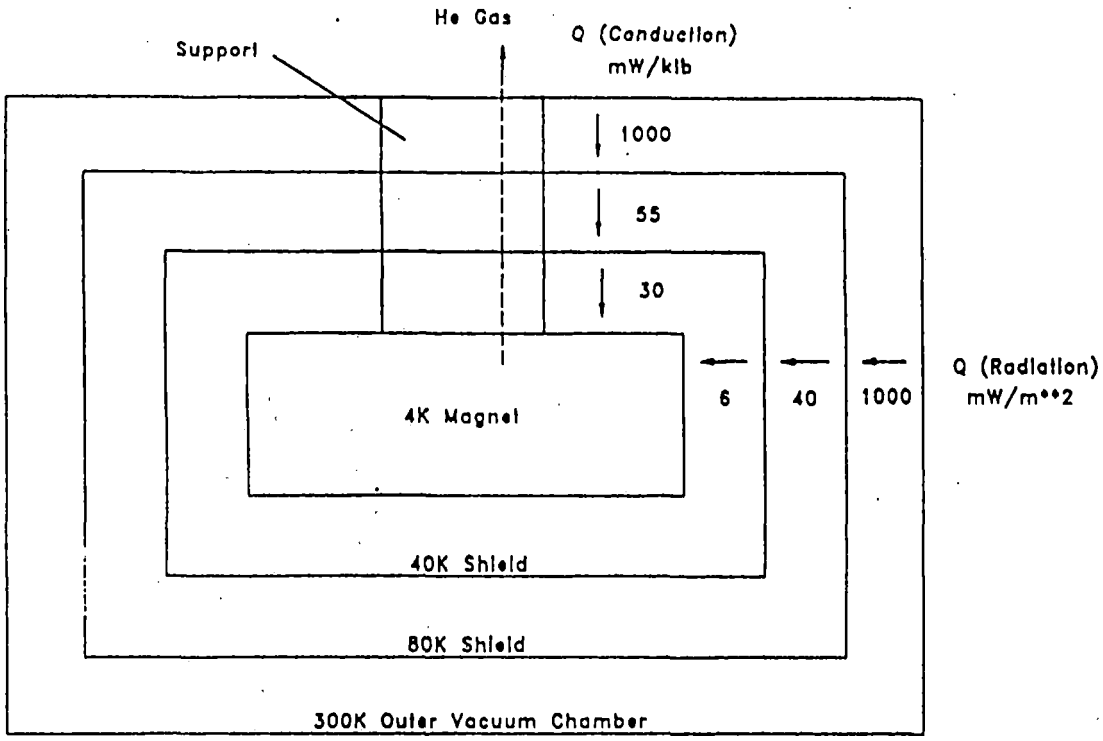

CRYOGENICS:

- 4K magnet must be cooled by pool boiling.
- 40K shield and support intercept cooled by vapor from pool boiling.
- 80K shield and support intercept and eddy currenly shield cooled by LN2 or 80K refrigerator.

Magnet/cryostat: cryogenic description (System 2 – pool boiling, no refrigerators required)
Figure 2-17

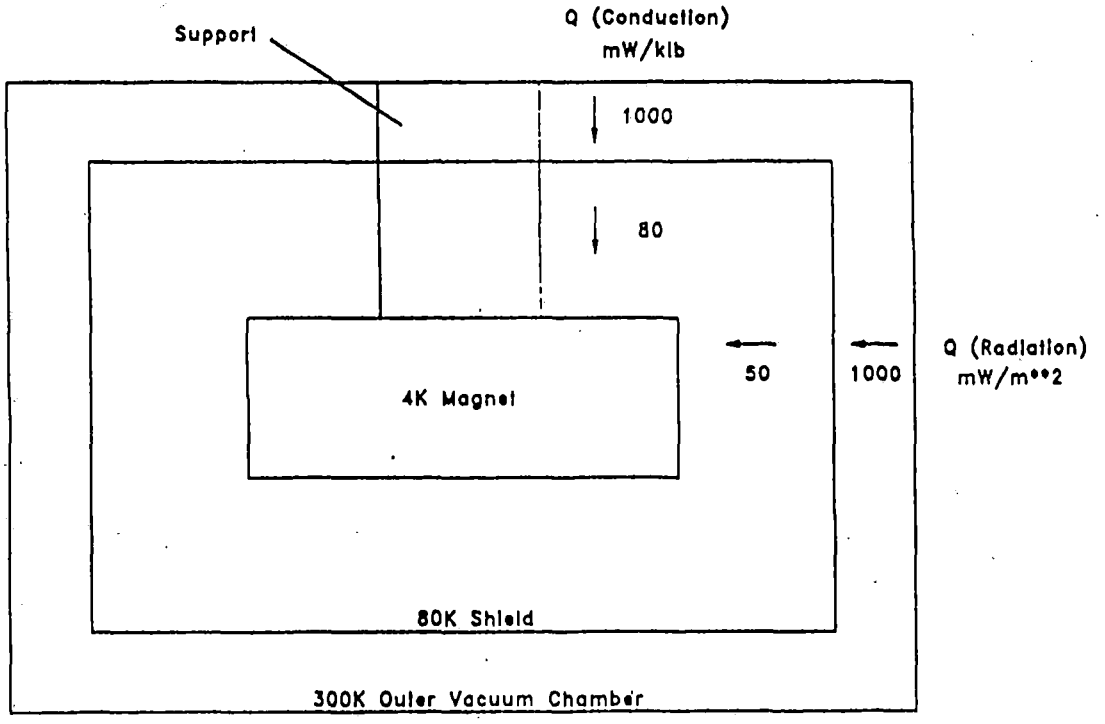

CRYOGENICS:

- 4K magnet cooled by pool boiling or 4K refrigerator.
- 80K shield and support intercept and eddy current shield cooled by LN2 or 80K refrigerator.

Magnet/cryostat: cryogenic description (System 3 – 80K shield only)
Figure 2-18

SUPERCONDUCTING MAGNET SYSTEM
LEVITATION AND PROPULSION CRYOSTAT
CONFIGURATION I

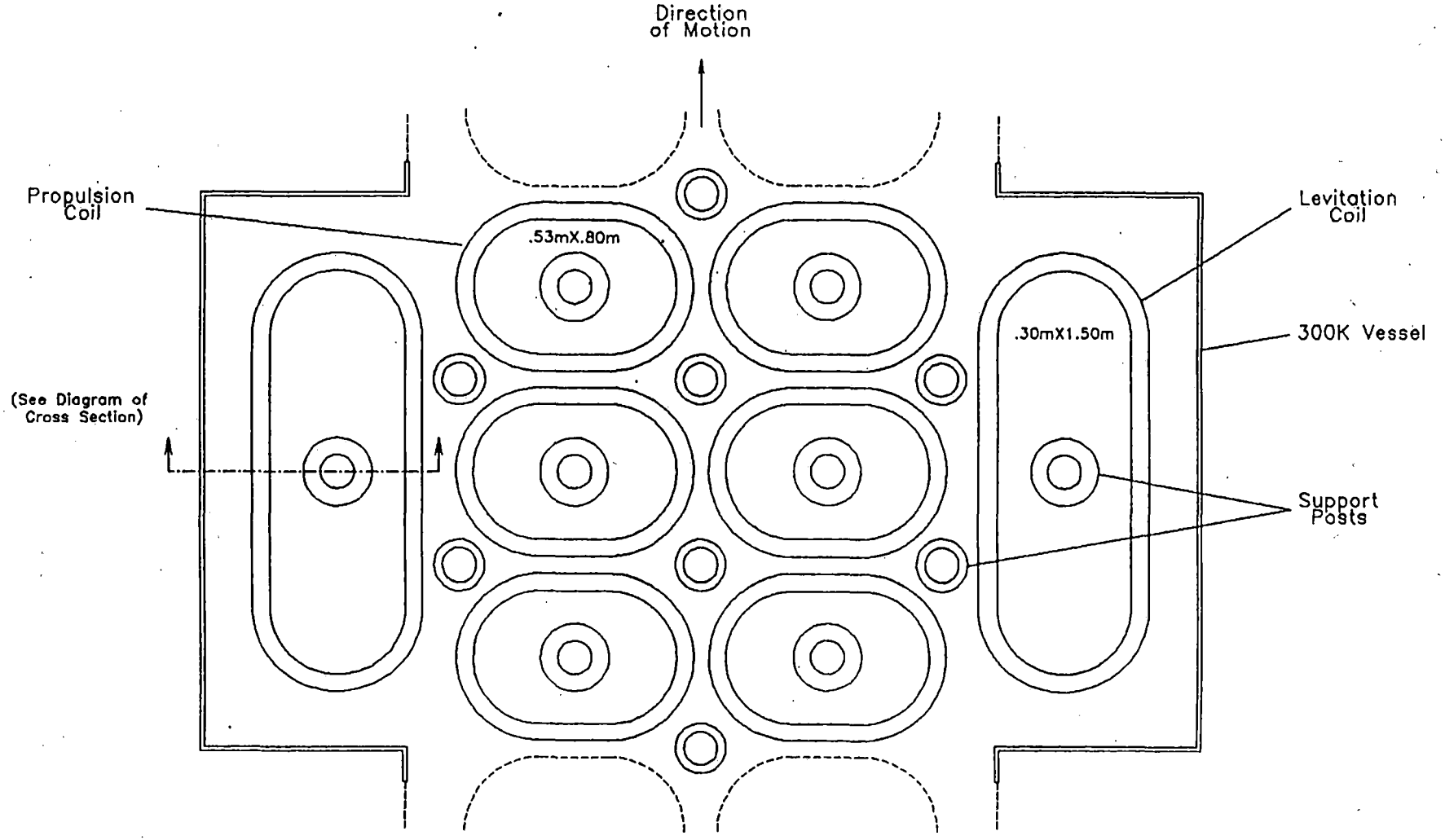

Figure 2-19

SUPERCONDUCTING PROPULSION MAGNET

COMPONENTS

1	Superconductor	6	80K Vessel
2	Coil Form	7	Foil Shields
3	Liquid Helium	8	20K Shield
4	4K Vessel	9	Cylindrical Supports
5	Liquid Nitrogen	10	300K Al Container

FEATURES

- Operating Loads:
  - 4.2 kN Horizontal
- Coil Dimensions:
  - Mean Length 0.53 m
  - Mean Width 0.80 m

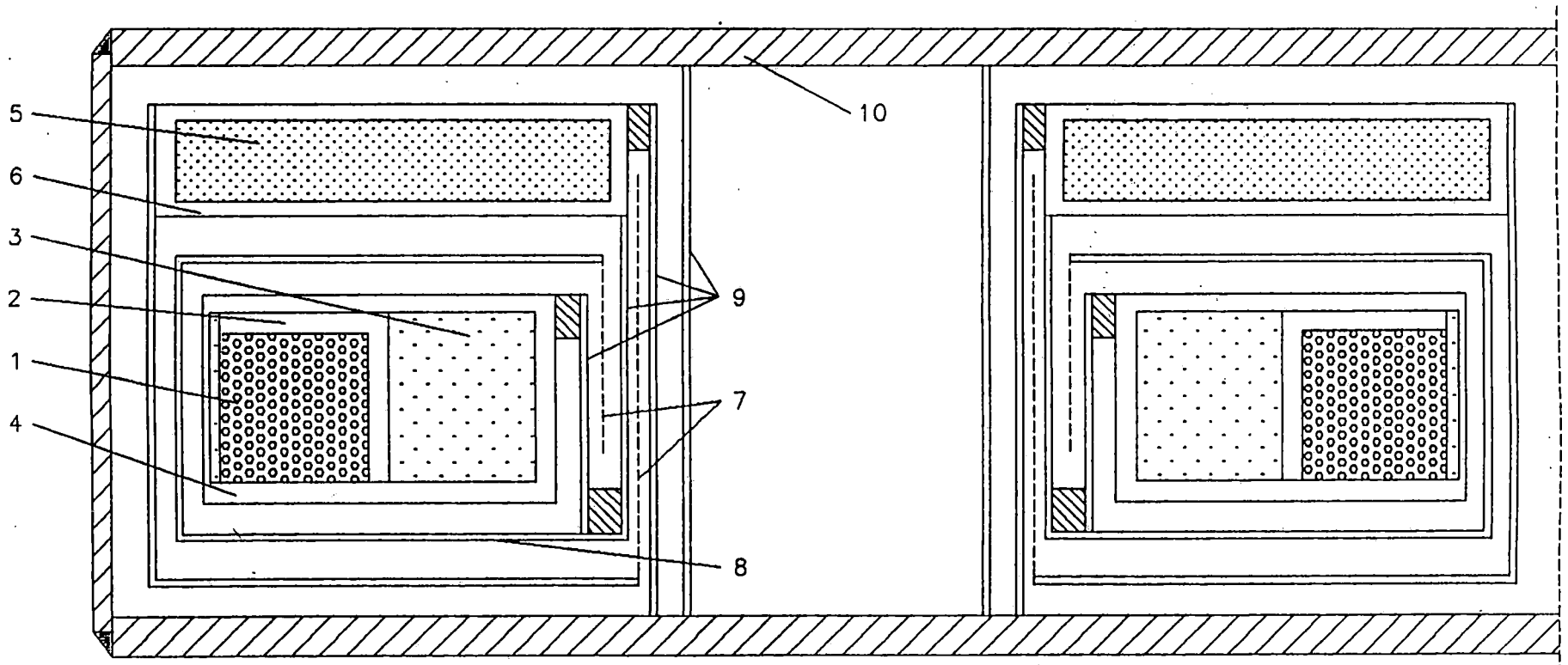

Figure 2-20

SUPERCONDUCTING LEVITATION MAGNET

COMPONENTS

1	Superconductor	6	80K Vessel
2	Coil Form	7	Foil Shields
3	Liquid Helium	8	20K Shield
4	4K Vessel	9	Cylindrical Supports
5	Liquid Nitrogen	10	300K Al Container

FEATURES

- Operating Loads:
  30 kN Vertical
- Coil Dimensions:
  Mean Length 1.50 m
  Mean Width 0.30 m

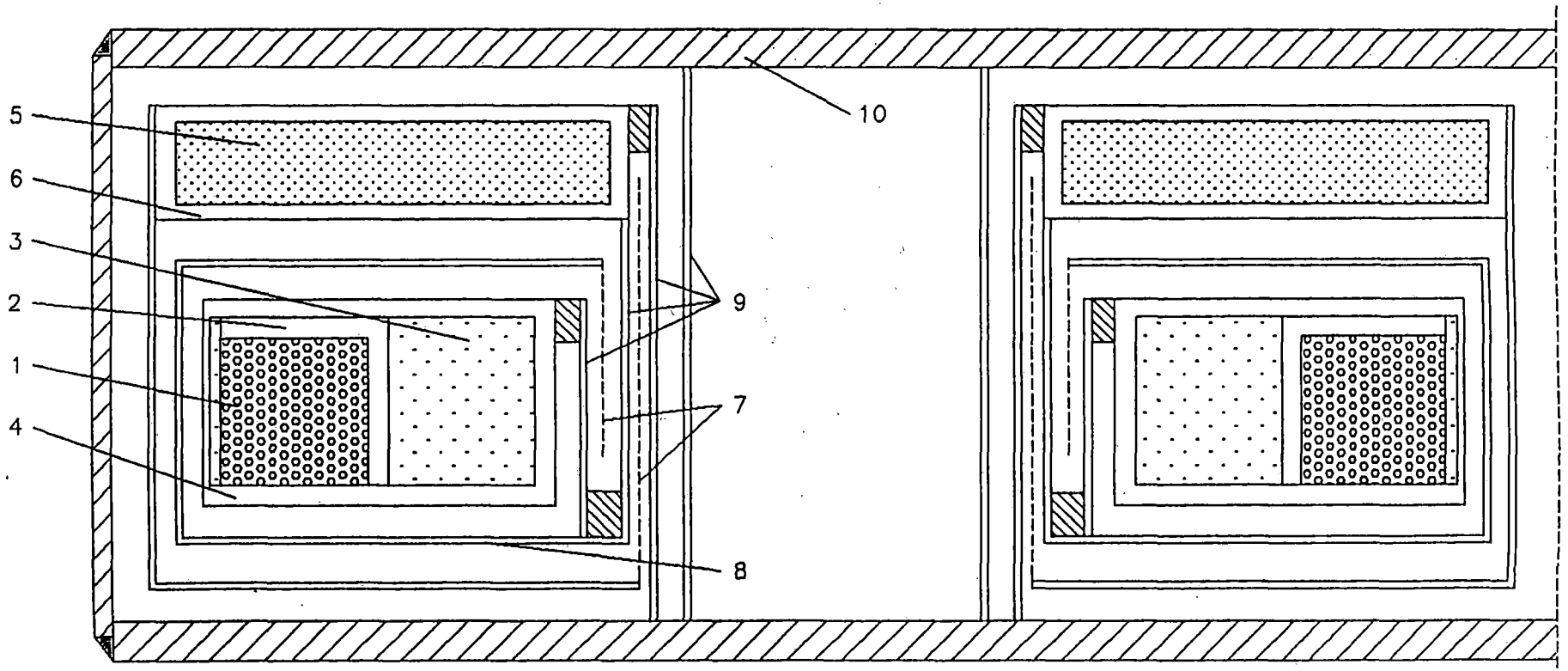

LEVMGT

Figure 2-21

CRYOSTAT FOR LEVITATION MAGNET

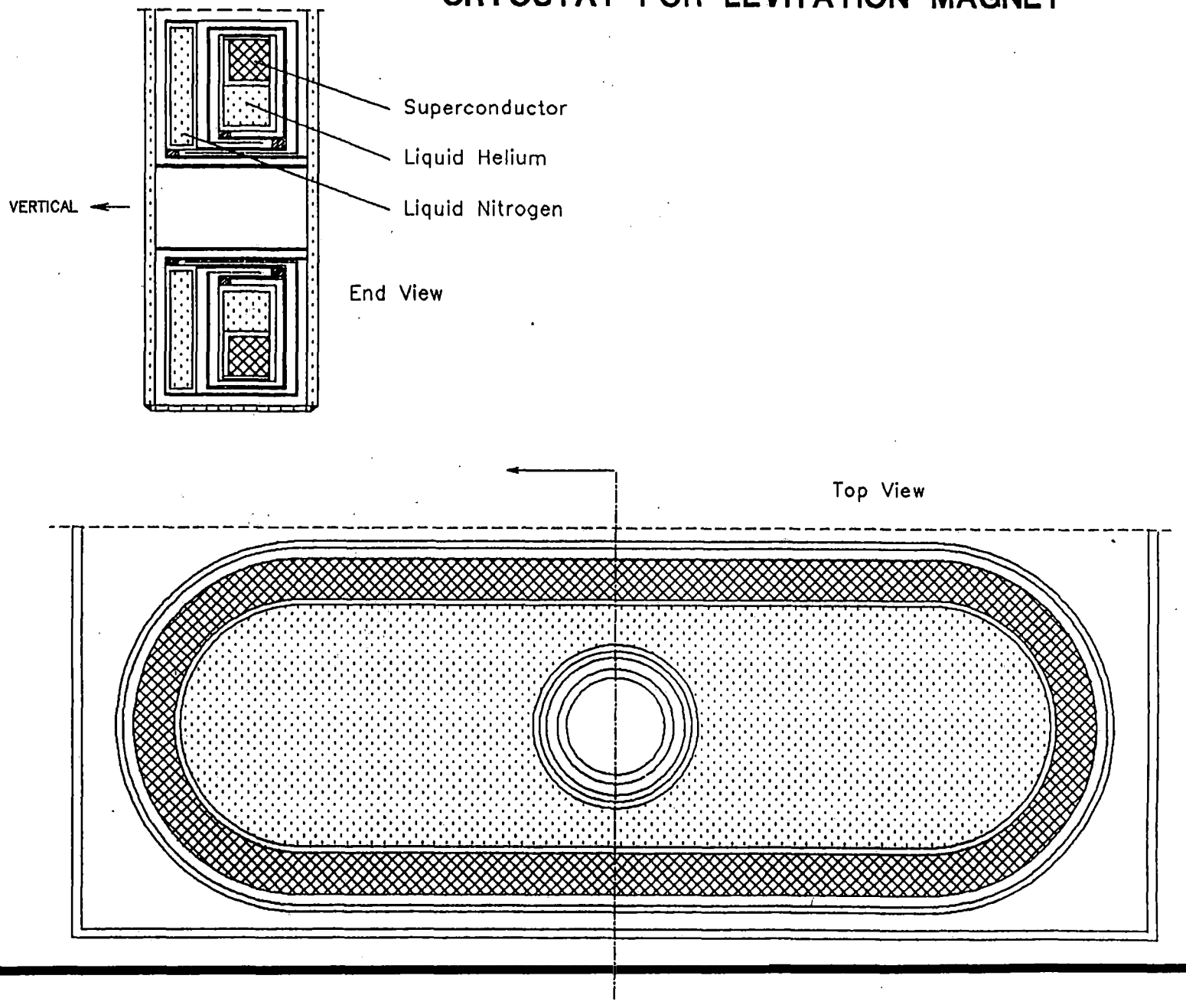

Figure 2-22

SUPERCONDUCTING MAGNET SYSTEM

LEVITATION AND PROPULSION
TYPE VI CONFIGURATION

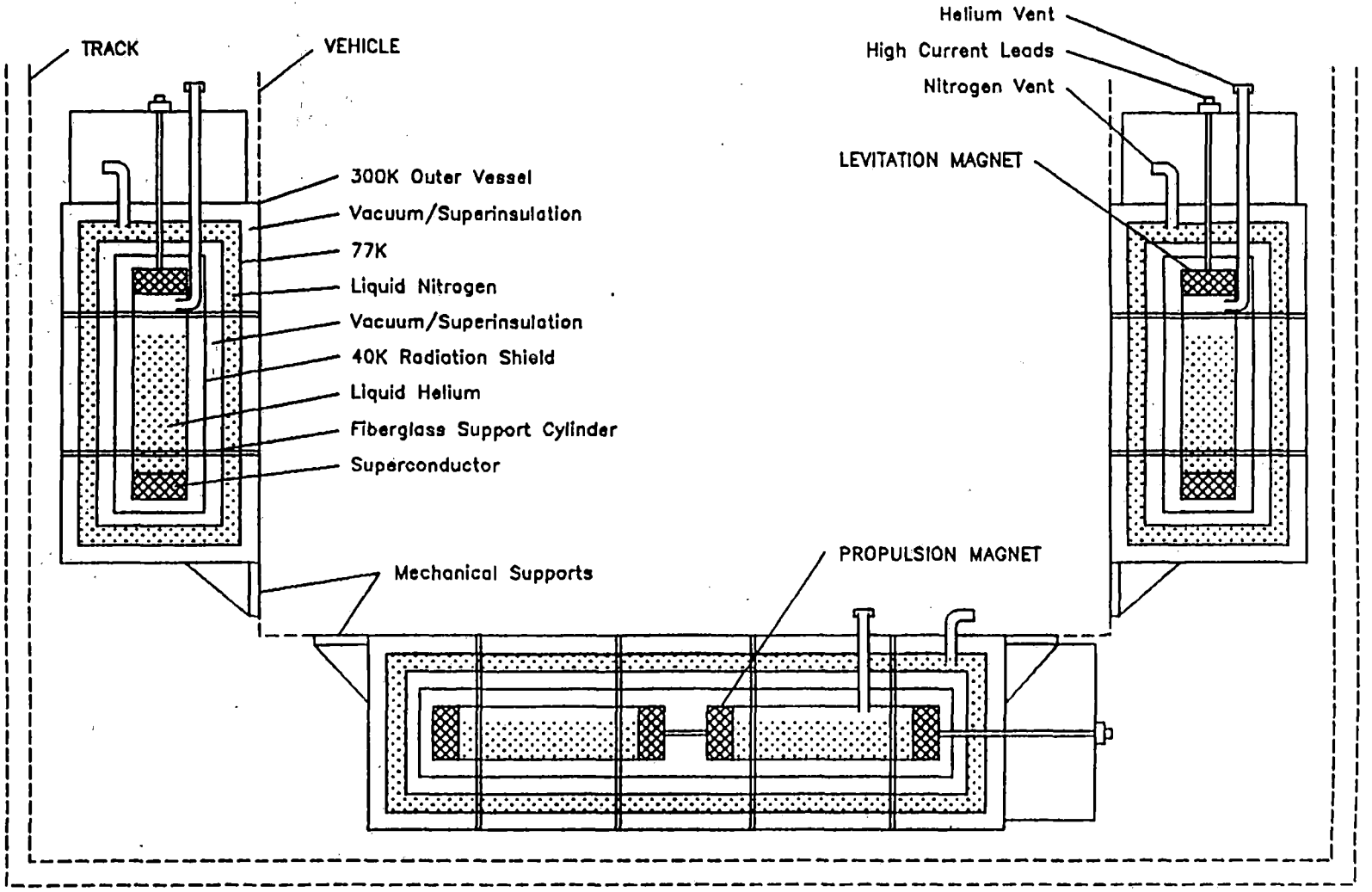

Figure 2-23

4. The total service space available for the magnets per car is assumed to be a box which is roughly:

- 30 m ¥ 3.4 m ¥ 0.8 m.
- This box has volume of approximately 80,000 liters.
- The total area of the sides of this box is approximately 250 m^2
- It is assumed that 40% of this area (100 m^2) will radiate to the heat shields of the cryostats.
- The heat load of the cryogenic piping is neglected. Bear in mind that the heat load of the piping for a continuous 4 K supply can be larger than the heat load of all the cryostats.

5. The heat load calculations are based on data for MRI magnets and the SSC accelerator.

6. We view these results as the "Best" one can do with each of these cryogenic systems.

- Practical considerations or adverse design choices will increase these cryogenic requirements.
- Lateral loads have been ignored, so that the total of loads to be supported from 4 K will be greater than 445,000 kN.
- Likewise when all the radiation area is taken into account, it is expected to exceed 100 m^2.
- For convenience of scaling, the heat loads are based on 445,000 kN per car and 100 m^2 of radiation per car.

7. To create some feeling for what these loads mean, we have assumed some reasonable fraction of the service volume being occupied with cryogens.

- Some storage is desirable to back-up the refrigerators and provide for power failure.
- We would expect that we would want to recover and recycle all of the helium.
- The use of LN_2 looks promising in order to significantly reduce the size and power requirements of an on-board refrigerator.
- The use of open cycle liquid helium should be considered only if every possible method can be used to minimize boil-off. We view this possibility as very unlikely.

A summary of heat loads is shown in Table 2-6. The computed heat loads for the 77 K shield and 20 K shields compare well with data from MRI systems and SSC cryostats, as shown in Table 2-7.

Table 2-6

Maglev Superconducting Magnet Cryogenic Performance

	System 1	System 2	System 3
For 50 tons			
$Q_{conduction}$			
Q_{4K}	1.0	3.0	8.0
Q_{shield}	7.0	5.5	–
Q_{80K}	100	100	100
For 100 m²			
$Q_{radiation}$			
Q_{4K}	0.3	0.6	5.0
Q_{shield}	4.5	4.0	–
Q_{80K}	100	100	100
Q_{total} (watts)			
Q_{4K}	1.3	3.6	13.0
Q_{shield}	11.5	9.5	–
Q_{80K}	200	200	200
Q_{total} (liter/hr)			
LHe	1.8	5.0	18.0
Shield	need 20K refr.	–	–
LN_2	4.4	4.4	4.4
Pot Life – 4,000 liters each			
LHe (days)	93	33	9
LN_2 (days)	38	38	38

Table 2-7

Magnet Cryogenic Heat Load Estimates

Conventional heat loads with 77 K shield and vapor-cooled shield at 20 K (comparison)

	SSC Dipoles	IGC MRI Systems
Radiation (300K to 77K)	0.75 W/m²	< 1.0 W/m²
Radiation (20K to 4K)	0.004 W/m²	< 0.002 W/m²
Cold Mass Support Conduction (300K to 77K) (Watts per 445 kg of supported mass)	1.12 W/1,000 kg	1.12 – 2.24 W/1,000 kg
Cold Mass Support Conduction (20K to 4K) (Watts per 445 kg of supported mass)	0.018 W/1,000 kg	0.011 – 0.022 W/1,000 kg

Using the heat loads, an estimate of the storage time or pot life was made. The pot life of the helium ranges from 9-90 days depending on the shield configuration. Liquid nitrogen storage is estimated to last about 38 days independent of the shield configuration.

Refrigerator for Liquid Helium

It is difficult to size the liquid helium refrigerator without having a detailed design for the cryostats and interconnecting helium supply line. However, using the heat loads in Table 2-6 we can make some estimates of the helium refrigerator capacities required. In all these estimates we have assumed that the eddy current losses in the cryostat are negligible and that the magnets are operated in the persistent mode with power leads retracted.

A summary of the liquid helium refrigerator requirements is shown in Table 2-8. The most likely or possible refrigeration power requirement is 16 kW for the refrigerator plus 25 kW for compressor cooling. This power can be used as the basis of power for cooling requirements. Note that an important parameter in the table is the power required to cool the compressors, which can be substantial for a mobile vehicle. For land-based compressors, the cooling is usually obtained from chillers or water circulation. Some of the cooling required for the compressor may be obtained from air flow as the vehicle moves down the guideway.

An analysis of cryogen consumption per vehicle, and efficiency and refrigerator weight is shown in Tables 2-7, 2-8, 2-9, and 2-10. Some important observations can be made from this data and the overall system requirements, even without a detailed design:

- From the data it is apparent that it is most efficient to use one refrigerator per car rather than a multiple of smaller ones. The smaller units must pay a penalty in cost, weight, volume, input power, and cycle efficiency.
- The smallest or most optimistic size considered was 2 watts at 4 K. The size and power requirements are modest. This small size is unrealistic when the necessary continuous feed liquid supply line is taken into consideration.

Table 2-8

4 K Refrigerator Requirements for Maglev Vehicle

(Assumes one refrigerator per car and that LN_2 is on-board)

	Min.	Most Likely	Max.
Capacity of 4 K refrigerator	2 watts	20 watts	200 watts
Power Required	4 kW	16 kW	80 kW
Weight of refrigerator	445 kg	2,225 kg	9,000 kg
Fraction of car weight (445,000 kg)	1%	5%	20%
Volume of refrigerator	1.5 m^3	6 m^3	20 m^3
Fraction of service volume (80 m^3)	0.8%	8%	25%
Specific work	300 kW/4 kW	2,000 to 1	800 to 1400 to 1
Carnot efficiency	4%	10%	20%
LN_2 required for refrigerator	0	5 L/hr	25 L/hr
LN_2 required for cryostats	5 L/hr	5 L/hr	5 L/hr
Total LN_2 required	5 L/hr	10 L/hr	30 L/hr
Power required for compressor cooling	6 kW	25 kW	125 kW

Table 2-9

Cryogen Consumption per Maglev Vehicle

Assume each car weighs ~ 50 tons

	20 K - 4 K LHe Liquid Helium		300 K - 80 K LN_2 Liquid Nitrogen	
	Watt	L/hr	Watt	L/hr
Conduction				
Vert. 50 tons	1.0	1.4	100	2.2
Horiz. (Braking) 0.5g	0.5	0.7	50	1.1
Radiation 50%	0.4	0.6	130	2.9
TOTAL	1.9	2.7	280	6.2

Assume 4,000 liter of each LHe and LN_2 containers

Pot Life Hours	1,480	645
Number of Days	62	27

Total of 10% of service volume occupied with LHe and LN_2

Table 2-10

Cryogen Heat Loads per Car (Calculations)

Conduction 20 K - 4 K

To support weight of car

Assume Q = 0.022 W/1,000 kg

Assume weight of car = 445,000 kN

Qcar = 0.0225 W/kg x 44,500 kg

= 1 Watt per car

= 1.4 liter/hr LHe per car

Radiation 20 K - 4 K

Area top and bottom = 2 x 3.4 x 30 = 204 m^2

sides = 2 x 33.4 x 0.8 = 53 m^2

Assume 0.003 Watt/m^2 x 257 ~ 1 liter/hr per car

Assume A_{EFF} = 50%

The Q = 1/2 x 1 = 0.5 liter/hr per car helium boil-off

Q Total 20 K - 4 K

$Q_T = Q_{support} + Q_{radiation}$

= 1.4 + 0.5

~ 2 liter/hr per car

Volume Service Compartment

Vol= 0.8 m x 3.4 x 30

≈ 80 m^3

= 80,000 liters

Assume 5% is LHe

Vol_{LHe} = 4,000 liters

Time to boil away

4,000 liters/2 liters per hour = 2,000 hours

÷ 24 = 83 days

Table 2-11

Cryogen Heat Loads per Car (Calculations)

Assume LN_2 300K - 77 K

Radiation 1 Watt/m^2

$Q = 50\% \times 257\ m^2 \times 1\ Watt/m^2$

$= 130$ Watt

Conduction 300 K - 77 K

$Q = 2.25\ W/1{,}000\ kg \times 44{,}500\ kg$

$= 100$ Watt

$Q_{TOTAL} = 130+100 = 230$ Watts 300K - 77 K

Let us also assume 4,000 liters of LN_2

Then:

$$\frac{\frac{45\ Watt/hr}{liter}}{230\ Watt} = \frac{0.2\ hr}{liter} \approx \frac{5\ liter}{hr}$$

$$\frac{4{,}000\ liters}{} = 800\ hr \div 24 = 33\ days$$

WT_{LN2} 4,000 liters x 0.40 kg/liter

$= 3.5$ turns $\div$ 50 turns $\approx$ 7% of total

- On the other end of the sizes considered, the 200 watt machine is not realistic either. It would require a significant fraction of the train's space and power.
- In the middle of these two extremes is a 20 watt, 4 K machine that looks feasible. It would be 5% of the weight and need 8% of the service volume. It would require 16 kW of power to be transferred to the levitated train.
- At this point, one might be tempted to put a design limit of 10 watts at 4 K on both the cryostats and the liquid helium supply line.
- This 4 K supply line that needs to run the full length on each car might require as much design work as the cryostats. At a minimum, it will also require an 80 K cooled radiation shield. Just figuring out how to plumb it in will require considerable effort. Hopefully we will be able to piggy-back on previous design efforts.
- It is obvious that realistic limits need to be established for the size of the 4 K refrigerator *before* one proceeds with a detailed design of the cryostat or the superconducting coil it houses.
- It may not make sense to design a super efficient cryostat if the losses are overwhelmed by the unavoidable transfer system.
- Anything short of a "systems" approach is not likely to be effective. Care should be taken to ensure that one part of the design does not get too far ahead of the other.
- For this simple analysis we have assumed that LN_2 would be stored on board. This would reduce power requirements and help in the case of a power outage. When the system is better defined, it may well be that this is not necessary.

Figures 2-24 through 2-27 show efficiency and weight data for the proper refrigerator choice. Note that HTSC coils operating at 20 K can operate with no liquid cryogen by using a refrigerator no larger than the minimum size refrigerator used for 4 K.

Figure 2-24.

Efficiency of liquid helium temperature refrigerators

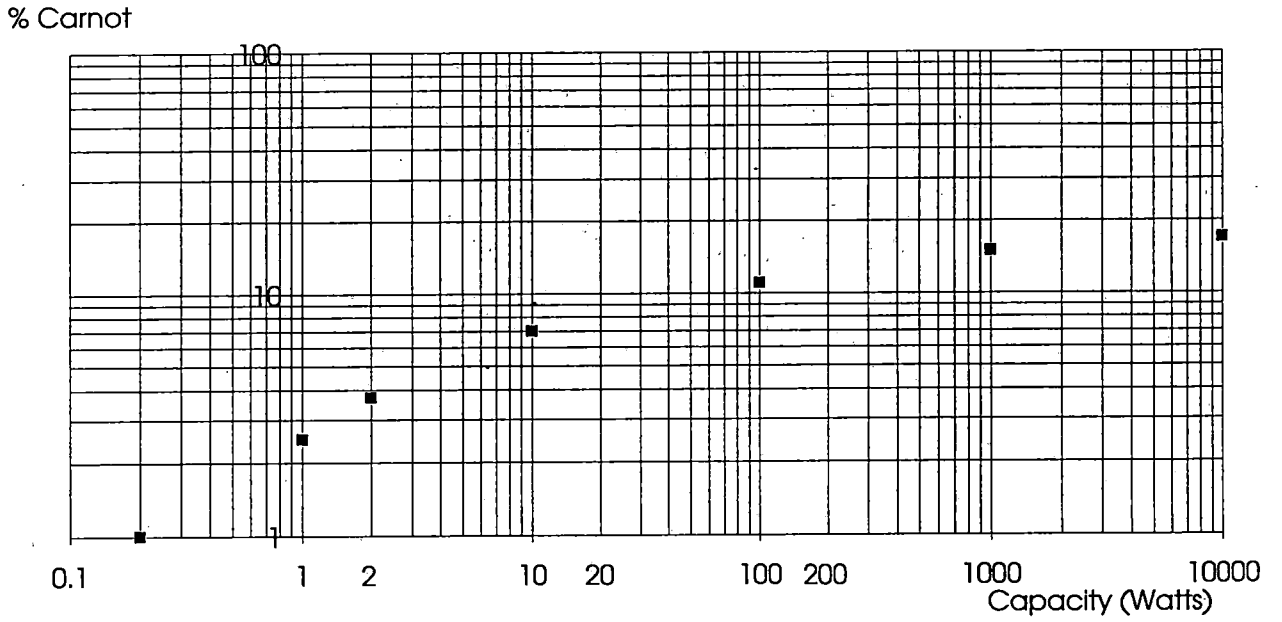

Figure 2-25.

Specific work requirements of liquid helium temperature refrigerators

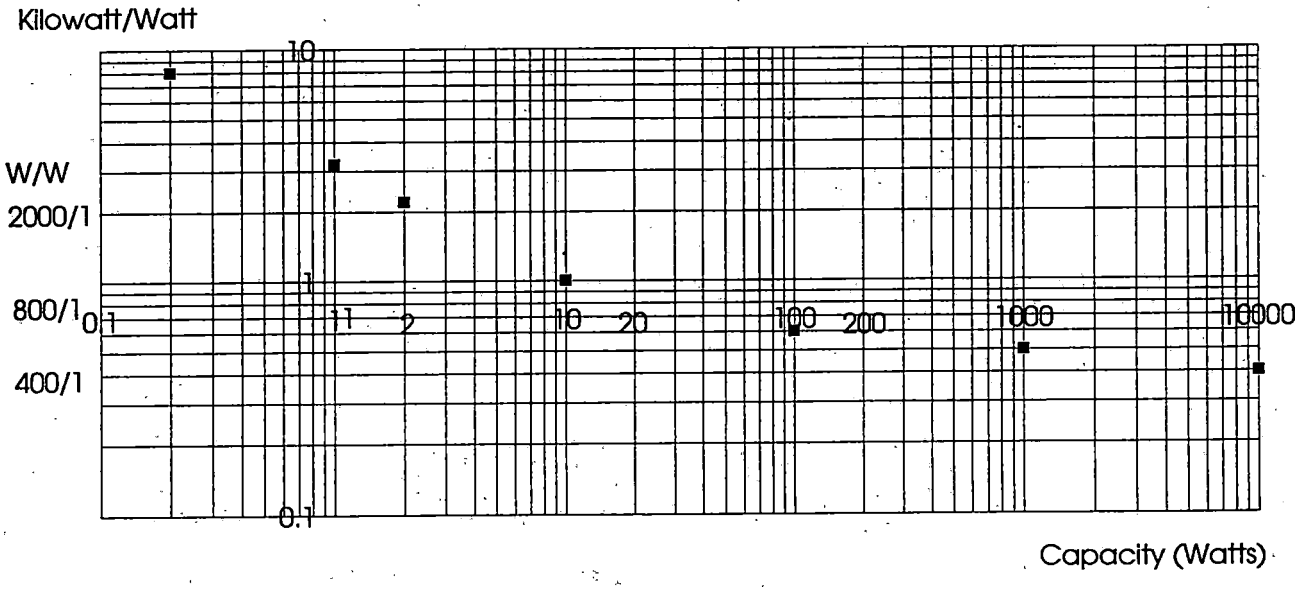

Figure 2-26.

Weight of liquid helium temperature refrigerators

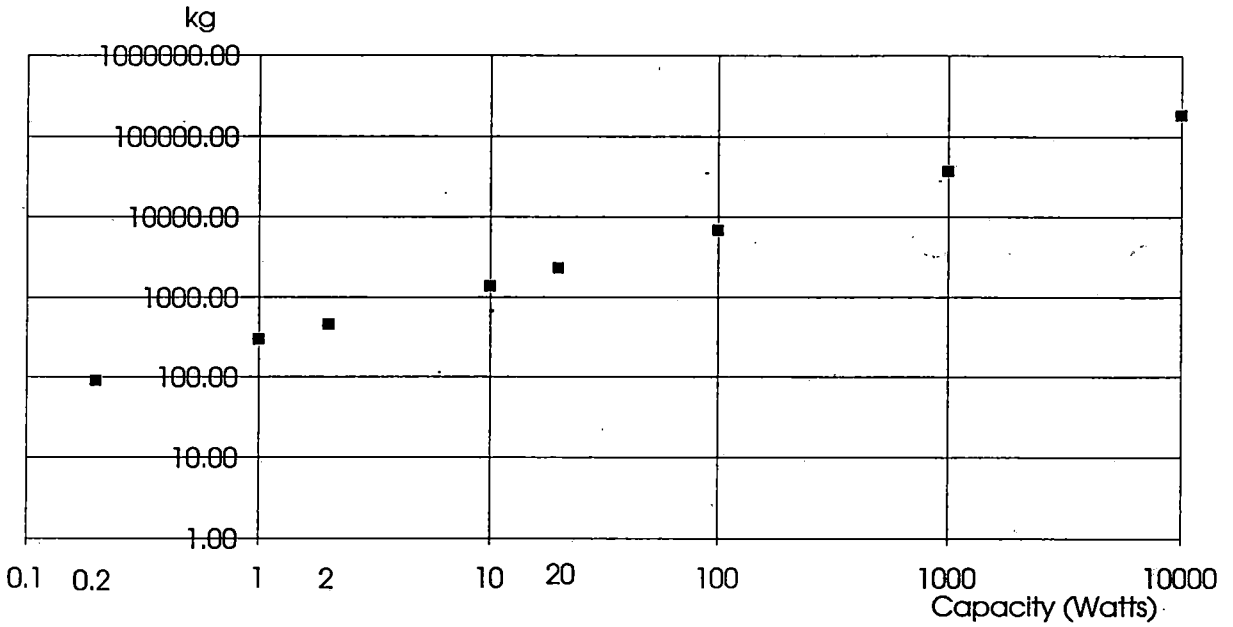

Figure 2-27.

Volume of liquid helium temperature refrigerators

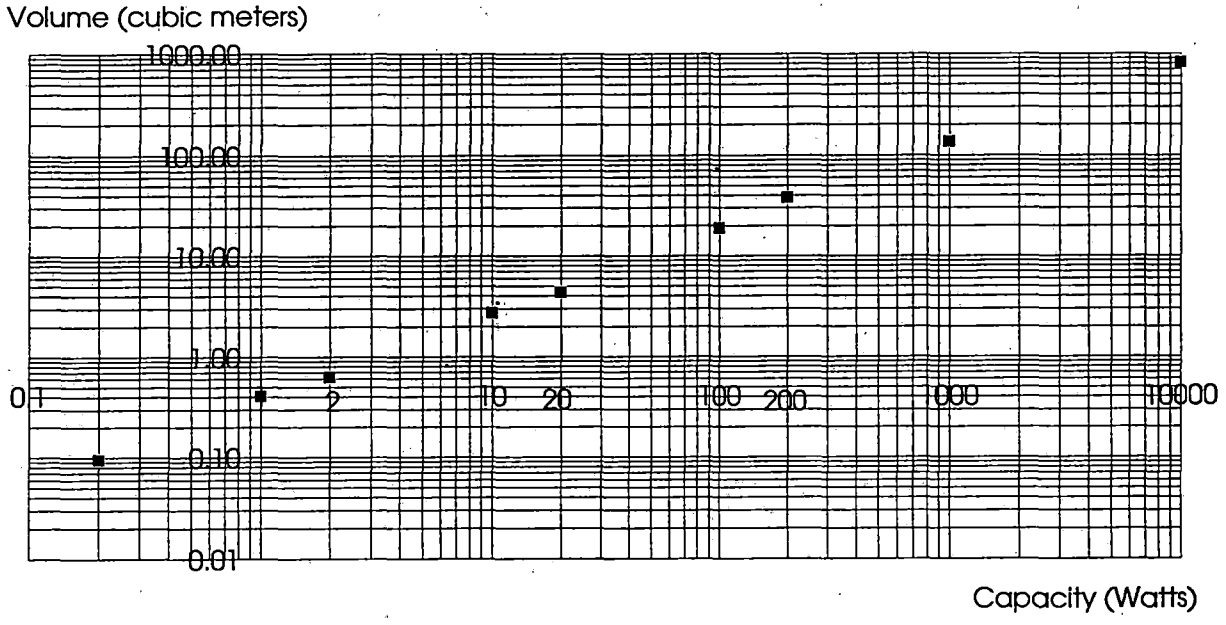

2.5 Magnetic Shielding

Unshielded Magnet Field Profiles

Magnet field profiles were generated in the passenger compartment in order to determine the magnetic shielding requirements and design.

Region of Interest

The passenger compartment in the study is 25 meters long by 3.4 meters wide. A portion of the compartment corresponding to one magnet cell has been examined which is representative of the entire train because the magnet pattern repeats. The magnetic field was computed from the nearest magnets in the cell, neglecting neighboring cells.

The train axis is defined as the y axis, which is also the direction of motion, the horizontal axis perpendicular to motion is labeled the x axis, and the vertical axis is the z axis. Profiles were taken at floor level (z = 0 cm), seat level (z = 50 cm), and head level (z = 150 cm). Three locations along the axis of the train were studied including the midplane (y = 0), the center of the propulsion magnet pair, and two positions forward of the midplane (y = 30 cm and y = 60 cm).

Unshielded Profiles of Configuration I

A layout of configuration I is shown in Figure 2-28 which consists of six horizontal propulsion magnets and two horizontal levitation magnets. The magnitude of the field generated by the propulsion and levitation coils at the midplane is shown in Figure 2-29 at the floor level, seat level, and head level. The field ranges from 80 to 112 Gauss. Similar plots forward of the midplane (Figures 2-30 and 2-31) indicate the field ranges from 80 to 118 Gauss at y = 30 cm and 48 to 100 Gauss at y = 60 cm. The magnetic field profiles are quite complicated because the magnets are designed with alternating polarity to minimize the field in the passenger compartment.

RELATIVE LOCATIONS OF PROPULSION AND LEVITATION COILS

CONFIGURATION I

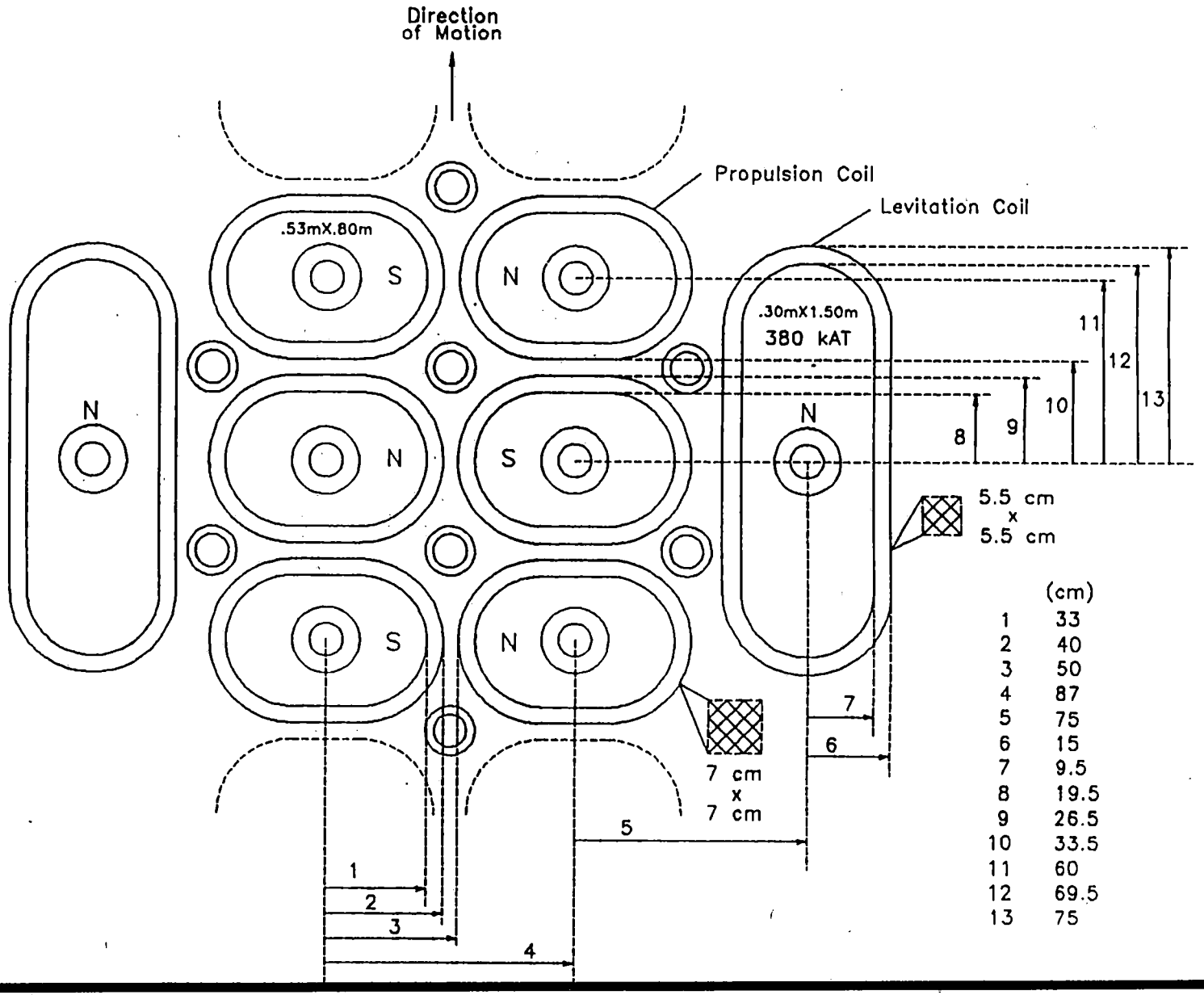

Figure 2-28

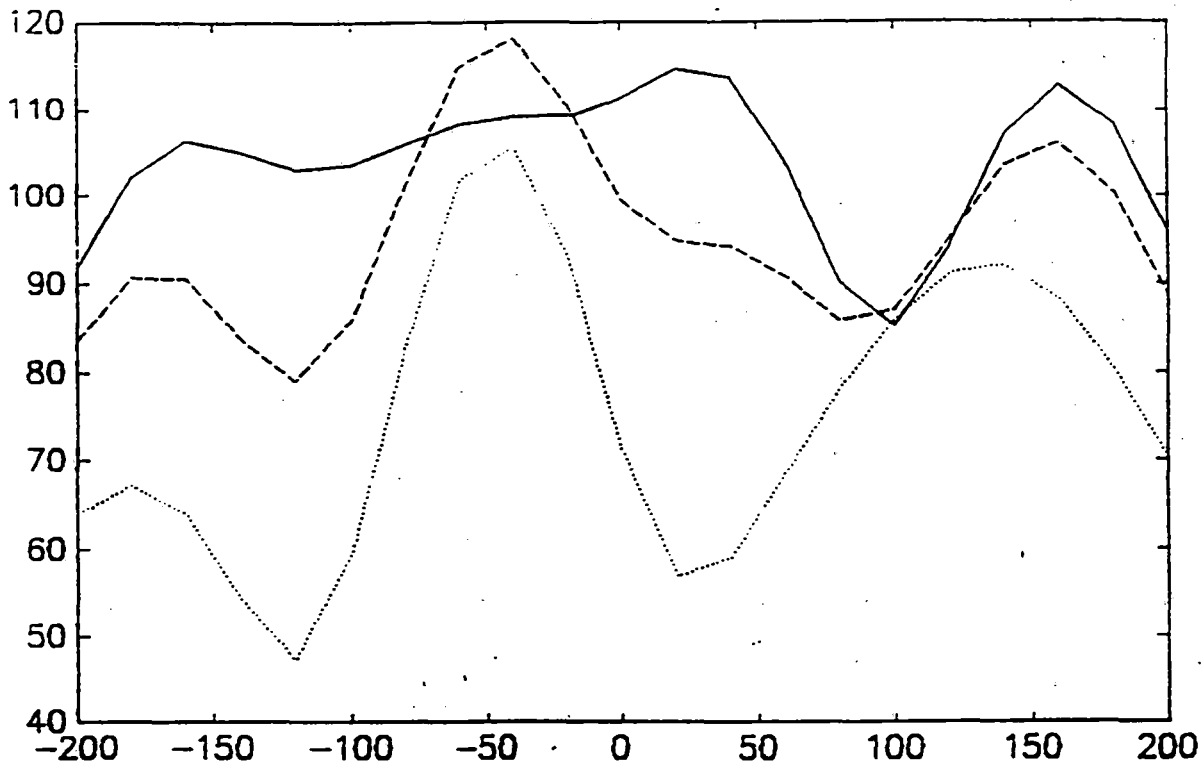

Configuration I.

The total magnetic field profile at the floor level

(a) In the midplane of the propulsion magnet (solid).
(b) In the plane 30 cm beyond propulsion magnet midplane (dashed).
(c) In the plane 60 cm beyond propulsion magnet midplane (dotted).

Figure 2-29

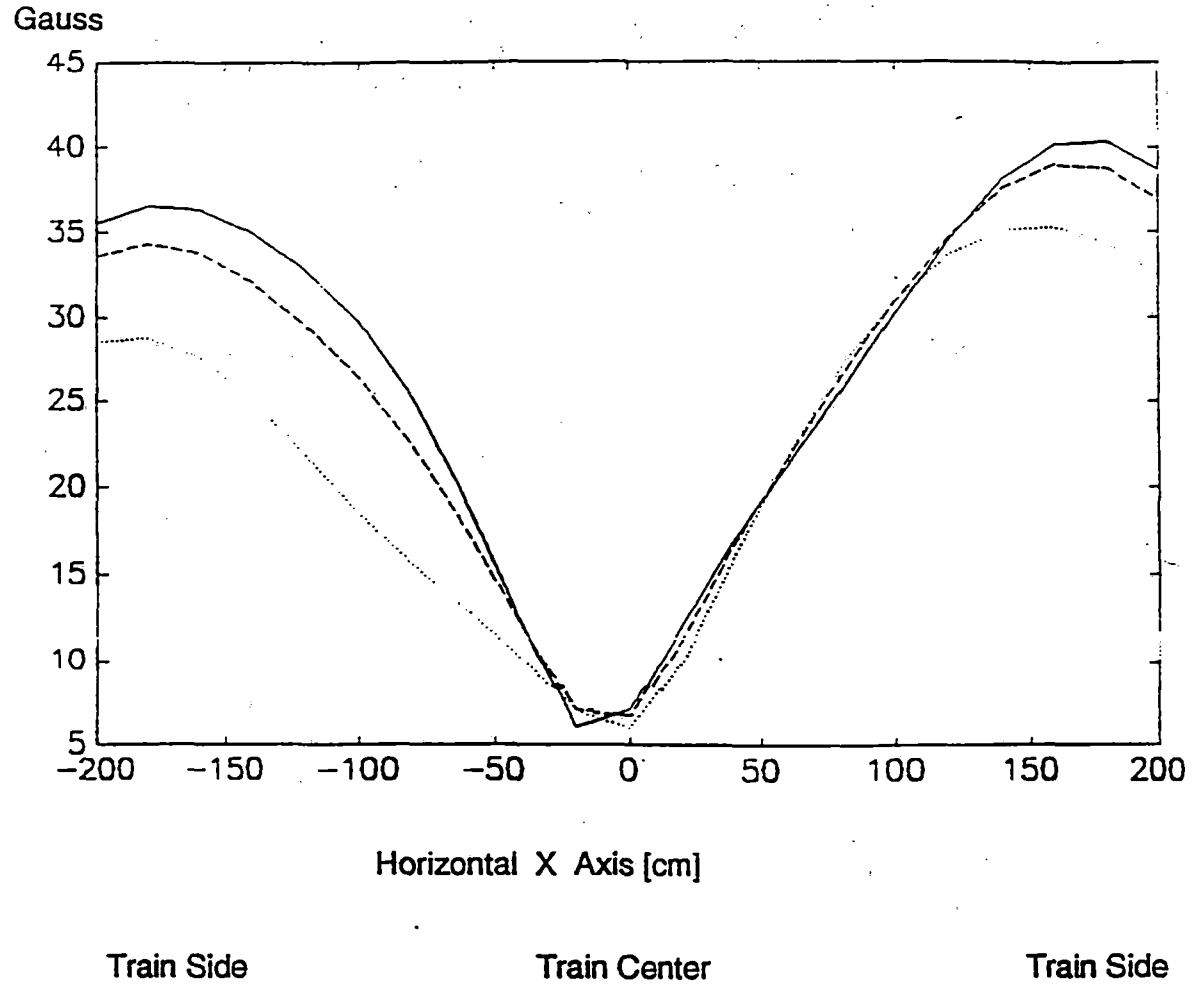

Configuration I

The total magnetic field profile 50 cm above floor level

(a) In the midplane of the propulsion magnet (solid).
(b) In the plane 30 cm beyond propulsion magnet midplane (dashed).
(c) In the plane 60 cm beyond propulsion magnet midplane (dotted).

Figure 2-30

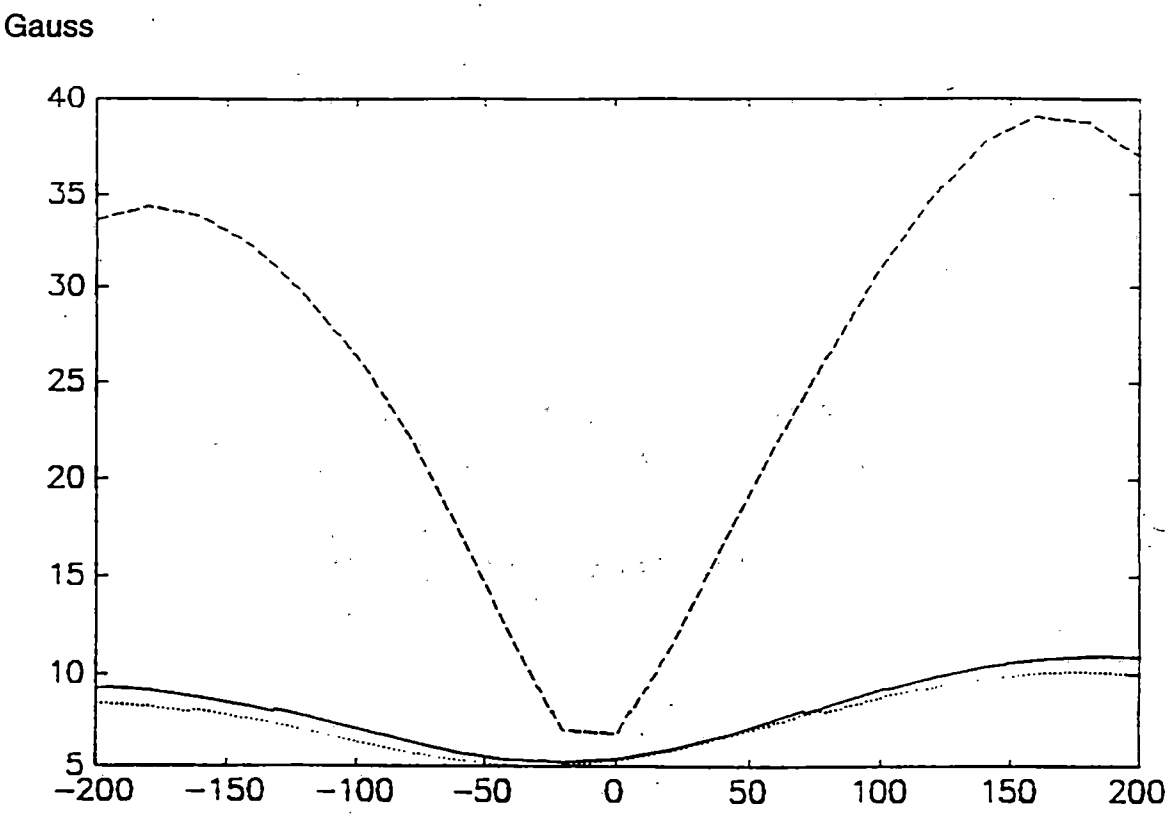

Configuration I

The total magnetic field profile 150 cm above floor level

(a) In the midplane of the propulsion magnet (solid).
(b) In the plane 30 cm beyond propulsion magnet midplane (dashed).
(c) In the plane 60 cm beyond propulsion magnet midplane (dotted).

Figure 2-31

Unshielded Profiles of Configuration VI

Configuration VI is shown in Figures 2-32 and 2-33. This configuration consists of two horizontal levitation magnets and six vertical propulsion magnets.

The field profiles at the floor at the midplane and forward of the midplane are shown in Figure 2-34. The field ranges from 10 to 115 Gauss at the midplane, 8 to 105 Gauss at y = 30 cm, and 8 to 80 Gauss at y = 60 cm.

The field profiles at seat level are shown in Figure 2-35. The field ranges from 20 to 42 Gauss. At head level this range drops to 10 to 12 Gauss, as shown in Figure 2-36.

Actively Shielded Magnets

One method of devising an actively shielded magnet is to add a coil of opposite polarity between the passenger compartment and the magnet to be shielded. The exact location, dimensions, and current in the shielding coil are dictated by the geometry and shielding requirements.

For simplicity a single circular propulsion coil was analyzed. The results are generally applicable to a collection of circular or racetrack coils.

In Figure 2-37, the field profile of an unshielded 600 kAT coil is shown at floor level, seat level, and head level. The profile is symmetric so that only one-half of the profile is shown. The field is higher (500 Gauss compared to 120 Gauss) than for a group of alternating coils wherein the fields tend to cancel one another's contributions.

MAGLEV 2000

PROPULSION AND LEVITATION COILS

CONFIGURATION VI

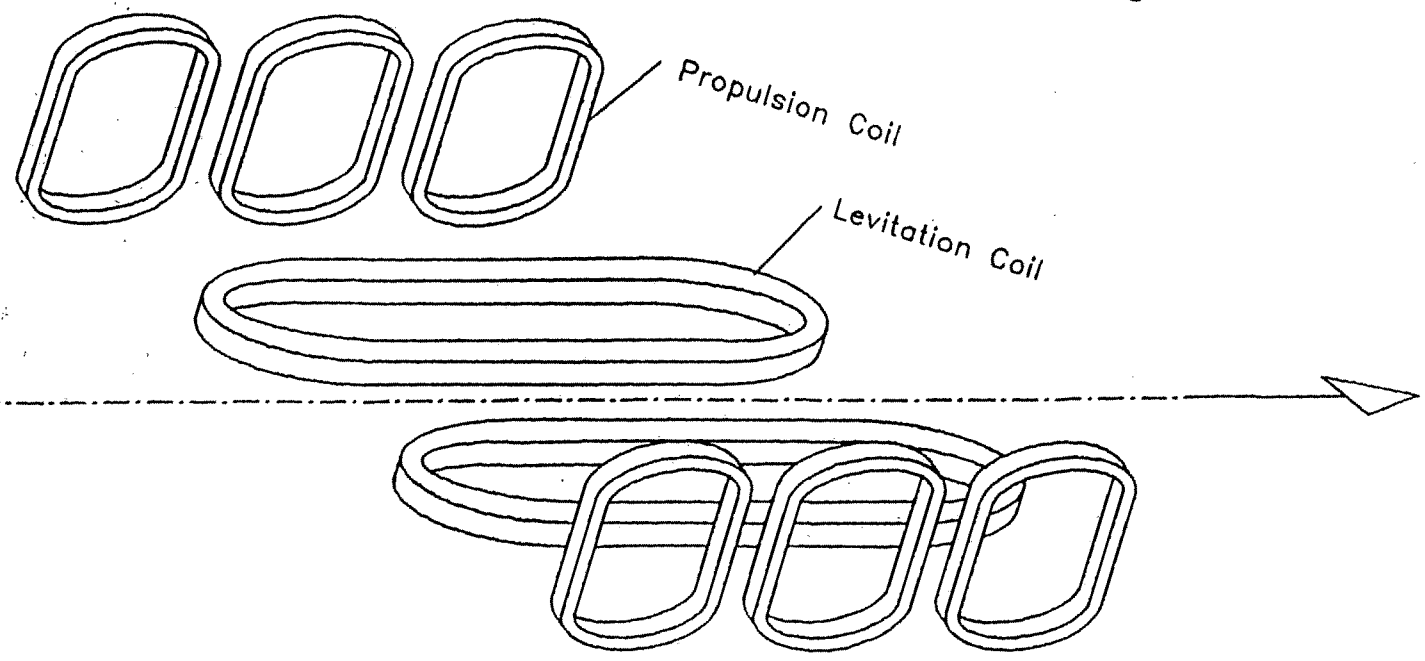

Figure 2-32

RELATIVE LOCATIONS OF PROPULSION AND LEVITATION COILS

CONFIGURATION VI

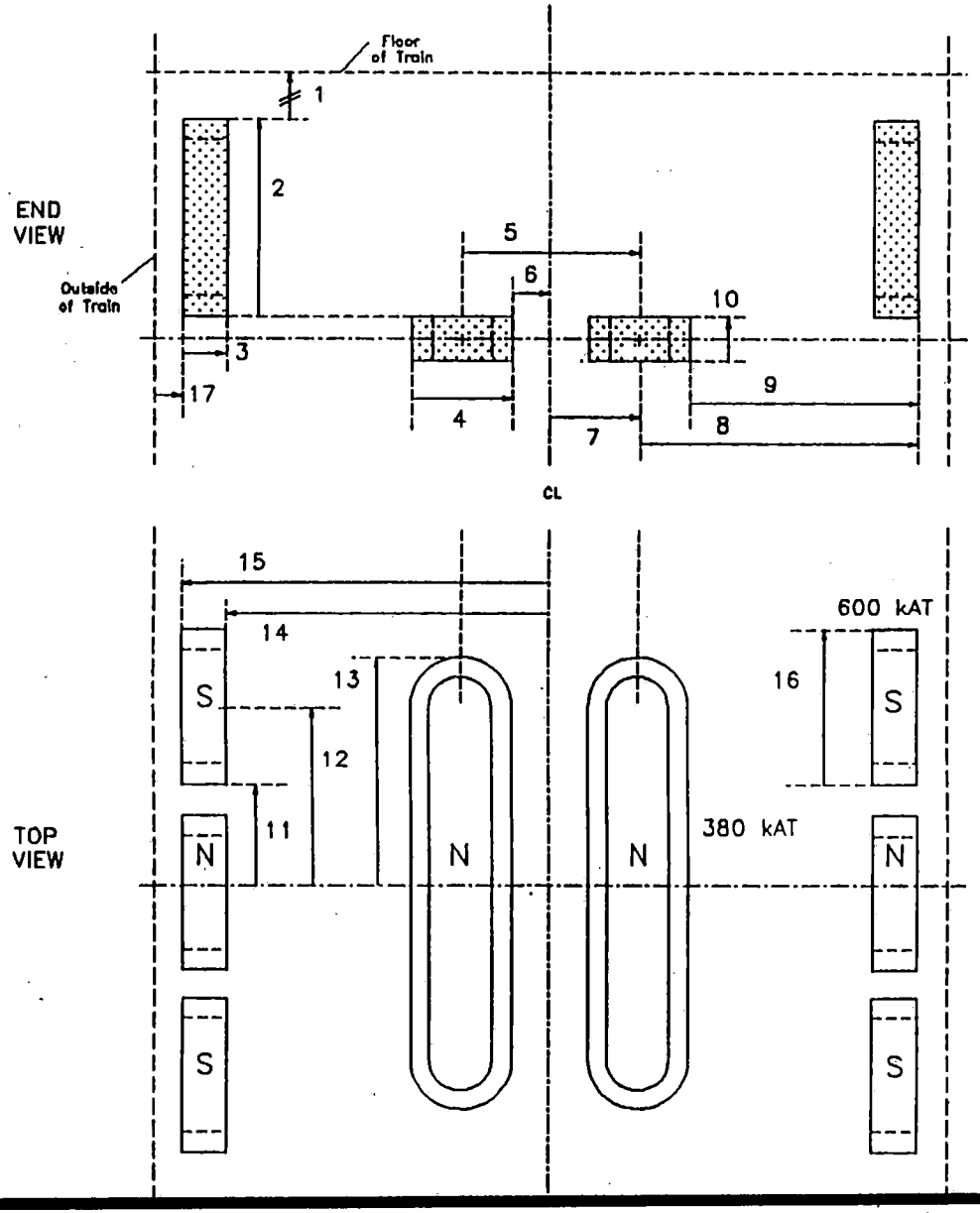

	(cm)
1	17.5
2	80
3	7
4	30
5	190
6	80
7	95
8	65
9	50
10	5.5
11	33.5
12	60
13	75
14	158
15	165
16	53
17	5

Figure 2-33

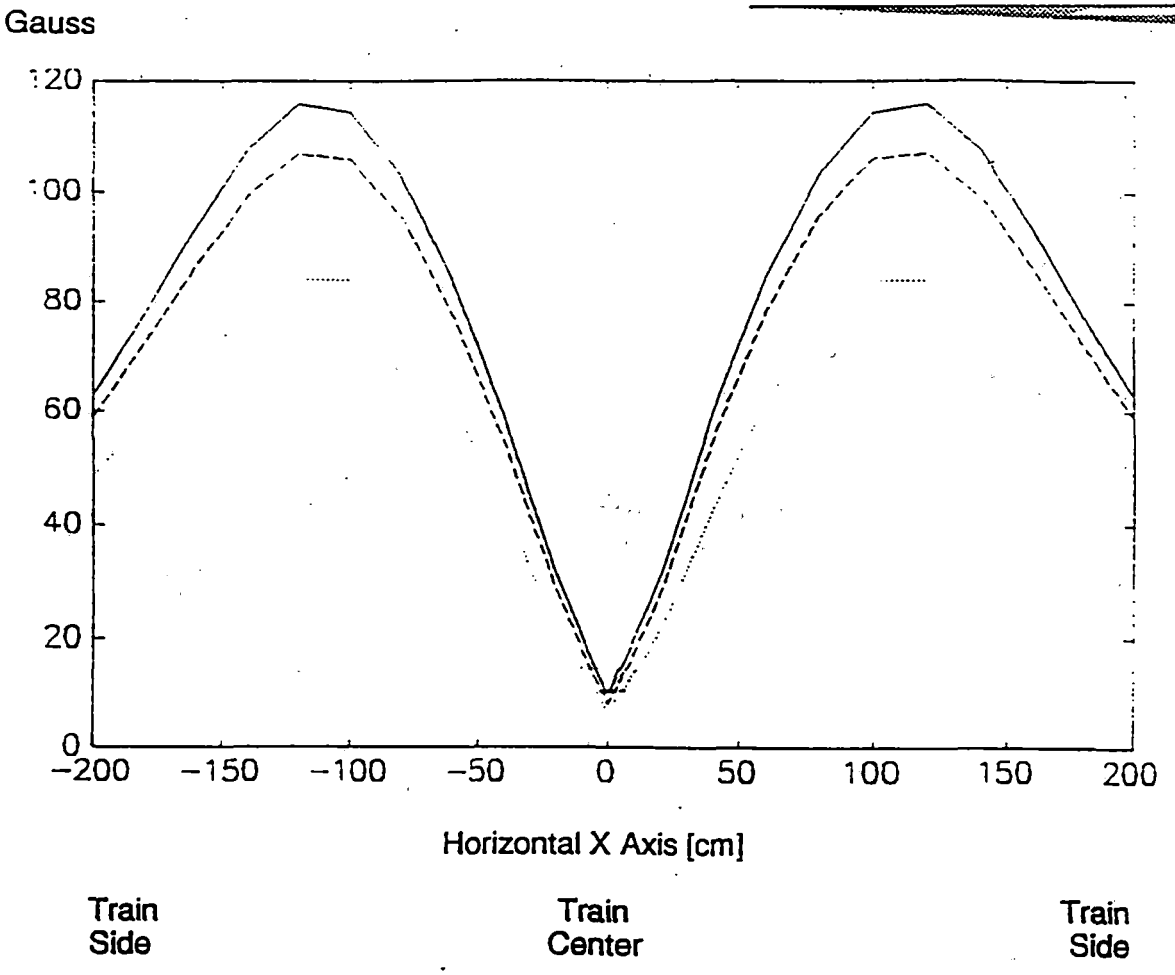

Configuration VI

The total magnetic field profile at the floor level

(a) In the midplane of the propulsion magnet (solid).
(b) In the plane 30 cm beyond propulsion magnet midplane (dashed).
(c) In the plane 60 cm beyond propulsion magnet midplane (dotted).

Figure 2-34

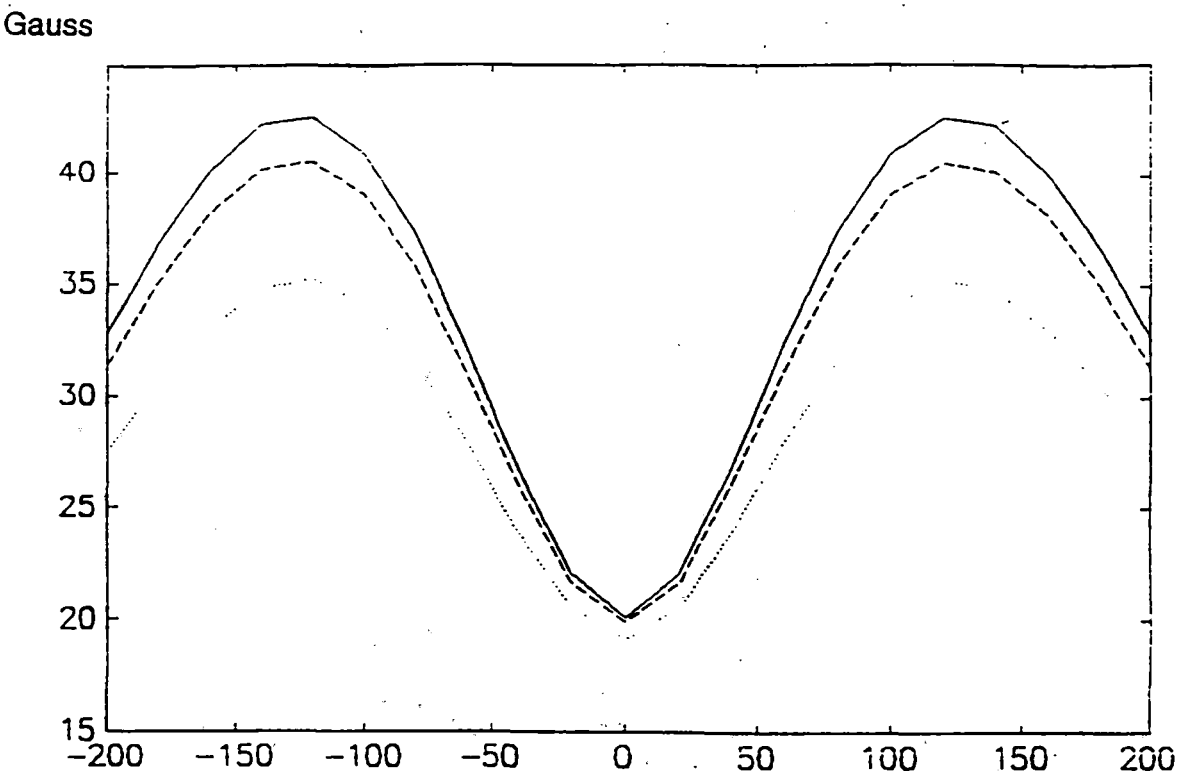

Configuration VI

The total magnetic field profile 50 cm above floor level

(a) In the midplane of the propulsion magnet (solid).
(b) In the plane 30 cm beyond propulsion magnet midplane (dashed).
(c) In the plane 60 cm beyond propulsion magnet midplane (dotted).

Figure 2-35

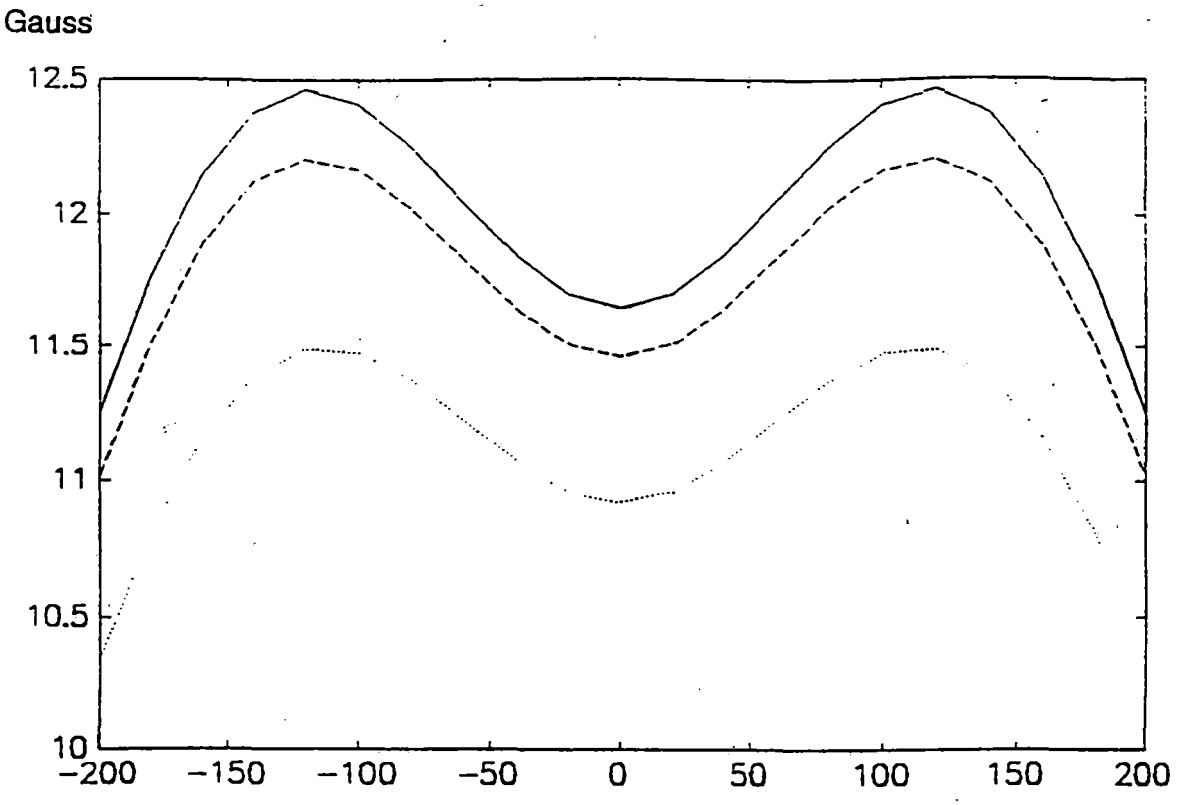

Configuration VI

The total magnetic field profile 150 cm above floor level

(a) In the midplane of the propulsion magnet (solid).
(b) In the plane 30 cm beyond propulsion magnet midplane (dashed).
(c) In the plane 60 cm beyond propulsion magnet midplane (dotted).

Figure 2-36

FIELD PROFILE FOR THE PROPULSION MAGNET

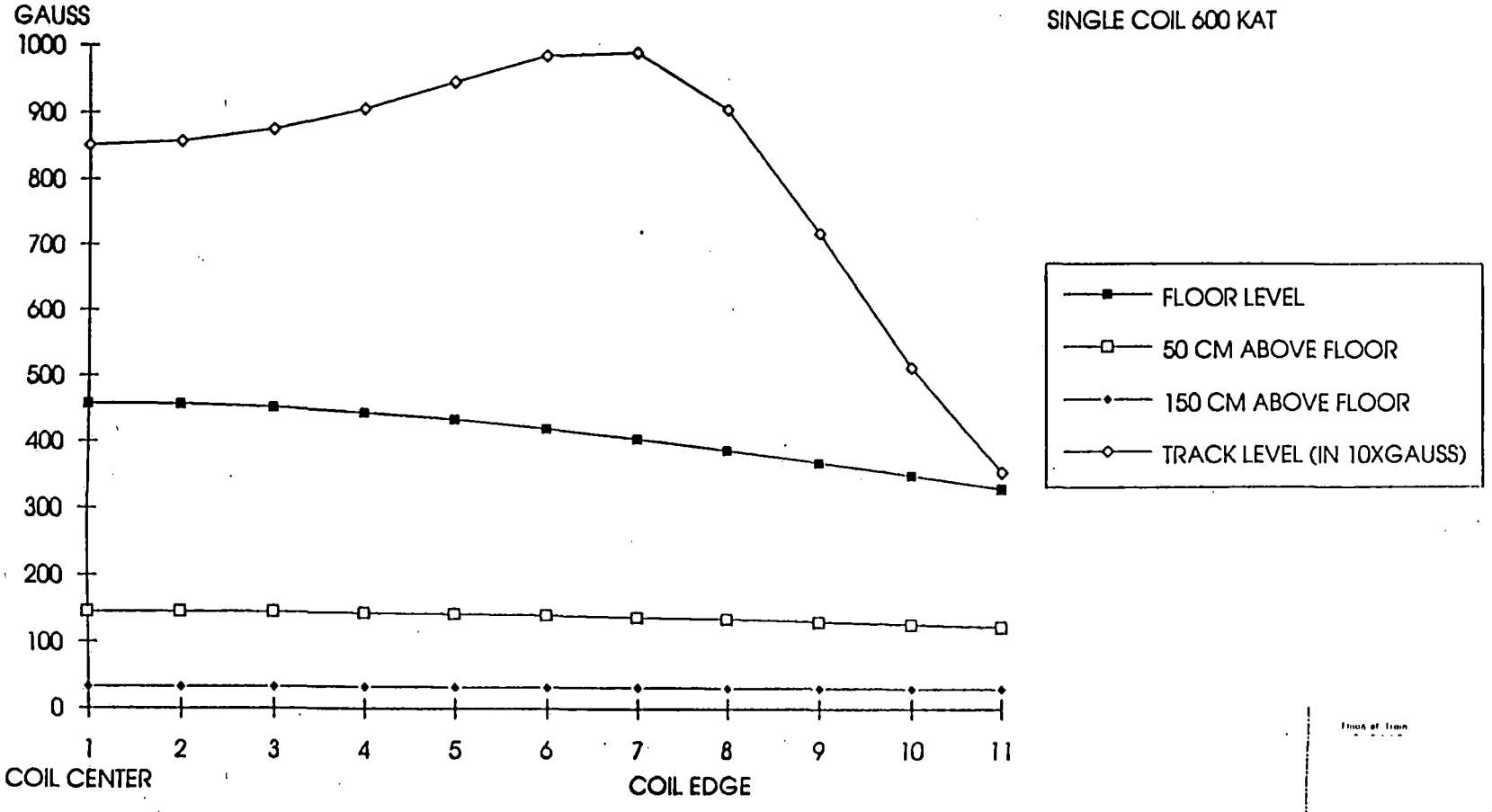

Figure 2-37

Shielding Effect

The addition of a shield magnet reduces both the field in the passenger compartment and the field at the track. This requires that the propulsion coil or levitation coil be driven at a higher current to compensate for the loss of field due to the shield in order to maintain the same lift or propulsion. The shield, in turn, must be driven at a higher field to remove field in the passenger compartment. This process will lead to higher currents in the shield and magnet until both the track field and the passenger fields are acceptable.

Figure 2-38 shows this effect quite clearly. A 600 kAT coil is shielded by another 600 kAT coil with the same dimensions and placed 10 cm above the main coil. The shield coil reduces the field in the passenger compartment from 500 to 150 Gauss, but also drops the field at the track.

Optimization

Two cases are presented as examples of shield optimization. In the first case shown in Figure 2-39, a coil of size 2.8 x 7 cm is placed 10 cm above the main coil and the current in the coil is adjusted until the field above the center of the coil at the passenger floor is approximately zero (0.08 Gauss). In regions above the floor, the field in the passenger compartment is higher.

In a second example shown in Figure 2-40, an attempt is made to lower the field more uniformly in the passenger compartment. Here the radius of the shield coil is adjusted to reduce the field all over the passenger compartment (not just at a point). The currents in the magnet and shield are adjusted so that the field at the track is not reduced from the required value.

More sophisticated optimization methods can be employed to reduce the passenger compartment field. These methods are constrained by the geometry of the train. Nevertheless, practical shields which reduce the passenger field to less than 10% of the unshielded values are easily attainable.

FIELD PROFILE FOR THE PROPULSION MAGNET

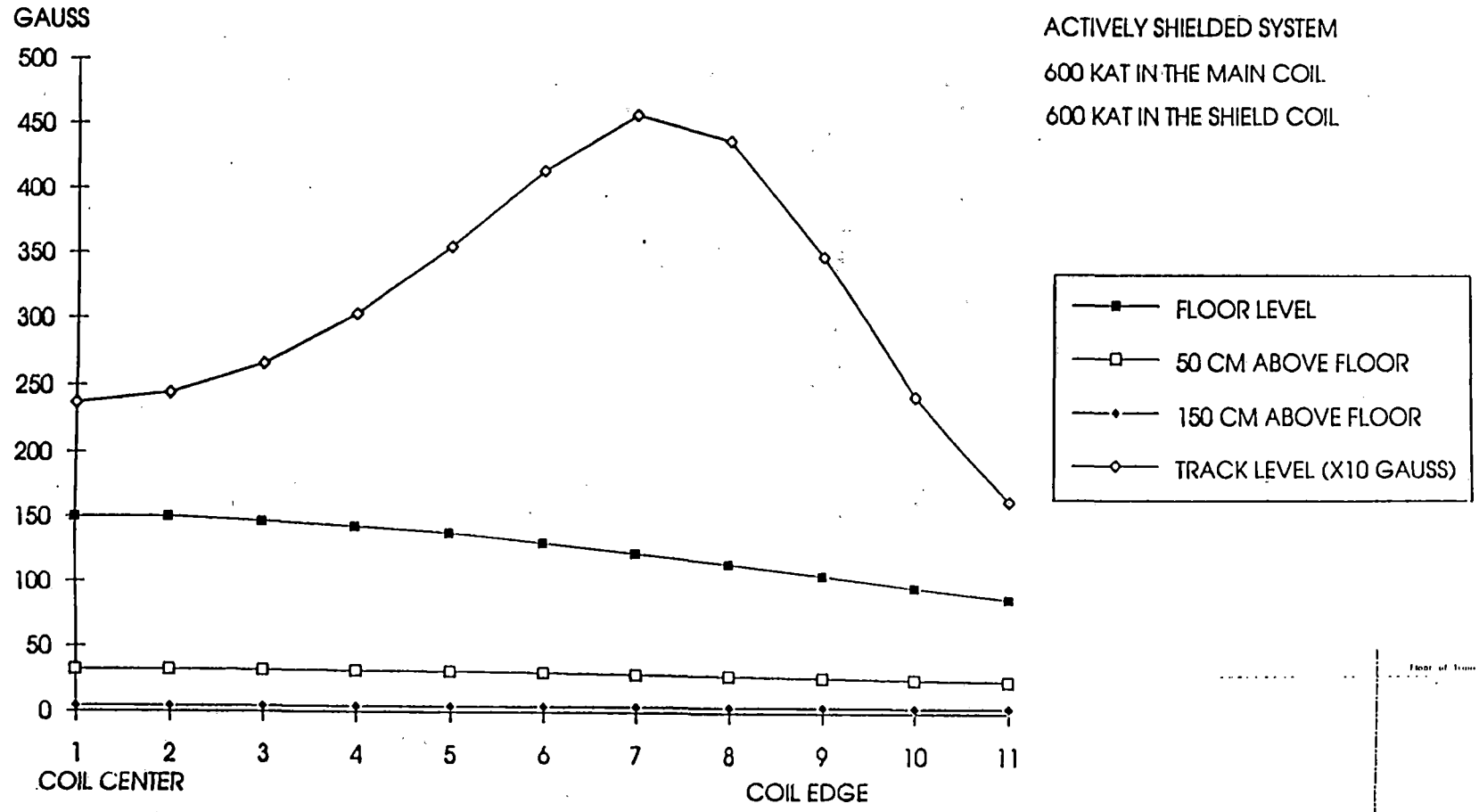

Figure 2-38

FIELD PROFILE FOR THE PROPULSION MAGNET

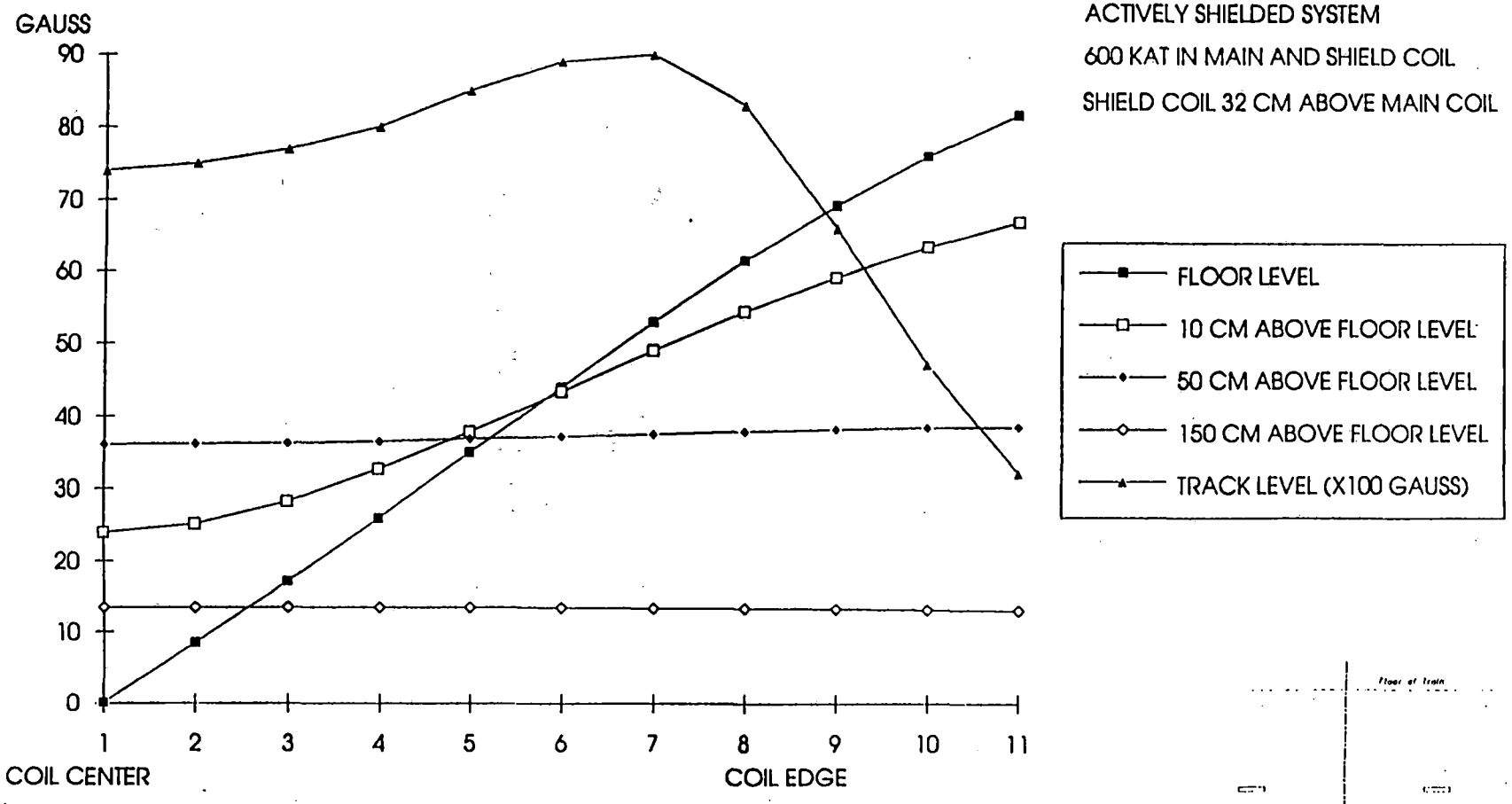

Figure 2-39

FIELD PROFILE FOR THE PROPULSION MAGNET

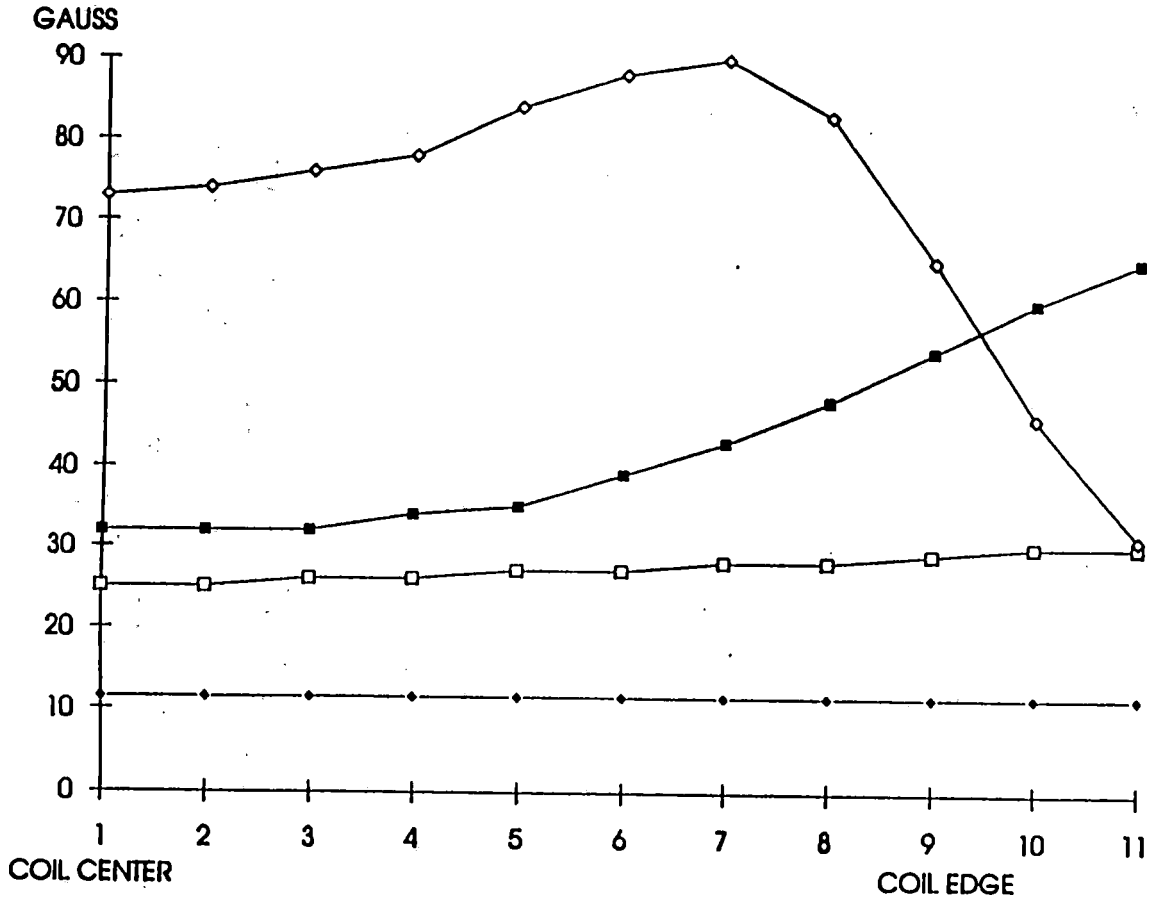

ACTIVELY SHIELDED SYSTEM
600 KAT IN MAIN AND SHIELD COIL
SHIELD COIL 32 CM ABOVE MAIN COIL
AND WITH 2 CM LARGER RADIUS

- FLOOR LEVEL
- 50 CM ABOVE FLOOR LEVEL
- 150 CM ABOVE FLOOR LEVEL
- TRACK LEVEL (X100 GAUSS)

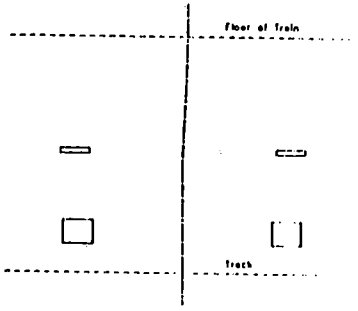

Figure 2-40

Passive Shielding

Method

A simple model was developed to study the effectiveness of an iron shield over a circular coil. The model is capable of analyzing several layers of different materials. In the cases studied, a single layer of highly permeable material (vanadium superemendur) was used. Several thicknesses of this material were examined.

Passive Shielding Examples

The example used consists of a circular propulsion coil with the shield located immediately below the passenger floor. For the first case shown in Figure 2-41, the shield is 5 cm thick. The field is 5 Gauss at the floor, 2.5 Gauss at the seat, and 0.7 Gauss at the head. These values are at the midplane (y = 0).

In the second example shown in Figure 2-42, the shield is 3 cm thick. As expected, the field rises to 8 Gauss at the floor, 4.1 Gauss at the seat, and 1.2 Gauss at head level.

Passive Shield Summary

The study indicates that a field reduction of a factor of 50 can be achieved by a 3 cm shield and a factor of 100 by a 5 cm shield. The shield material is vanadium superemendur, a highly permeable material. For a train system consisting of 6 horizontal propulsion magnets and two horizontal levitation magnets, a 3 cm passive shield may reduce the peak field in the passenger compartment to below 2.5 Gauss. A 5 cm shield could reduce the field below 1.5 Gauss. This is based on a linear extrapolation of the simplified model studied. A more detailed finite element analysis will be required to refine this estimate to include nonlinear, nonsuperpositional effects.

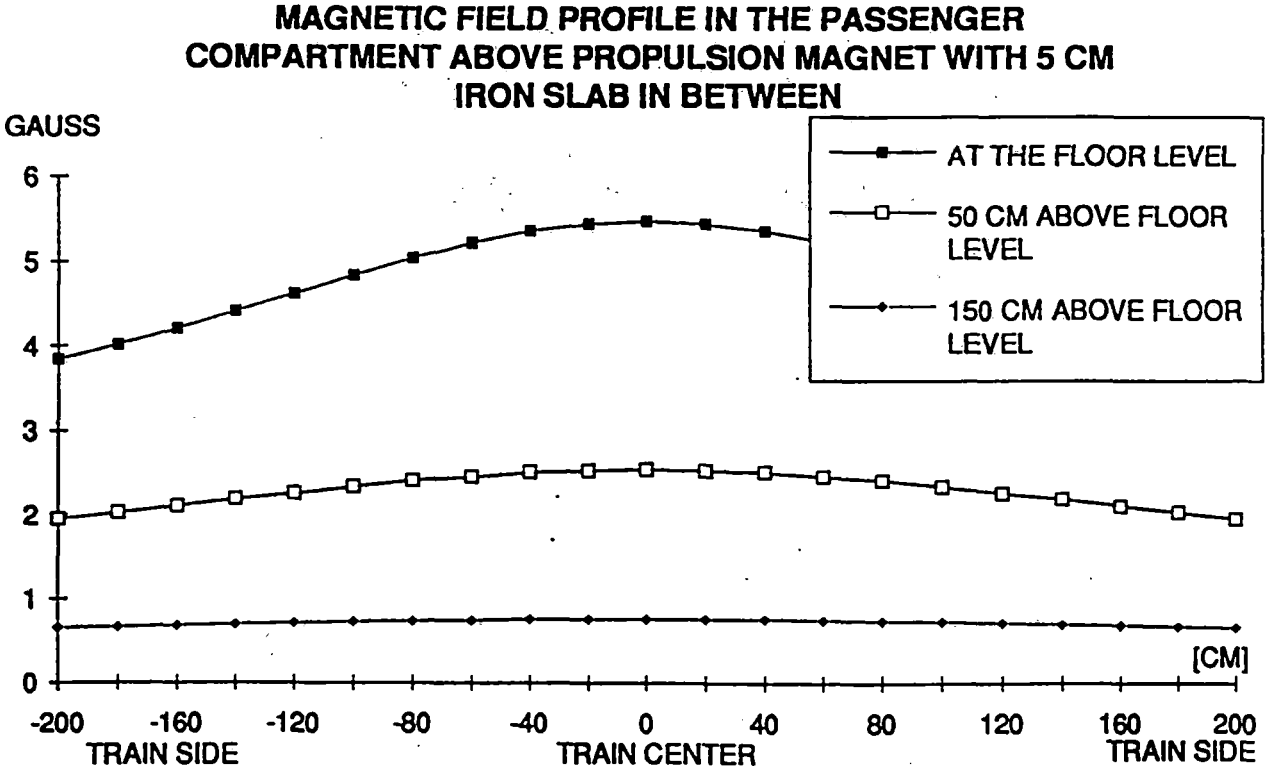
MAGNETIC FIELD PROFILE IN THE PASSENGER COMPARTMENT ABOVE PROPULSION MAGNET WITH 5 CM IRON SLAB IN BETWEEN
GAUSS
6
5
4
3
2
1
0
AT THE FLOOR LEVEL
50 CM ABOVE FLOOR LEVEL
150 CM ABOVE FLOOR LEVEL
[CM]
-200
-160
-120
-80
-40
0
40
80
120
160
200
TRAIN SIDE
TRAIN CENTER
TRAIN SIDE

Figure 2-41

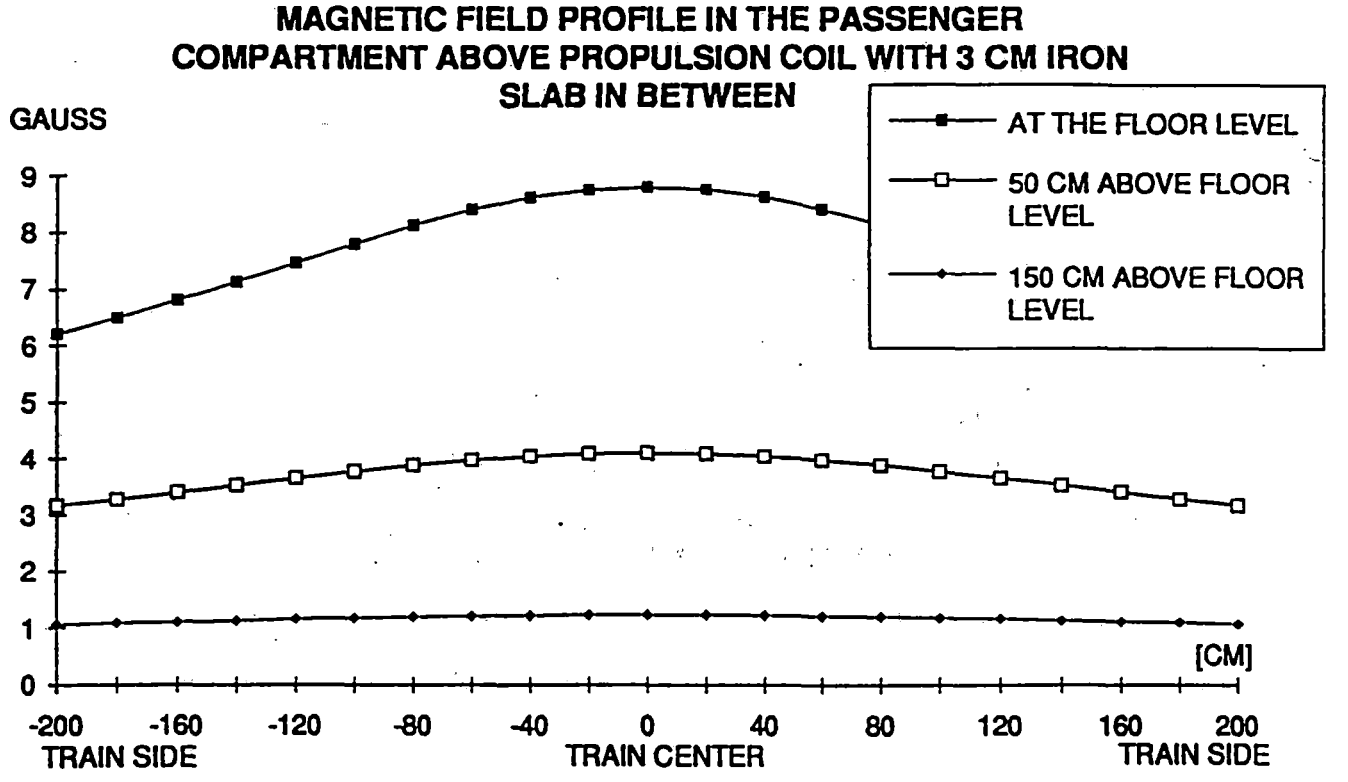
MAGNETIC FIELD PROFILE IN THE PASSENGER COMPARTMENT ABOVE PROPULSION COIL WITH 3 CM IRON SLAB IN BETWEEN
GAUSS
AT THE FLOOR LEVEL
50 CM ABOVE FLOOR LEVEL
150 CM ABOVE FLOOR LEVEL
9
8
7
6
5
4
3
2
1
0
[CM]
-200
-160
-120
-80
-40
0
40
80
120
160
200
TRAIN SIDE
TRAIN CENTER
TRAIN SIDE

Figure 2-42

REFERENCES

Conductor Design	Source
Figure 2-9-1	ASI Manufacturing Data
Figure 2-9-2	Reed, Clark, *Advances in Cryogenic Materials*
Figure 2-9-3	DOE/EPRI Assessment of High T_c Superconductors
Figure 2-9-4	Sato, Hikata, Iwasa, *Applied Physics Letters*
Figure 2-9-5	GE Research Report, December 1991
Figure 2-10	M. Wilson, *Superconducting Magnets*
Figure 2-11	NBS Data Sheet

Refrigeration

Figures 2-24 – 2-27 T. R. Strobridge and D. B. Chelton

LITERATURE REVIEW

I. General Levitation

1. J. R. Hogan, "Comparison of Lift and Drag Forces on Vehicle Levitation by Eddy Current Repulsion for Variations and Normal Flux Magnets with One or Two Tracks," Sept. 1974.

2. John R. Reitz, "Forces on Moving Magnets Due to Eddy Currents," *Journal of Applied Physics*, Vol. 41, No. 5, Apr. 1970.

3. E. R. Laithwate, "Electromagnetic Levitation," IEEE Proceedings, Vol. 112, No. 12, Dec. 1965.

4. Richard D. Thornton, "Design Principles for Magnetic Levitation." *Proceedings of the IEEE*, Vol. 61, No. 5, May 1973.

5. Shung-Wu Lee, "Force on Current Coils Moving over a Conducting Sheet with Application to Magnetic Levitation," *Proceedings of the IEEE*, Vol. 62, No. 5, May 1974.

6. Richard D. Thornton, "Magnetic Levitation and Propulsion, 1975," *IEEE Transactions on Magnets*, Vol. Mag-11, No. 4, July 1975.

7. J. R. Reitz, "U.S. Department of Transportation Program in Magnetic Suspension (Repulsion Concept)," Toronto Intermag Conference, May 14-17, 1974.

8. J. F. Eastham, "Experiments on the Lateral Stabilisation and Levitation of Linear Induction Motors," Toronto Intermag Conference, May 14-17, 1974.

9. G. T. Danby, "Force Calculations for Hybrid (Ferro-Nullflex) Low-Drag Systems," Toronto Intermag Conference, May 14-17, 1974.

10. J. P. Howell, "Stability of Magnetically Levitated Vehicles Over a Split Guideway," *IEEE Transactions on Magnetics*, Vol. Mag-11, No. 5, Sept. 1975.

11. J. F. Eastham, "Full-Scale Testing of a High Speed Linear Synchronous Motor and Calculation on End Effects," *IEEE Transactions on Magnetics*, Vol. 24, No. 6, Nov. 1988.

12. P. E. Burke, "Dual Linear Synchronous Motor for Maglev Vehicles," *IEEE Transactions on Magnetics*, Vol. Mag-13, No. 5, Sept. 1977.

13. Sakae Yamamura, "Electromagnetic Levitation System by Means of Salient-Pole Type Magnets Coupled with Laminated Slotless Rails."

14. R. H. Borcherts, "Lift and Drag Forces for the Attractive Electromagnetic Suspension System."

15. M. Iwamoto, "Magnetic Damping Force in Electrodynamically Suspended Trains."

16. H. T. Coffey, "Dynamic Performance of the SRI Maglev Vehicle."

17. P. E. Burke, "The Calculation of Eddy Losses in Guideway Conductors and Structural Members of High-Speed Vehicles."

18. C. H. Tang, "A Review of the Magneplane Project," *IEEE Transactions on Magnetics*," Vol. Mag-11, No. 2, March 1975.

19. C. A. Guderjahn, "Magnetic Suspension and Guidance for High Speed Rockets by Superconducting Magnets," *Journal of Applied Physics*," Vol. 40, No. 5, April 1969.

20. R. G. Rhodes and B.E. Nulhall, *Magnetic Levitation for Rail Transport*, Clareton Press, 1981.

21. E. R. Laithwaite, *Linear Electric Motors*, Nills and Bosh Ltd., 1971.

22. E. R. Laithwaite, *Propulsion Without Wheels*, Tlart Publishing Company, NY, 1966.

23. J. R. Powell and G. Danby, "Magnetically Suspended Train for Very High Speed Transport," *Proceedings of the 4th IECEC Conference*, Washington, 1969.

II. Superconductivity Aspect

1. H. Tsuchishima, "Superconducting Magnet and On-Board Refrigeration System on Japanese Maglev Vehicle," *IEEE Transactions on Magnetics*, Vol. 27, No. 2, March 1991.

2. O. Tsukamoto, "Development of Superconducting Linear Induction Motor for Steel Making Processes," *IEEE Transactions on Magnetics*, Vol. 27, No. 2, March 1991.

3. Boon-Teck Ooi, "Electromechanical Dynamics in Superconducting Levitation Systems," *IEEE Transactions on Magnetics*, Vol. Mag-11, No. 5, Sept. 1975.

III. General Maglev

1. William F. Hayes, "Magnetic Field Shielding for Electrodynamic Vehicles," IEEE, 1987.

2. Gordon R. Slemon, "The Canadian Maglev Project on High-Speed Interurban Transportation," *IEEE Transactions on Magnetics*, Vol. Mag-11, No. 5, Sept. 1975.

3. Stephen Kuznetsov, "Commercialization of Maglev Technology for U.S. Baseline Interurban System: An Industrial Perspective," presented at Eighth International Convention on High Speed Rail, Anaheim, CA, May 6, 1991.

4. *Conceptual Design and Analysis of the Tracked Magnetically Levitated Vehicle Technology Program (TMLV). Repulsion Scheme. Volume I. Technical Studies.* The Philco-Ford Corporation. Prepared for Federal Railroad Administration, Feb. 1975.

5. O. Tsukamoto, "A New Magnetic Levitation System with AC Magnets," *IEEE Transactions on Magnetics*, Vol. 24, No. 2, March 1988.

6. Yoshiro Kyotani, "Recent Progress by JNR on Maglev," *IEEE Transactions on Magnetics*, Vol. 24, No. 2, March 1988.

7. A. H. Greene, "LSM Control of Maglev Vehicle Ride Quality."

8. "Magnetically Levitated High-Speed Ground Transportation System for New York State." Prepared for The New York State Energy Research and Development Authority, July 10, 1990.

9. G. R. Slemon, "A Linear Synchronous Motor for High-Speed Ground Transport," Toronto Intermag Conference, May 14-17, 1974.

10. P. C. Sen, "On Linear Synchronous Motor (LSM) for High-Speed Propulsion," *IEEE Transactions on Magnetics*, Vol. Mag-11, No. 5, Sept. 1975.

11. J. Meins, "The High Speed Maglev Transportation System Transrapid," *IEEE Transactions on Magnetics*, Vol. 24, No. 2, March 1988.

12. W. S. Brown, "The Effect of Long Magnets on Inductive Maglev Ride Quality,"*IEEE Transactions on Magnetics*, Vol. Mag-11, No. 5, Sept. 1975.

13. Y. Iwasa, "An Operational 1/25-Scale Magneplane System with Superconducting Coils," *IEEE Transactions on Magnetics*, Vol. Mag-11, No. 5, Sept. 1975.

14. K. Oberretl, "Transients and Oscillations in the Repulsive Magnetic Levitation System," *IEEE Transactions on Magnetics*, Vol. Mag-11, No. 5, Sept. 1975.

15. T. Umemori, "Study on Miniaturization of Electromagnet for DC Linear Motor," *IEEE Transactions on Magnetics*, Vol. Mag-16, No. 5, Sept. 1980.

16. David W. Jackson, "Magneplane Power Supply Costs."

17. G. Bohn, "The Magnetic Train Transrapid 06."

18. Hisashi Tanaka, "JR Group Proves Maglev Frontiers," *Railway Gazetta International*, July 1990.

19. Yoshihiro Kyotani, "Present Status of JNR Maglev Development."

20. New York State Technical and Economic Maglev Evaluation," prepared for New York State Energy Research and Development Authority, 1990.

21. L. R. Johnson, D. M. Rote, J. R. Hull, H. T. Coffey, J. G. Daley and R. F. Giese, "Maglev Vehicles and Superconductor Technology," Argonne National Laboratory, 1989.

GUIDEWAY EVALUATION

3.1 Existing Systems Integration

3.1.1 Description of Guideway Configurations

The 5 guideway configurations chosen for this evaluation are described in detail below and shown in Figures 3-1 thru 3-21. The 5 configurations are:

Type I	Flat-Top Guideway
Type II	Wrap Around or Clamp Type Guideway
Type III	Trough or Semicircular Guideway
Type IV	Inverted "T" Guideway
Type V	U-shaped or Channel Guideway.

The levitation and propulsion systems for each of these configurations have been designed (see Sections 1.0 and 2.0) and positioned on the guideway for optimum operation. The dimensions of the guideway are based on the requirements of these systems. Each of these guideways offers a unique solution for the support of a Maglev transportation system; and any of the 5 can be designed to provide a reliable means of support for a high-speed mass transportation system. The comparisons provided herein will demonstrate relative advantages and disadvantages of each of the configurations.

The 5 guideways are constructed of similar materials and installed using similar installation techniques. The primary structural element used to support all 5 guideway configurations is a precast, prestressed concrete girder supplied by a vendor and delivered to the jobsite ready for installation. A further discussion of the construction, transportation, and installation of the guideway girder is provided in Section 3.1.6.

One of the unique structural material design considerations is the potential interaction between ferrous metal in the guideway girder and the magnetic fields created by the levitation and propulsion systems. The prestressing tendons, reinforcing bars and anchor bolts are items that pose a potential interference problem. The solution chosen for the interference problem between the magnetic fields and the prestressing tendons is to maintain a minimum girder depth that ensures at least a one-meter separation between the LSM and the levitation ladders and the tendons. This solution has minimal impact on the design of the girder. Only the shorter spans (50- and 75-ft) are restricted by this minimum depth criteria.

The reinforcing and the anchor bolts on top of the guideway cannot be moved away or shielded from the magnetic fields. Therefore, the simplest solution is to use a non-magnetic material for both the reinforcing and the anchor bolts. The materials investigated were stainless steel, aluminum, and fiber-reinforced plastic (FRP) anchor bolts and FRP concrete reinforcing. The materials chosen for use in this study were FRP anchor bolts and FRP concrete reinforcing. Unfortunately, current technology for FRP concrete reinforcing has not advanced to the point where strength design procedures and standards have been developed. For this reason, the girder design philosophy has been limited to a simple beam philosophy. This implies that (1) there are no continuous spans over column supports, (2) the maximum design moment and deflection occur at the center of the span, and (3) the top of the girder is always in compression. Maintaining the top of the girder in compression minimizes the design stresses in the FRP reinforcing. This design philosophy allows the use of FRP reinforcing without extending the technical aspects of the material beyond the known application possibilities.

The use of FRP anchor bolts to secure the LSM and the levitation ladders to the girder is within the current technology available from vendors that manufacture the bolts. Also, the LSM and ladders are set in a recessed grout pocket that provides additional lateral support.

Future development of non-ferrous materials for reinforcing and bolts may allow the use of continuous beams which will help reduce the depth of the cross-section while maintaining the deflection criteria.

The girders are designed to rest on mechanically adjustable supports. Each of these supports may be adjusted vertically to level the girder during installation and to maintain the girder's level during operation. In order to maintain a level support system during operations, the supports will be interconnected by a sensor system that will continuously monitor the position of the girders relative to each other and to adjacent girders. In addition, an audio sensing system that can identify the "sound" response as the vehicle passes over the girders and can compare the response to a previously determined base line response will be utilized to plan maintenance and replacement operations for the life of the guideway system. The development of the sensor system and the mechanically adjustable supports are not a part of this study, but a cost for these systems has been included in the guideway costs provided later.

The girders are designed for expansion and contraction due to temperature variations. One end (fixed end) of the girder is secured by a steel pin that is cast with the concrete support and fits within a steel sleeve cast with the girder; the maximum horizontal movement, laterally and longitudinally, is 5 mm. The other end (sliding end) of the girder is secured by a steel pin that is cast with the concrete support and fits within a steel channel cast in the girder; the maximum allowable lateral horizontal movement is 5 mm and longitudinal movement is 40 mm. The longitudinal expansion and/or contraction of the girder is dependent on the weather conditions for the area where the guideway is located. For the purposes of this report, a 100°F differential has been chosen. The girders will be arranged so that both girders on a column support will have either fixed or sliding ends. This will cause the forces created on the structural system at a particular column support to be in opposite directions and reduce the net effects of temperature variations. The effects of temperature variations from the top to the bottom of the girder are not investigated in this report. One possible solution to minimize the effects of temperature variations from top to bottom of the girder is to paint the top surface a reflective white. The cost for painting the girder has been included in this estimate.

The elevation criteria for each guideway requires a minimum clearance above roadways similar to bridge overpasses. Figure 3-22 defines the minimum vertical clearance from the ground to a bridge overpass to the underside of the guideway girder. The clearances used in

this study vary from 4.5 m (15 ft) representing the clearance over a ground-level roadway to 16.8 m (55 ft) above a bridge overpass. The elevation of the top of the guideway will vary according to the depth of the cross-section required for each specific span analyzed.

The following describes each of the configurations in greater detail and provides additional information on the constructability of each.

TYPE I (Reference Figures 3-1, 3-2 and 3-3)

The Type I guideway is a flat-top configuration and is the simplest of all the guideways to design, fabricate, and install. The basic structural shape that provides support is a rectangular box beam. The girder will be cast with recessed areas formed for the installation of the levitation ladders and the LSM assembly. The fabrication process will include casting the girder, drilling and setting the FRP anchor bolts in epoxy, setting the levitation ladders, and filling the void area with nonshrink grout to provide a smooth, level surface.

The level installation of the LSM assembly is critical to the optimum operation of the propulsion system. In order to set the LSM as level as possible, the area of the recess is formed deeper than the LSM support tray. A nonshrink grout leveling pad is poured first and allowed to harden. This will account for any recess irregularities that may be encountered with each individual girder. The LSM assembly is placed on the level grout pad and secured using the FRP anchor bolts, which are located by the girder fabricator using the actual dimensions of the assembly. The recessed area where the anchor bolts are located along each side of the assembly is grouted level with the top of the girder and the top of the LSM. The surface of the finished product is a level, plane surface without obstructions.

The perception that nothing "visible" is keeping the vehicle from sliding off the guideway is one objection to this type of guideway. The shape of the flat-top guideway has been economized for the shorter spans, which provides a flange extension beyond the web that will allow a portion of the vehicle structure to wrap around the edge of the girder (see Figures 3-2 and 3-3.) This shape will provide a more positive method for ensuring that the vehicle will stay on the girder than the normal box shape (Figure 3-1) that is used for the longer spans.

The guideway is elevated on either a single- or a double-column support (see Figures 3-4 and 3-5. The double column and beam system are designed as a structural frame.

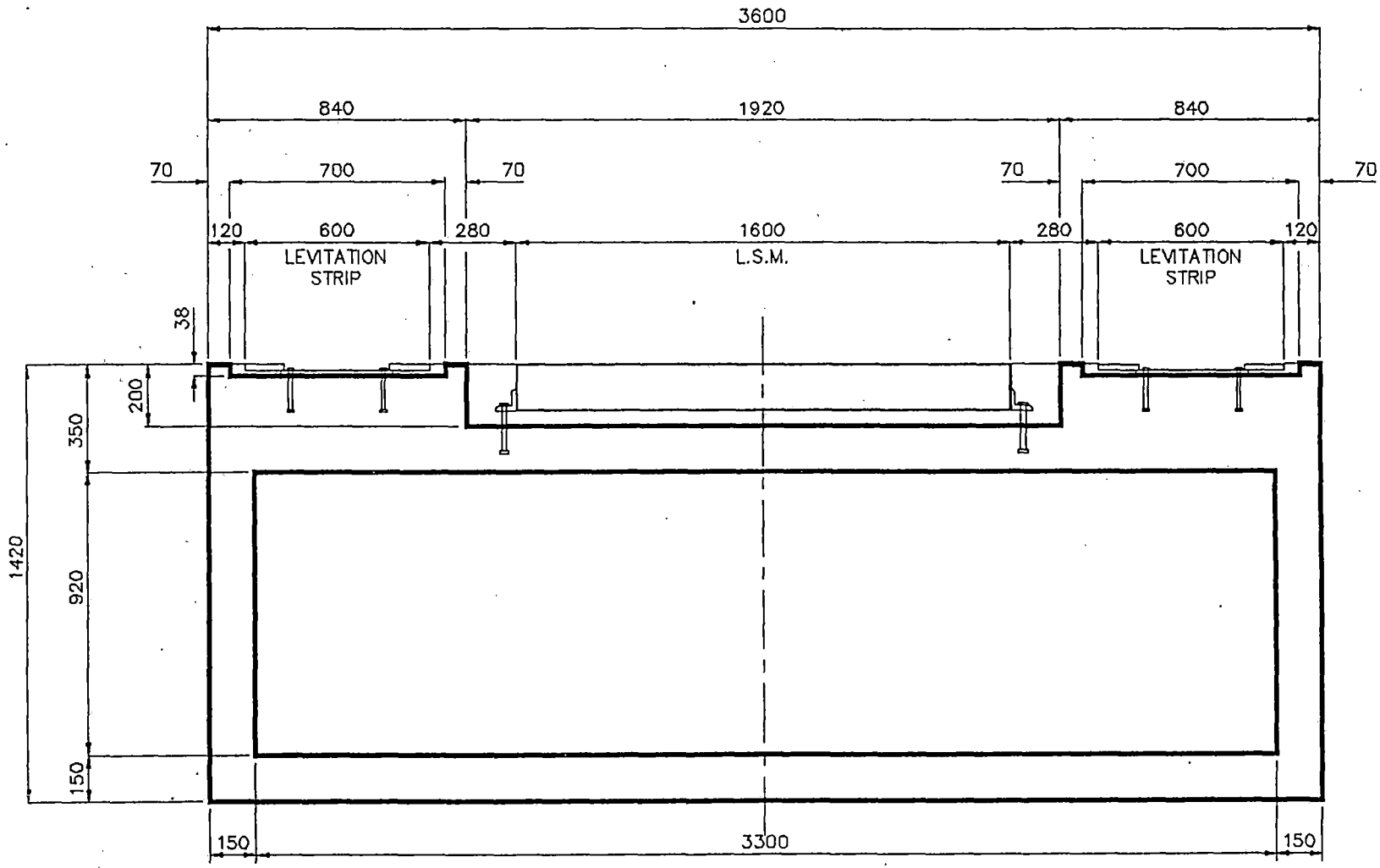

TYPE I – GUIDEWAY SECTION
FIGURE 3-1

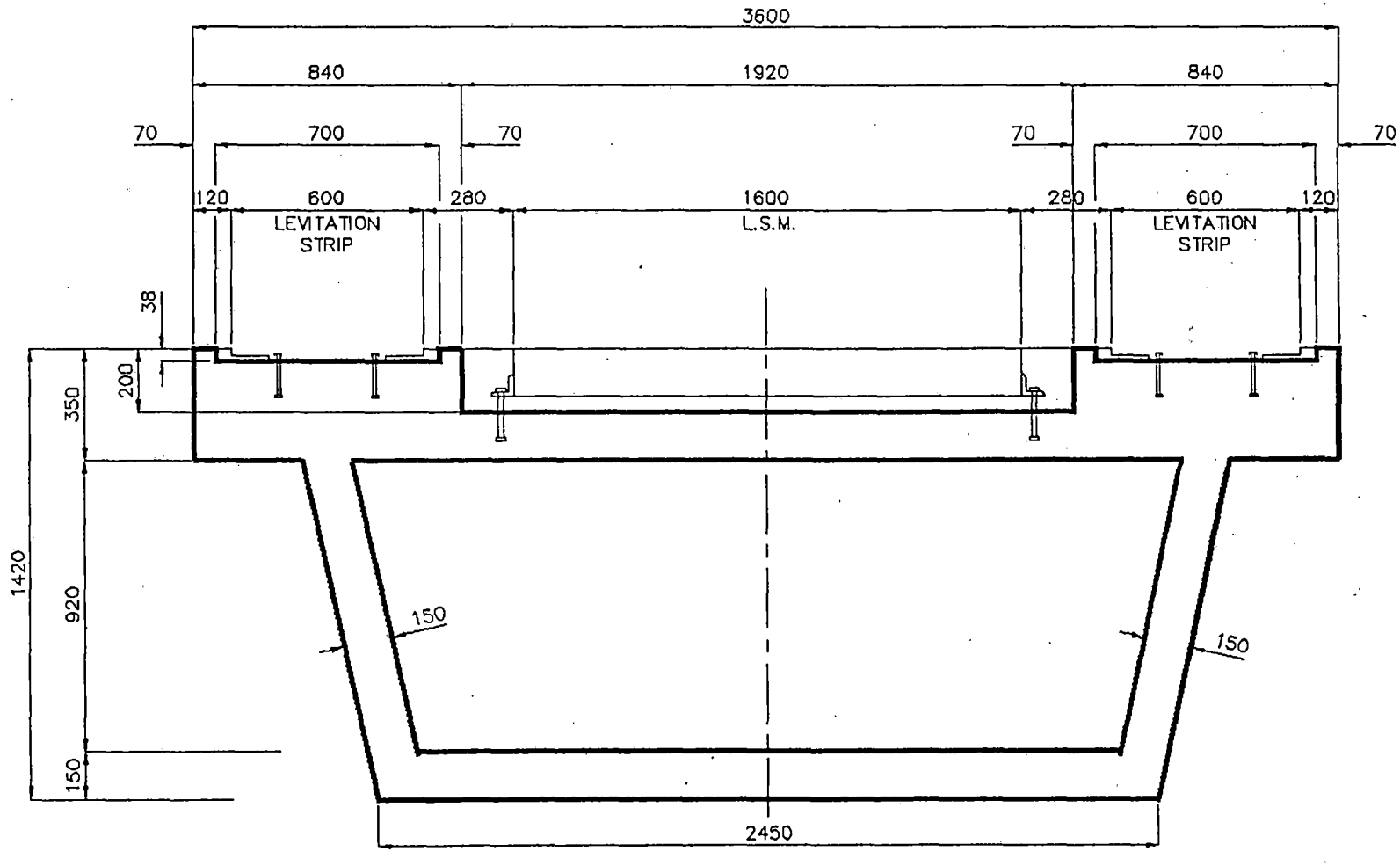

TYPE I A – GUIDEWAY SECTION
FIGURE 3–2

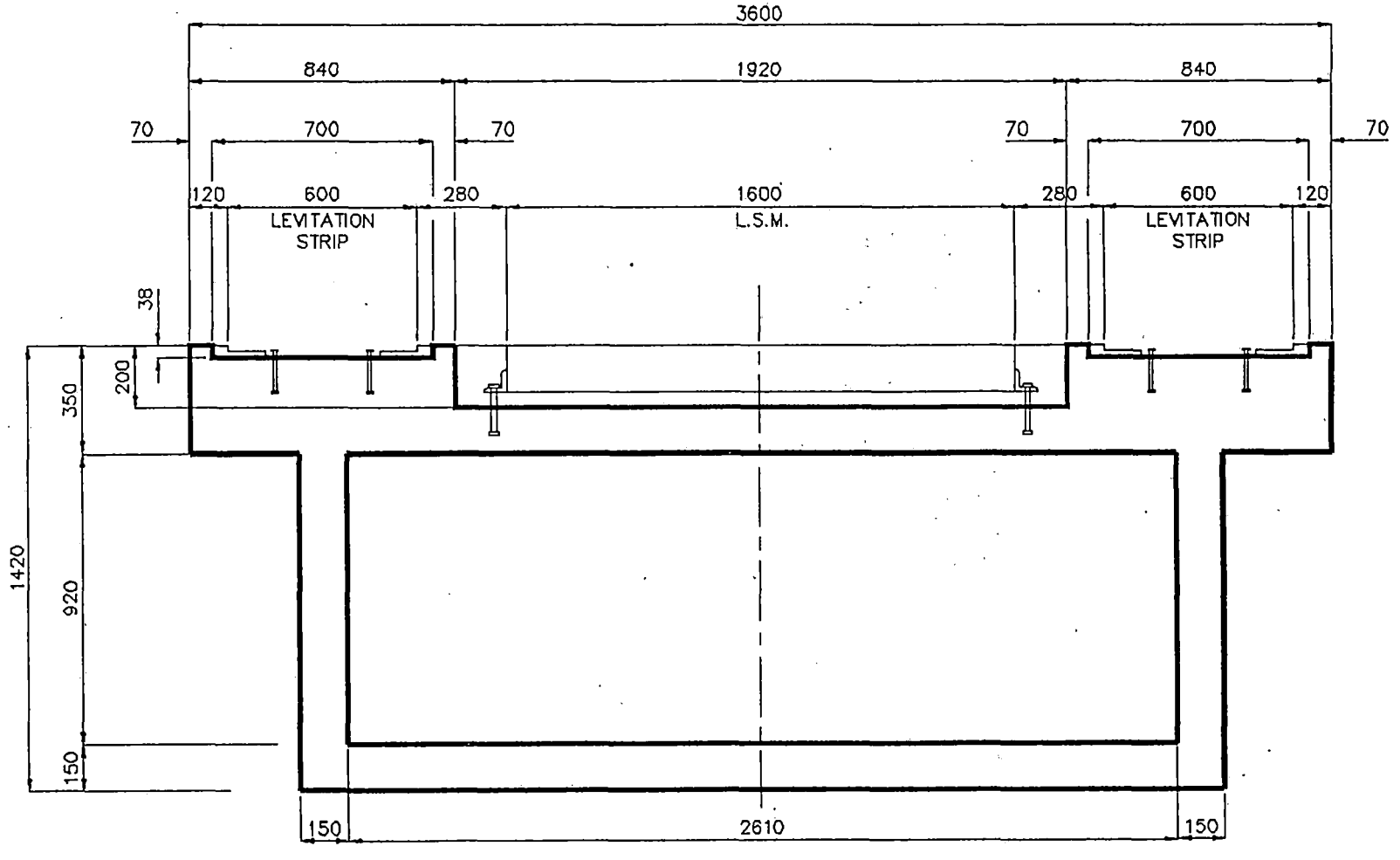

TYPE I B – GUIDEWAY SECTION
FIGURE 3-3

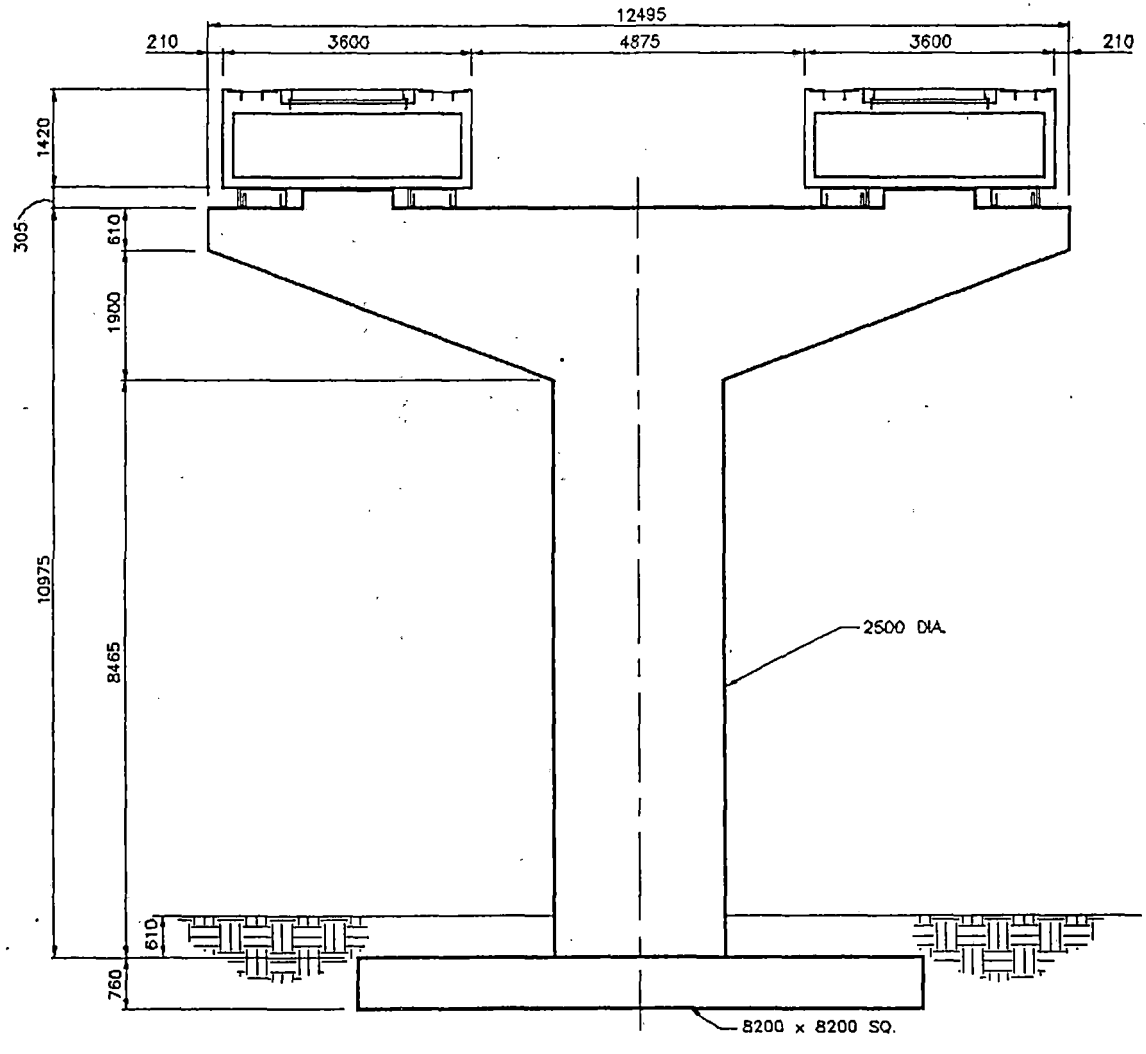

TYPE I – GUIDEWAY ELEVATION SINGLE COLUMN
FIGURE 3-4

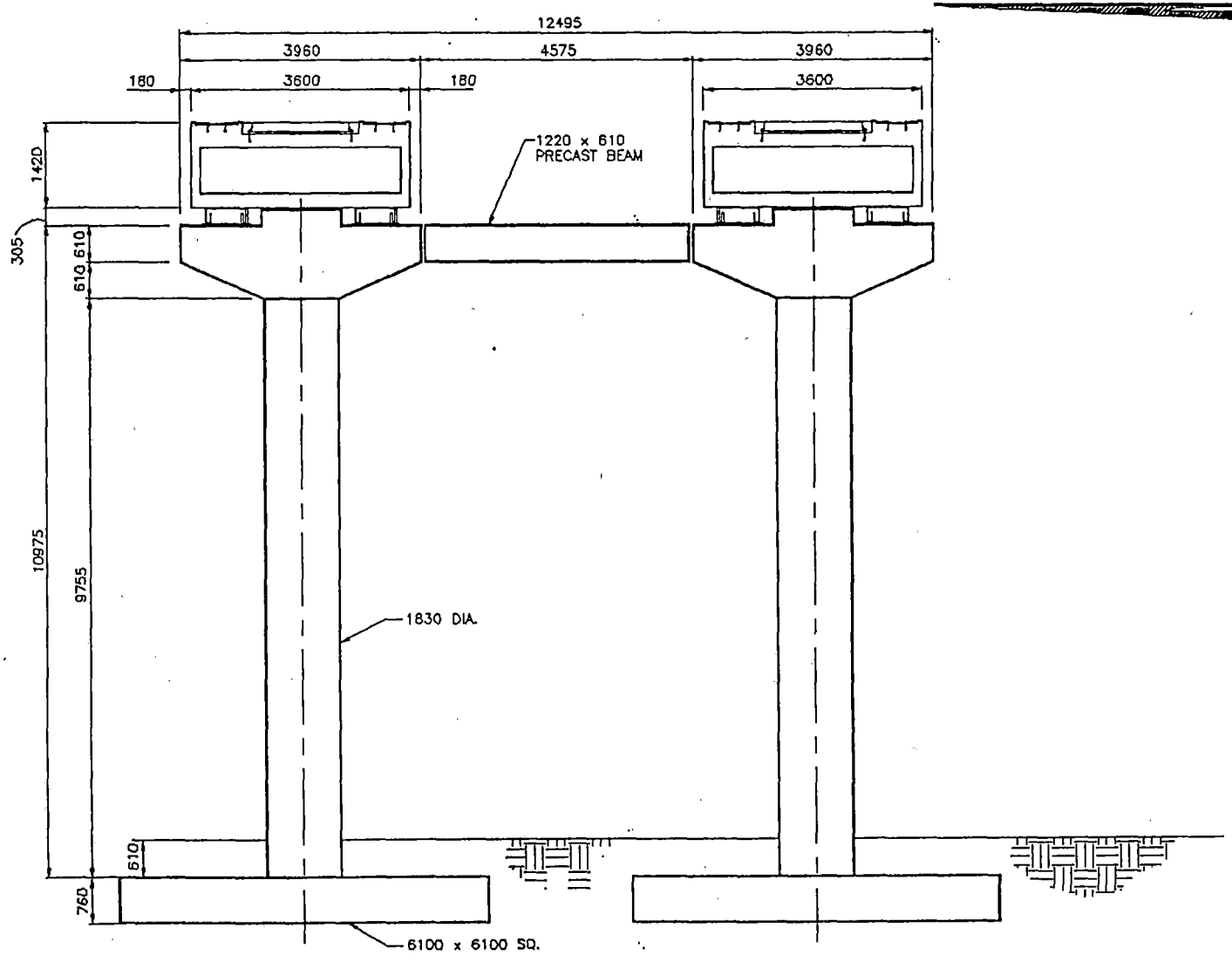

TYPE I – GUIDEWAY ELEVATION DOUBLE COLUMN
FIGURE 3-5

TYPE II (Reference Figure 3-6)

The Type II guideway is a wrap-around or clamp-type configuration. The basic structural shape providing support is an I-shape with flange top and bottom and a single center web. The girder will be cast with recessed areas for the installation of the levitation ladders. The LSM is divided in half and is mounted below the top flange on each side of the girder and levelled using the installation bolts and shims. Grouting will be minimized. All bolts will be FRP, as was the case for the Type I.

The levitation ladders are installed as in Type I. The sides of the top flange are deepened to allow the installation of an aluminum strip to be used in conjunction with a magnet on the vehicle under-carriage to maintain the horizontal alignment of the vehicle. A minimum clearance of 500 mm is provided below the top flange to allow room for the vehicle magnet assembly and structure. The bottom flange was "filled in" to help provide a better bearing area at the supports. The top surface of the guideway is a level, plane surface without obstructions.

The wrap-around effect offers greater confidence that the vehicle will stay with the guideway than any of the other guideway configurations.

The guideway is elevated the same as the Type I (see Figures 3-7 and 3-8).

TYPE III (Reference Figures 3-9, 3-10 and 3-11)

The Type III guideway is a trough or semicircular configuration. The basic structural shape providing support is identical to the Type I, a rectangular box beam. The curved portion on top of the girder will be cast after the box beam is complete. The curved section will have a central area blocked-out for the installation of the LSM. The area between the LSM and the side of the girder will be filled in continuously and a curved surface formed as the concrete reaches the proper elevations. A recess for the installation of the aluminum levitation ladders will be formed in the curved top surface. Great care must be exercised to ensure that concrete surfaces are true and correct.

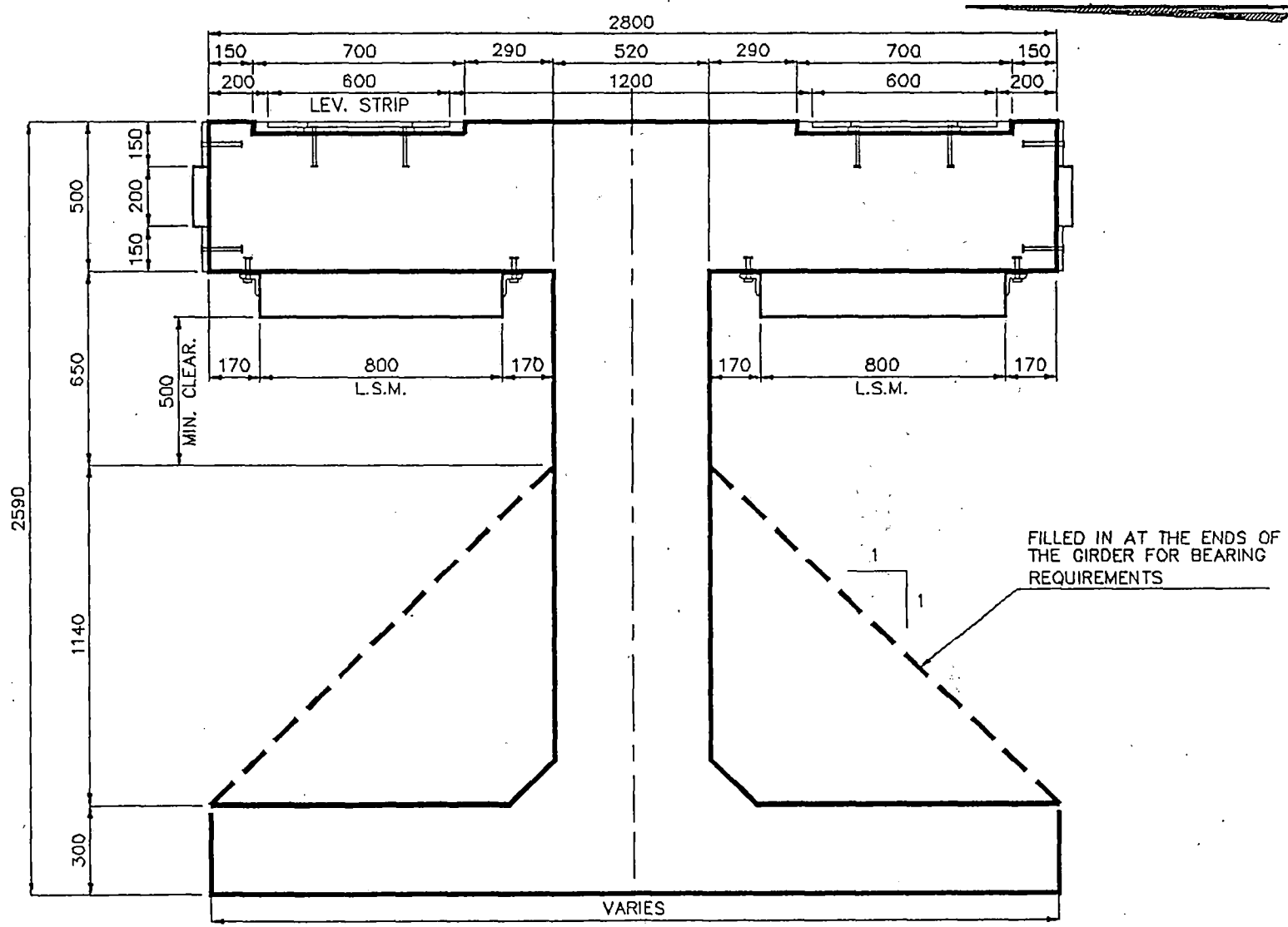

TYPE II – GUIDEWAY SECTION
FIGURE 3–6

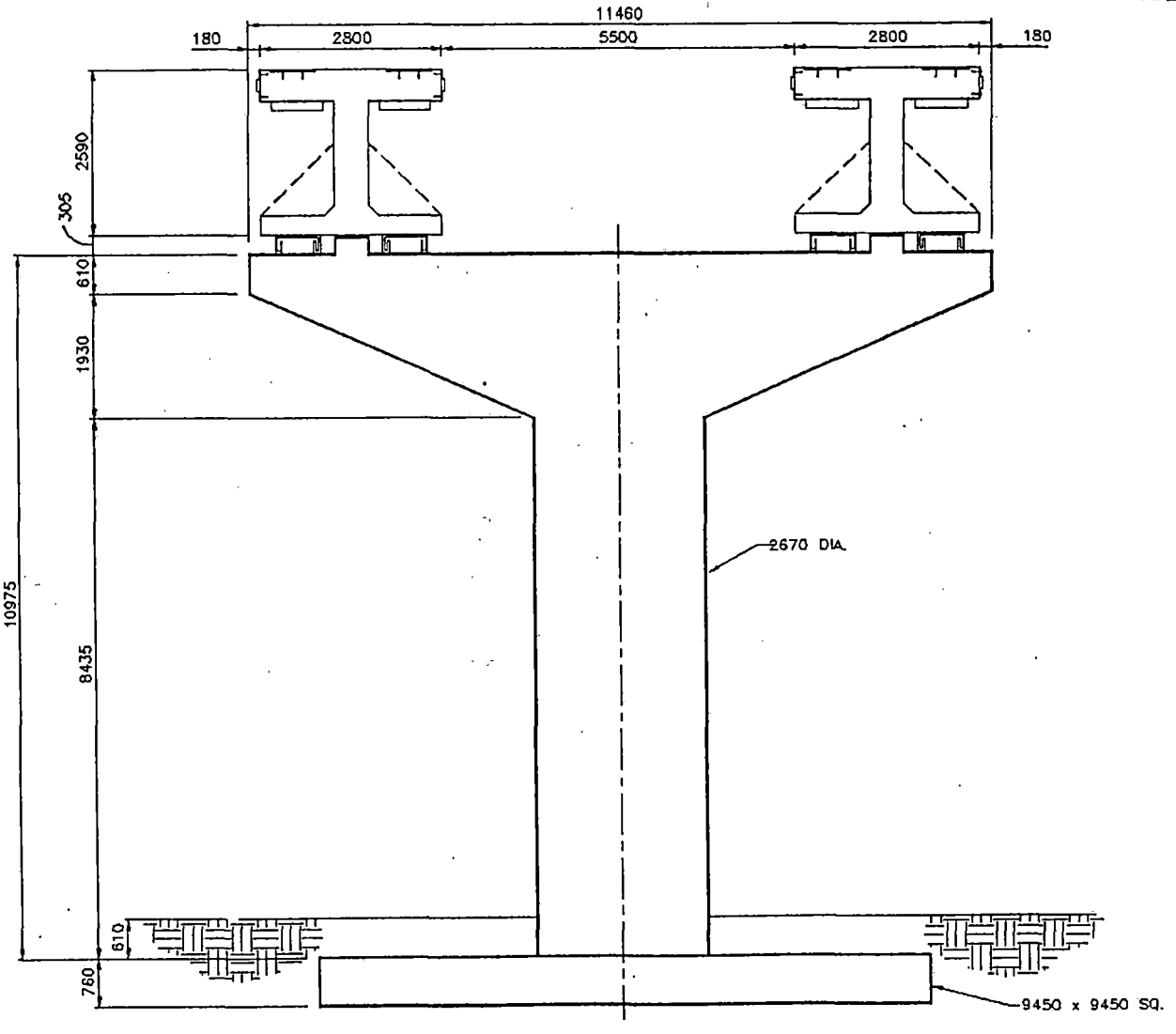

TYPE II – GUIDEWAY ELEVATION SINGLE COLUMN
FIGURE 3-7

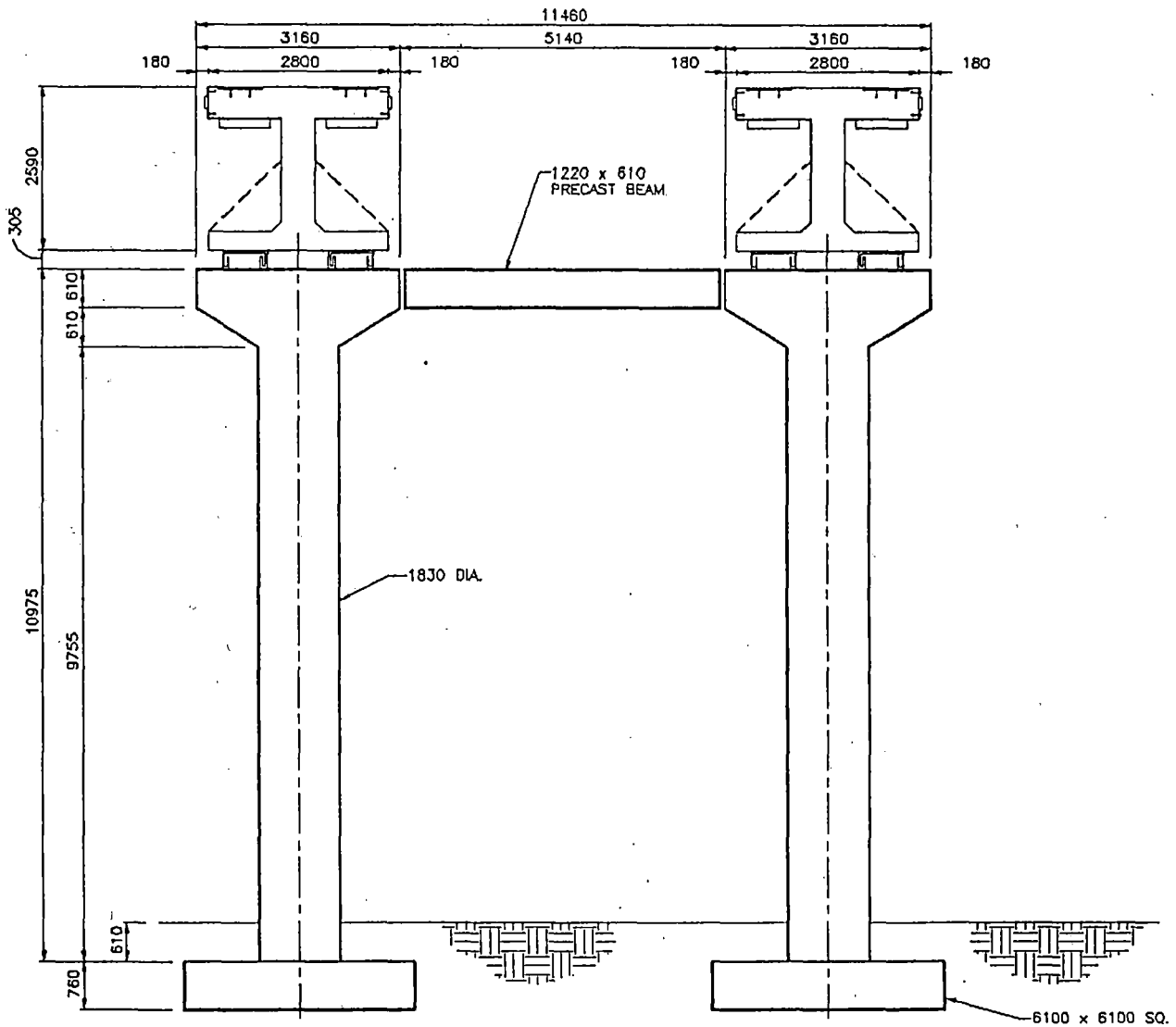

TYPE II – GUIDEWAY ELEVATION DOUBLE COLUMN

FIGURE 3-8

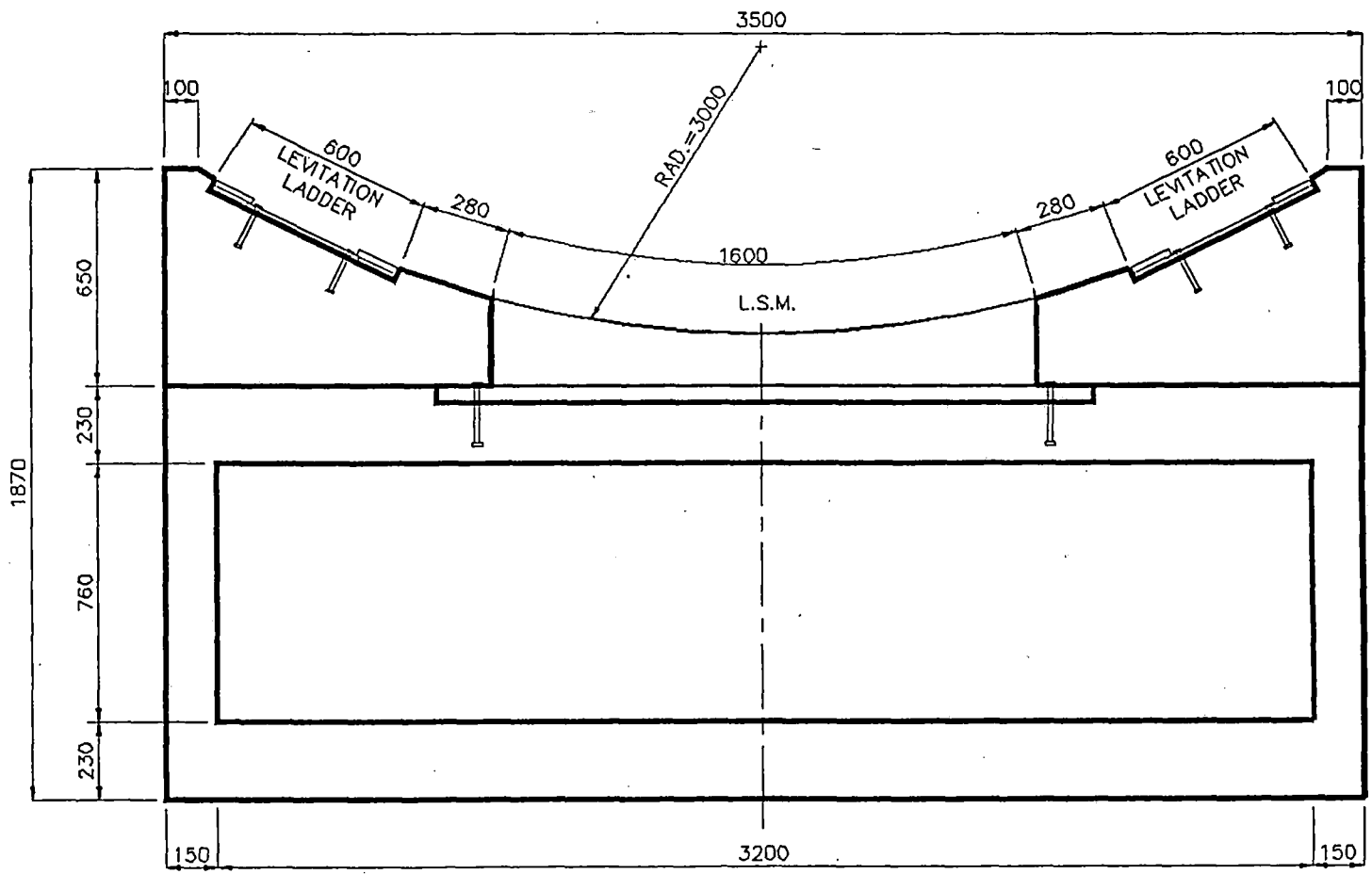

TYPE III – GUIDEWAY SECTION
FIGURE 3-9

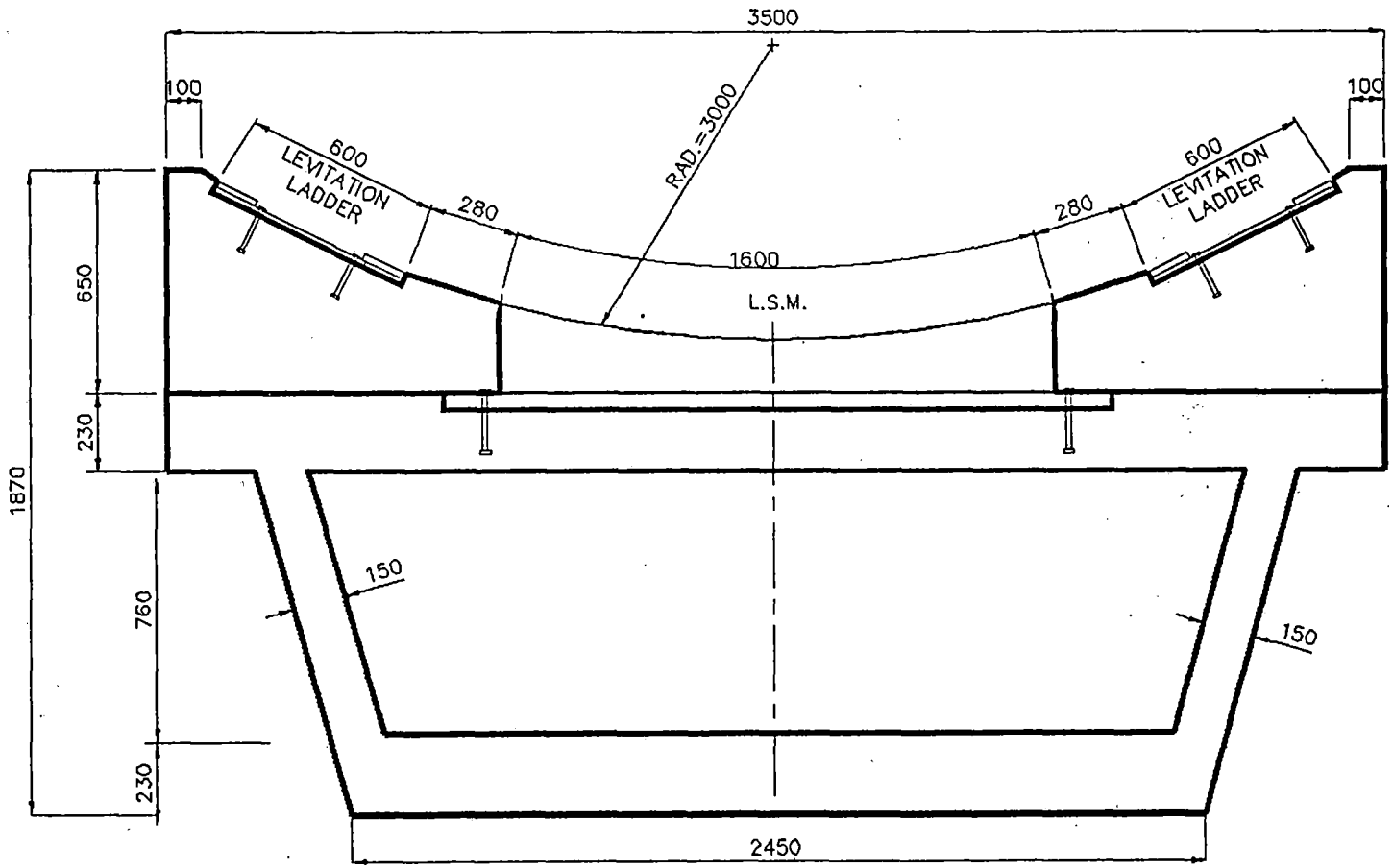

TYPE III A – GUIDEWAY SECTION
FIGURE 3–10

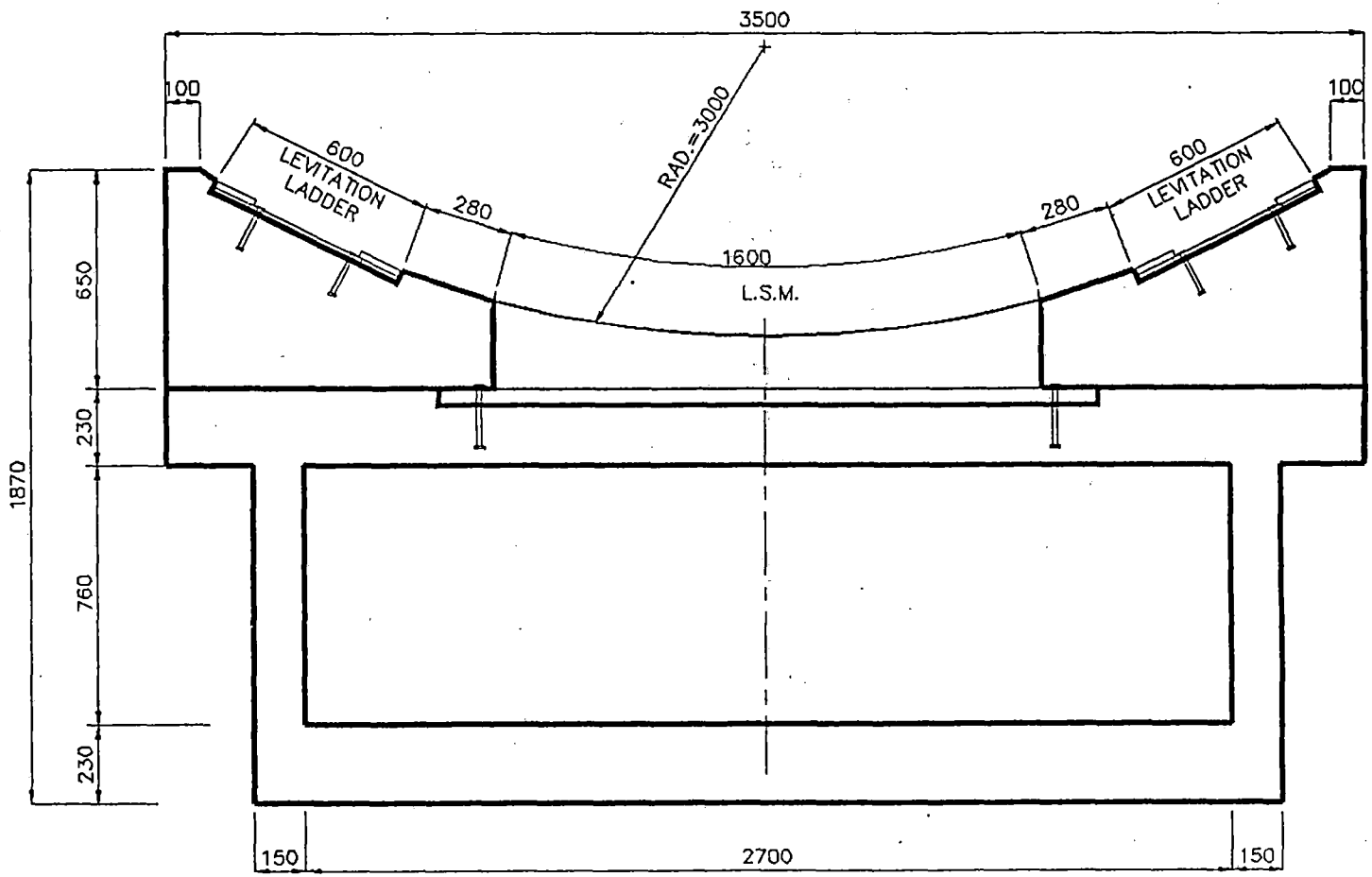

TYPE III B – GUIDEWAY SECTION
FIGURE 3–11

The top flange of the box section and the areas along the sides of the LSM that support the levitation ladders must be reinforced with FRP reinforcing rods. Similar to the Type I installation, the level installation of the LSM is critical to the optimum operation of the propulsion system. The LSM and the aluminum levitation ladders will be installed similar to the Type I installation. The shape of the girder has been economized similar to the Type I girder (see Figures 3-10 and 3-11).

Again, one potential objection is that there is nothing "visible" keeping the vehicle from sliding out of the trough.

The guideway is elevated the same as the Type I (see Figures 3-12 and 3-13).

TYPE IV (Reference Figures 3-14, 3-15, and 3-16)

The Type IV guideway is an inverted "T" configuration. The basic structural shape providing support is identical to the Type I, a rectangular box beam. In this case, a central web is extended above the box to form a vertical wall that is used to mount the LSMs. The vertical wall will be cast on top of the completed box beam. The LSM is divided in half and mounted on opposite sides of the central wall. The wall is formed so that the face of the wall at the top and the face of the LSM are in line. The top of the wall will be formed to provide a surface for a guidance wheel from the vehicle to impact in case the vehicle strays too far laterally. All the reinforcing in the wall must be FRP or other nonmagnetic material.

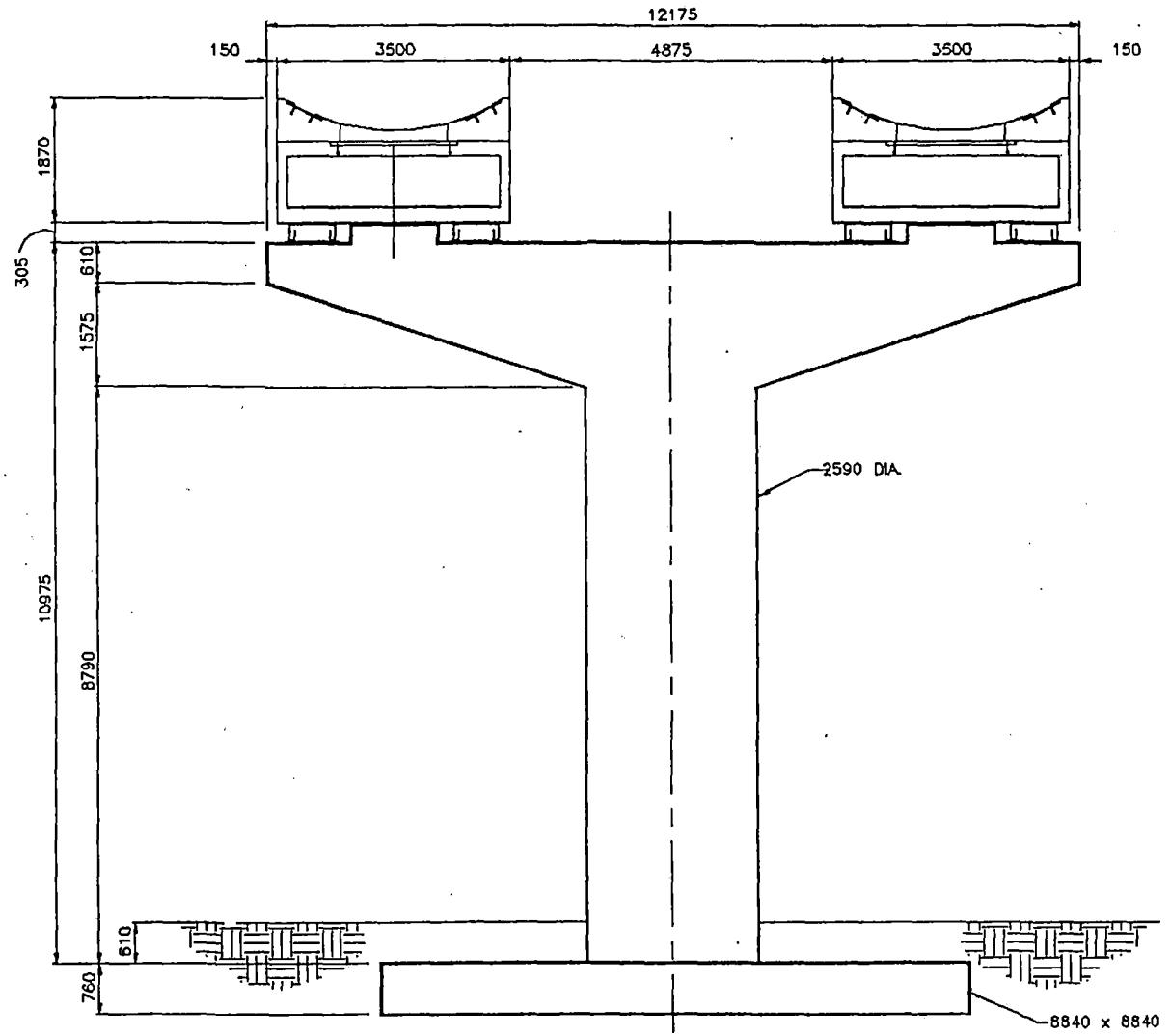

TYPE III – GUIDEWAY ELEVATION SINGLE COLUMN
FIGURE 3-12

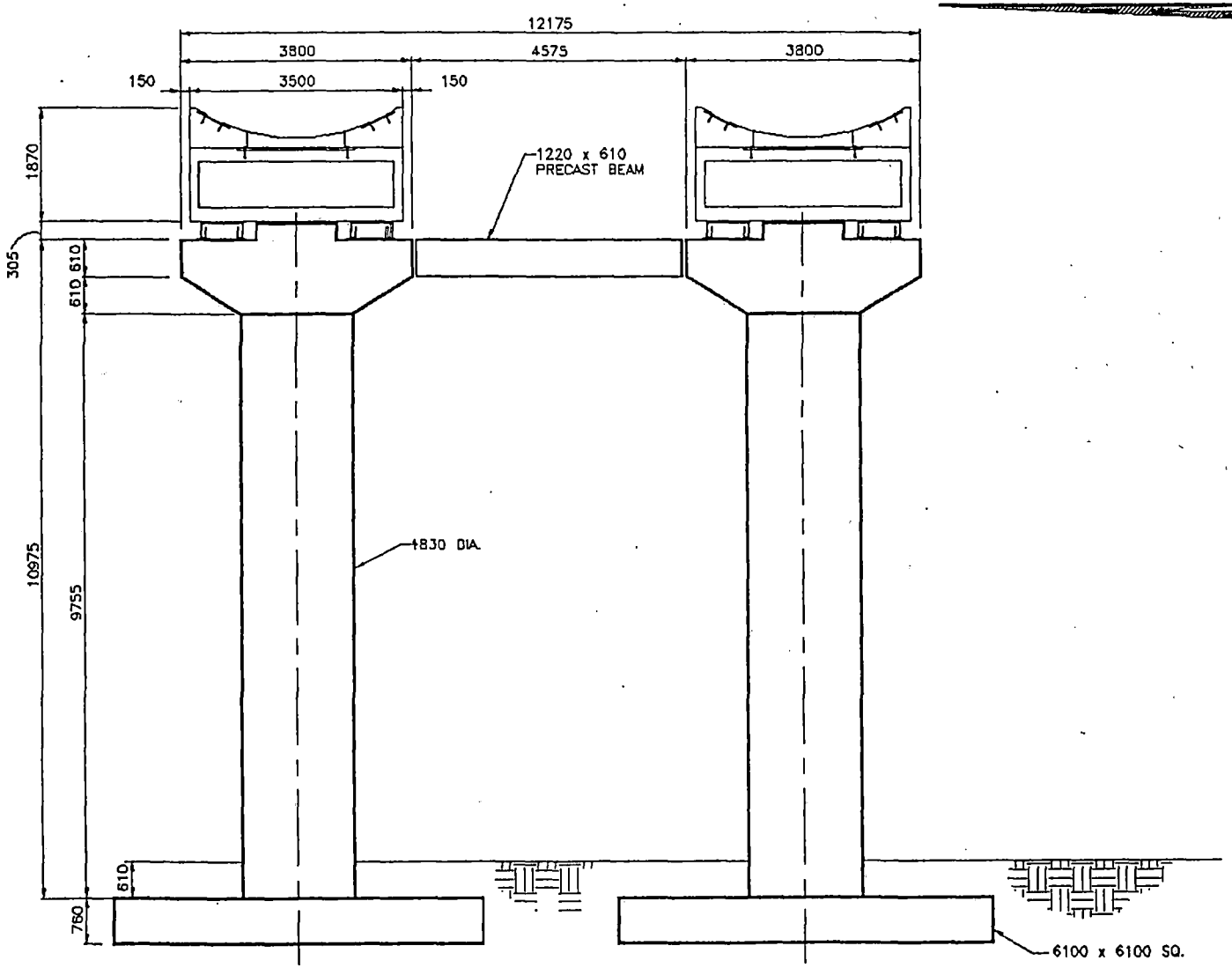

TYPE III – GUIDEWAY ELEVATION DOUBLE COLUMN
FIGURE 3-13

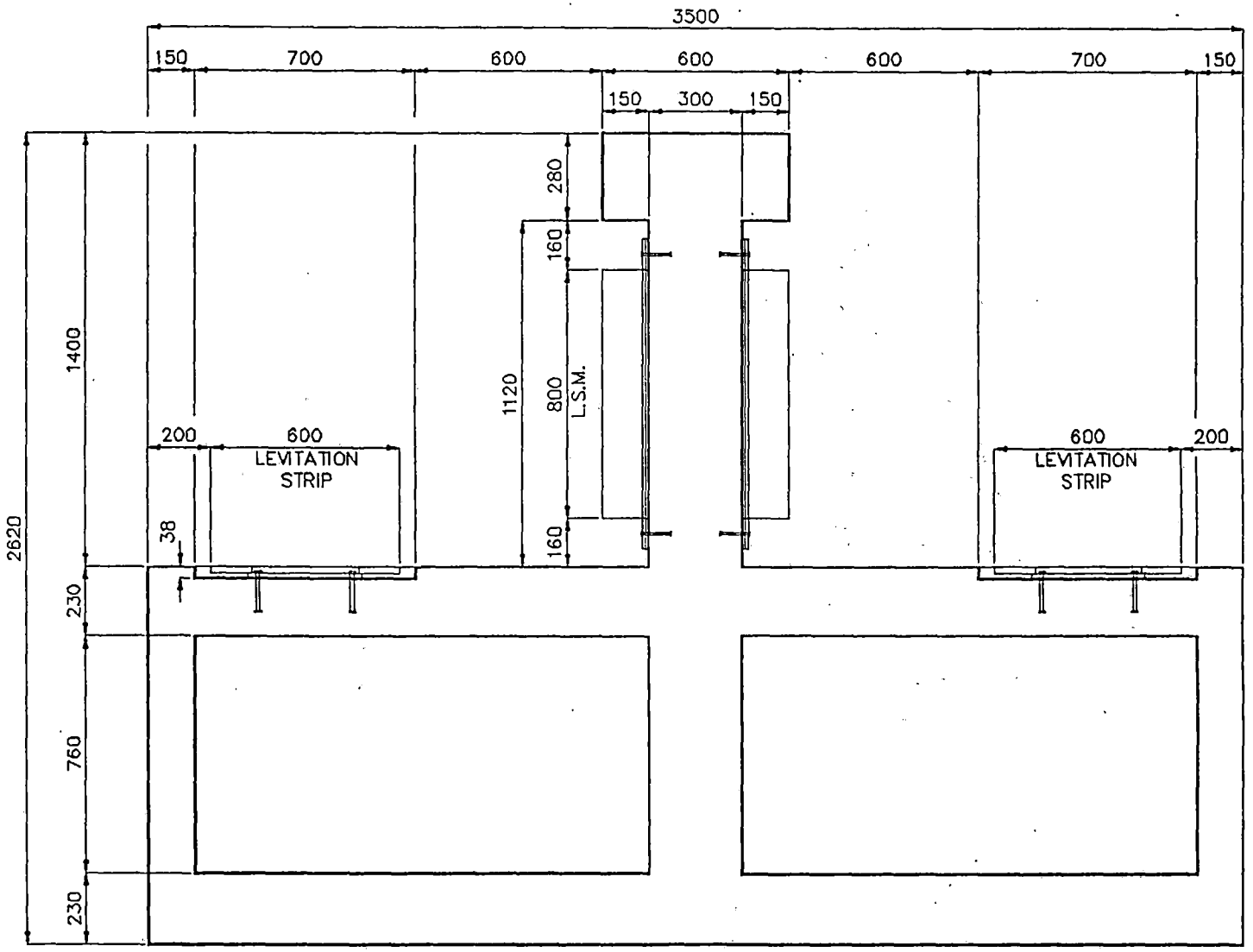

TYPE IV – GUIDEWAY SECTION
FIGURE 3–14

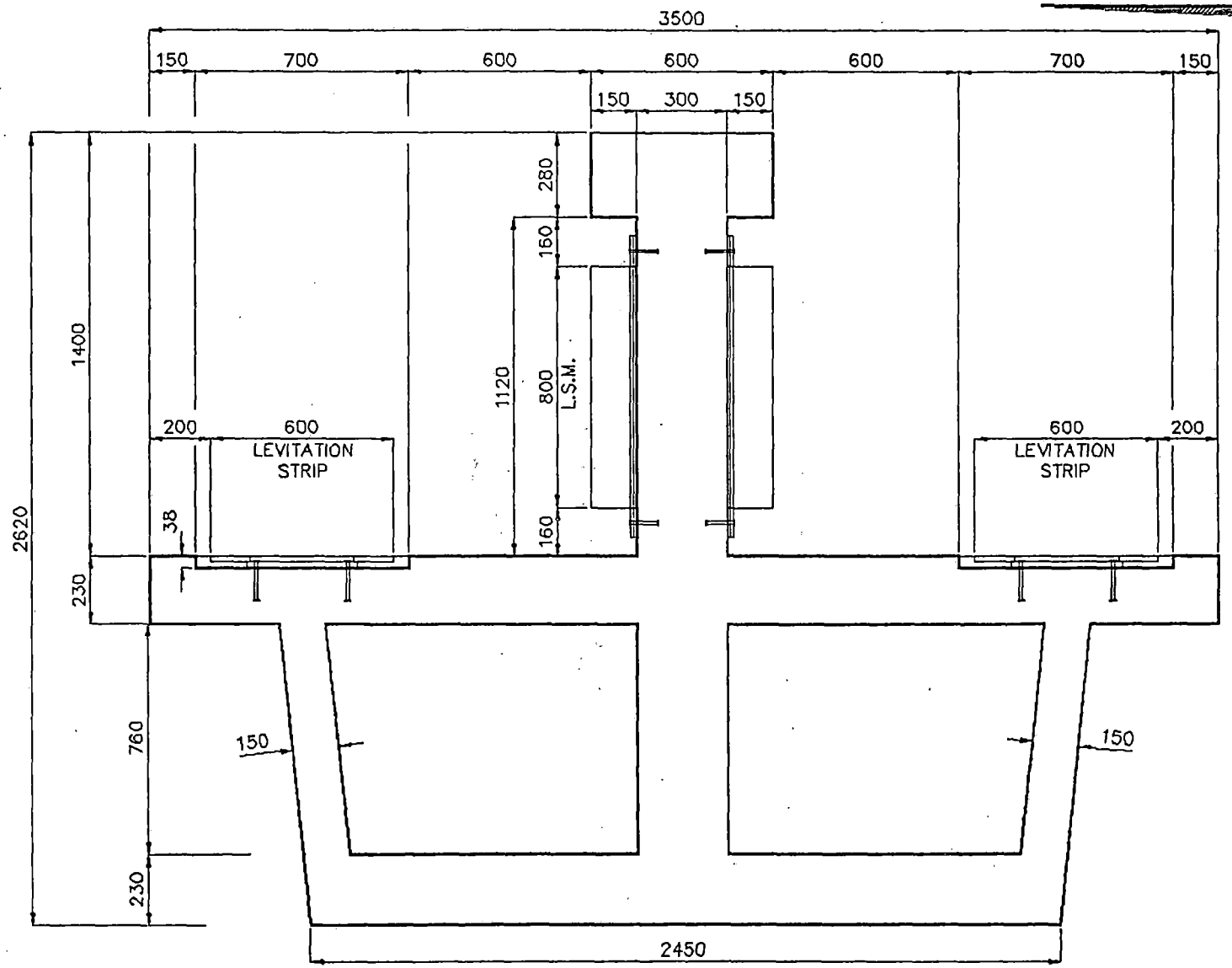

TYPE IV A – GUIVDEWAY SECTIVON
FIGURE 3–15

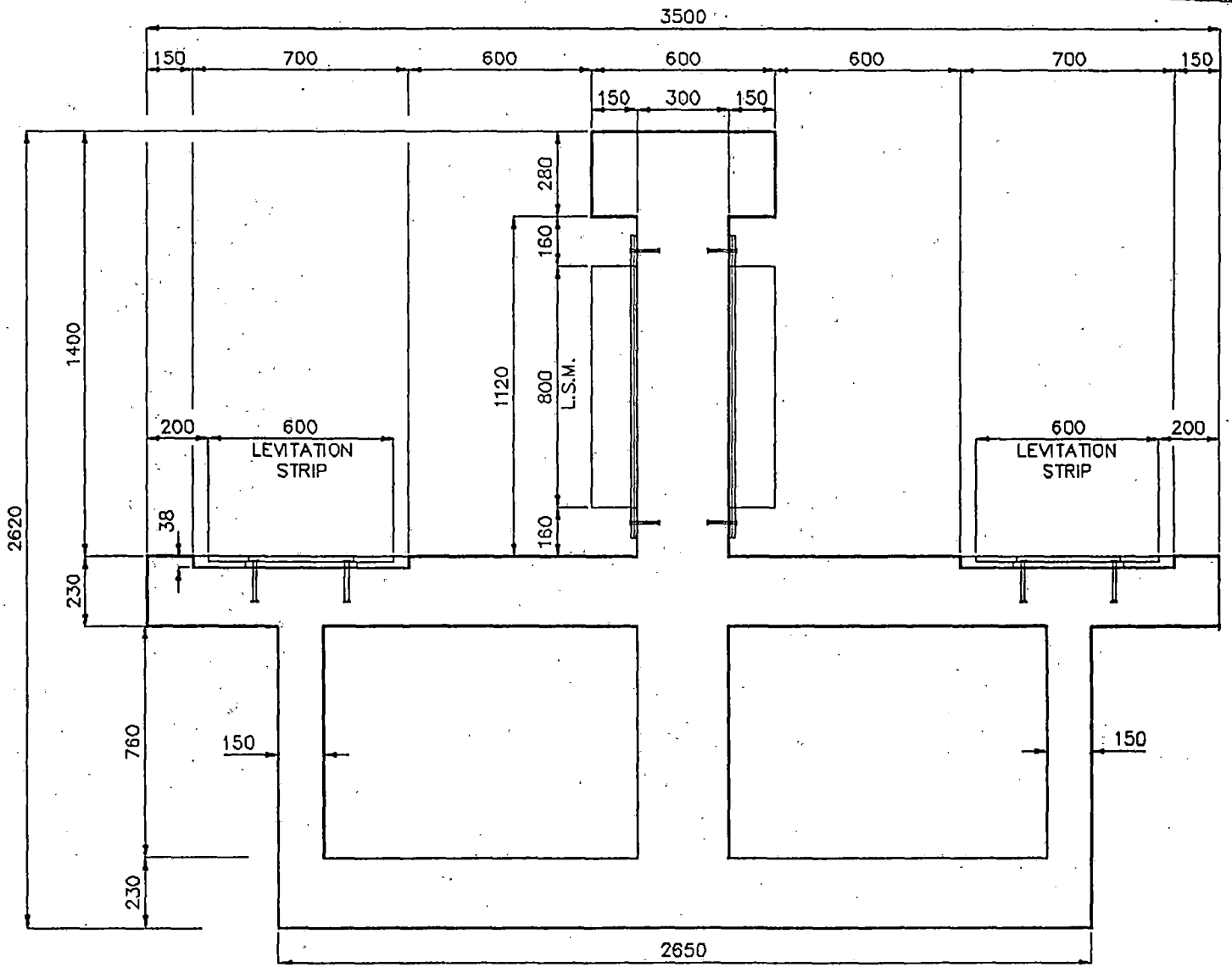

TYPE IV B – GUIDEWAY SECTION
FIGURE 3–16

The vehicle straddles the wall and is levitated by levitation ladders at either side of the guideway. The levitation ladders are installed as described in the Type I description. The LSM are mounted on the center wall and are levelled using FRP bolts and shims. The critical fabrication concern is the center wall above the main support girder. This wall must be cast after the box beam is completed. This will increase the fabrication time and cost for this guideway. The vehicle straddling the center wall offers a greater confidence that the vehicle will stay with the guideway than the Type I or Type III.

The shape of the girder has been economized for the shorter spans similar to Type I (see Figures 3-15 and 3-16).

The guideway is elevated the same as the Type I (see Figures 3-17 and 3-18).

TYPE V (Reference Figure 3-19)

The Type V guideway is an U-shaped configuration. The basic structural shape providing support is still the rectangular box beam. The overall width of the guideway is increased in order to position the vehicle within the U-shape. The LSM is divided in half and mounted on the side walls similar to the Type IV. The shape of the interior face of the wall is formed similar to the Type IV to protect the LSMs and to provide a surface at the top of the wall for a guidance wheel from the vehicle to impact the wall in case the vehicle strays too far laterally. All the reinforcing in the sidewalls must be FRP or other nonmagnetic material.

The levitation ladders are mounted in the floor of the U-shaped channel and installed as described in the Type I description. As in the Type IV guideway, the sidewalls will have to be cast after the box beam is completed. This will increase fabrication time and cost for the guideway. Because the vehicle operates within the confines of the U-shape, this concept offers increased confidence that the vehicle will stay with the guideway but adds the possibility of a "bumper car" effect. The aerodynamics aspects of this guideway are not clear at this time and will not be addressed in this study.

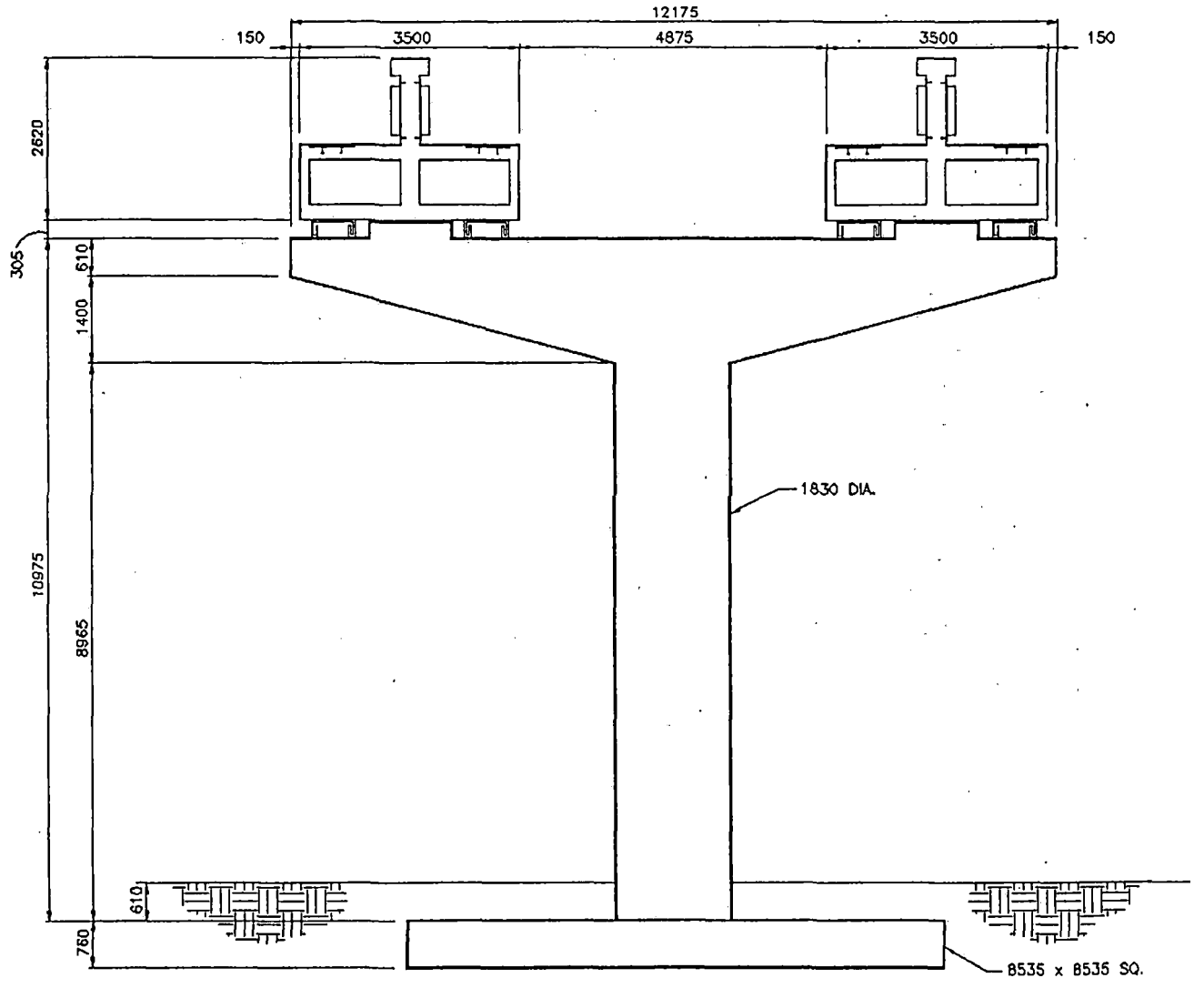

TYPE IV – GUIDEWAY ELEVATION SINGLE COLUMN
FIGURE 3-17

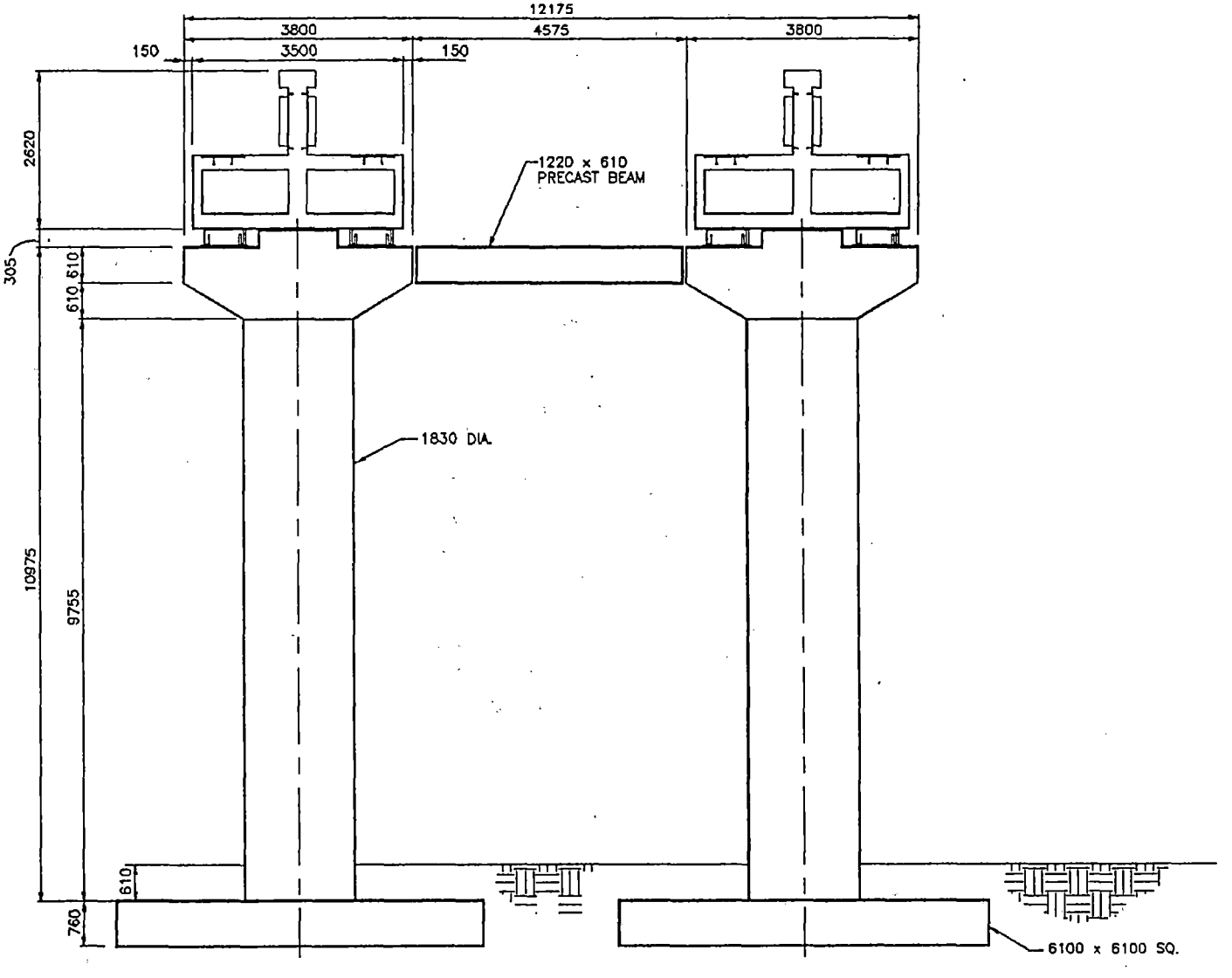

TYPE IV – GUIDEWAY ELEVATION DOUBLE COLUMN
FIGURE 3–18

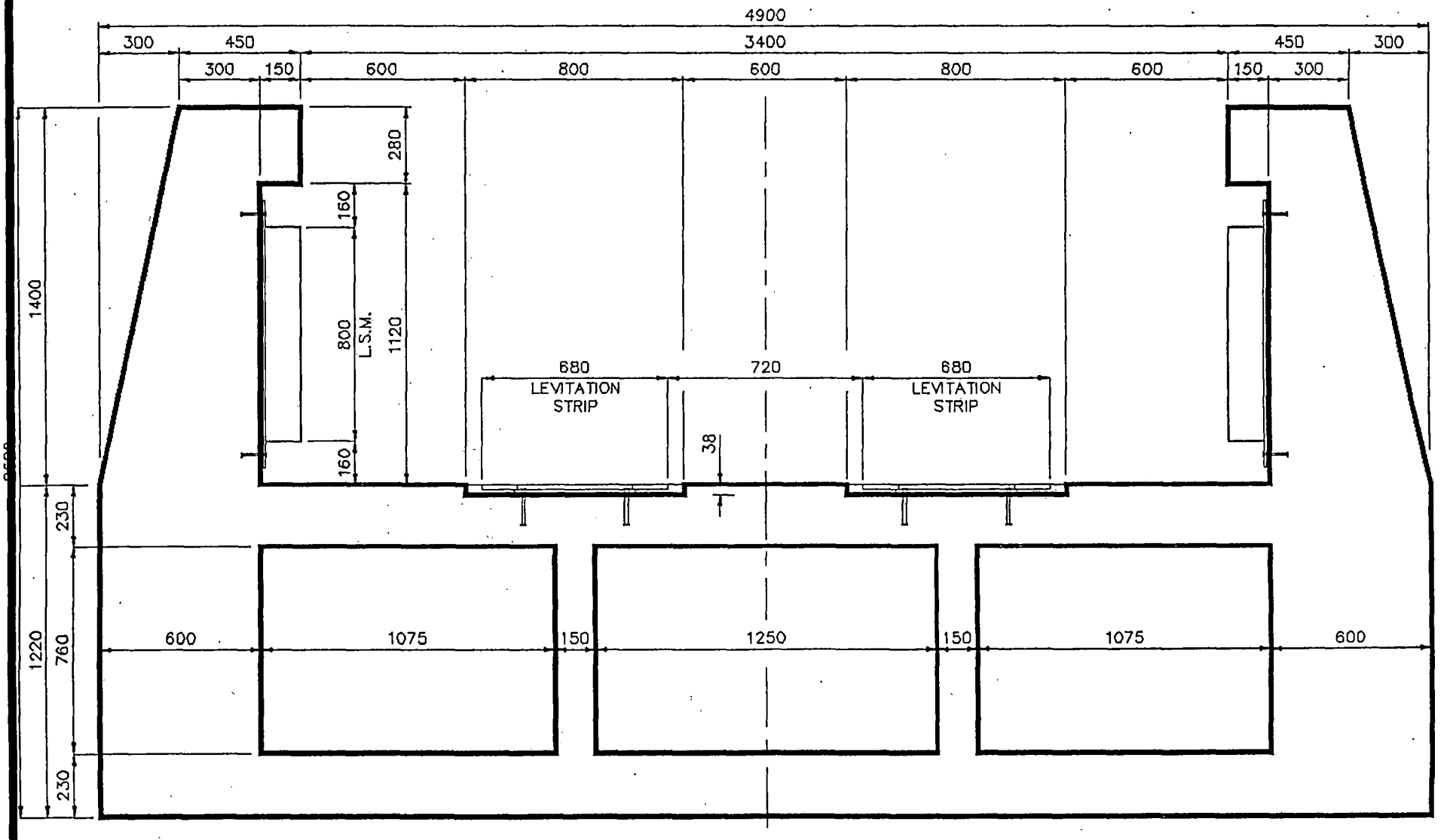

TYPE V – GUIDEWAY SECTION
FIGURE 3-19

The guideway is elevated the same as the Type I (see Figures 3-20 and 3-21).

The guideway configurations described above and shown in Figures 3-1 thru 3-21 provide a general summary of the current research efforts for Maglev guideway support systems. However, a complete design/construction estimate utilizing the same design criteria and parameters for all 5 configurations has not been performed. The primary effort of this study is to design each of the configurations and prepare a construction cost estimate for each. This will enable a rigorous comparison of each system and the advantages and limitations they present.

3.1.2 Guideway Design Criteria/Parameters

The design criteria, design allowables, and material properties and strengths used in the design effort are provided below:

DESIGN CRITERIA/PARAMETERS

ENVIRONMENTAL CRITERIA

Reference Standard:	ASCE 7-88 Minimum Design Loads for Buildings and Other Structures
Structure Classification:	Category III (ASCE 7-88 Table 1)
Wind Criteria:	Structure only; Basic Wind Speed 161 km/h (100 mph), Exposure C, at hurricane oceanline, 50-year recurrence interval
	Structure with vehicle operating; Basic Wind Speed 80.5 km/h (50 mph), Exposure C, at hurricane oceanline, 50-year recurrence interval

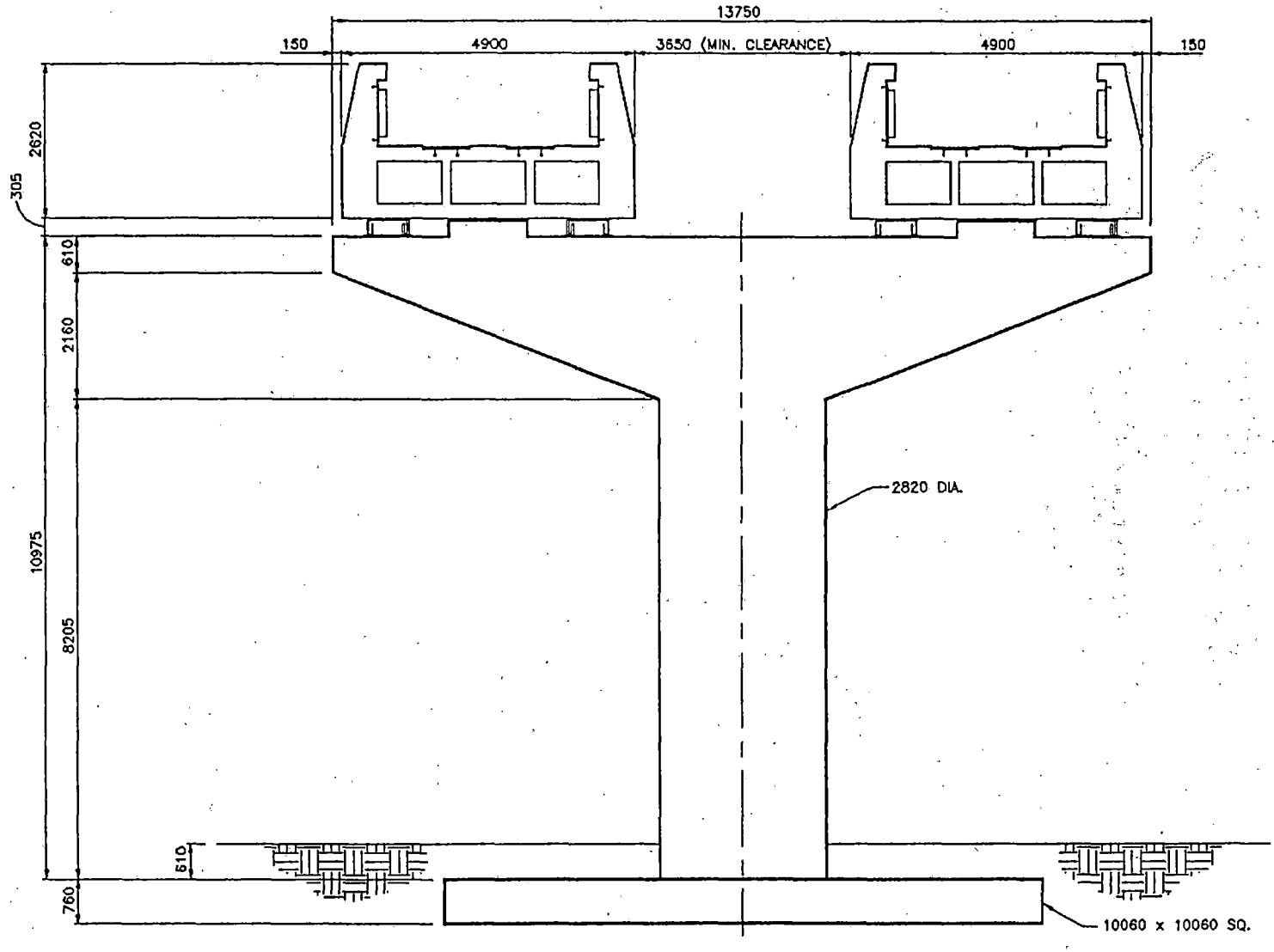

TYPE V – GUIDEWAY ELEVATION SINGLE COLUMN
FIGURE 3-20

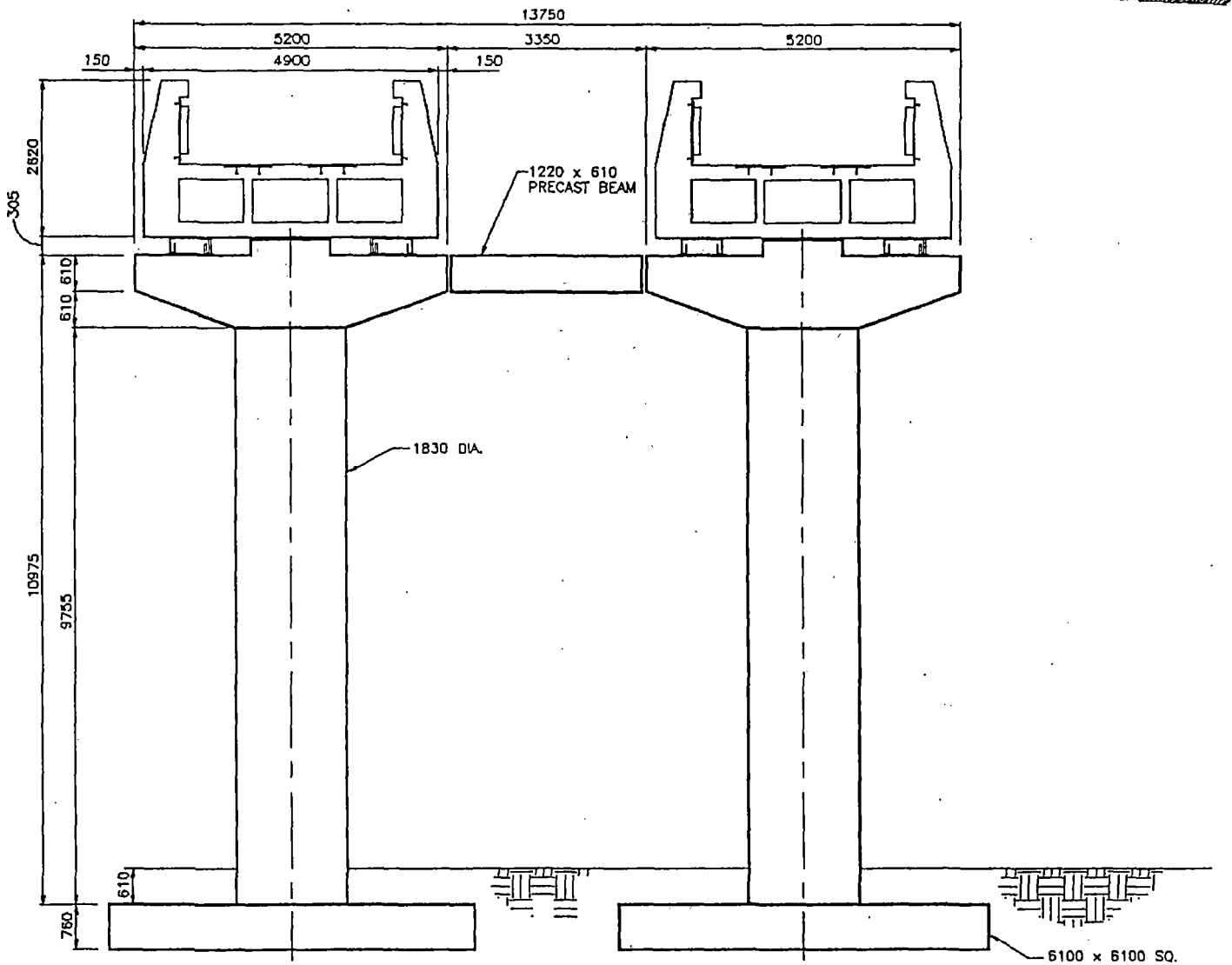

TYPE V – GUIDEWAY ELEVATION DOUBLE COLUMN
FIGURE 3-21

Seismic Criteria:	Zone 2 and/or Zone 4
Snow/Ice Criteria:	Ground Snow Loads (p_g) 1 kPa (20 psf), 51 mm (2 inch) ice accumulation
Frost Criteria:	Design Penetration 1 meter (3 feet) (establishes min. foundation depth)

FOUNDATION CRITERIA

Spread Footing:	Allowable gross bearing pressure of 192 kPa (4,000 psf) at 1.4 meters (4.5 feet) below finished grade

MATERIALS

Structural Steel:	ASTM A36, fy = 413685 kPa (60000 psi)
Concrete:	Foundation (cast-in-place)-ACI 318, f'c = 27,579 kPa (4,000 psi) Column (cast-in-place) - ACI 318, f'c = 27,579 kPa (4,000 psi) T-beam (cast-in-place) - ACI 318, f'c = 27,579 kPa (4,000 psi) Girder (precast) - ACI 318, f'c = 41,369 kPa (6,000 psi)
Concrete Reinf.:	Cast-in-place reinforcing - ASTM A615 Grade 60 Prestressing tendons - ASTM A615 123 tonnes (270 kips) Reinforcing near magnets - FRP
Anchor Bolts:	Clear of magnetic field - ASTM A36 In magnetic field - FRP
Connection Bolts:	Clear of magnetic field - ASTM A325 In magnetic field - FRP

DIMENSIONAL PARAMETERS

Guideway Height:	Varies from a ground clearance of 4.57 m (15 ft) to 16.76 m (55 ft) from grade to bottom of concrete girder; baseline design will be 10.67 m (35 ft)
Guideway Length:	Varies from 15.2 m (50 ft) to 61.0 m (200 ft) from centerline to centerline of supports; baseline design will be 30.5 m (100 ft)
Width:	Minimum two way traffic with minimum 4.9 m (16 ft) clear between each vehicle
Vehicle support :	Reference sketches for the 5 systems under investigation

STRUCTURAL DESIGN CRITERIA

Deflection Criteria:	Column (lateral) - Height/250, Height/500* and Height/750
	Girder (vertical) - Span/1000, Span/2000* and Span/4000
	* - denotes baseline design
Foundation Stability Criteria:	Overturning - 2.0 Factor of safety
	Sliding - 1.5 Factor of safety

VEHICLE CRITERIA

Height	2.75 m (9 ft) from top of concrete guideway
Width	3.05 m (10 ft) 4 seats/row
Length	22.9 m (75 ft) per car (3 car typical train); 20 rows of seats per train (2.5' per seat) + 25' of space at end of vehicle
Weight	Empty - 1265.0 kg/m (850 plf)
	Full - 1265.0 + 90.7 kg (200#)/person w/luggage X 4 seats/row X 20 rows / 22.9 m = 1590.0 kg/m (1070 plf)

The criteria and loads described above are combined to form the loadings that the guideway structure must be designed to resist. The load combinations that will be used to design the structure are outlined in the Load Combination Matrix Table.

LOAD COMBINATION MATRIX

			Operating (Normal)	Operating w/Emer. Stop	Operating w/Wind	Operating w/Seismic
Vertical Loads	Dead Loads	Girder wt.	x	x	x	x
		Lev+LSM	x	x	x	x
		Cables, etc	x	x	x	x
		Ice/snow**	x	x	x	x
		Misc	x	x	x	x
	Live Loads	Vehicle wt.	x	x	x	x
		Passengers	x	x	x	x
		Braking	x		x	x
		Emer. Stop		x		
Lateral Loads	Wind	Structure			x	
		Vehicle			x	
	Seismic*	Structure				x
		Vehicle				x
Long. Loads	Seismic*	Structure				x
		Vehicle				x

* Note for seismic loads, Zone 2 and Zone 4 are both considered. For Zone 4 seismic loads the full lateral or longitudinal load is combined with a 30% orthogonal load

** 2" ice accumulation + 20-psf ground snow load

3.1.3 Guideway Conceptual Designs

The descriptions and details in Section 3.1.1 are a result of an analysis of various structural systems using the criteria/parameters discussed in Section 3.1.2. The actual design of each item of the overall structure was an iteritive process based on economy of section and constructability. The girders were considered precast, pre-assembled, and pre-tested in a shop before shipment (if possible); the foundations, columns, and T-beams were all cast-in-place using the same basic dimensions to ensure the use of prefabricated forming materials. The design dimensions provided on each of the Figures 3-1 thru 3-21 represent the results from the analysis and design using the criteria/parameters from Section 3.1.2, and the baseline deflection criteria, height requirement, and width requirement combined with a vehicle length equal to the span of the girder.

3.1.4 Cost Criteria

The items provided below are the basis for the development of construction costs for the guideway structure and associated systems:

Engineering/Geotechnical Support
Temporary Construction Facilities
Site Preparation and Finishing
Cast-in-place Foundation
Cast-in-place Columns and T-beams
Precast Concrete Girder (including Aluminum Levitation Ladders and LSM)
Shop Installation of Levitation Strips, LSM, Sensor System, Cables, and Wiring
Precast Concrete Girder Installation and Hook-up
Contractor contingency, overhead, and profit.

The cost for the items shown above was estimated for various designs. From these estimates, cost were developed for specific construction activities that could be quantified from

the design effort. For example, the total cost for cast-in-place concrete for the foundation is $290/cubic yard of concrete in the foundation. This cost includes engineering, construction personnel, construction equipment, materials, profit, and overhead. The following data was used to estimate the guideway construction cost.

ITEM	COST	COST
Construction Facilities	$51,200/mi	$31,814/km
Site Preparation & Finishing	$225,280/mi	$139,983/km
Guardrail	$1,220/column	$1,220/column
Foundations	$290/yd^3	$379/m^3
Column & T-beam	$350/yd^3	$457/m^3
Girder	$385/yd^3	$503/m^3
Girder Installation & Paint	$2,816,000/mi	$1,749,781/km
LSM & Levitation Installation	$1,400,000/mi	$869,920/km
LSM	$483,000/mi	$302,000/km

3.1.5 Guideway Cost Summary

The cost of each of the guideway configurations is provided below for the base case, which has been developed using the following criteria/parameters:

Column Spacing	30.5 m
Ground Clearance	10.67 me
Girder Vertical Deflection Limit	Span/2000
Column Lateral Deflection Limit	Height/500
Seismic Zone	2
Girder Strength	41,369 kPa
Foundation Gross Allowable Base Pressure	192 kPa

GUIDEWAY COST SUMMARY

Type I	$10,044,000/mi	$6,241,000/km
Type II	$11,669,000/mi	$7,251,000/km
Type III	$10,836,000/mi	$6,733,000/km
Type IV	$11,293,000/mi	$7,017,000/km
Type V	$12,675,000/mi	$7,876,000/km

The costs provided above reflect an estimate of the engineering, fabrication, and construction associated with a large civil project. The use of these numbers must be limited onlt to a comparison of the total cost between the different guideway configurations. The design of the guideways and the assimilated cost data are not associated with any particular region, nor is it a final detailed design. For example, a review of the data presented above indicates that Type I has an overall constructed cost less than Type V but does not indicate the total cost for the construction of either guideway.

3.1.6 Guideway Construction Problems

The most cost-effective method of construction and installation includes the delivery of the girder prewired with all control cables installed, levitation ladders secured, and grouted in position, LSM secured and grouted in position, assembly-tested to ensure continuity for each girder, and the electronic/controls connections to the next girder prepared and ready for field installation. The entire assembly for a single girder is shipped as a unit to the construction site, lifted by one or two cranes into position, leveled, and then electrically connected to the next girder. The shorter spans for Types I, III, and IV can be constructed in this manner.

However, the weight and size of the longer spans for Types I, III, and IV, and all spans for Types II and V preclude fabrication and shipping of a complete girder. Special permits are available for shipping oversized, overweight items. For a Maglev system, there would be many shipments over an extended time period that would result in traffic congestion, escorts, etc. The solution for this situation is to construct the guideway in segments. Each guideway girder would be composed of a series of segments that would be supported in place by a structural steel truss. After the segments are positioned, they are post-tensioned together to form the continuous guideway. The size and number of segments are dependent on the cross-section of the girder required for the span investigated. There are other possible solutions, including cast-in-place girders and onsite casting of the girders. The delivery of the girders in multiple pieces minimizes the ability to prewire and test the LSM and levitation system.

Another potential construction problem is the space availability at the construction site.

The foundations designed for the column supports are quite large. The designs associated with both the Seismic Zone 4, longer spans, and the taller columns require foundations that may not fit within the median space for many Interstate ROWs. There are two possible solutions for this construction problem: pile foundations and drilled caissons. Based on a brief investigation of both cases it was determined that the costs are equal to or greater than the spread footing costs. The design effort for either of these cases would require the assumption of too many design variables for the results to be of any value, i.e., lateral deflection criteria is one of the key elements in the design and would be greatly dependent on a soil-pile interaction which, when assumed, would have little or no meaning. Therefore, this effort was limited to the discussion found here.

3.2 Cost Relationships

The construction cost of the guideway is dependent on many variables, including site location, congestion of other facilities, terrain, accessibility of construction materials, type of soils supporting the structure, material strengths, length of span, number of supporting columns, height of structure, and the vehicle supported. The variables that have been estimated and a cost impact prepared are:

- single versus double columns,
- span length,
- height of the structure,
- girder vertical deflection criteria,
- column lateral deflection criteria,
- Seismic Zone influence, and
- girder material strength.

The cost relationships are presented in graphical and tabular form in Appendix 3.A-1 through 3.A-216.

3.3 Innovative Configurations

The 5 guideway configurations discussed in Sections 3.1 and 3.2 summarize the primary guideway shapes that have been investigated and documented in the literature. The development of a new configuration hinges on the operation of the levitation and propulsion systems. Of the 5 guideways, Type I is the simplest and least costly to construct, and Type II appears to be the safest to operate because of the wrap-around effect. A new configuration that incorporates properties from both of these shapes is a box shape that is narrower than the Type I and allows the sides of the vehicle to extend below the top surface along the sides of the box. The levitation system is located on top, and the propulsion system is located along the sides of the box. This shape is Type VI. The dimensions of the box for a single-column support are shown in Table 3-51, and the cost relationship compared to the other Types is shown on Chart 3-37.

The cost of Type VI is penalized, as were the other shapes, due to the 1-m separation distance between the LSM and the prestressing tendons. Since the LSM is located on the side of the box, (below the top), the depth of the box, even for short spans is approximately 2.5 m. When adequate research has been completed and the interaction problem between the magnetic fields and the metal tendons has been solved, this shape could be very advantageous.

3.4 Multiple Uses

The multiple use of Maglev Rights-of-Way (ROWs) and Infrastructures Study provides a brief survey and examination of the main issues facing the feasibility and viability of developing a Maglev guideway system designed to achieve multiple transit and nontransit goals. The approach used in this study included the following:

A. SURVEY OF LITERATURE

A comprehensive survey of literature on Maglev technology and economic feasibility was conducted. The survey focused on those studies which help estimate the

potential savings gained by incorporating elements of non-transit with the infrastructure.

B. COLLECTING DATA FROM PRIMARY SOURCES

Data were gathered about particular elements of infrastructure and related consumer uses. Attempts were made to gather general cost estimates from utility companies for each potential element of nontransit infrastructure. However, due to time and resource constraints, reliable and useful cost data could not be generated. The main constraint is the limited knowledge of the economics and financial feasibility of Maglev systems. Most of the experimentation to date has been performed in Germany and Japan. The cost data available reflects the cost structure of production factors in these countries. Also, because of the limited budget for this project, the scope of work is limited to those elements of multiple uses for which data are readily available.

C. PROJECT PROPOSAL

The cost savings anticipated by incorporating multiple uses into the Maglev system depends upon the legal and institutional conditions and the economic demands for the additional functions. These considerations dictate the need for systematic and detailed studies conducted on the following:

- The legal and institutional constraints, including problems associated with ROWs-established design standards of AASHTO, AREA, etc.
- Economic feasibility, including detailed market studies performed on each selected potential site. Such market studies will give special attention to demand for, and supply of, each element of nontransit use.

3.4.1 Background

A recent Transportation Research Board (TRB) report, "Special Report 233 - In Pursuit of Speed: New Options for Intercity Passenger Transport," drew some interesting observations, reference "Cost Estimates for Maglev Infrastructures Based on Corridor Study Reports," pg. 3-48. The report concluded that, although Maglev offers speeds up to 300 mph, more research is needed both to determine the potential for lower costs and to assess the viability of this technology. The report recommended a careful review of both the potential market for Maglev and the National Maglev Initiative results. It concluded that high-speed ground transportation could make travel easier for millions of Americans but that this mode of travel would not come cheaply. Such transport systems would attract riders from other types of transportation but are unlikely to gain enough passengers to cover the full costs. Subsidies will be necessary, and the country will need changes in its institutional systems for transportation. The viability of Maglev depends more upon creative methods of decreasing the investment cost per mile, including multiple use of the infrastructure.

Maglev technology, having evolved over the last three decades, now potentially represents a new option for high-speed ground transportation (HSGT). At present, the Maglev system competes with high-speed rail (HSR) for intercity passenger transportation. Maglev technology is now at an advanced stage of commercialization in Japan and Germany, and extensive tests have been carried out on these German and Japanese models.

The real problem facing Maglev system implementation is the lack of research showing that Maglev technology has reached a stage where **total user fees can cover the total cost.** The capital cost of the Maglev system, as well as HSR, is primarily determined by the construction cost of the guideway; vehicle cost is estimated at only a fraction of the total capital cost. The TRB Report 233 (1991) gives estimates for guideway costs as 50 to 80% of total capital cost, including up to 10% for the ROW. The report cites vehicle cost as 10 to 20%. The capital cost of the ROW is seen as highly sensitive to the specific characteristics of the corridor.

Whether or not cost savings through multiple-use design of Maglev guideway structure and ROWs could contribute a substantial saving has not been tested in relation to Maglev system implementation in the United States. Yet, there are indications that the viability of Maglev in the United States critically depends upon reducing construction costs of the guideway. The Maglev guideway system, designed to achieve multiple transit and nontransit goals, may result in cost reductions. Another critical factor is the potential income generated from rider and nonrider use. User fees and nonuser benefits must be of such magnitude that they will gain support from both private and public sectors.

With respect to the issue of cost saving, the following basic technological choices must also be made:

- **Choice of Maglev Technology System type:** Electromagnetic System (EMS) or electrodynamic (EDS). Design of the guideway system possible nontransit use of ROWs requires selection of either EMS or EDS.
- **Choice of system:** Develop U.S. Maglev system or franchise foreign systems such as the German or the Japanese systems.

If the German or the Japanese Maglev systems are franchised, the adaptation of their technology systems to U.S. standards has to be addressed. This may call for changes in design, regulation, or institutional arrangements. These adaptations may impose additional constraints on the use of ROWs for the selected Maglev technology system.

This preliminary study is one of the first attempts to address the issue of cost-sharing through the multiple use of Maglev ROWs and structures. The study also provides the following:

- Bibliographies of the literature, highlighting those which are significant.
- An outline of the main issues, requiring examination in a market.
- Economic feasibility, as well as institutional studies, to determine viability of private sector leadership in Maglev system implementation in the United States.

3.4.2 Survey of Literature

The literature on joint use and cost sharing in the design of Maglev System guideway structure, as well as on potential constraints, is limited. The American Association of State Highway Transportation officials (AASHTO) has discussed some of the issues. Specifically, a need exists to address the modality of joint use of Maglev guideways. A fact emerging from the survey of existing literature is that the concept of joint use for the Maglev system has yet to be worked out in the coming years.

Both domestic and international publications on Maglev systems are included in the literature survey. The survey focuses on most recent publications and covers Maglev concepts, technology, cost, methods of evaluation, and safety and environmental issues. A number of publications cover the TransRapid Maglev System of Germany and the MLU002 Electrodynamic Levitation and HSST-03, Japanese versions of Maglev.

Almost all the cost estimates for the Maglev system in the United States rely primarily on data from the TransRapid System. These Maglev feasibility studies have yielded cost estimates between $11 million and $63 million per mile. Some cost data for implemented projects in Germany and Japan does exist but is of limited value for the U.S. economic environment. For example, the following project costs are listed below:

- Shinkansen-Tokaido line averaged $13 million per mile.
- Osaka-Okayama extension was $17.6 million per mile.
- Okayama-Yakata extension $23.4 million per mile.

The TransRapid guideway structure, with both concrete and steel beam guideways, is estimated at about 63% of the capital cost, while equipment costs stand at 28% and vehicle costs at only 9%. This indicates that significant cost saving on guideway construction could make the Maglev system profitable.

A most relevant document on joint use and cost sharing is "The Market Analysis of the Business Opportunity in the Telecommunication Industry." This document was prepared

for Bay Area Rapid Transit (BART) by Bechtel Civil, Inc., in August 1986, reference "Comparison of Results for BART Options," pg. 3. A comparison of cost savings for 3 alternatives, for joint use of rail ROWs, is shown in Appendix A-2. The ROWs lease was estimated at $2,500.00/km/yr/customer. Thus, the lease per year for a single customer traveling 500 km amounts to $1.25 million. If the Maglev system operates the telecommunication service, the return on investment ranges from 18 to 48% for the alternatives considered. This indicates the size of savings from a single-utility joint use.

3.4.3 Sources

Public service agencies and electric power, telephone, and other utility companies were questioned on the need, compatibility, and possible cost savings through joint use of ROWs. They also were asked about problems associated with the electromagnetic field that results from Maglev system implementation.

With respect to compatibility and cost savings, the organizations were unwilling to estimate, on the grounds that the questions had meaning only with respect to specific corridors. However, they did express interest in participating in a concrete project. The effect of electromagnetic fields on the operations of utility companies in joint use varies according to the utilities used. As far as the telecommunications system is concerned, the field will have little impact as long as fiber optic cables are used for trunk lines. The corrosive effect of stray current on oil or gas pipelines may be significant, but technology is available to prevent such effects from taking place.

3.4.4 Issues to be Examined

The following proposal outlines the main issues that need to be addressed.

A. MARKET AND ECONOMIC FEASIBILITY STUDY

The critical factor restraining the active interest of U.S. industries in Maglev is the lack of clearly visible, ensured markets and opportunities for profit in the implementation of the Maglev system. The opinion of those in the industry is that "the market is too far away and uncertain to warrant spending resources on research and development." National Maglev Initiative evaluation of international and U. S. Maglev system concepts will require exhaustive studies on market and economic feasibility for use of HSGT in each of the 12 corridors identified in Appendix A-1. The proposed studies will accomplish the following:

- Focus on the market and economic feasibility of the Maglev system.
- Update and evaluate competitiveness and commercial viability of Maglev system/EMS/EDS.
- Incorporate cost savings that could result from guideway structural designs for joint use, and establish actual joint use of ROWs with public utility companies.
- Focus and highlight external/public benefits and cost savings that may result in energy, environmental improvement, relief of traffic congestion, technology spinoff, etc.
- Examine other important issues which include ROW acquisitions, research and development funds, and appropriate government cost sharing.

The results of site-specific market and economic feasibility studies of the Maglev system are critical for potential private-sector financing and implementation of the selected Maglev system, whether it be an international franchise or domestically developed Maglev system.

The question of whether cost savings will be generated from the joint use of Maglev guideway structures, ROWs, and public utility services cannot be answered satisfactorily in general terms. Yet, Maglev system implementation is heavily contingent on significant cost savings that can provide comparative advantages over competing systems.

B. INSTITUTIONAL AND PUBLIC POLICY ISSUES

The Federal Highway Administration (FHWA) makes decisions on federally-aided highways and their ROWs on a case-by-case basis -- there are no set rules. Current laws require payment, at fair market value, for state-owned ROWs. Therefore, changes in federal policy to favor Maglev may be required.

In addition, a number of institutional and public policy issues need to be addressed if the U.S. private sector is to assume leadership in the development and implementation of the Maglev system.

Among the main institutional issues is the legal framework under which Maglev will develop. For instance, one issue concerns the pros and cons of Maglev system exemption from Interstate Commerce Commission oversight due to Maglev system competition with deregulated airlines.

Another important issue relates to the need for the implementation of an innovative financing system and an appropriate institutional mechanism to help finance the Maglev system.

Also to be considered under the institutional and policy issues are ROW acquisitions, government/industry development funds, etc.

While research proceeds on refining the Maglev technology system concept, an urgent need exists to continue working on economic and financial feasibility, as well as on institutional and public policy areas.

3.4.5 Conclusion

The study for Multiple Use of Maglev Right-of-Ways and Infrastructure findings can be summarized briefly as follows:

A. LACK OF CONCRETE STUDIES

Although a number of feasibility studies were performed for some potential Maglev corridors, no concrete studies which include the joint-use of ROWs, based on the Maglev system, exist. The BART study of ROW joint use for telecommunication services indicates that the potential for cost savings does exist.

B. NEED FOR SPECIFIC STUDIES

Generic studies are useful for providing a general overview of the issues. However, the joint use of ROW studies will have the most impact when they focus on specific corridors.

C. KEY CHALLENGES

Among the key challenges facing Maglev systems are conducting market and economic feasibility studies and developing innovative methods to solve institutional and public policy issues.

Table 3-1

COMPARISON OF RESULTS FOR BART OPTIONS

The potential value of BART's ROW, if used as a telecommunications corridor, was determined by evaluating four alternative options, or cases, that could be pursued as business opportunities:

- A Base Case which assumes that BART installs and sells fiber and leases right-of-way, but does not otherwise enter the telecommunications business. A company in the telecommunications business (Operator) would market the services and operate the system.
- An Alternative 1 to the Base Case which assumes that BART enters the telecommunications business and assumes all functions as an Operator.
- An Alternative 2 to the Base Case which assumes BART installs only enough fiber to satisfy pre-committed demand, sells the fiber during a two-year period, and demand, sells the fiber during a two-year period, and derives ROW revenues. No other services are provided.
- An Alternative Base Case which adds the San Ramon/Pleasanton area to the Base Case.

COMPARISON OF RESULTS FOR BART OPTIONS
(Thousand Dollars, 1986)

	Base Case	Alternatives 1	2	Alternatives Base Case*
Total Revenues (10 Year Totals)	6,974	26,797	3,906	8,025
Expenses (10 Year Totals)	104	9,696	129	104
Net Income (10 Year Totals)	6,870**	7,758	7,921**	
Capital Cost (10 Year Totals)	2,749	4,279	1,116	3,519
Net Cash Flow (10 Year Totals)	4,121	7,592	2,662	4,402
Present Value of Net Cash Flows @10%				
Rate of Return on Investment	28%	18%	48%	21%
Payback (Year)	3	5	1	4

*Includes the San Ramon/Pleasanton possible corridor
**Assumes no income taxes paid

SOURCE: Bechtel Civil, Inc.,"MARKET ANALYSIS OF THE BUSINESS OPPORTUNITIES IN THE TELECOMMUNICATION INDUSTRY", (Prepared for BART)

Table 3-2

COST ESTIMATES FOR MAGLEV INFRASTRUCTURE BASED ON CORRIDOR STUDY REPORTS

Corridor	Length	Date of Study	Source of Sponsor	Cost of Corridors millions per mile	Source
Detroit-Chicago	280	1985	Michigan Department of Transportation	19	CIGGT 1986
Philadelphia-Pittsburgh	352	1985	Pennsylvania HSR Commission	63	CIGGT 1986
Montreal-Ottawa	115	1984	Transport Canada Transportation Development Center	14	CIGGT 1986
Vancouver-Portland	342	1984	Washington Department of Transportation	50	CIGGT 1986
Tampa-Orlando-Miami	314	1984	Florida HSR Commission	27	CIGGT 1986
Quebec-Windsor	653	1984	VIA Rail Canada	11	CIGGT 1986
Las-Vegas-Los Angeles	230	1983	City of Las Vegas	17	CIGGT 1986
Toronto-Montreal	376	1980	Transport Canada Transportation Development Center	20	CIGGT 1986
Chicago-St. Louis	282	1984	Federal Reserve Bank of Chicago	18	CIGGT 1986
Las Vegas-Los Angeles	267	1990	Maglev Working Group	18	CIGGT 1986
Pittsburg-Airport	19	1990	Maglev Working Group	33	
		1990	Federal Railroad Administration	31	
		1987	Transrapid	20	FRA 1990

Note: All figures are in 1991 dollars.
50 percent not elevated.

SOURCE: TRB/NRC, "IN PURSUIT OF SPEED - NEW OPTIONS FOR INTERCITY PASSENGER TRANSPORT", Report 233, Washington, D. C. 1991

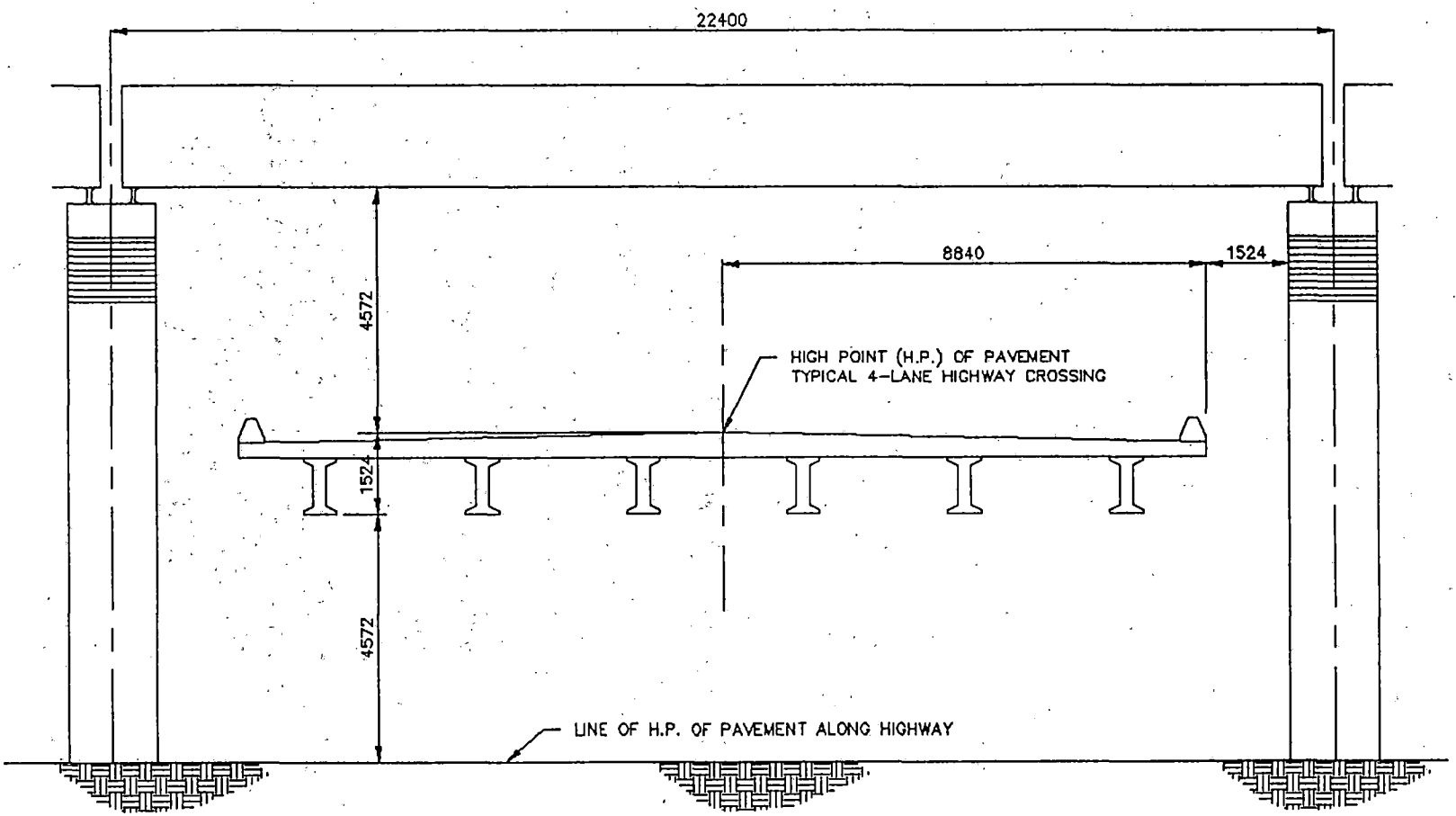

TYPICAL HIGWAY CLEARANCE
FIGURE 3-22

PROPERTY OF FRA
RESEARCH & DEVELOPMENT
LIBRARY

Guideway Structural Design and
Power/Propulsion/Braking in Relation to
Guideways, Final Report, Babcock & Wilcox, 1993 -
11-Advanced Systems

SMEAD CO VP365A